PJNM

Philippine Journal of Nuclear Medicine

Vol. 21 No. 1 **January to June 2026**

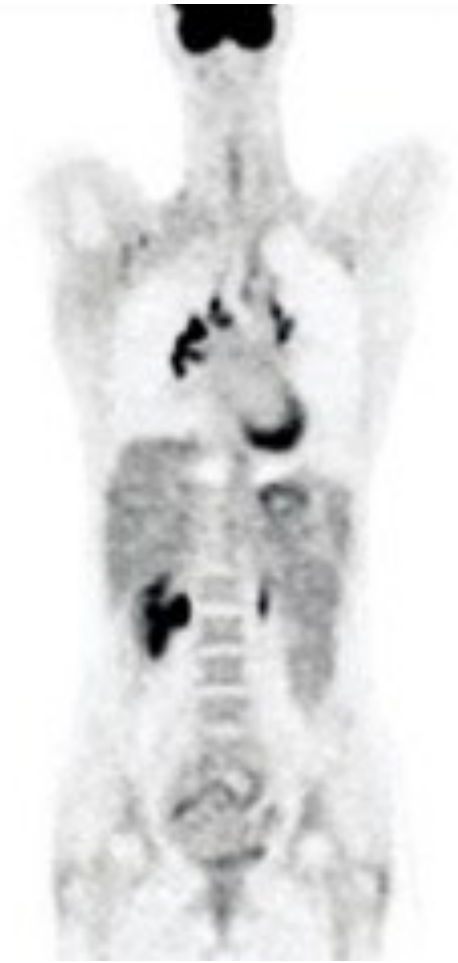

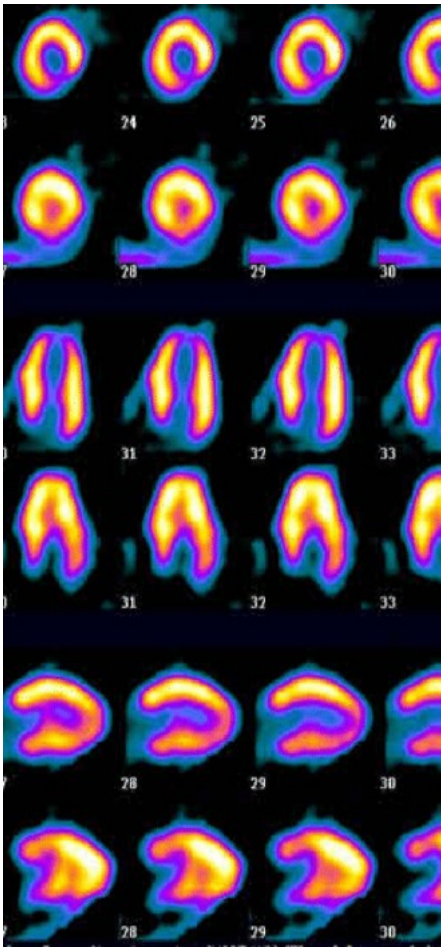

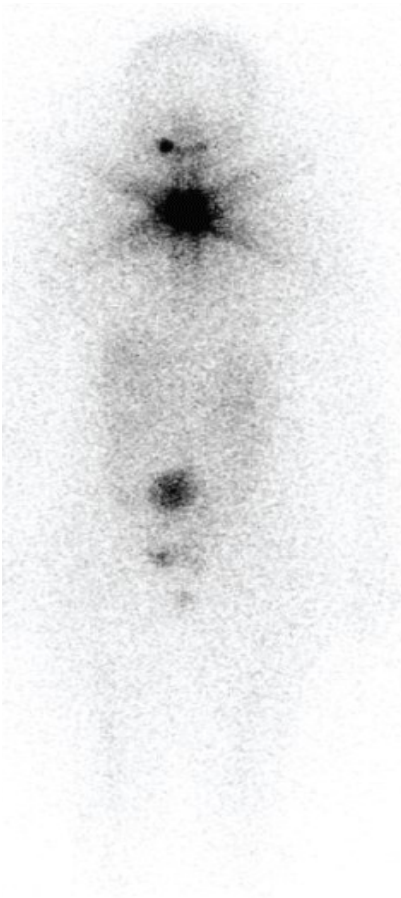

Contents:

Philippine Journal of Nuclear Medicine

Volume 21 No. 1
January to June 2026

Official Publication of the Philippine Society of Nuclear Medicine

The Philippine Journal of Nuclear Medicine is a peer-reviewed journal published by the Philippine Society of Nuclear Medicine. Subscription is free to all PSNM members in good standing as part of their membership privileges.

The Journal will be primarily of interest to medical and paramedical personnel working in nuclear medicine and related fields. Original works in clinical nuclear medicine and allied disciplines in physics, dosimetry, radiation biology, computer science, radiopharmacy, and radiochemistry are welcome. Review articles are usually solicited and published together with related reviews. Case reports of outstanding interest are likewise welcome. PSNM documents and position papers of interest to the reader will also be published as necessary.

Manuscripts for consideration should be sent to:

The Editor, Vincent Peter C. Magboo, MD
Philippine Journal of Nuclear Medicine
c/o Philippine Society of Nuclear Medicine
Unit 209 One Beatriz Tower Condo
4 Lauan St. cor. Aurora Blvd
Project 3, Quezon City 1102, Philippines
Contact. No.: +63 (966) 976 5676
Email: vcmagboo@up.edu.ph
philnucmed@gmail.com

All business communications and requests for complimentary copies should be addressed to the above.

ISSN 1655-9266

INFORMATION FOR AUTHORS

EDITORIAL POLICY

The Philippine Journal of Nuclear Medicine is the official peer-reviewed publication of the Philippine Society of Nuclear Medicine. The Journal accepts original articles pertinent to the field of nuclear medicine. Articles may be on any of the following: clinical and basic sciences, case reports, technical notes, special contributions, and editorials.

Submission of manuscripts

The submitted manuscript package should consist of: (1) the full text (including tables) in Microsoft Word, plain text or ConTeXt document format; and (2) high-resolution JPEG files of all images used in the manuscript. The complete manuscript package may be submitted as a compressed (.ZIP) file by email to philnucmed@gmail.com, or in an optical disc (CD/DVD) and mailed to

> The Editor: Philippine Journal of Nuclear Medicine, c/o Philippine Society of Nuclear Medicine, Unit 209 One Beatriz Tower Condo, 4 Lauan St. cor. Aurora Blvd., Project 3, Quezon City 1102, Philippines.

Manuscripts should be accompanied by a cover letter signed by the author responsible for correspondence regarding the manuscript. The cover letter should contain the following statement:

"All copyright ownership is transferred to the Philippine Journal of Nuclear Medicine upon acceptance of the article _____. This manuscript has been seen and approved by all the authors. The authors stipulate that the material submitted to the Philippine Journal of Nuclear Medicine is an original work and has not been submitted to another publication for concurrent consideration. Any human and/or animal studies undertaken as part of the research are in compliance with regulations of our in stitution(s) and with generally accepted guidelines governing such work."

The cover letter should also give any additional information that may be helpful to the Editor. Signed cover letters sent by email should be in PDF format.

MANUSCRIPT FORMAT

Manuscripts must be written in English, and printed on letter-sized white bond paper, 8.5 in x 11 in (21.6 cm x 27.9 cm). The text should be on one side of the paper only, single-spaced, with at least 1.5 in (4 cm) margins on all sides. Each of the following sections must begin on separate pages and in the following order: title page, abstract, text, acknowledgments, references, tables (each on a separate page), and legends. Pages should be consecutively numbered beginning with the title page. The first line of paragraphs should be indented by at least five spaces.

Title page

The title page should include: (1) a concise but informative title; (2) a short running head or footline of no more than 40 characters; (3) a complete byline, with first name, middle initial, and last name of each author and highest adacemic degrees; (4) the complete affiliation for each author, with the name of departments and institutions to which the work should be attributed; (5) disclaimers, if any; (6) the name, address, and telephone number of the author responsible for correspondence about the manuscript; and (7) the name and address of author to whom reprint requests should be directed.

Abstract and key words
An abstract of no more than 300 words should state the purpose of the study or investigation, summary of methodology, major findings, and principal conclusions. New and important aspects of the study or observations should be emphasized. No figures, abbreviations or reference citations are to be used in the abstract.

Text

The text of original scientific and technical articles is usually divided into the following sections: Introduction, Materials and Methods, Results, Discussion, and Summary or Conclusion.

Case reports are divided into the following sections: Introduction, Case Report, Discussion, and Conclusion. They should contain a concise description of one to three patients, emphasizing the nuclear medicine aspects and include methodology, data and correlative studies. Procedures should be described in sufficient detail to allow other investigators to reproduce the results.

Other articles, e.g. review articles, position papers, or editorials, should introduce a problem or question, present evidence, and conclude with an answer. Generally, review articles should have extensive documentation. Literature citations should represent the breadth and depth of the subjects being reviewed. The organization of review articles will depend greatly on the subject matter and material.

Generic names must be used throughout the text. Instruments and radiopharmaceuticals must be identified by manufacturer name and address in parentheses.

Acknowledgments

Persons or agencies contributing substantially to the work, including any grant support, must be acknowledged.

References

References must be cited in consecutive numerical order at first mention in the text and designated by the reference number in parentheses. References appearing in a table or figure should be numbered sequentially with those in the text.

The reference list must be numbered consecutively as in the text. The journal follows Index Medicus style for references and abbreviates journal names according to the List of Journals Indexed in Index Medicus. 'Unpublished observations' and 'personal communications' should not be used as references, although written—not verbal—communications may be noted as such in the text. The author is responsible for the accuracy of all references and must verify them against the original document.

For journal articles with six or less authors, all authors must be listed. For those with seven or more authors, only the first three are listed, and "et al." is added to the end of the list.

> Seabold JE, Conrad GR, Kimball DA, Ponto JA and Cricker JA. Pitfalls in establishing the diagnosis of deep venous thrombophlebitis by indium-111 platelet scintigraphy. J Nucl Med 1988;29:1169–1180.

For book and book chapters:

> Williams LJ. Evaluation of parathyroid function. In: Brock LJ, Stein JB, eds. The parathyroid and its diseases. 4th ed. New York: Wiley; 1985:196–248.
>
> Goodyear B. Bone marrow transplantation in severe combined immunodeficiency syndrome. In: Gree HJ, Blackscmith R, eds. Proceedings of the fourth biennial meeting of the International Society of Transplantation. Houston: International Society of Transplantation; 174: 44–46.

For journal article in electronic format:

> Author. Title. Journal name. Online publishing date. Available from: URL address.

Tables

Each table should be typed double-spaced on a separate page. Do not submit tables as photographs. Tables should be self-explanatory and should supplement, not duplicate, the text. Each table must be cited in consecutive numerical order in the text. Tables should be numbered consecutively with a Roman number following the word TABLE.

Illustrations

Illustrations should clarify and augment the text. Figures should be sharp and of high quality. Glossy photographs of line drawings rendered professionally on white drawing paper in black India ink, with template or typeset lettering, should be submitted. High quality computer-generated art is also acceptable. Letters, numbers, and symbols should be clear and of sufficient size to retain legibility after reduction.

Each illustration must be numbered and cited in consecutive order in the text. Illustrations should be identified on a gummed label. Legends should be typed double-spaced on a separate page. Figures should be numbered with an Arabic number following the word FIGURE.

Units of measurement

Use of the International System of Units (SI) is standard. Measurements of length, height, weight, and volume must be reported in metric units. Other measurements must be reported in the units in which they were made. Alternative units (non-SI units) should be added in parentheses by the author, if indicated.

Abbreviations and symbols

Only standard abbreviations and symbols should be used in the text. At first mention, the complete term, followed by its abbreviations in parentheses, must be used in the text. Standard units of measure should not be expanded at first mention. Consult a style manual, if necessary.

REVIEW PROCEDURE

Submitted manuscripts are peer-reviewed for originality, significance, adequacy of documentation, reader interest, composition, and adherence to the guidelines. Manuscripts are returned to the author for revision if suggestions and criticisms have been made. All accepted manuscripts are subject to editing for scientific accuracy, clarity, and style.

PHILIPPINE SOCIETY OF
NUCLEAR MEDICINE

MIDYEAR CONVENTION

RADIATION SAFETY REFRESHER COURSE

AUGUST 01, 2026
NOVOTEL MANILA ARANETA CITY

SAVE THE DATE!

Message from the President of the Society

Warm greetings to my colleagues and friends,

We continue to move forward with steady confidence as we navigate both the opportunities and challenges of our specialty. As hybrid imaging and theranostics become more firmly integrated into clinical practice, nuclear medicine in the Philippines continues to mature in both scope and influence. Increasingly, we find ourselves contributing to multidisciplinary teams and shared clinical decisions that directly shape patient care - reflecting our growing relevance within the broader healthcare landscape.

The Philippine Journal of Nuclear Medicine embodies this progress and remains central to our mission of advancing education, research, and quality practice. Long established as a platform for resident and fellow scholarship, the Journal now invites a broader and more inclusive exchange of ideas across the Society. I encourage practicing physicians to share their clinical experiences and practice-based insights, and allied medical professionals to contribute their expertise in quality, safety, education, and innovation. Each perspective strengthens our collective understanding and supports the continuous improvement of our specialty.

May this Journal continue to serve as a welcoming and credible space for rigorous inquiry, collaboration, and mentorship. Through shared knowledge and purposeful scholarship, we move forward together - shaping a specialty that continues to grow in relevance, impact, and heart, in keeping with the mission and values of our Society.

With warm regards,

Michele A. Duldulao - Ogbac, MD, FPSNM

President, Philippine Society of Nuclear Medicine (2025-2027)

GE HealthCare

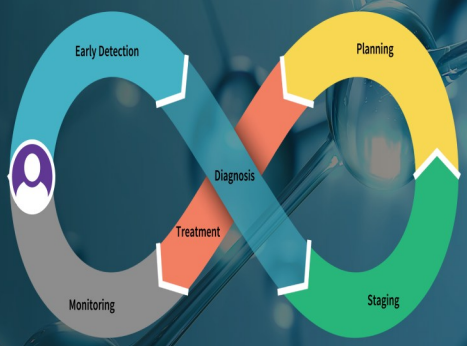

It's time for a Theranostics revolution

Cyclotron Solutions
PETtrace™ 800 Cyclotron
^{68}Ga Liquid Target
^{68}Ga Solid Target

Radiochemistry
FASTlab™ 2 New Edition Developer

Discovery PET/CT
Solutions with high sensitivity, Precision DL, Q.Clear & MotionFree to image ^{68}Ga for diagnosis, staging or restaging

Digital SPECT/CT
Solutions to image and quantitate ^{177}Lu imaging accurately to personalise patient treatment

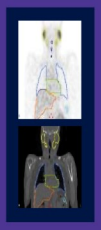

Digital AI applications for Effective quantitation including automatic **AI-based segmentation**

Discovery

Diagnosis

Treatment

GE HealthCare

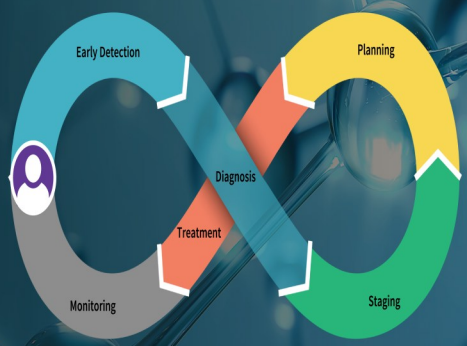

It's time for a Theranostics revolution

Cyclotron Solutions
PETtrace™ 800 Cyclotron
^{68}Ga Liquid Target
^{68}Ga Solid Target

Radiochemistry
FASTlab™ 2 New Edition Developer

Discovery PET/CT
→ Solutions with high sensitivity, Precision DL, Q.Clear & MotionFree to image ^{68}Ga for diagnosis, staging or restaging

Digital SPECT/CT
Solutions to image and quantitate ^{177}Lu imaging accurately to personalise patient treatment

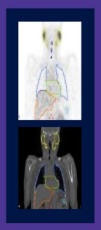

Digital AI applications for Effective quantitation including automatic **AI-based segmentation**

Discovery | Diagnosis | Treatment

The Utility of Cardiac PYP Scintigraphy in the Diagnosis of Transthyretin Cardiac Amyloidosis: A Case Report

Dominic Alcantara, MD, Nicole Patricia Hui, MD, Edward Bengie Magsombol, MD

Department of Nuclear Medicine, The Medical City, Ortigas Avenue, Pasig City, Philippines
E-mail address: alcantaradomz@gmail.com

ABSTRACT

Cardiac amyloidosis is a rare form of restrictive cardiomyopathy characterized by protein deposition in the heart. There are gaps in the Philippine literature regarding its incidence, suggesting underdiagnosis. Conventional imaging with echocardiography and cardiac magnetic resonance (MR) are valuable for diagnosis but they cannot distinguish between the transthyretin (ATTR) and light chain (AL) types. Differentiating between the two is crucial due to their distinct prognoses and treatment approaches. Endomyocardial biopsy is the gold standard for confirming diagnosis, however it is invasive with risk of complications. We present a case of an elderly Filipino male who developed easy fatigability for five days after recovering from a mild coronavirus disease (COVID-19) infection. Chest radiograph revealed right-sided pleural effusion. Biomarkers for cardiac ischemia showed elevated Troponin I and normal NT-pro-BNP levels. Electrocardiogram showed sinus rhythm with 1st degree atrioventricular block. Initially, he was diagnosed with post-COVID cardiomyopathy and pneumonia, and was started on empiric antimicrobial therapy. Echocardiography revealed preserved left ventricular (LV) ejection fraction and Grade 2 LV diastolic dysfunction. Cardiac MR showed findings suggestive of cardiac amyloidosis, prompting further investigation. Subsequently, Technetium-99m pyrophosphate (PYP) cardiac scintigraphy showed elevated heart-to-contralateral lung ratios and a myocardial uptake semiquantitative grade of 3. These corresponded to a positive scan which led to the diagnosis of ATTR cardiac amyloidosis and obviated the need for biopsy. In summary, cardiac PYP scintigraphy is reliable in the diagnosis of ATTR cardiac amyloidosis especially in cases where conservative management is preferred.

***Keywords**: ATTR, cardiac transthyretin amyloidosis, PYP scan, technetium-99m pyrophosphate scintigraphy*

INTRODUCTION

Cardiac amyloidosis is a rare disease caused by extracellular deposition of misfolded proteins called amyloid fibrils in the myocardium, which eventually leads to restrictive cardiomyopathy and heart failure [1]. This disorder can be divided to two main types: deposition of transthyretin (ATTR) from liver-synthesized proteins, and deposition of immunoglobulin light chains (AL) from an abnormal proliferation of plasma cells. If left untreated, cardiac amyloidosis is highly fatal with a median survival time of less than 1 year for the AL type and 4 years for the ATTR type [2]. There is growing enthusiasm in subtyping the disease as a result of three key areas of advancements: non-invasive cardiac imaging for diagnosis, emerging therapy with the ATTR kinetic stabilizer Tafamidis, and observational studies in the Asian population indicating that it may be underdiagnosed [1, 3]. Conventional cardiac imaging with echocardiography and cardiac magnetic resonance (MR) are valuable for the diagnosis, but they cannot differentiate between the two types .

Given their distinct prognoses and treatment approaches, it is crucial to distinguish between AL and ATTR. The gold standard in confirming the diagnosis is via endomyocardial biopsy with Congo red staining with apple-green birefringence under polarized light, immunohistochemistry typing and/or mass spectrometry. However, this is an invasive procedure and carries a low but notable risk of cardiac injury and perforation. Biopsy is thus reserved for equivocal cases with discordant clinical and imaging findings [3, 5].

We report a case of an elderly Filipino male who presented with acute heart failure and pneumonia after recovering from a mild coronavirus disease (COVID-19) infection. During the course of management, he benefited from a technetium-99m pyrophosphate (PYP) scan which led to a definitive diagnosis. The objective of this report is to highlight the utility of cardiac PYP scanning in the diagnosis of ATTR cardiac amyloidosis in an elderly patient with preference for conservative management

CASE PRESENTATION

An 85 year old Filipino male presented with easy fatigability and exertional dyspnea of 5 days duration. This was noted to be a week after recovering from febrile episodes with a positive COVID-19 rapid antigen test result. For the past medical history, he has hypertension, a small right kidney attributed to previous nephritis, chronic hyponatremia, and a history of treated pulmonary tuberculosis. His blood pressure was 140/80 mmHg, and on physical examination there was noted bilateral basal crackles. Plain chest radiograph showed right-sided pleural effusion.

Biomarkers for cardiac ischemia and heart failure were also investigated. The Troponin I level was elevated at 26.8 pg/mL (Reference value < 12) and the NT-pro-BNP level was within normal at 405 pg/mL (Reference value < 450 for people over age 75). Electrocardiography (ECG) showed sinus rhythm with 1st degree atrioventricular (AV) block, but otherwise no evident acute ischemic changes. He was initially diagnosed with post-COVID cardiomyopathy and pneumonia, and was started on empiric antimicrobial therapy. Sputum culture with gram staining were positive for moderate growth of Acinetobacter baumannii and Enterobacter cloacae with various resistance and sensitivity profiles, after which the antibiotic was shifted to Meropenem.

Transthoracic echocardiography was performed for assessment of heart failure and possible myocarditis, which showed the following findings: normal left ventricular (LV) cavity size, concentric LV remodeling, LV ejection fraction of 62.9% by Simpson's biplane method, Grade 2 LV diastolic dysfunction, right ventricular (RV) hypertrophy, aortic sclerosis with aortic annular calcification, and mitral sclerosis with moderate mitral regurgitation. Overall, echocardiography pointed to heart failure with reserved ejection fraction, with Grade 2 diastolic dysfunction as a typical finding in possible cardiac amyloidosis. Subsequently, cardiac magnetic resonance (CMR) imaging was done for further evaluation of cardiomyopathy, which showed diffuse patchy late gadolinium enhancement involving the LV segments, likewise enhancement of the RV and atrial walls, and abnormal contrast kinetics in the blood and myocardium. These imaging findings were suggestive of cardiac amyloidosis, prompting further work-up to differentiate between AL and ATTR. In the interim, serum assay for free light chain proteins were sent for analysis which all returned as negative .

After conventional cardiac imaging, the patient was referred to our nuclear medicine department for a cardiac PYP scan. The scan was performed by administering Technetium-99m pyrophosphate intravenously, imaging the patient 1 hour and 3 hours post-injection, and acquiring anterior (Figure 1) and posterior views of the thorax. Complementary single photon emission computed tomography (SPECT) of the thorax was also acquired for better anatomic localization (Figure 2) .

On 1-hour imaging, there was a diffuse cardiac tracer uptake greater than the adjacent skeletal activity (Figure 1A). Tracer activity in the ribs was nearly absent. On 3-hour imaging, similar findings were observed (Figure 1B). Using the anterior image, a circular region of interest (ROI) was applied on the area of the heart and the same size of ROI was applied on the area of the contralateral lung, which allowed calculations for the heart-to-contralateral lung (H:CL) ratio. On 1- and 3-hour images, the H:CL ratio was elevated at 1.6 and 1.8, respectively (normal is < 1.5 and < 1.3, respectively). The intensity of cardiac tracer uptake was compared with the skeletal uptake, corresponding to a positive scan with semiquantitative grade of 3. Overall, this led to the diagnosis of ATTR cardiac amyloidosis.

Possible treatment with Tafamidis, including its risks, benefits, and cost was discussed with the patient and family. Due to financial constraints, the patient refused treatment. Considering his advanced age and preference, conservative management was done and the family was counselled regarding disease prognosis. They were also advised on the importance of further testing with genotyping to identify disease subtype such as hereditary variant (ATTRv) or wild type (ATTRwt).

DISCUSSION

ATTR cardiac amyloidosis has historically been considered a rare disease and there are gaps in the scientific literature regarding its incidence in Asia including the Philippines [3]. The disease disproportionately affects older adult males and people of African descent. Considering available data in the Asian population, recent findings from a Japanese observational cohort study revealed that the estimated incidence of ATTR cardiomyopathy was approximately 1 per 10,000 person-years among those > 65 years old [4]. Majority of the diagnosis was made by PYP scintigraphy with negative monoclonal protein markers. To help increase recognition of the disease, practical

recommendations for the Asian population were developed by Lin et al which listed a summary of 'red flags' upon presentation, prompting timely referral and further work-up [3]. Relevant to our case is the acute development of heart failure with preserved ejection fraction in an elderly patient, which can be considered a red flag and prompt investigation for cardiac amyloidosis in suspect cases. The initial diagnosis was complicated due to the concomitant presence of pneumonia and recent history of viral respiratory infection (COVID-19), hence evaluation for possible post-COVID cardiomyopathy was pursued. Eventually, the presence of cardiac MR findings suggestive of cardiac amyloidosis helped direct referral for cardiac PYP scintigraphy. A summary on typical imaging features using multiple modalities for cardiac amyloidosis is given in Table 1 for reference [6].

Bone-avid radiotracers such as technetium-99m (Tc-99m) labelled pyrophosphate (PYP), diphosphono-propanodicarboxylic acid (DPD), and hydroxymethylene disphosphonate (HMDP) have been shown to preferentially bind to the myocardium in patients with ATTR cardiac amyloidosis. The exact mechanism for the differential uptake in ATTR rather than AL is still unknown. However, it has been suggested that cardiac

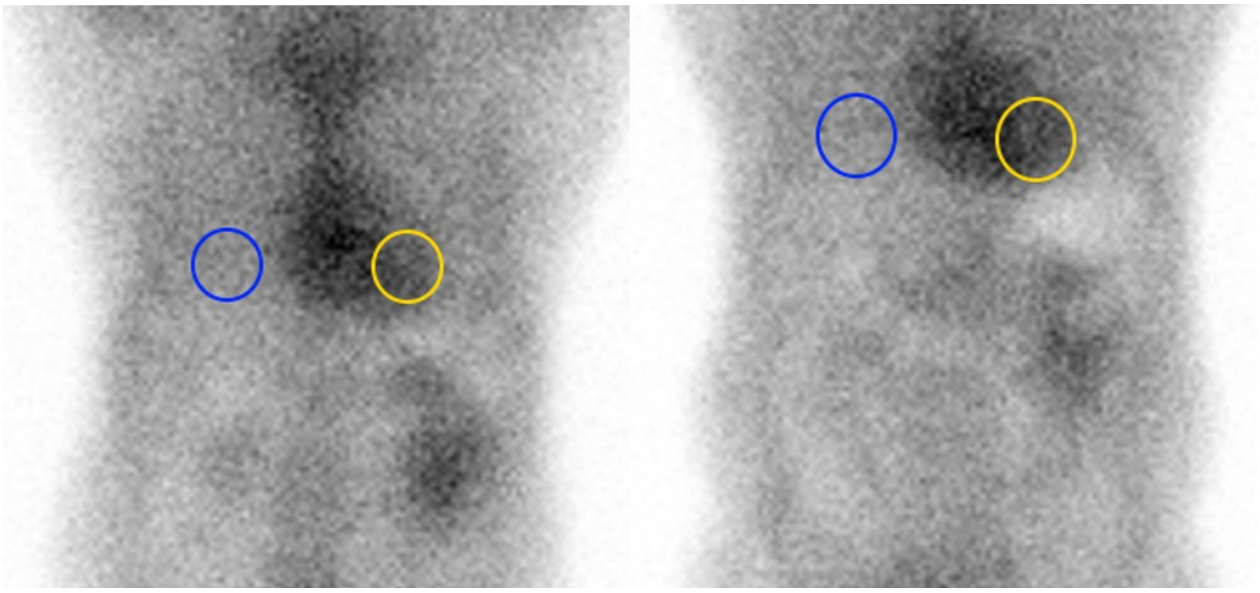

FIGURE 1. Cardiac PYP scan with anterior planar images 1 hour (left) and 3 hours (right) post-injection showed a region of diffuse tracer uptake in the heart (yellow circle). Tracer activity to denote rib contour is nearly absent. The contralateral lung region was also determined (blue circle) to compute for the H:CL ratio. Physiologic activity is noted in the kidneys with a relatively small right kidney .

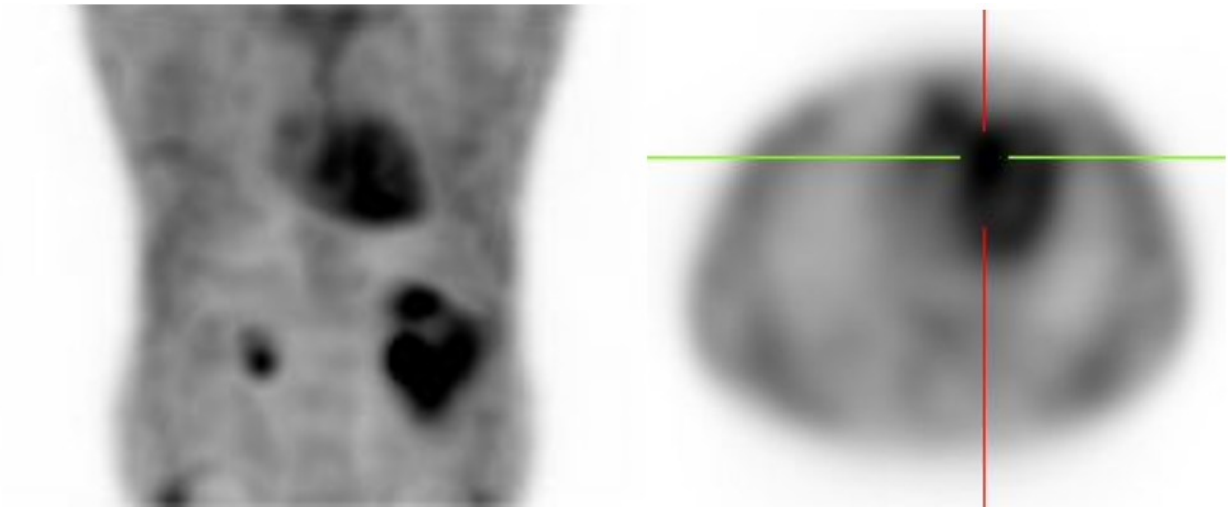

FIGURE 2 Complementary SPECT imaging of the cardiac PYP scan at 1 hour post-injection (left) with selected axial slice (right) at the level of the myocardium (red and green partial cross). This allowed better localization of tracer activity in the visualized thorax when correlated with the planar images

TABLE 1. Summary of multiple cardiac imaging modalities for the diagnosis of cardiac amyloidosis

	Echocardiography	Cardiac Magnetic Resonance	Positron emission tomography with F-18 Florbetapir or Florbetaben	Technetium-99m labelled bone scan* with PYP, DPD, or HMDP
Typical imaging features of cardiac amyloidosis	LV wall thickness > 12 mm Relative apical sparing of global longitudinal strain ratio ≥ Grade 2 diastolic dysfunction	LV wall thickness > upper limit of normal for sex on steady-state free precession cine view Global extracellular volume > 0.40 Diffuse late gadolinium enhancement Abnormal gadolinium kinetics typical for amyloidosis, myocardial nulling prior to blood pool nulling	Target to back-ground (LV myocardium to blood pool) ratio > 1.5 Retention index > 0.030 per minute	Grade 2 or 3 myocardial uptake of radiotracer Heart-to-contralateral lung ratio of ≥ 1.5 on 1-hour images, or ≥ 1.3 on 3-hour images

*Findings in bone scintigraphy are suggestive of the transthyretin type of cardiac amyloidosis

LV = left ventricular; PYP = pyrophosphate; DPD = diphosphonopropanodicarboxylic acid; HMDP = hydroxymethylene disphosphonate

ATTR contains relatively higher calcium content, making it more avid for bone seeking tracers [7]. In a retrospective study by Gilmore et al. (2016) that evaluated 1217 patients with suspected cardiac amyloidosis, it was shown that bone scintigraphy was 99% sensitive and 86% specific for cardiac ATTR, with false positives almost exclusively due to cardiac AL. More importantly, the combined findings of negative biomarkers for monoclonal proteins and scintigraphic features of increased myocardial tracer uptake compared to adjacent bone showed a specificity and positive predictive value for cardiac ATTR amyloidosis of 100% [8]. Thus in the appropriate clinical context, cardiac scintigraphy with bone seeking radiotracers is highly reliable in distinguishing ATTR from AL. In addition, advantages of scintigraphy include its non-invasive nature and evaluation for systemic or extracardiac involvement of amyloidosis.

To standardize and improve the evaluation of cardiac amyloidosis, a diagnostic algorithm was developed by the American Society of Nuclear Cardiology in joint consensus with other specialty societies. They recommend clinical diagnosis of ATTR cardiac amyloidosis when all of the following criteria are met: a Tc-99m PYP, DPD, or HMDP scan showing Grade 2 or 3 myocardial tracer uptake, with negative serum free light chain assay, and presence of typical cardiac imaging features in echocardiography, cardiac MR, or positron emission tomography [6, 7]. The grading of cardiac tracer uptake is based on the semiquantitative method developed by Perugini et al: Grade 0 shows no cardiac uptake and normal rib uptake, Grade 1 refers to cardiac uptake less than rib uptake, Grade 2 is cardiac uptake with intensity similar to the ribs, and Grade 3 corresponds to cardiac uptake greater than rib uptake, with mild or absent rib activity [9]. As an adjunct to interpretation, quantitative assessment with H:CL ratios can be helpful. An H:CL ratio of ≥1.5 at 1-hour imaging or ≥ 1.3 at 3-hour imaging can indicate ATTR cardiac amyloidosis. However, this can be a source of false positive when only 1-hour imaging is performed. This may present as slow radiotracer clearance from the blood pool and LV cavity, usually seen in patients with low cardiac output [10]. Other sources for false positives may be due to myocardial infarction, rib fracture near the area of the heart, or hydroxychloroquine toxicity [11]. It is thus recommended to acquire complementary SPECT for better localization. Acquiring both early and delayed imaging may also increase confidence in interpreting tracer kinetics .

In conclusion, recognition of appropriate clinical context is necessary for a timely diagnosis of cardiac amyloidosis. In the presence of typical cardiac MR findings and negative biomarkers for the AL type, a positive cardiac PYP scan can reliably confirm the diagnosis of ATTR cardiac amyloidosis. This is especially beneficial in cases where a conservative approach to management is preferred, as invasive endomyocardial biopsy is no longer needed to establish the diagnosis

DECLARATIONS

The authors declare there are no conflicts of interest, financial or otherwise.

Patient Consent

The authors obtained informed consent for chart review and case reporting from the patient. The study was done in compliance with the national Data Privacy Act of 2012.

ACKNOWLEDGEMENT

The authors acknowledge the following sections of The Medical City for their support: Cardiovascular Institute, Department of Radiology, and Department of Nuclear Medicine.

REFERENCES

1. Kittleson, M. M., Maurer, M. S., Ambardekar, A. V., Bullock -Palmer, R. P., Chang, P. P., Eisen, H. J., Nair, A. P., Nativi-Nicolau, J., Ruberg, F. L., & American Heart Association Heart Failure and Transplantation Committee of the Council on Clinical Cardiology (2020). Cardiac Amyloidosis: Evolving Diagnosis and Management: A Scientific Statement From the American Heart Association. Circulation, 142(1), e7–e22. https://doi.org/10.1161/CIR.0000000000000792.
2. Alexander, K. M., Orav, J., Singh, A., Jacob, S. A., Menon, A., Padera, R. F., Kijewski, M. F., Liao, R., Di Carli, M. F., Laubach, J. P., Falk, R. H., & Dorbala, S. (2018). Geographic Disparities in Reported US Amyloidosis Mortality From 1979 to 2015: Potential Underdetection of Cardiac Amyloidosis. JAMA cardiology, 3(9), 865–870. https://doi.org/10.1001/jamacardio.2018.2093.
3. Lin, W., Chattranukulchai, P., Lee, A. P., Lin, Y. H., Yu, W. C., Liew, H. B., & Oomman, A. (2022). Clinical recommendations to diagnose and monitor patients with transthyretin amyloid cardiomyopathy in Asia. Clinical cardiology, 45(9), 898–907. https://doi.org/10.1002/clc.23882.
4. Takashio, S., Tokitsu, T., Matsukawa, M., Sakaino, N., Fujimoto, K., Sakamoto, T., Noda, K., Tsunoda, R., Misumi, I., Hirai, N., Doi, H., Koide, S., Mizuno, Y., Hirose, T., Kurokawa, H., Kajiwara, I., Ohba, K., Miyamoto, S., Araki, S., Yamamoto, E., … Kumamoto Cardiac Amyloid Survey Investigators (2022). Incidence, clinical characteristics, and diagnostic approach in transthyretin amyloid cardiomyopathy: The Kumamoto Cardiac Amyloidosis Survey. Journal of cardiology, 80(1), 49–55. https://doi.org/10.1016/j.jjcc.2022.01.002.
5. Kavita, A., Abdul Onny, M. A., Suppiah, S., Abdul Aziz, A. F., Hashim, H., Raja Shariff, R. E., & Ng, C. S. (2021). A challenging road to diagnosing transthyretin cardiac amyloidosis and using technetium-99m pyrophosphate bone scintigraphy in nuclear cardiology - A case report. The Medical journal of Malaysia, 76(5), 762–767.
6. Dorbala, S., Ando, Y., Bokhari, S., Dispenzieri, A., Falk, R. H., Ferrari, V. A., Fontana, M., Gheysens, O., Gillmore, J. D., Glaudemans, A. W. J. M., Hanna, M. A., Hazenberg, B. P. C., Kristen, A. V., Kwong, R. Y., Maurer, M. S., Merlini, G., Miller, E. J., Moon, J. C., Murthy, V. L., Quarta, C. C., … Bourque, J. M. (2020). ASNC/AHA/ASE/EANM/HFSA/ISA/SCMR/SNMMI expert consensus recommendations for multimodality imaging in cardiac amyloidosis: Part 2 of 2-Diagnostic criteria and appropriate utilization. Journal of nuclear cardiology : official publication of the American Society of Nuclear Cardiology, 27(2), 659–673. https://doi.org/10.1007/s12350-019-01761-5.
7. Dorbala, S., Ando, Y., Bokhari, S., Dispenzieri, A., Falk, R. H., Ferrari, V. A., Fontana, M., Gheysens, O., Gillmore, J. D., Glaudemans, A. W. J. M., Hanna, M. A., Hazenberg, B. P. C., Kristen, A. V., Kwong, R. Y., Maurer, M. S., Merlini, G., Miller, E. J., Moon, J. C., Murthy, V. L., Quarta, C. C., … Bourque, J. M. (2019). ASNC/AHA/ASE/EANM/HFSA/ISA/SCMR/SNMMI expert consensus recommendations for multimodality imaging in cardiac amyloidosis: Part 1 of 2-evidence base and standardized methods of imaging. Journal of nuclear cardiology : official publication of the American Society of Nuclear Cardiology, 26(6), 2065–2123. https://doi.org/10.1007/s12350-019-01760-6.
8. Gillmore, J. D., Maurer, M. S., Falk, R. H., Merlini, G., Damy, T., Dispenzieri, A., Wechalekar, A. D., Berk, J. L., Quarta, C. C., Grogan, M., Lachmann, H. J., Bokhari, S., Castano, A., Dorbala, S., Johnson, G. B., Glaudemans, A. W., Rezk, T., Fontana, M., Palladini, G., Milani, P., … Hawkins, P. N. (2016). Nonbiopsy Diagnosis of Cardiac Transthyretin Amyloidosis. Circulation, 133(24), 2404 – 2412. https://doi.org/10.1161/CIRCULATIONAHA.116.021612.
9. Perugini, E., Guidalotti, P. L., Salvi, F., Cooke, R. M., Pettinato, C., Riva, L., Leone, O., Farsad, M., Ciliberti, P., Bacchi-Reggiani, L., Fallani, F., Branzi, A., & Rapezzi, C. (2005). Noninvasive etiologic diagnosis of cardiac amyloidosis using 99mTc-3,3-diphosphono-1,2-propanodicarboxylic acid scintigraphy. Journal of the American College of Cardiology, 46(6), 1076–1084. https://doi.org/10.1016/j.jacc.2005.05.073.
10. Zhu, Y., Pan, R., Peng, D., Dong, Q., & Zhu, X. (2022). Pitfalls of the Semi-Quantitative Analyzing 99mTc-Pyrophosphate Planar Images for Diagnosing Transthyretin Cardiac Amyloidosis: A Possible Solution. Diagnostics (Basel, Switzerland), 12(1), 94. https://doi.org/10.3390/diagnostics12010094.
11. Gerber, J., & Miller, E. J. (2021). Optimal interpretation of Tc99m PYP in 2020: Avoiding the million-dollar mistake. Journal of nuclear cardiology : official publication of the American Society of Nuclear Cardiology, 28(2), 503–506. https://doi.org/10.1007/s12350-020-02503-8.

KHealth
BRING GOOD THINGS TO LIFE

Careview
BRING GOOD THINGS TO LIFE

Taking the Lead in PET/CT Imaging and Innovative Radiopharmaceuticals

PRODUCTS OF KHEALTH:

- [18F]-FDG
- [18F]-FBB
- [18F]-FPSMA
- [177LU]-LUPSMA

CAREVIEW MANAGED CENTERS:

National Kidney and Transplant Institute
East Ave., Diliman Quezon City

CENTURIA PET/CT CENTER
G/F Centuria Medical Makati, Kalayaan Ave., Cpr. Salamanca, Makati City

AUF MEDICAL CENTER
McArthur Highway, Barangay Salapungan, Angeles City, 2009

Careview PET/CT Center Manila
850 United Nations Ave, Paco, Manila

MARY MEDIATRIX MEDICAL CENTER
THE HUB OF HEALTHCARE EXPERTS
J.P. Laurel Highway, Lipa City Batangas

Careview Cancer Center BGC
31st Street Cor. Second Ave., Crescent Park West, Bonifacio Global City

Philippine General Hospital
Taft Ave, Ermita, Manila

Careview PET/CT Center Valenzuela
Unit 111b-d, McArthur Highway, Brgy Karuhatan, Valenzuela City

SCAN THE QR CODE
(For us to call you)

LET US HELP YOU SECURE YOUR SCHEDULE

RESERVATION HOTLINE NOS | 7777-4080
+63 9176805371

PARTNER WITH US: info@khealthcorp.com | admin@careviewcorp.com

Two in One: A Rare Case of Two Horseshoe Kidneys Identified in an Ischiopagus Tripus Conjoined Twins using [^{99m}Tc] Tc-DMSA Scintigraphy

Leo D. Milay, MD, Arnel E. Pauco, MD

Radioisotope Laboratory, Division of Nuclear Medicine, University of the Philippines - Philippine General Hospital
E-mail address: leo.milay@gmail.com; arnelpauco@gmail.com

ABSTRACT

Ischiopagus tripus conjoined twins is an extremely rare condition presenting with multiple congenital anomalies. To date, there has been no such documented case that underwent ^{99m}Tc-dimercaptosuccinic acid ([^{99m}Tc] Tc-DMSA) scintigraphy for the evaluation of renal parenchymal function. We report the first case of an ischiopagus tripus conjoined twins with two horseshoe kidneys assessed using [^{99m}Tc] Tc-DMSA. Using the planar geometric analysis and volumetric counting via SPECT/CT, split renal functions (SRFs) were determined to be within normal limits. These findings were corroborated by contrast-enhanced computed tomography (CT) and magnetic resonance imaging (MRI) which demonstrated unremarkable enhancement pattern on all phases and with intact parenchymal thickness in both horseshoe kidneys. This study highlights the usefulness of [^{99m}Tc] Tc-DMSA scan in assessing baseline renal parenchymal function in such complex case of conjoined twins prior the planned separation.

***Keywords**: Ischiopagus tripus, conjoined twins, horseshoe kidney, DMSA scintigraphy, SPECT/CT*

INTRODUCTION

Conjoined twins represent one of the rarest congenital anomalies occurring with a varying worldwide incidence of approximately 1:50,000-1:200,000 births. Ischiophagus conjoined twinning is even rarer representing only 6%-11% of all conjoined twins [1]. In this case report, we present the first documented case of ischiopagus tripus conjoined twins with multiple congenital anomalies (imperforate anus, fused liver, two horseshoe kidneys with single urinary bladder and urethra) that underwent renal cortical scintigraphy [^{99m}Tc] Tc-DMSA for the evaluation of renal parenchymal function as requested by the pediatric surgery department as part of the preoperative workup for the planned separation.

CASE SUMMARY

The conjoined twins, fused at the pelvis with three appendages, were born preterm (36 weeks) to a then 31-year-old Filipino primigravid via caesarian section (Figure 1). Prenatal ultrasound on the 2nd trimester of pregnancy detected twin gestation with multiple congenital anomalies. During the course of pregnancy, the mother was admitted several times due to threatened preterm labor, with an episode of urinary tract infection during the third trimester. No other prenatal maternal illnesses nor complications were noted. Upon delivery of the twins, both demonstrated good cry and activity. Ileostomy was performed on the first day of life for the management of a single imperforate anus and they were eventually admitted to a neonatal intensive care unit for 27 days. They were subsequently discharged well on room air and interim hospital stay revealed no further medical complications.

At one year and seven months old, the conjoined twins were referred to our institution for surgical planning prior to possible separation. CT urography and MRI revealed two horseshoe kidneys (one for each of the twin) fused in the inferior poles with fused urinary bladders. Additionally, they were also found to have fused liver parenchyma and single abdominal cavity with fused lower gastrointestinal tract. On the seventh day of admission, the patients had developed acute urinary tract infection and were treated with oral antibiotics.

To rule out pyelonephritis and scarring, in addition to determining baseline renal parenchymal function, [^{99m}Tc] Tc-DMSA scan was requested by the pediatric surgery service. The conjoined twins were sedated prior the procedure. Each twin was given 55.5 MBq (1.5 mCi) of [^{99m}Tc] Tc-DMSA. Planar images of the kidneys in the

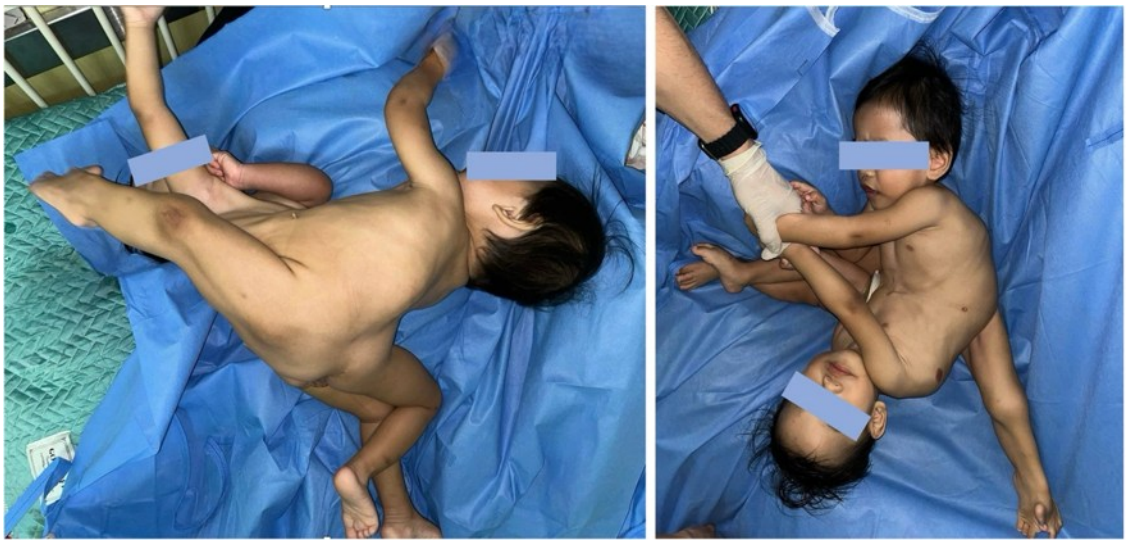

FIGURE 1 Ischiopagus tripus conjoined twins fused at the pelvis and with three appendages .

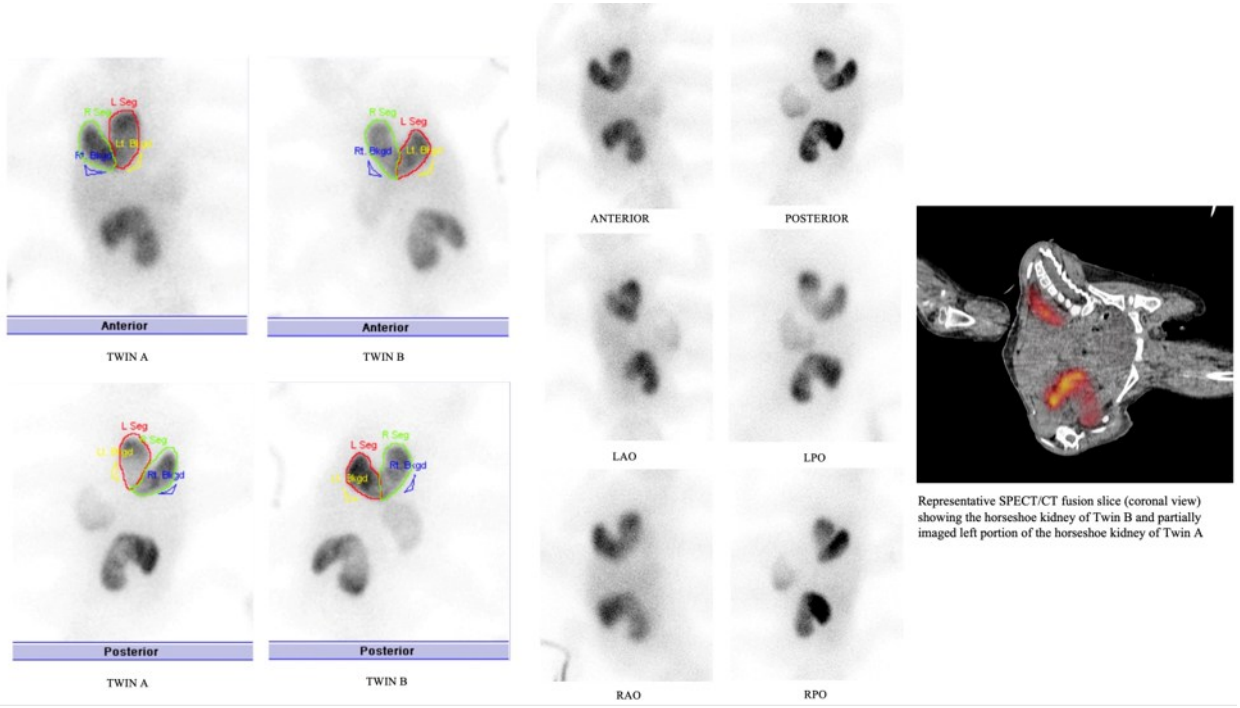

FIGURE 2 Planar images in anterior, posterior, and oblique views and representative SPECT/CT coronal view of the horseshoe kidneys obtained two hours after administration of [^{99m}Tc] Tc-DMSA .

anterior, anterior oblique, posterior, and posterior oblique views were obtained two hours after injection (Figure 2). Single photon emission computed tomography combined with computed tomography scan (SPECT/CT, Siemens Symbia T model) was also acquired thereafter. To determine the split renal function (SRF) of the left and right kidneys of each twin, regions of interests (ROIs) were drawn by visual approximation of the midline of each horseshoe kidney. Geometric mean analysis of the anterior and posterior counts was performed. Volumetric SPECT/CT quantification was also performed and results were compared with the planar method.

[^{99m}Tc] Tc-DMSA scintigraphy showed that the horseshoe kidneys demonstrated fairly homogeneous cortical tracer uptake seen in different planar projections. No definite scintigraphic evidence of parenchymal defect such as diffuse or sharp indentation in renal contour with thinning of cortex, loss of renal volume, or absent activity was observed in both planar and SPECT/CT images. Geometric analysis showed that for Twin A, SRF was 50.2% for the left kidney and 49.8% for the right kidney. For Twin B, SRF was 54.8% and 45.2% for the left and right kidneys, respectively. SRF values are within normal limits (45 to 55%) [2]. In terms of the total counts

SRF was also determined using volumetric counting via attenuation-corrected SPECT/CT images. Average voxel counts were used per regions of interests. For Twin A, SRF was 48.3% for the left kidney and 51.7% for the right kidney. For Twin B, SRF was 54.2% and 45.8% for the left and right kidney, respectively. In terms of the sum of average voxel counts for each whole horseshoe kidney, differential function was 48.0% and 52.0% for Twin A and Twin B, respectively; with Twin B's horseshoe kidney having consistently slightly higher counts, similar on the planar method.

MRI and CT urography done a month earlier also demonstrated that both kidneys were directed anterolaterally, being in different planes not parallel to the gamma camera detectors. Both had unremarkable enhancement pattern on all phases and with intact parenchymal thickness. No renal masses nor lithiasis was seen. These findings corroborated the normal findings observed in [^{99m}Tc] Tc-DMSA scan.

DISCUSSION

The incidence of horseshoe kidney is approximately 1:500 in the normal population with a male preponderance of 2:1 [3]. There is no clear published data regarding its incidence in conjoined twins. Moreover, the incidence of two horseshoe kidneys in conjoined twins is likewise undetermined. About a third of horseshoe kidneys are often asymptomatic with most cases identified incidentally. A number of complications can occur such as ureteric obstruction, impaired urinary drainage, hydronephrosis, vesicoureteric reflux, infection, and scarring due to the intrinsic anatomic defect [4].

Traditional imaging methods like X-rays and intravenous urograms, along with more sophisticated cross-sectional techniques such as ultrasound, CT, and MRI, are crucial in assessing horseshoe kidneys. Among these, contrast-enhanced CT is currently the preferred method for evaluating horseshoe kidneys and their positioning relative to nearby anatomical structures. It also plays an important role in the evaluation of potential complications and surgical planning [5]. Ultrasound may lack the sensitivity required to reliably detect renal parenchymal defects compared to [^{99m}Tc] Tc-DMSA scintigraphy when evaluating renal anomalies especially in pediatric population [6]. [^{99m}Tc] Tc-DMSA scan has also been shown to be the most reliable method in for evaluation of renal cortical scarring [7].

[^{99m}Tc] Tc-DMSA scan binds to the sulfhydryl groups in proximal tubules in the renal cortex having 40–65% of the administered activity present in the cortex 2 hours after injection with longer retention than other renal imaging radiopharmaceuticals. With this, it is considered as the gold standard imaging method to assess renal parenchymal defects (ex. hypoplasia, dysplasia, scars) and in determination of SRF [8]. Contrast-enhanced CT shows comparable sensitivity and specificity to [^{99m}Tc] Tc-DMSA scan in detecting acute pyelonephritis. However, CT involves higher exposure to ionizing radiation and carries risks of contrast reactions and contrast-induced nephropathy [9]. MRI, including diffusion-weighted MRI, is a promising approach for imaging pyelonephritis, offering the benefits of no ionizing radiation exposure and no requirement for iodinated contrast agents. However, it typically involves sedation or general anesthesia, particularly for younger children, coupled with a longer study period [10].

Utilizing [^{99m}Tc] Tc-DMSA scintigraphy, the two horseshoe kidneys of the conjoined twins were clearly delineated in the planar images. No definite scintigraphic evidence of cortical dysfunction was appreciated in both planar and SPECT images. Additionally, tracer accumulation seen in between the two horseshoe kidneys corresponded to the fused lobulated urinary bladder on CT. Normal differential functions of the left and right aspects of each horseshoe kidney were calculated for each twin using geometric mean analysis of the anterior and posterior planar images. Quantification of DMSA uptake using SPECT/CT yielded fairly similar results, with SRFs within normal limits.

Efforts have been made to measure DMSA uptake in the kidneys using both SPECT and planar images, but these approaches are not extensively adopted or documented, needing additional validation [2]. Some study suggests that differences in SRF determination between the two are clinically negligible [11]. Others note that around 25% of planar DMSA scintigraphies indicating an abnormal SRF in pediatric patients may appear normal when evaluated using SPECT/CT. This discrepancy likely arises from the inability of planar imaging to correct for attenuation, which can underestimate the function of the kidney with the poorest function when assessed by geometric mean (GM) and as such, planar scans indicating an abnormal SRF in pediatric patients should ideally be complemented with SPECT/CT [12].

CONCLUSION

Our study showed that [^{99m}Tc] Tc-DMSA scan remains a reliable method in ruling out of renal parenchymal abnormalities as corroborated by CT and MR imaging findings. This study likewise demonstrated its usefulness in clearly revealing the existence of two horseshoe kidneys in a conjoined twins and in the evaluation of its SRFs via both planar and SPECT methods, yielding fairly similar results providing pre-operative baseline renal function prior the planned separation. A follow-up study can be done in the future for comparison, or if the twins would be separated successfully.

In line with this, the utility of quantifying DMSA uptake in the kidneys using SPECT/CT in addition with planar images remains underexplored and necessitates additional validation, notably if abnormal SRF was determined in planar imaging.

DECLARATIONS

The authors declare no conflicts of interest, financial or otherwise.

REFERENCES

1. Mohammad, S. A., AbouZeid, A. A., Ahmed, K. A., Abd-Elhamed, A. M., & Rawash Eldieb, L. M. (2023). Postnatal imaging of conjoined twins: a customized multimodality approach. Pediatric radiology, 53(11), 2291–2304. https://doi.org/10.1007/s00247-023-05709-3.
2. Vali, R., Armstrong, I.S., Bar-Sever, Z. et al. (2022). SNMMI procedure standard/EANM practice guideline on pediatric [^{99m}Tc]Tc-DMSA renal cortical scintigraphy: an update. Clin Transl Imaging 10, 173–184. https://doi.org/10.1007/s40336-022-00484-x.
3. Schiappacasse, G., Aguirre, J., Soffia, P., Silva, C. S., & Zilleruelo, N. (2015). CT findings of the main pathological conditions associated with horseshoe kidneys. The British journal of radiology, 88(1045), 20140456. https://doi.org/10.1259/bjr.20140456.
4. Cascio, S., Sweeney, B., Granata, C., Piaggio, G., Jasonni, V., & Puri, P. (2002). Vesicoureteral reflux and ureteropelvic junction obstruction in children with horseshoe kidney: treatment and outcome. The Journal of urology, 167(6), 2566–2568.
5. Shah, H. U., & Ojili, V. (2017). Multimodality imaging spectrum of complications of horseshoe kidney. The Indian journal of radiology & imaging, 27(2), 133–140. https://doi.org/10.4103/ijri.IJRI_298_16.
6. Marceau-Grimard, M., Marion, A., Côté, C., Bolduc, S., Dumont, M., & Moore, K. (2017). Dimercaptosuccinic acid scintigraphy vs. ultrasound for renal parenchymal defects in children. Canadian Urological Association journal = Journal de l'Association des urologues du Canada, 11(8), 260–264. https://doi.org/10.5489/cuaj.4257.
7. Bhatnagar, V., Mitra, D. K., Agarwala, S., Kumar, R., Patel, C., Malhotra, A. K., & Gupta, A. K. (2002). The role of DMSA scans in evaluation of the correlation between urinary tract infection, vesicoureteric reflux, and renal scarring. Pediatric surgery international, 18(2-3), 128–134. https://doi.org/10.1007/s003830100680.
8. Mohamadien, N. R., Mohamed, M. S., Mekkaway, M. A., Ali, W. A., & Diab, W. A. (2023). 99mTc-DMSA renal cortical scanning: a comparison of planar, SPECT, and SPECT/CT imaging for the detection of renal cortical scarring. Egyptian Journal of Radiology and Nuclear Medicine, 54(1), 218. https://doi.org/10.1186/s43055-023-01156-0.
9. Craig, W. D., Wagner, B. J., & Travis, M. D. (2008). Pyelonephritis: radiologic-pathologic review. Radiographics: a review publication of the Radiological Society of North America, Inc, 28(1), 255–328. https://doi.org/10.1148/rg.281075171.
10. Sriman, R., Venkatesh, K., Mathew, C., Pankaj, M., & Shankar, R. (2020). Validity of diffusion-weighted magnetic resonance imaging in the evaluation of acute pyelonephritis in comparison with contrast-enhanced computed tomography. Polish journal of radiology, 85, e137–e143. https://doi.org/10.5114/pjr.2020.93669.
11. Cao, X., Xu, X., Grant, F. D., & Treves, S. T. (2016). Estimation of Split Renal Function With 99mTc-DMSA SPECT: Comparison Between 3D Volumetric Assessment and 2D Coronal Projection Imaging. AJR. American journal of roentgenology, 207(6), 1324–1328. https://doi.org/10.2214/AJR.16.16307.
12. Reichkendler, M. H., Berg, R. M. G., de Nijs, R., Nørgaard, H., Schmidt, I. M., & Borgwardt, L. (2020). Planar scan vs. SPECT/low-dose CT for estimating split renal function by 99mTc-DMSA scintigraphy in children. European journal of nuclear medicine and molecular imaging, 47(3), 729–733. https://doi.org/10.1007/s00259-019-04575-2.

FRAX Scores with and without Bone Mineral Density for Osteoporosis Treatment Decisions among Patients at Jose R. Reyes Memorial Medical Center

Louen Mark T. Visaya, MD

Department of Nuclear Medicine, Jose R. Reyes Memorial Medical Center
E-mail address: louenmarkvisaya@gmail.com

ABSTRACT

Objective:

To evaluate the concordance between Fracture Risk Assessment Tool (FRAX) scores calculated with and without bone mineral density (BMD) in predicting osteoporosis treatment needs among Filipino patients at Jose R. Reyes Memorial Medical Center, and to identify patient characteristics that influence this concordance.

Methodology:

A retrospective study of 1,566 patients aged 40-90 years who underwent DXA scan from 2020-2024 was conducted. Clinical risk factors were collected from medical records, and FRAX scores were calculated with and without femoral neck BMD. Treatment recommendations were based on a threshold of ≥3% for 10-year hip fracture probability. Concordance between FRAX scores with and without BMD was analyzed across various demographic and clinical characteristics.

Results:

The overall concordance rate between FRAX scores with and without BMD was 87% (1,362/1,566). FRAX with BMD suggested treatment for 12.3% (n = 192) of patients, while FRAX without BMD suggested treatment for 6.1% (n = 96). Significant factors associated with discordance included female sex (14.3% vs 3.2% in males, p<0.001), advanced age (31.8% discordance in ≥80 years), lower BMI (33.3% discordance in underweight), and osteoporosis status (32.7% discordance). The highest discordance was observed in patients with FRAX scores in the 4-5.9% range (66.7% discordance). Among discordant cases, 76.5% (n = 156) were instances where FRAX with BMD suggested treatment while FRAX without BMD did not.

Conclusion:

While FRAX without BMD demonstrates good overall concordance with FRAX with BMD, significant discordance exists in specific patient subgroups. BMD testing should be prioritized for women over 60 years, patients ≥80 years old, those with low BMI, and individuals with intermediate FRAX scores without BMD (2-5.9%). This strategic approach to BMD testing can optimize resource allocation while ensuring comprehensive fracture risk assessment for high-risk patients in resource-limited settings.

Keywords*: FRAX score, bone mineral density, osteoporosis, treatment decisions, concordance, Filipino population, fracture risk assessment*

INTRODUCTION

Osteoporosis is a significant health concern worldwide, characterized by low bone mass and structural deterioration of bone tissue [1,2]. The most critical clinical outcome of osteoporosis is the occurrence of insufficiency fractures, with common sites in the vertebra, distal forearm, and hips [1,2,3]. Thus, Fracture Risk Assessment Tool (FRAX) and bone mineral density (BMD) measurements are central to osteoporosis diagnosis and management [3,4,5].

BMD accounts for approximately 70% of bone strength and serves as a representative measure of bone mass [3]. A decline in BMD is directly associated with an increased risk of fractures. The measurement of BMD at the hip or spine is a strong indicator, comparable to the use of blood pressure and serum cholesterol in predicting cardiovascular disease [3].

Despite the utility of BMD measurements, a significant limitation was highlighted in the 1994 WHO report [1]. It stated that the majority of fragility fractures occur in individuals who do not meet the BMD criteria for osteoporosis, defined as a BMD of ≤ -2.5 standard deviations (SD) below the young normal mean [1]. This BMD threshold has high specificity for diagnosing osteoporosis; however, its sensitivity is relatively low, ranging from about 30 to 50% under most reasonable assumptions. This means that many individuals who sustain fractures have BMD values above the diagnostic threshold for osteoporosis, indicating a need for additional risk factors to be considered in fracture risk assessment [1].

While BMD is widely available and a proven predictor of fracture risk, other non-BMD factors such as age, previous fracture, falls, and certain medications also significantly contribute to fracture risk[1-6]. These factors are independent of BMD and, when combined, enhance the sensitivity of fracture risk assessments, improving the strategies for treatment intervention[1, 3 - 5]. The advent of the FRAX tool became instrumental in this regard as it integrates hip BMD and clinical risk factors to estimate a 10-year probability of major osteoporotic fracture (MOF) and hip fracture. It is particularly useful in identifying individuals at high risk of fracture, guiding clinical decisions for those with a T-score in the osteopenic range [1 - 5].

While incorporating BMD into FRAX calculations is the preferred method for fracture risk assessment, studies have shown that FRAX scores without BMD can still provide valuable insights into fracture risk[2,7-10]. This method leverages clinical risk factors to estimate fracture risk, although it may not capture the nuanced risk profiles that BMD provides.

Research from India suggests that FRAX-derived thresholds for osteoporosis treatment can be effectively applied without BMD and can be a pragmatic approach in resource-poor settings potentially reducing overtreatment and ensuring that treatment is accessible to those in need [6,7]. The Thai study by Teeratakulpisarn et al. found that while FRAX scores with and without BMD yielded concordant osteoporosis treatment recommendations in most cases, factors like older age, lower BMD, and borderline FRAX scores without BMD were associated with discordant results [8].

In the Philippine setting the recommended method for assessing fracture risk, among the at-risk population, is using FRAX with BMD however in settings where BMD measurement via DXA is unavailable or not feasible it is suggested that FRAX without BMD be used [3]. However no local data exploring the concordance of treatment decisions are available as of the writing of this study.

OBJECTIVE

General Objective

To evaluate the concordance between FRAX scores calculated with and without bone mineral density (BMD) in predicting the need for osteoporosis treatment among patients at Jose R. Reyes Memorial Medical Center.

Specific Objectives

- To determine the rate of concordance between treatment recommendations based on FRAX scores with and without BMD in the study population
- To identify patient characteristics and clinical factors that influence the concordance between FRAX with and without BMD assessments

METHODOLOGY

Medical records of patients at the Department of Nuclear Medicine of Jose R. Reyes Memorial Medical Center who underwent a DXA scan from 2020-2024 was retrospectively reviewed. Patients aged 40 to 90 years of age were included. Bone mineral density of the femoral neck and risk factors based from the FRAX tool including age, sex, body measurements (weight and height),

fracture history (both personal and parental hip fractures), lifestyle choices (smoking and alcohol consumption), medical conditions (rheumatoid arthritis and disorders strongly associated with secondary osteoporosis), medication use (glucocorticoids) were recorded.

Participants already receiving treatment for Osteoporosis were excluded from the study.

RESEARCH DESIGN

This paper employed a retrospective study design involving existing medical records of patients at the Department of Nuclear Medicine of the Jose R. Reyes Memorial Medical Center who underwent a DXA scan from 2020-2024.

SAMPLE SIZE COMPUTATION

At 95% confidence level and 0.05 margin of error, the minimum sample size needed to determine concordance rate between FRAX scores calculated with and without bone mineral density (BMD) in predicting the need for osteoporosis treatment is at least 209. The calculation is based on the resulting concordance rate of 83.78% from the results of the study of Teeratakulpisarn et. al. (2020).

$$n = \frac{Z^2 \times p \times (1-p)}{e^2} = \frac{1.96^2 \times 0.8378(1-0.8378)}{0.05^2} \approx 209$$

n = minimum sample size or minimum number of subjects
z = value from the standard normal distribution corresponding to desired confidence level (Z = 1.96 for 95% confidence level)
p = expected prevalence at 83.3%
e = desired precision 0.05

DATA COLLECTION

A review of records was done to collect demographic and clinical risk factors as well as data of Dual-energy X-ray absorptiometry (DXA) to measure the non-dominant hip BMD. Body Mass Index (BMI) was calculated as weight in kilograms divided by the square of height in meters (kg/m^2) and categorized using the Asia-Pacific Standard. All BMD measurements were obtained using the Hologic Horizon® DXA System. BMD T-scores were also extracted and categorized under normal (T-score ≥ -1), osteopenia (T-score < -1 but > -2.5), or osteoporosis (T-score ≤ -2.5). Calculation of FRAX scores with and without hip BMD was done using the FRAX tool adjusted to the Filipino population reference. FRAX results were then categorized as either concordant or discordant in reference to the recommended cutoff for medical treatment (10-year probability of hip fracture ≥ 3%).

DATA ANALYSIS

Descriptive statistics, such as mean and standard deviation, was used to present continuous data while frequency and percentage were used for categorical data. In comparing the two groups (concordance vs non concordance) or determining possible factors associated with concordance, t-test was used for continuous while chi square or fisher exact test was used for categorical data. Level of significance is set at 5%.

RESULTS

The study included a total of 1,566 patients, with a gender distribution heavily skewed towards women. Table I presents the demographic data of the study population. Results show that the significant majority were females (88.1%, n = 1380) compared to male (11.9%, n = 186). The mean age of participants was 66.7 ± 10.4 years, with males being older (72.1 ± 6.8 years) than females (65.9 ± 10.6 years).

Physical characteristics varied between genders, with males having higher mean weight (60.2 ± 12.3 kg vs 56.5 ± 12.0 kg), greater height (160.0 ± 6.2 cm vs 149.7 ± 6.6 cm), and lower BMI (23.6 ± 4.6 vs 25.2 ± 5.1) compared to females. The overall mean BMI was 25.0 ± 5.0. Bone mineral density (BMD) measurements were higher in males (0.66 ± 0.13 g/cm²) compared to females (0.59 ± 0.12 g/cm²). However, females had higher Hip Fracture FRAX scores both with BMD (1.60 ± 2.24 vs 0.85 ± 0.75) and without BMD (1.20 ± 1.18 vs 0.81 ± 0.56) compared to males.

FRAX with and without BMD resulted in a decision to treat in 192 (12.3%) and 96 participants (6.1%), respectively. Analysis of FRAX questionnaire responses revealed that 57.9% (n = 906) of the study population did not have any clinical risk factors. Figure 1 presents the distribution of each risk factor as reported in the questionnaire.

Among those reporting risk factors, secondary osteoporosis was the most prevalent (26.1%, n = 408), followed by smoking (5.7%), alcohol consumption (5.0%), parental history of hip fracture (3.8%), and personal history of fracture (3.4%). Less common risk factors included rheumatoid arthritis (1.5%) and glucocorticoid use (0.4%)

TABLE 1. Demographic data of the study population

	Total (n = 1566)	Male (n = 186)	Female (n = 1380)
Age (years)	66.7 ± 10.4	72.1 ± 6.8	65.9 ± 10.6
Body weight (kg)	57.0 ± 12.1	60.2 ± 12.3	56.5 ± 12.0
Height (cm)	150.9 ± 7.3	160.0 ± 6.2	149.7 ± 6.6
BMI (kg/m^2)	25.0 ± 5.0	23.6 ± 4.6	25.2 ± 5.1
Femoral neck BMD (g/cm^2)	0.60 ± 0.12	0.66 ± 0.13	0.59 ± 0.12
Femoral neck T-score	-2.14 ± 1.03	-1.66 ± 1.13	-2.20 ± 0.99
FRAX score of hip fracture			
Without BMD (%)	1.2 ± 1.1	0.8 ± 0.6	1.2 ± 1.2
With BMD (%)	1.5 ± 2.1	0.9 ± 0.8	1.6 ± 2.2
FRAX score suggesting treatment (≥ 3%)			
Without BMD, n (%)	96 (6.1)	0 (0)	96 (7.0)
With BMD, n (%)	192 (12.3)	6 (3.2)	186 (13.5)

Data are presented as mean ± standard deviation and proportions for continuous and categorical variables respectively.

BMI - body mass index; BMD - bone mineral density

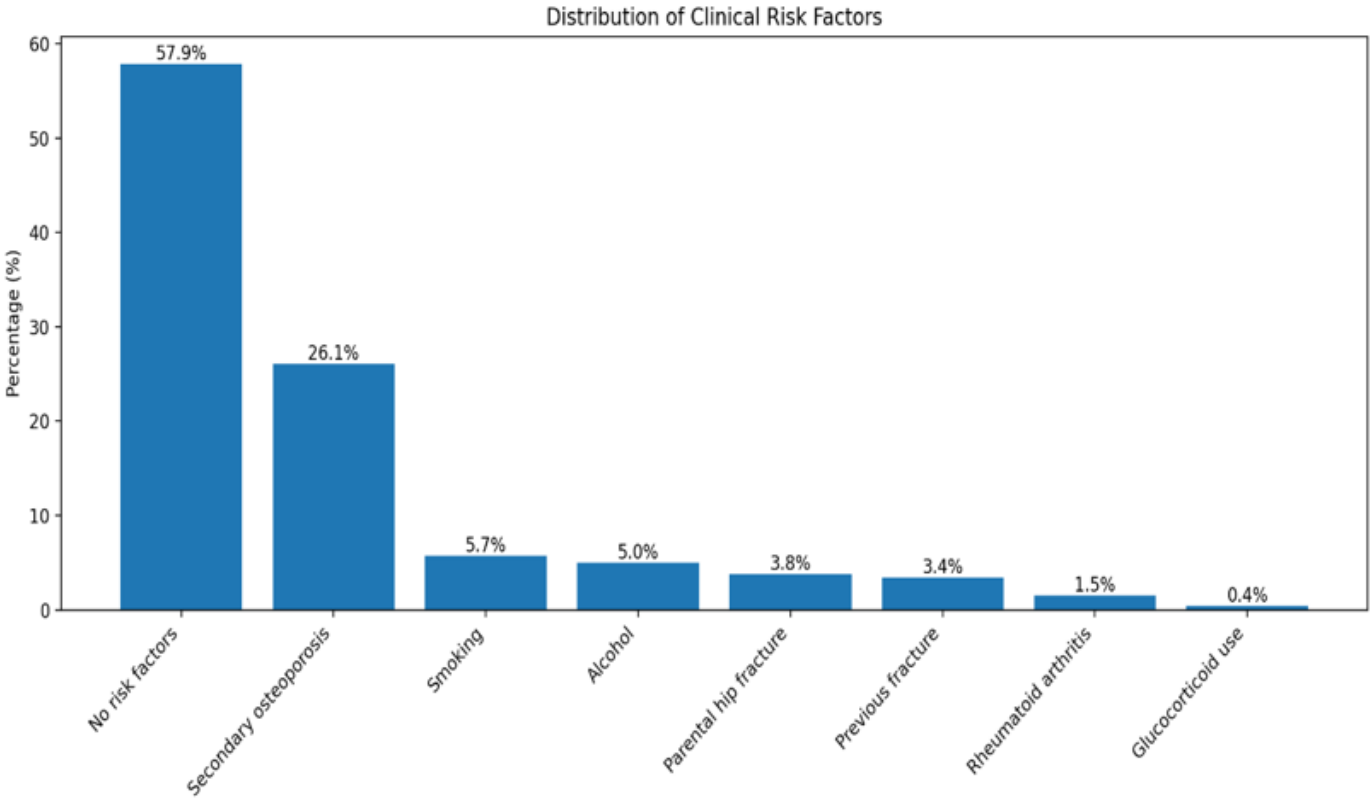

FIGURE 1 Distribution of each risk factor based on the FRAX questionnaire.

Table 2 presents the distribution of treatment recommendations across various demographic and clinical subgroups, including sex, age, BMI status, and BMD status.

Using a treatment threshold of ≥3% for 10-year hip fracture probability, FRAX with BMD suggested treatment for 12.3% (n = 192) of patients, while FRAX without BMD suggested treatment for 6.1% (n = 96) of patients. Gender differences were observed, with FRAX with BMD recommending treatment for 3.2% (n = 6) of males and 13.5% (n = 186) of females, while FRAX without BMD recommended treatment only for females (7.0%, n = 96).

Age-related trends were evident, with no treatment recommended for individuals under 50 years old by either method. The highest number of recommended treatments was in the 70-79 years age group for both FRAX with BMD (n = 108) and FRAX without BMD (n = 42).

BMI and BMD status also influenced treatment recommendations. FRAX with BMD recommended treatment across all BMI categories, while FRAX without BMD recommended treatment mostly for underweight patients (33.3%, n = 48). No treatments were recommended for patients with normal BMD status by either method. For individuals with osteoporosis, FRAX with BMD recommended more than twice the number of treatments compared to FRAX without BMD (180 vs 84 patients, respectively).

The overall concordance between FRAX with and without BMD was 87% (n = 1362), with discordance observed in 13% (n = 204) of cases. Factors significantly associated with discordance ($p < 0.001$) included female sex, older age, lower BMI, lower femoral neck BMD, and lower femoral neck T-score (Table 3). The concordance was highest for younger age groups, higher BMI categories, and normal to osteopenic BMD status. Discordance was most pronounced in the ≥ 80 years age group (31.8%), underweight BMI category (33.3%), and those with osteoporosis (32.7%).

FRAX scores without BMD showed a clear trend in discordance rates, with the highest discordance (66.7%) observed in the 4-5.9% probability range, while perfect concordance was seen for probabilities ≥ 6%. The characteristics of subjects with discordant results were analyzed. Table 4 presents a detailed breakdown of these discordant cases. Among the discordant cases, 76.5% (n = 156) were instances where FRAX with BMD suggested treatment while FRAX without BMD did not, and 23.5% (n = 48) were cases where FRAX without BMD suggested treatment while FRAX with BMD did not. These discordant cases showed significant differences in age, BMI, femoral neck BMD, and T-scores (all $p < 0.001$).

DISCUSSION

This study aimed to evaluate the concordance between FRAX scores calculated with and without bone mineral density (BMD) in predicting osteoporosis treatment needs among patients at Jose R. Reyes Memorial Medical Center. The findings revealed important insights into the use of FRAX scores and their implications for clinical practice, particularly highlighting scenarios where BMD measurements significantly enhance fracture risk assessment.

While the overall concordance rate between FRAX scores calculated with and without BMD was 87%, indicating substantial agreement between the two methods, similar to previous studies at around 74 - 87% [6-8, 10], the study's findings revealed clinical scenarios where BMD measurements provided essential additional information for treatment decisions. This suggests that while FRAX without BMD could serve as an initial screening tool, the integration of BMD measurements significantly improves the risk assessment accuracy in specific patient populations.

Sexual differences were observed in the concordance rates, with males showing higher concordance (96.8%) compared to females (85.7%). This disparity might be attributed to the generally higher BMD values observed in males in the study. The significant discordance in females (14.3%) indicates that relying solely on FRAX without BMD could potentially miss a substantial number of high-risk female patients. This gender difference in concordance rates aligns with previous studies that have reported variations in FRAX performance between males and females [11], suggesting that BMD testing may be particularly valuable for female patients, where FRAX scores without BMD may underestimate fracture risk.

Age emerged as a significant factor influencing concordance, with rates decreasing markedly to 68.2% for those 80 years and older. This striking decrease in concordance with age strongly suggests that BMD measurements become increasingly crucial for accurate risk assessment in older populations. Previous studies have also reported lower concordance in the older population [7, 8]. The integration of BMD data appears

TABLE 2. Treatment decisions using FRAX with and without BMD. Treatment threshold -

	FRAX with BMD		FRAX without BMD	
	Treatment	No treatment	Treatment	No treatment
All subjects (n = 1566)	192	1374	96	1470
Sex				
Male (n = 186)	6	180	0	186
Female (n =1380)	186	1194	96	1284
Age group				
<50 years (n = 126)	0	126	0	126
50-59 years (n = 216)	6	210	0	216
60-69 years (n = 558)	60	498	12	576
70-79 years (n = 534)	108	426	42	492
≥80 years (n = 132)	18	114	42	90
BMI status				
Underweight (n = 144)	42	102	48	96
Normal (n = 366)	66	300	36	330
Overweight (n = 306)	30	276	0	306
Obese (n = 750)	54	696	12	738
BMD status				
Normal (n = 234)	0	234	0	234
Osteopenia (n = 708)	12	696	12	696
Osteoporosis (n = 624)	180	444	84	540

particularly valuable in older adults where factors beyond clinical risk factors significantly influence fracture risk. For patients ≥ 80 years, the nearly 32% discordance rate when BMD is excluded suggests that relying solely on FRAX without BMD could lead to significant underestimation of fracture risk in this vulnerable population. This finding underscores the complexity of fracture risk assessment in older adults, where factors beyond BMD, such as fall risk and frailty, play crucial roles [12].

Body Mass Index (BMI) significantly affected concordance rates, with higher concordance observed in overweight (90.2%) and obese (94.4%) participants compared to those who are underweight (66.7%) or with normal BMI (77.1%). The substantial discordance in underweight patients (33.3%) strongly indicates that BMD measurements are essential for accurate risk assessment in this group. This trend is consistent with other studies showing greater concordance in those with above-normal BMI [6, 7, 13]. The impact of BMD inclusion appears most critical in patients with lower BMI, suggesting that these patients should be prioritized for BMD testing.

Perhaps the most striking findings emerged in the analysis of BMD status and FRAX probability ranges. While perfect concordance was observed for individuals with normal BMD and those with osteopenia, the concordance rate dropped significantly to 67.3% for individuals with osteoporosis. Of the 624 participants with osteoporosis, 180 (28.8%) would have been

TABLE 3. Factors affecting concordance between FRAX with and without BMD

	Concordant result (n = 1362)	Discordant result (n = 204)	p-value
All subjects	1362/1566 (87%)	204/1566 (13%)	
Sex			< 0.001
Male, n (%)	180 (96.8%)	6 (3.2%)	
Female, n (%)	1182 (85.7%)	198 (14.3%)	
Age (years)	65.6 ± 10.3	73.7 ± 7.8	< 0.001
Age group			< 0.001
< 50 years, n (%)	126 (100%)	0 (0%)	
50-59 years, n (%)	210 (97.2%)	6 (2.8%)	
60-69 vears, n (%)	498 (89.3%)	60 (10.7%)	
70-79 years, n (%)	438 (82%)	96 (18%)	
≥ 80 vears, n (%)	90 (68.2%)	42 (31.8%)	
BMI (kg/m^2)	25.5 ± 5.0	21.9 ± 4.4	< 0.001
BMI status (%)			< 0.001
Underweight, n (%)	96 (66.7%)	48 (33.3%)	
Normal BMI, n (%)	282 (77.1%)	84 (22.9%)	
Overweight, n (%)	276 (90.2%)	30 (9.8%)	
Obese, n (%)	708 (94.4%)	42 (5.6%)	
Femoral neck BMD (g/cm^2)	0.62 ± 0.11	0.45 ± 0.07	< 0.001
Femoral neck T-score	-1.9 ± 0.9	-3.5 ± 0.5	< 0.001
BMD status (%)			< 0.001
Normal BMD, n (%)	234 (100%)	0 (0%)	
Osteopenia, n (%)	708 (100%)	0 (0%)	
Osteoporosis, n (%)	420 (67.3%)	204 (32.7%)	
FRAX score of hip fracture without BMD	0.98 ± 1.04	2.25 ± 1.09	< 0.001
FRAX without BMD group, n (%)			< 0.001
< 2	1236 (93.2%)	90 (6.8%)	
2-3.9	102 (50%)	102 (50%)	
4-5.9	6 (33.3%)	12 (66.7%)	
6-7.9	12 (100%)	0 (0%)	
≥8	6 (100%)	0 (0%)	

Data are presented as mean ± standard deviation and proportions for continuous and categorical variables respectively. P-value < 0.05 was considered statistically significant. BMI - body mass index; BMD - bone mineral density

TABLE 4. Characteristics of subjects with discordant FRAX results.

Characteristics	Discordant FRAX result (n = 204)		p-value
	FRAX with BMD suggest treatment (n = 156)	FRAX without BMD suggest treatment (n = 48)	
All subjects (%)	156/204 (76.5)	48/204 (23.5)	
Sex (%)			0.37
Male	6 (3.8)	0 (0)	
Female	150 (96.2)	48 (100)	
Age (years)	72.1 ± 7.4	78.8 ± 6.8	< 0.001
Age group (%)			< 0.001
<50 years	0 (0)	0 (0)	
50-59 years	6 (3.8)	0 (0)	
60-69 years	54 (34.6)	6 (12.5)	
70-79 years	84 (53.8)	12 (25)	
≥80 years	12 (7.7)	30 (62.5)	
BMI (kg/m^2)	22.8 ± 4.5	18.8 ± 1.9	< 0.001
BMI status (%)			< 0.001
Underweight	24 (15.4)	24 (50)	
Normal	60 (38.5)	24 (50)	
Overweight	30 (19.2)	0 (0)	
Obese	42 (26.9)	0 (0)	
Femoral neck BMD (g/cm2)	0.43 ± 0.07	0.51 ± 0.04	< 0.001
Femoral Neck T-score	-3.64 ± 0.46	-2.86 ± 0.34	< 0.001
BMD status			
Normal	0	0	
Osteopenia	0	0	
Osteoporosis	156	48	

Data are presented as mean ± standard deviation and proportions for continuous and categorical variables respectively. P-value < 0.05 was considered statistically significant. BMI - body mass index; BMD - bone mineral density

recommended for treatment based on FRAX with BMD, but not by FRAX without BMD. This substantial discordance in the osteoporotic group demonstrates that FRAX without BMD may significantly underestimate fracture risk in those who need treatment most. Critical discordance patterns also emerged in specific FRAX probability ranges, with the highest discordance (66.7%) observed in the 4-5.9% range and significant discordance (50%) in the 2-3.9% range. These findings strongly suggest that BMD testing is essential for patients with intermediate FRAX scores, where treatment decisions are most likely to be influenced by BMD data.

Based on these findings, we propose a strategic approach to BMD testing, prioritizing female patients (particularly those over 60 years), patients ≥80 years of age, individuals with low or normal BMI, and patients with FRAX scores without BMD in the 2-5.9% range. While FRAX without BMD can serve as an initial screening tool, the study's findings strongly support the integration of BMD measurements for comprehensive fracture risk assessment. The significant discordance rates in specific patient populations demonstrate that relying solely on FRAX without BMD could potentially miss a substantial number of high-risk patients who would benefit from treatment. This is particularly critical in resource-limited settings, where strategic allocation of BMD testing resources could significantly improve the identification and management of high-risk patients.

These findings provide valuable insights into the use of FRAX scores with and without BMD in the Filipino population. By identifying factors that influence concordance rates and highlighting the crucial role of BMD measurements in specific patient groups, we can refine our approach to osteoporosis screening and management, particularly in resource-limited settings. This strategic approach ensures that BMD testing resources are allocated to those patients who would benefit most from the additional diagnostic information, ultimately improving the accuracy of fracture risk assessment and treatment decisions.

CONCLUSION

Comprehensive analysis of FRAX score calculations at Jose R. Reyes Memorial Medical Center revealed an 87% agreement between assessments made with and without BMD measurements, demonstrating substantial consistency in treatment recommendations across both methods. This finding suggests that FRAX without BMD can serve as a valuable initial screening tool for fracture risk assessment in our Filipino population, particularly in settings where BMD testing resources may be limited.

Through detailed examination of patient data, several critical patterns emerged that significantly influenced the alignment between these two assessment methods. Gender emerged as a key factor, with men showing notably higher consistency (96.8%) compared to women (85.7%) in treatment recommendations. Age played a crucial role, with marked differences appearing in elderly populations, particularly those 80 years and older where agreement dropped to 68.2%. Body composition also proved influential, as underweight (66.7%) and normal BMI (77.1%) individuals showed lower consistency compared to overweight (90.2%) and obese (94.4%) participants.

Most notably, analysis identified specific patient subgroups where BMD measurements provided crucial additional information for treatment decisions. Patients with confirmed osteoporosis showed a significant drop in concordance to 67.3%, while those with intermediate FRAX scores (2-5.9%) demonstrated the highest rates of divergence in treatment recommendations. These findings point to specific populations where BMD testing might be most valuable: women over 60 years, patients ≥80 years of age, individuals with low or normal BMI, and those with intermediate FRAX scores without BMD.

These insights support implementing a tiered approach to fracture risk assessment in clinical practice, particularly in resource-limited settings. While FRAX without BMD serves as an effective initial screening tool, strategic allocation of BMD testing to identified high-risk groups can optimize resource utilization while ensuring comprehensive care for those most likely to benefit from additional assessment. Future research should focus on validating these findings across diverse Filipino populations and evaluating the long-term clinical outcomes of this strategic approach to osteoporosis management.

LIMITATIONS OF THE STUDY

The study is specifically concerned with the concordance of FRAX scores at the time of DXA procedure. It does not intend to monitor or measure treatment decision outcomes following the initial assessment. The study is limited to patients at Jose R. Reyes Memorial Medical Center, which may not represent the entire Filipino population. As such, the findings may not be generalizable to other regions or ethnic groups within the Philippines. The FRAX tool itself has inherent limitations, as it may not capture all the nuanced risk profiles, especially when BMD is not included in the calculation. The reliance on record review for data collection may introduce bias if the records are incomplete or inaccurate.

DISCLOSURES

The author of this study has no conflicts of interest to disclose.

ETHICAL CONSIDERATIONS

The study was conducted with authorization and and permission secured from the Jose R. Reyes Memorial Medical Center Institutional Review Board (IRB). Adhering to the highest ethical standards ensured the protection of participants' rights and welfare throughout

the research process.

ACKNOWLEDGMENTS

This research paper would not have been possible if not for the contributions of certain individuals to which I am sincerely grateful. First and foremost, I thank the Almighty God for providing me the wisdom and strength to persevere through the challenges encountered along the way. I wish to express my deepest gratitude to Dr. Alyssa Granda for providing not only emotional but also technical support during difficulties. I could not have overcome the hurdles of this journey without her patience and encouragement. I also extend my sincere thanks to Dr. Ivan David, my training officer, for his invaluable guidance in helping me realize the research direction I felt most passionate about. To my parents, I am forever thankful for your unwavering support in all my endeavors. Finally, I dedicate this work to my patients, to whom I have committed my life in service.

REFERENCES

1. Kanis, J. A., Johansson, H., Harvey, N. C., & McCloskey, E. V. (2018). A brief history of FRAX. Archives of osteoporosis, 13(1), 118. https://doi.org/10.1007/s11657-018-0510-0.
2. Kanis, J. A., Harvey, N. C., Johansson, H., Odén, A., Leslie, W. D., & McCloskey, E. V. (2015). FRAX and fracture prediction without bone mineral density. Climacteric : the journal of the International Menopause Society, 18 Suppl 2, 2–9. https://doi.org/10.3109/13697137.2015.1092342.
3. Li-Yu, J., Sison-Aguilar, A., Tabu, I., Bautista, J., Co, E. V., Española, S. S., Fernandez, M. E., Gabat-Tan, J., Guison-Bautista, T., Lugue-Lizardo, L., Maglonzo, E. I., Martinez, E., Medina, D., Ngalob-Samonte, Q., Orillaza, N., Jr, Padua, M. R., Patricio, J., Ronquillo, J., Roxas-Panuda, M. C. A., Urbanozo-Corpuz, H., … Osteoporosis Clinical Practice Guideline Task Force (2025). Philippine Clinical Practice Guidelines on Screening, Diagnosis, Management and Prevention of Primary Osteoporosis and Fragility Fractures Among Postmenopausal Women and Older Men. Journal of the ASEAN Federation of Endocrine Societies, 40(2), 18–26. https://doi.org/10.15605/jafes.040.02.27.
4. Abu Dhabi Department of Health. (2019). DOH guideline on the screening for osteoporosis. https://www.doh.gov.ae/-/media/D9596EA3C6B749B8ABF61FBD1DD7EF15.ashx
5. Li-Yu, J., Perez, E. C., Cañete, A., Bonifacio, L., Llamado, L. Q., Martinez, R., Lanzon, A., Sison, M., Osteoporosis Society of Philippines Foundation, Inc. (OSPFI), & Philippine Orthopedic Association (POA) Clinical Practice Guidelines Task Force Committee on Osteoporosis (2011). Consensus statements on osteoporosis diagnosis, prevention, and management in the Philippines. International journal of rheumatic diseases, 14(3), 223–238. https://doi.org/10.1111/j.1756-185X.2011.01626.x.
6. Nagendra, L., Bhavani, N., Menon, V. U., Pavithran, P. V., Menon, A. S., Abraham, N., Nair, V., & Kumar, H. (2021). FRAX-based osteoporosis treatment guidelines for resource-poor settings in India. Archives of osteoporosis, 16(1), 69. https://doi.org/10.1007/s11657-021-00931-8.
7. Asirvatham, A. R., Balachandran, K., Kannan, S., Balasubramaniam, S. K., & Mahadevan, S. (2018). FRAX First - Pragmatic Approach in Resource Poor Settings. Indian journal of endocrinology and metabolism, 22(6), 757–759. https://doi.org/10.4103/ijem.IJEM_412_18.
8. Teeratakulpisarn, N., Charoensri, S., Theerakulpisut, D., & Pongchaiyakul, C. (2021). FRAX score with and without bone mineral density: a comparison and factors affecting the discordance in osteoporosis treatment in Thais. Archives of osteoporosis, 16(1), 44. https://doi.org/10.1007/s11657-021-00911-y.
9. Kanis, J. A., McCloskey, E., Johansson, H., Oden, A., & Leslie, W. D. (2012). FRAX(®) with and without bone mineral density. Calcified tissue international, 90(1), 1–13. https://doi.org/10.1007/s00223-011-9544-7.
10. Lujano Negrete, A. Y., Skinner Taylor, C. M., Pérez Barbosa, L., et al. (2022). Ab1034 fracture risk by frax with and without bone mineral density, comparison of factors affecting concordance. Annals of the Rheumatic Diseases, 81(Suppl 1), 1640.2-1640. https://doi.org/10.1136/annrheumdis-2022-eular.4913.
11. Kanis, J. A., Harvey, N. C., Cooper, C., Johansson, H., Odén, A., McCloskey, E. V., & Advisory Board of the National Osteoporosis Guideline Group (2016). A systematic review of intervention thresholds based on FRAX : A report prepared for the National Osteoporosis Guideline Group and the International Osteoporosis Foundation. Archives of osteoporosis, 11(1), 25. https://doi.org/10.1007/s11657-016-0278-z.
12. Masud, T., Binkley, N., Boonen, S., Hannan, M. T., & FRAX (®) Position Development Conference Members (2011). Official Positions for FRAX® clinical regarding falls and frailty: can falls and frailty be used in FRAX®? From Joint Official Positions Development Conference of the International Society for Clinical Densitometry and International Osteoporosis Foundation on FRAX®. Journal of clinical densitometry : the official journal of the International Society for Clinical Densitometry, 14(3), 194–204. https://doi.org/10.1016/j.jocd.2011.05.010.
13. De Laet, C., Kanis, J. A., Odén, A., Johanson, H., Johnell, O., Delmas, P., Eisman, J. A., Kroger, H., Fujiwara, S., Garnero, P., McCloskey, E. V., Mellstrom, D., Melton, L. J., 3rd, Meunier, P. J., Pols, H. A., Reeve, J., Silman, A., & Tenenhouse, A. (2005). Body mass index as a predictor of fracture risk: a meta-analysis. Osteoporosis international : a journal established as result of cooperation between the European Foundation for Osteoporosis and the National Osteoporosis Foundation of the USA, 16(11), 1330–1338. https://doi.org/10.1007/s00198-005-1863-y.

Pure Yolk Sac Tumor- Post Pubertal Type with Lung and Nodal Metastasis on ^{18}F-FDG PET/CT Scan in a 37-Year Old Male Filipino: A Case Report

Kenji O. Ip, MD

Nuclear Medicine Section and PET/CT Center, Cardinal Santos Medical Center
E-mail address: kenjiip93@gmail.com

ABSTRACT

^{18}F-Fluorodeoxyglucose (^{18}F-FDG) Positron Emission Tomography/ Computed Tomography (PET/CT) is an advanced multimodality imaging tool that has become part of standard of care in oncological practice providing various utilities. Pure yolk sac tumor-postpubertal type (PYSTPPT) is an extremely rare and aggressive malignancy. PYSTPPT is an extremely rare type of germ cell tumor with an aggressive nature with only about 36 documented cases, two of which document use of FDG PET/CT imaging. Here we present the first local documented case of a 37-year-old, Filipino, male patient who initially presented with an enlarging right testicle, difficulty breathing and intractable back pain. He was diagnosed with PYSTPPT with locoregional and distant nodal metastasis with pulmonary metastases. An FDG PET/CT scan was utilized for staging and treatment evaluation. The patient underwent radical orchiectomy and chemotherapy using Bleomycin, Etoposide, and Cisplatin, and is currently in complete remission 3 months post-chemotherapy. The use of molecular imaging modalities such PET/CT scans enable convenient whole-body imaging and thorough assessment in staging, evaluating treatment response and disease monitoring of malignancies, especially aggressive types such as PYSTPPT. It also helps provide additional information in documenting rare or unusual diseases.

***Keywords**: Testicular Germ Cell Tumor, yolk sac tumor, Fluorodeoxyglucose F18, Positron-Emission Tomography*

INTRODUCTION

Testicular cancers are rare malignancies that only compromise about 1% of adult neoplasms. Histologically it is subdivided into the germ cell tumors (GCTs) and non-germ cell tumors with the former being more common, about 80-95% of total cases. In 2016, WHO has further subdivided GTCs into germ cell neoplasia in-situ (GCNIS) related GCTs and non-GCNIS related tumors [1 - 3]. Yolk sac tumors (YST) are the most common type of GCTs in infants and children, often as pure tumors. Conversely, in postpubertal individuals, pure YSTs are exceeding rare malignancies, compromising < 1% of testicular GSTs [2, 4 - 5]. Due to the rarity of the condition, there have only been about less than 36 reported cases to date and possibly the first documented case in the Philippines [2, 5 - 6]. PET/CT scans are becoming the mainstay imaging modality of choice in oncology due to its high sensitivity, ability to differentiate benign and aggressive pathology and evaluation of treatment outcomes [7]. By documenting the patient's clinical, radiologic, laboratory workup, treatment course, and outcome, we aim to contribute to the limited body of literature on this rare entity.

CASE DESCRIPTION

A 37-year-old, Filipino, male patient, with no previous illnesses nor surgery, is non-smoker and non-alcoholic beverage drinker, exercises regularly, with familial history of breast and colonic cancer in the paternal side. The patient presented with progressively enlarging right testicle for 9 months, with on and off sharp pain, and soreness. He had no other associated complaints or symptoms. Patient eventually sought consult wherein ultrasound of the testicles showed that the right testis turned into a fairly defined, complex, predominantly isoechoic mass with interspersed cystic components. Thereafter, he was advised for surgical management, and preoperative malignancy work up was done: Computed tomography (CT) of the abdomen showed enlarged heterogeneously enhancing right testis, serum alfa fetal protein (AFP) >51, 700 ng/ml (at 1:1000 dilution) and beta-human chorionic gonadotropin (β-HCG) 37.47 mIU/ml. Subsequently, the patient underwent right radical orchiectomy and a 13 x 9 x 8.5 cm solid, cream tan, right testicular mass weighing 537.9 grams, was removed. Serial sections show tumor replacement of the entire testicular parenchyma with a solid to partially cystic grayish white to tan cut surface with focal hemorrhage and necrosis. The tumor abuts the epididymis and tunica

albuginea without perforation of the tunica vaginalis. Histologic sections show a tumor with stellate and spindled tumor cells focally arranged in ringlets with in a myxoid stroma. Tumor cells with varying amounts of clear to eosinophilic cytoplasm lining loose meshwork off anastomosing channels and various cyst containing mucoid are also seen. Tumor cells forming rounded to elongated popular structures with glomeruloid appearance are noted with evidence of no lymphovascular invasion. Histopathology reported as yolk sac tumor, post-pubertal type.

Approximately 1 month after the surgery, there was note of a sharp decline in AFP and β-HCG levels, 6,690 ng/ml and < 2.39 mIU/ml respectively. Chest CT scan was also done for metastatic work up which showed tiny non-calcified pulmonary nodules in the right lung. Subsequent AFP and β-HCG levels show further decline 816 ng/ml and < 2.39 mIU/ml, respectively.

Within 3 months post-orchiectomy, there was note of rise in serum AFP 1,470 ng/ml. Subsequently, 5 months post-orchiectomy, there was onset of back pain, radiating to the left flank. It was initially attributed to muscle strain from household work and the patient self-medicated with celecoxib which provided no relief of symptoms. The pain was progressive and worse at nighttime which resulted to difficulty of sleeping especially when flat on bed. This prompted several emergency room (ER) consultations where in x-rays, ultrasound and CT scan showed no underlying pathology. During one of the ER consultations, the patient was admitted and started on tramadol 50mg/IV every 8 hours and pregabalin 75mg/tablet every 12 hours which gave little to no relief. Magnetic resonance imaging (MRI) of the lumbosacral spine was then done showing posterior disc bulges and desiccation, C4-C5 and C5-C6 levels, causing ventral thecal sac indentation with no spinal cord compromise; these findings however do not explain the excessive back pain. Patient then underwent 18F-Fluorodeoxyglucose (18F-FDG) PET/CT scan which showed hypermetabolic cervical, mediastinal, retroperitoneal, and pelvic lymphadenopathies with lung metastases with a recommended staging of IIIC (pT1bN3M1a, S3) based on the American Joint Committee on Cancer (AJCC) guideline. Thereafter, the patient underwent 3 cycles of BEP chemotherapy (Bleomycin, Etoposide and Cisplatin) in a span of 2 months.

8-months post-orchiectomy, follow-up 18-F FDG PET/CT scan showed complete resolution of the cervical lymphadenopathies and pulmonary metastasis with metabolic resolution and gross regression of the mediastinal, retroperitoneal, and pelvic lymphadenopathies. There was also significant decrease in AFP and β HCG levels, 4.44 ng/ml and < 2.39 mIU/ml, respectively. The patient was in remission for approximately 3 months.

9-months post-orchiectomy, the patient developed persistent dry cough with associated chest pain. X-ray was done showing fluid build-up in the right lung. A thoracentesis was done and blood-like red-fluid was aspirated. An 18-F FDG PET/CT scan was done showing hypermetabolic right lung mass, bilateral lung nodules, right pleural lesions with loculated effusion, left retroperitoneal mass and thoracic and abdominopelvic lymphadenopathies. A video-assisted thoracoscopic surgery (VATS) was done to remove a large portion of the right lung mass. The patient is currently undergoing TIP chemotherapy (Paclitaxel, Ifosfamide, and Cisplatin).

DIAGNOSTIC ASSESSMENT

A whole body ^{18}F-FDG PET/CT scan was performed 5 months post-orchiectomy and prior to initiation of chemotherapy. The maximum intensity projection (MIP) view showed multiple hypermetabolic lesions in cervical, thoracic, and abdominal region (Figure 1). For the cervical region, the scan revealed a non-enhancing mass in the left cervical area measuring 4.0 x 2.7 x 2.5 cm (CCxTxAP) with a maximum Standardized Uptake Value (SUVmax) of 12.3 on PET (Figure 2) with another similar lesion noted posterior to the left clavicle measuring 1.2 x 1.6 x 1.3 cm with SUVmax of 8.8 (Figure 3).

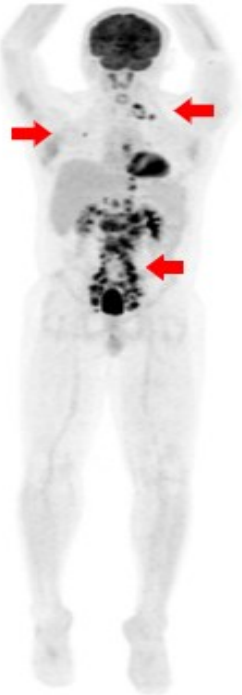

FIGURE 1 PET MIP image showing the multiple tracer uptake in the cervical, thoracic, and abdominal region (arrows)

TIMELINE

	Surgery Right orchiectomy			**Chemotherapy** Bleomycin, Etoposide and Cisplatin
January 2023 to September 2023	**September 2023 to October 2023**	**November 2023**	**December 2023 to January 2024**	**February 2024**
Symptom Palpable right testicular mass, progressively enlarging **Ultrasound** Complex right testicular mass wherein neoplasm was considered **Abdominal CT scan** Enlarged heterogeneously enhancing right testis **Tumor markers** Markedly elevated	**Histopathology** Yolk Sac Tumor, post pubertal type **Tumor markers** Sharp decline, still elevated	**Tumor markers** Further decline **Chest CT scan** Tiny non-calcified pulmonary nodules, right lung, inflammatory vs metastatic	**Symptom** Intractable back pain and difficulty in breathing **Tumor markers** Rising marker levels	**FDG PET/CT scan** Metastatic cervical, mediastinal, retroperitoneal, and pelvic lymphadenopathies, pulmonary metastases

		Surgery VATS, right **Chemotherapy** Paclitaxel, Ifosfamide, and Cisplatin
May 2024	**August 2024**	**September 2024**
FDG PET/CT scan Complete resolution of the metastatic cervical, lymphadenopathies and pulmonary metastases, metabolic resolution with gross regression of the metastatic mediastinal, retroperitoneal, and pelvic lymphadenopathies	**Symptom** Dry cough with associated chest pain **FDG PET/CT scan** Hypermetabolic findings are worrisome for recurrent metastatic disease: Thoracic and abdominopelvic lymphadenopathy Pleural lesions with loculated effusion in the right Bilateral lung nodules and right lung mass-like consolidation Left retroperitoneal mass, may be peritoneal or nodal in nature	

In the thoracic region, there were multiple FDG-avid varisized nodules scattered in both lungs, the largest is in the right upper lobe measuring 1.1 x 1.0 x 0.8 cm with SUVmax up to 6.6 (Figure 4). There were multiple enlarged mediastinal lymph nodes that extends into the retrocrural space, the largest measuring 1.8cm in short axis with SUVmax up to 15.0 (Figure 5).

In the abdominal region, the right testis was surgically absent with no undue FDG activity in the region. However, there were multiple FDG-avid enlarged lymph nodes in the retroperitoneal and pelvic regions. The largest in the left internal iliac chain measuring 2.7 cm in its short axis diameter. The retroperitoneal lymph nodes appeared to be encasing the abdominal aorta, renal arteries, inferior vena cava, bilateral common and internal iliac arteries, causing the anterior displacement of the pancreas and third segment of the duodenum (Figure 6).

THERAPEUTIC INTERVENTION

The patient was started on chemotherapy consisting of Bleomycin, Etoposide and Cisplatin. A total of 3 cycles were completed and a follow-up whole-body PET/CT scan was done after 1 month for restaging and evaluation of treatment response. In the follow-up PET/CT scan, it showed complete resolution of the non-enhancing, FDG-avid lesions in the left cervical area (Figure 7).

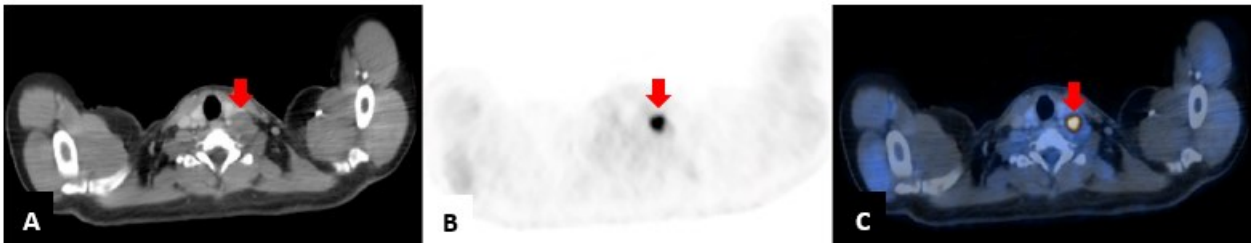

FIGURE 2 Axial view of the cervical region showing the (A) CT, (B) PET, and (C) Fused PET/CT images of the patient's initial whole-body PET/CT scan of the larger non-enhancing mass in the left cervical area (red arrows).

FIGURE 3 Axial view of the cervical showing the (A) CT, (B) PET, and (C) fused PET/CT images of the patient's initial whole-body PET/CT scan of the similar non-enhancing lesion posterior to the left clavicle (red arrows).

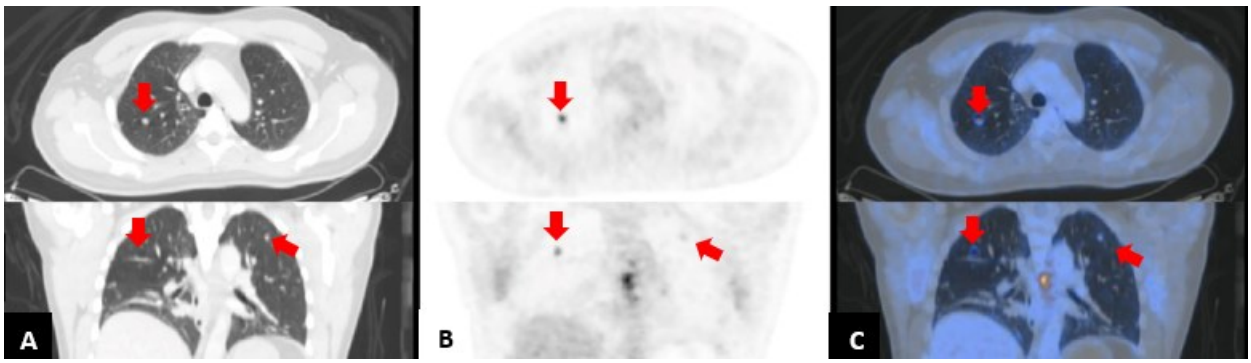

FIGURE 4 Axial and coronal view showing the (A) CT, (B) PET, and (C) fused PET/CT images of the patient's initial whole-body PET/CT scan with emphasis on the pulmonary nodules (red arrows) .

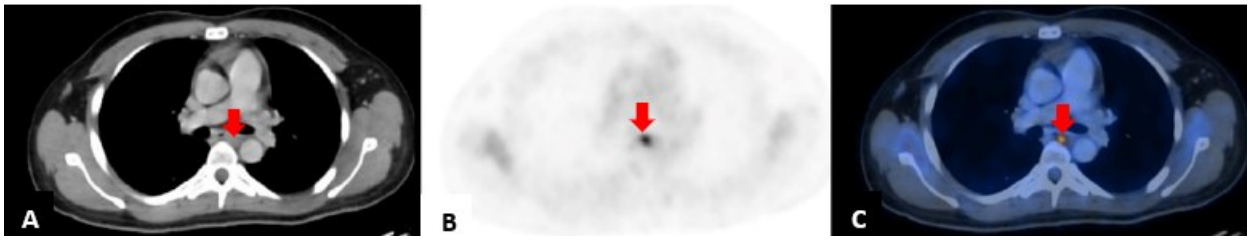

FIGURE 5 Axial view showing the (A) CT, (B) PET, and (C) fused PET/CT images of the patient's initial PET/CT scan showing the enlarged mediastinal lymph nodes that extends into the retrocrural space (red arrows) .

In the thoracic region, there was complete resolution of the multiple non-calcified, FDG-avid, varisized nodules in both lungs. (Figure 8). The previous multiple enlarged mediastinal lymph nodes extending into the retrocrural space are no longer FDG-avid and showed significant decrease in size and number, with few remaining unenlarged retrocrural lymph nodes, measuring up to 0.4 cm (Figure 9).

The surgical site remained unremarkable. The multiple enlarged lymph nodes in the retroperitoneal and pelvic regions were no longer FDG-avid and showed significant regression in number and sizes (Figure 10). The largest lymph node was in the aorto-caval region at L2 vertebral level, measuring 1.9 cm (previously 2.7 cm in the left internal iliac region). There was lesser degree of encasement of the inferior vena cava, abdominal aorta, and bilateral renal arteries. The bilateral common and internal iliac arteries were no longer encased, and the anterior displacement of the pancreas and third segment of the duodenum was resolved.

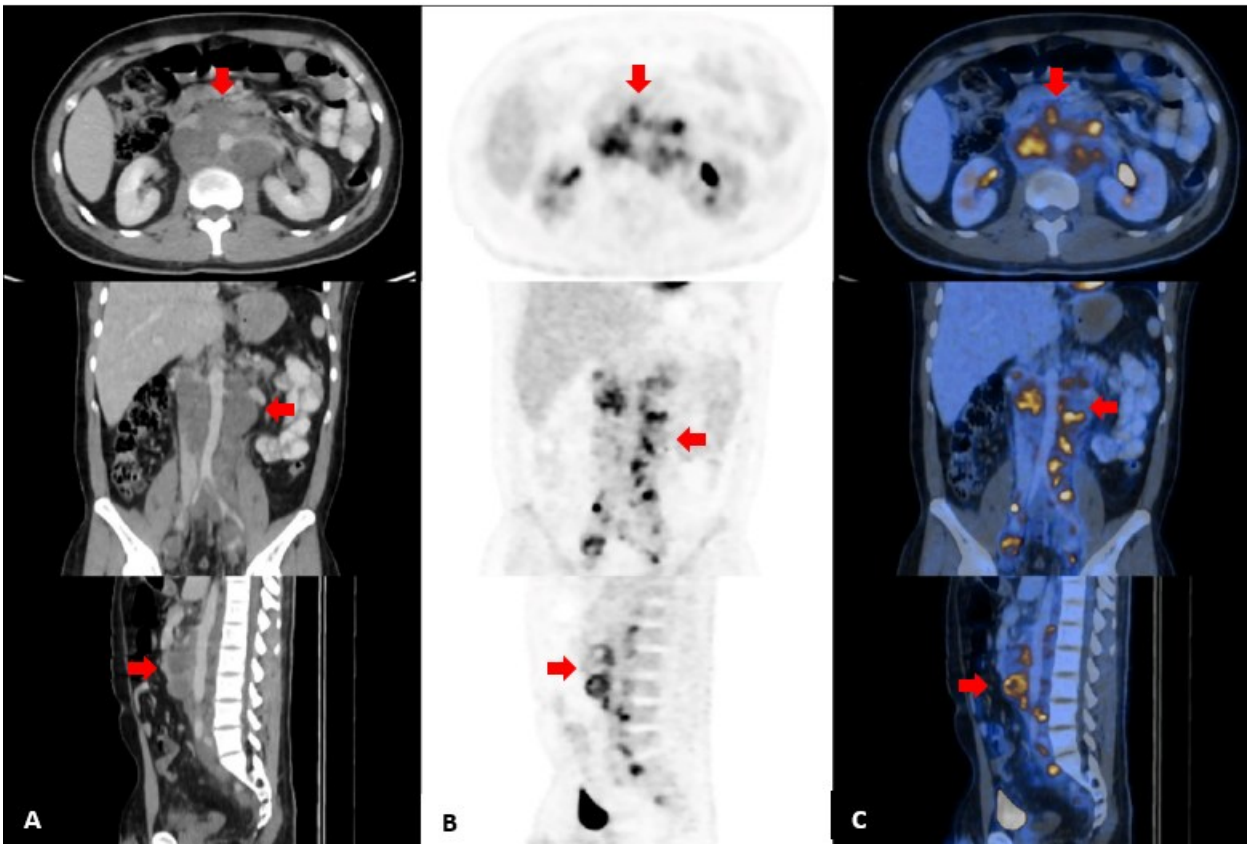

FIGURE 6 Axial, coronal, and sagittal view showing the (A) CT, (B) PET, and (C) fused PET/CT images of the patient's initial PET/CT scan showing the multiple FDG-avid enlarged lymph nodes in the retroperitoneal and pelvic region.

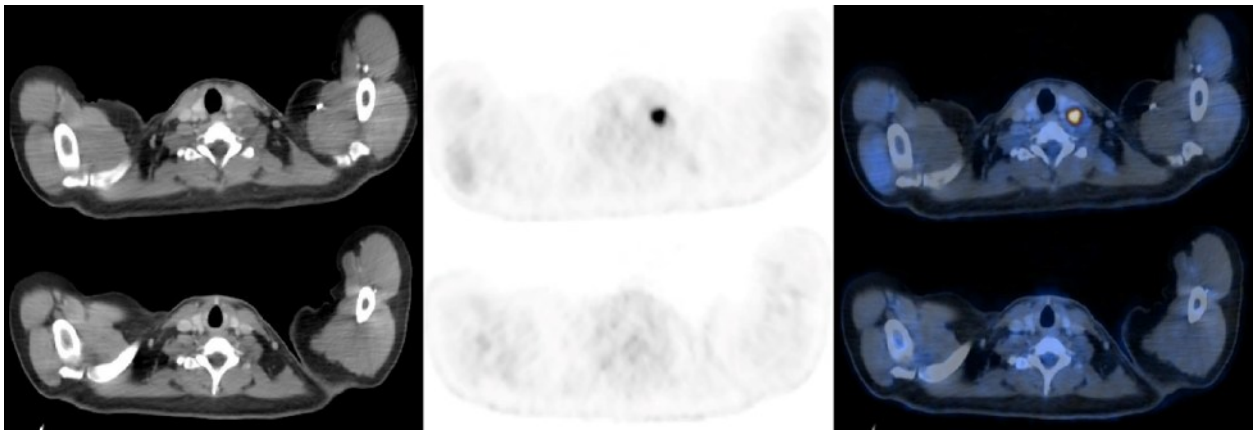

FIGURE 7 Axial view of the neck, the (A) CT, (B) PET, and (C) fused PET/CT images of the follow-up whole-body PET/CT scan showing resolution of the lesions in the left cervical region. Initial PET/CT scan (1st row) and follow-up PET/CT scan (2nd row) .

RELAPSE

In the interim, the patient developed dry cough with associated chest pain. Another 18F-FDG PET/CT scan was done and the MIP images revealed multiple FDG-avid lesions in the thorax and abdomen (Figure 11). There is interval development of marked irregular enhancing thickening of the right lung pleura with intense FDG uptake and minimal loculated effusion (SUVmax up to 11.7) (Figure 12).

There is also presence of an FDG-avid mass-like consolidation of the right upper and middle lobes (SUVmax 14.4) which compresses the traversing right pulmonary artery, superior pulmonary vein and their branches, and causes cut-off of the middle lobe bronchi (Figure 13). There is also interlobular septal thickening in the remaining pneumatized portions of the right lung. Non-calcified nodules, some with pleural attachment, are also seen in the right lower lobe, left upper lobe and lingula (Figure 14)

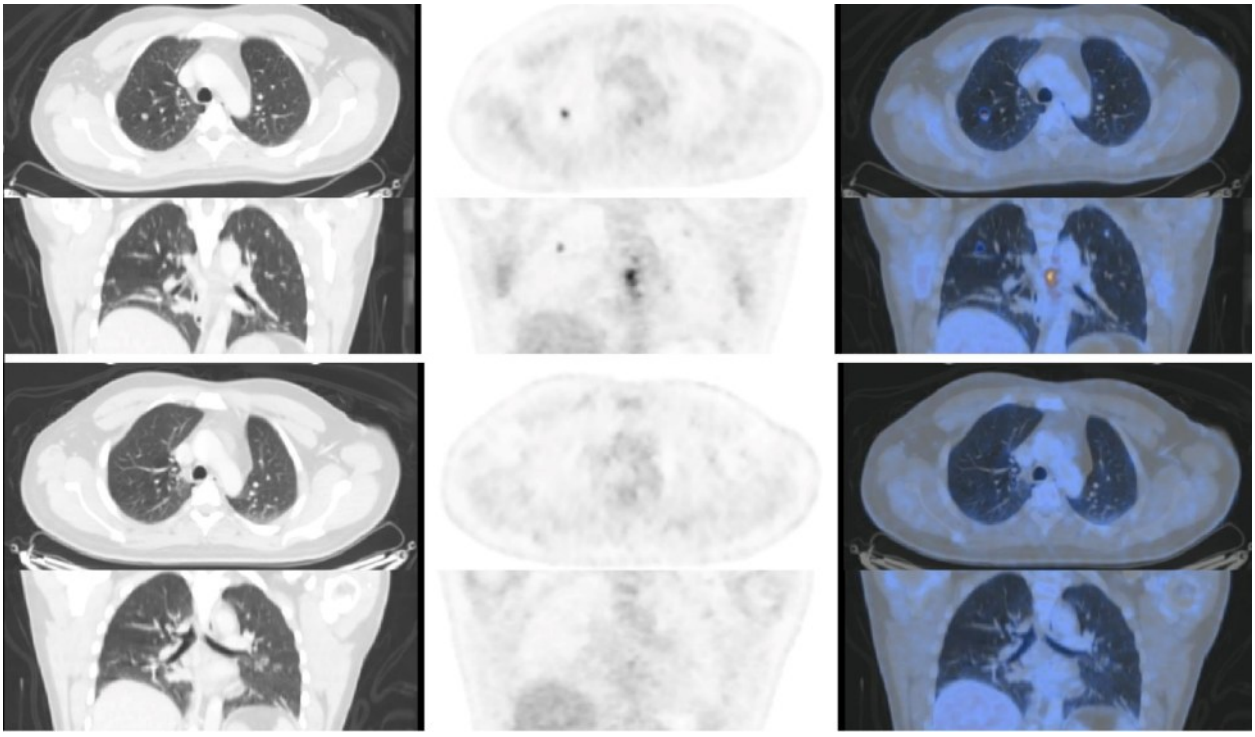

FIGURE 8 Axial and coronal view showing the (A) CT, (B) PET, and (C) fused PET/CT images of the patient's second whole-body PET/CT scan with emphasis on lung region showing resolution of the pulmonary nodules. Initial PET/CT scan (1st row) and follow-up PET/CT scan (2nd row).

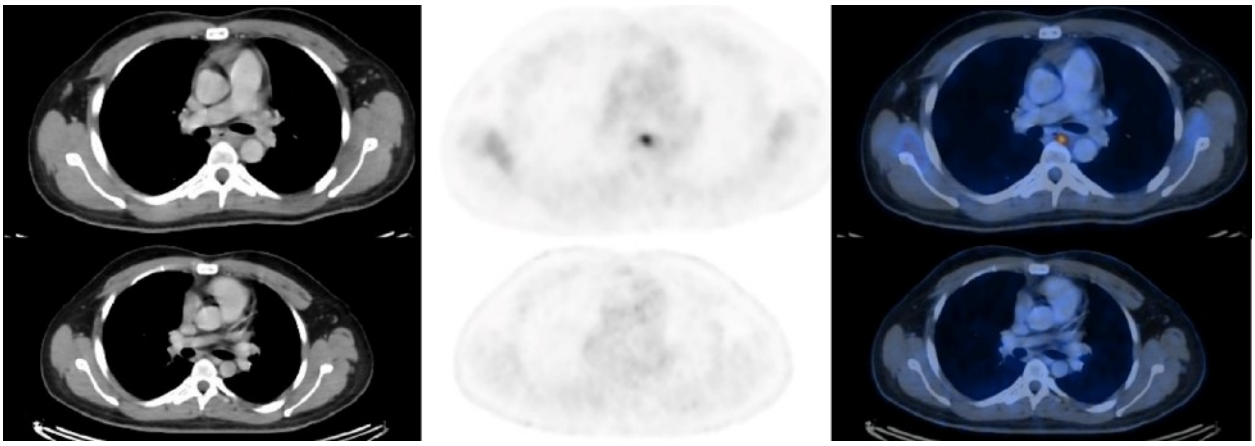

FIGURE 9 Axial view showing the (A) CT, (B) PET, and (C) fused PET/CT images of the patient's second whole-body PET/CT scan showing resolution of the mediastinal lymph nodes. Initial PET/CT scan (1st row) and follow-up PET/CT scan (2nd row).

Numerous prominent to enlarged FDG-avid lymph nodes are identified in the right upper paratracheal, bilateral lower paratracheal, subcarinal, paraesophageal, anterior cardiophrenic, right internal mammary, retrocrural, bilateral posterior intercostal regions (SUVmax up to 8.0). (Figure 15), retroperitoneal, mesenteric and iliac chains regions (SUVmax up to 10.4.) (Figure 16).

There is also presence of an FDG-avid (SUVmax 7.1) bilobed mass is identified in the left infrarenal retroperitoneal area, measuring 2.3 x 2.7 cm (Figure 17).

OUTCOME AND FOLLOW-UP

No adverse events were reported post PET/CT scans. Patient underwent VATS to remove the thoracic mass and is currently undergoing TIP chemotherapy.

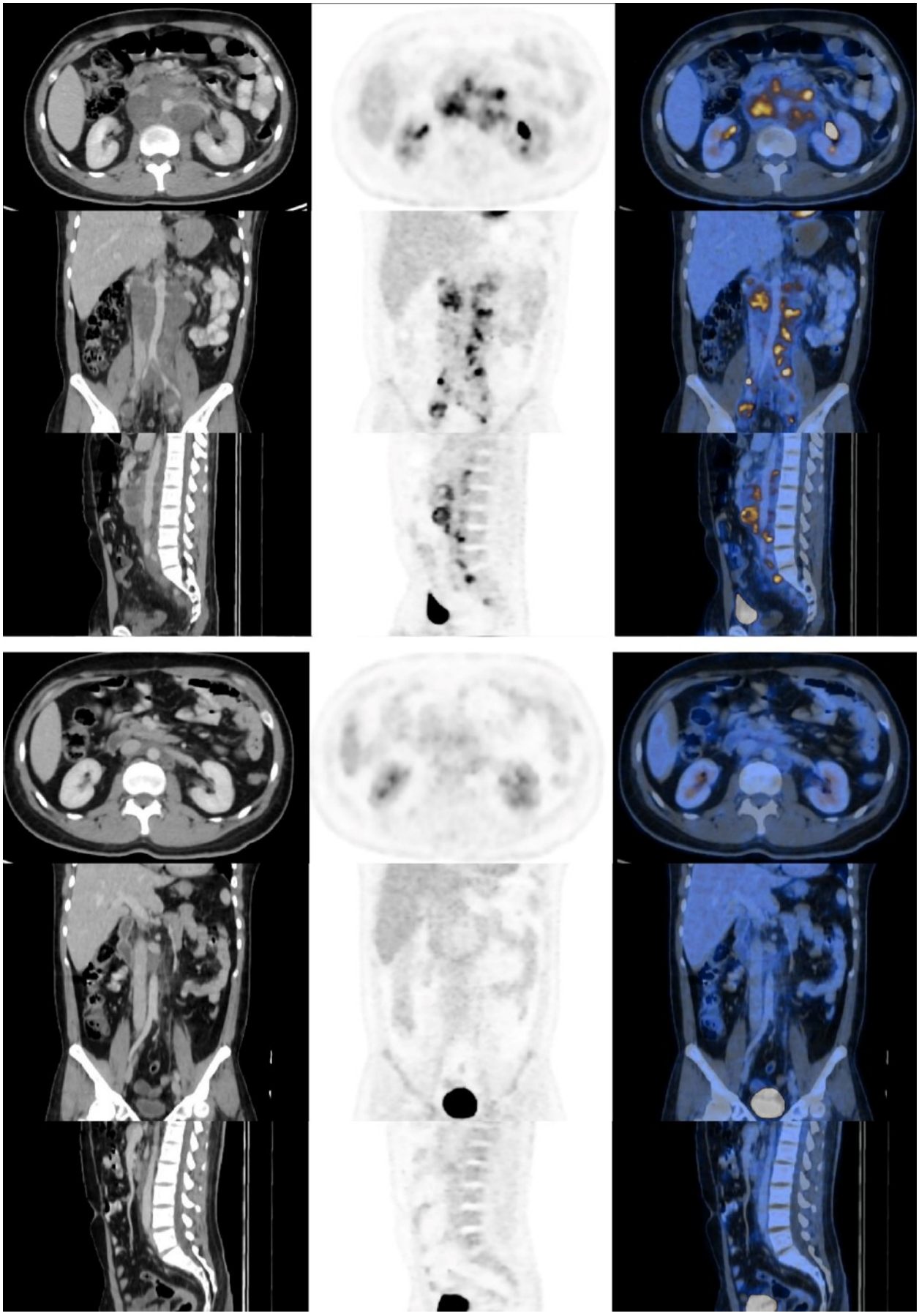

FIGURE 10 Axial, coronal and sagittal view showing the (A) CT, (B) PET, and (C) fused PET/CT images of the patient's second whole-body PET/CT scan showing resolution of the abdominal lymphadenopathies. Initial PET/CT scan (1st row) and follow-up PET/CT scan (2nd row) region.

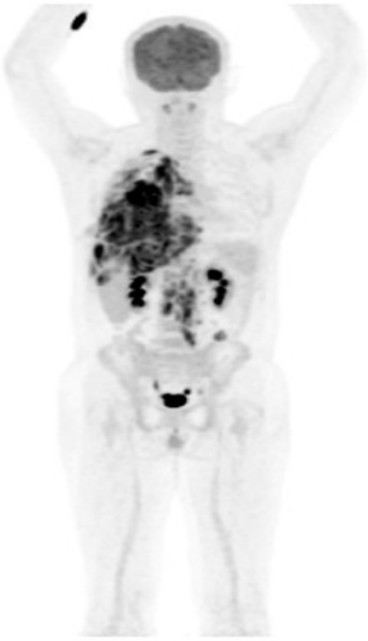

FIGURE 11 PET maximum intensity projection view of the patient's third whole-body PET/CT scan showing multiple FDG-avid lesions in the thoracic and abdominal regions.

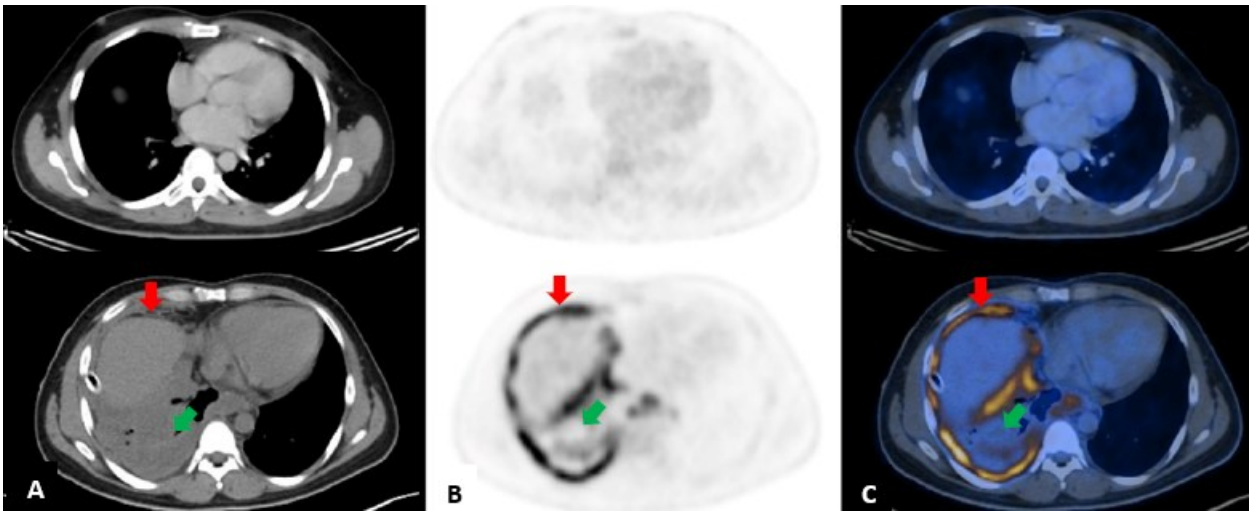

FIGURE 12 Axial view showing the (A) CT, (B) PET, and (C) fused PET/CT images of the patient's third whole-body PET/CT scan showing the FDG-avid irregular enhancing thickening of the right lung pleura (red arrow) and minimal loculated effusion (green arrow). Previous PET/CT scan (1st row) and latest PET/CT scan (2nd row) .

DISCUSSION

The 2016 WHO classification divides testicular GCTs into two main categories: those related to germ cell neoplasia in situ (GCNIS) and non-GCNIS related tumors. Non-GCNIS-related tumors include Type I, which consists of prepubertal teratomas and YSTs, and Type III, known as spermatocytic tumors, which lack chromosome 12p abnormalities. Type I testicular germ cell tumors (TGCTs) occur primarily in children and are either benign teratomas or malignant yolk sac tumors. Type III TGCTs are found in older men. In contrast, Type II GCNIS-related tumors are malignant, occur in adolescents and young adults, are associated with chromosome 12p abnormalities, and include seminomas, nonseminomas (such as embryonal carcinoma, teratomas, yolk sac tumors, and choriocarcinoma), as well as mixed and regressed GCTs [3 - 5].

Post-pubertal yolk sac tumors (YSTs) usually appear as part of mixed germ cell tumors (GCTs) or as recurrences after chemotherapy with unusual morphology, primarily affecting young to middle-aged men. Pure post-pubertal YSTs are extremely rare, less than 1% of testicular GCTs, and are more aggressive in clinical behavior. In most cases, surgical removal of a pure pre-pubertal YST through orchiectomy is curative. Currently, there is limited information regarding prognostic factors specifically associated with pure post-pubertal YSTs [2, 4 - 5].

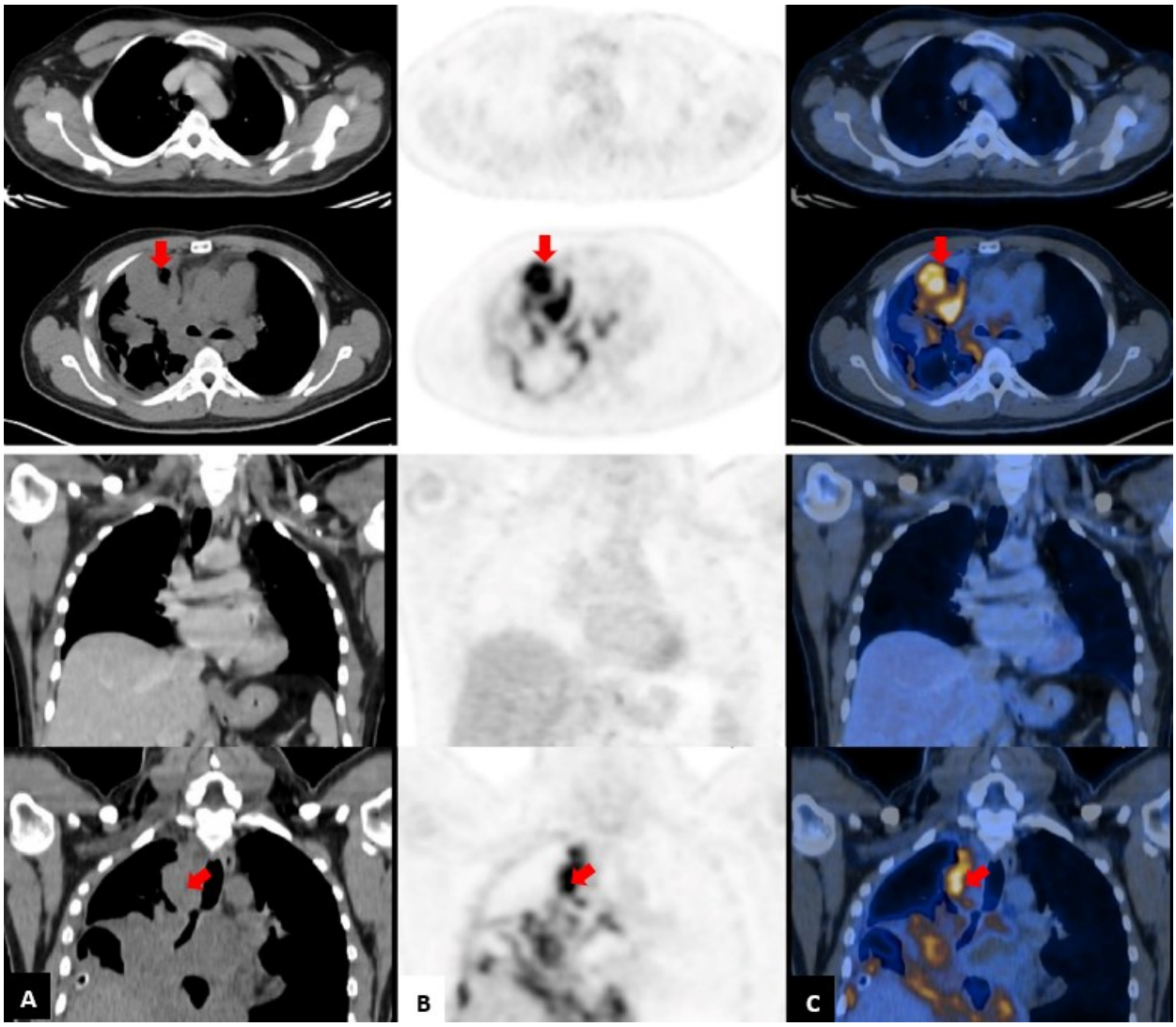

FIGURE 13 Axial view and coronal view showing the (A) CT, (B) PET, and (C) fused PET/CT images of the patient's third whole-body PET/CT scan showing the mass-like consolidation of the right upper and middle lobes (red arrow) with associated compression of adjacent structures. Previous PET/CT scan (1st row) and latest PET/CT scan (2nd row).

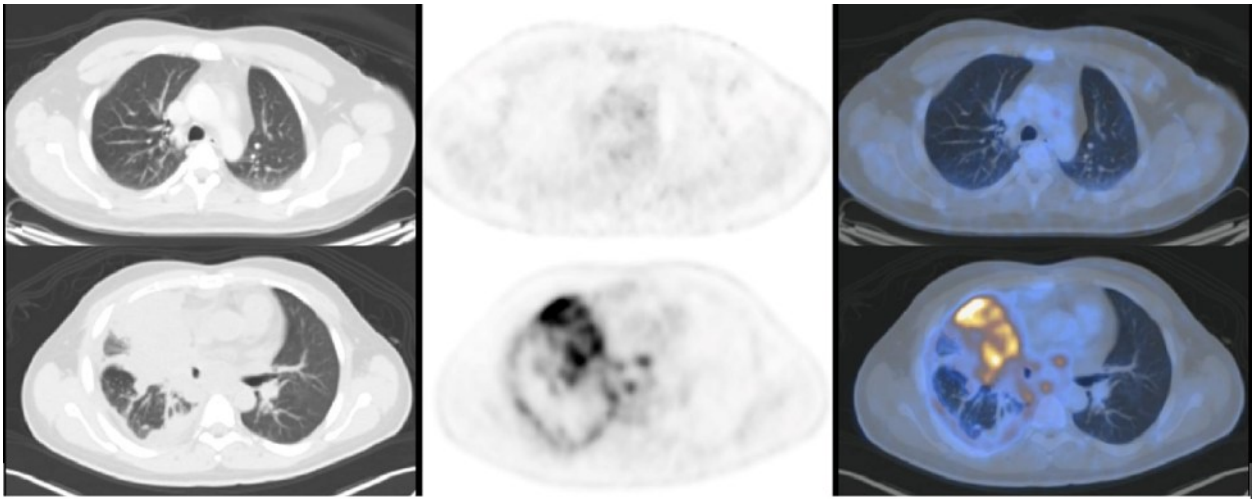

FIGURE 14 Axial view showing the (A) CT, (B) PET, and (C) fused PET/CT images of the patient's third whole-body PET/CT scan showing interlobular septal thickening in the pneumatized portions of the right lung and bilateral non-calcified nodules. Previous PET/CT scan (1st row) and latest PET/CT scan (2nd row).

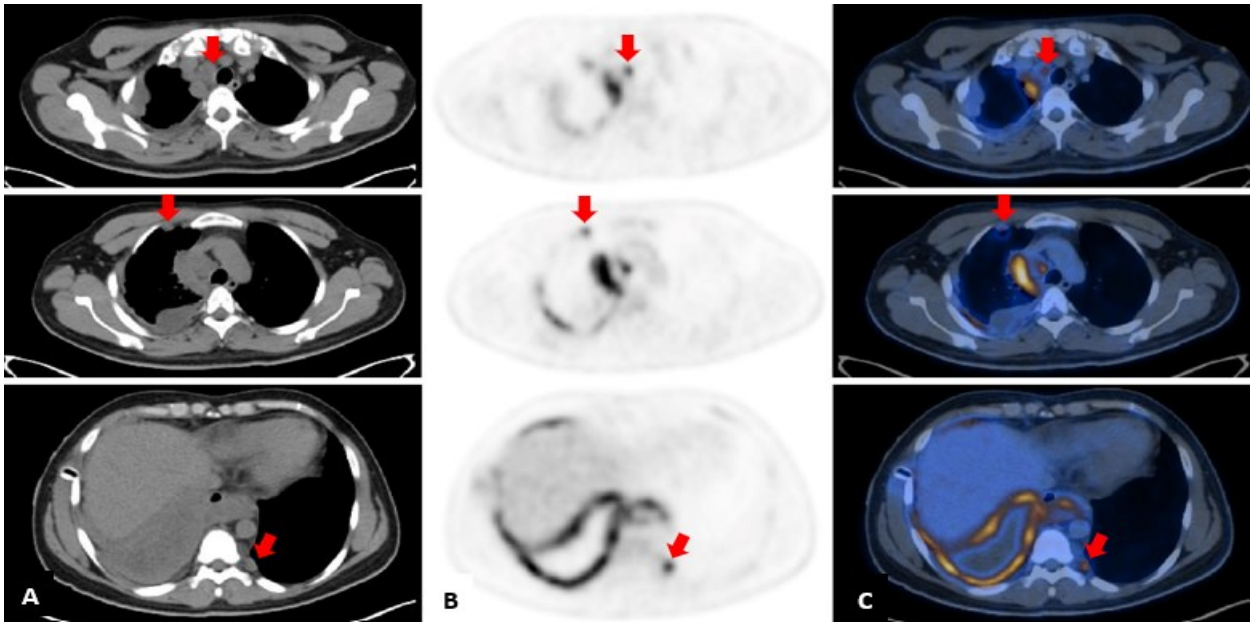

FIGURE 15 Axial view showing the (A) CT, (B) PET, and (C) fused PET/CT images of the patient's third whole-body PET/CT scan showing FDG-avid thoracic lymphadenopathies.

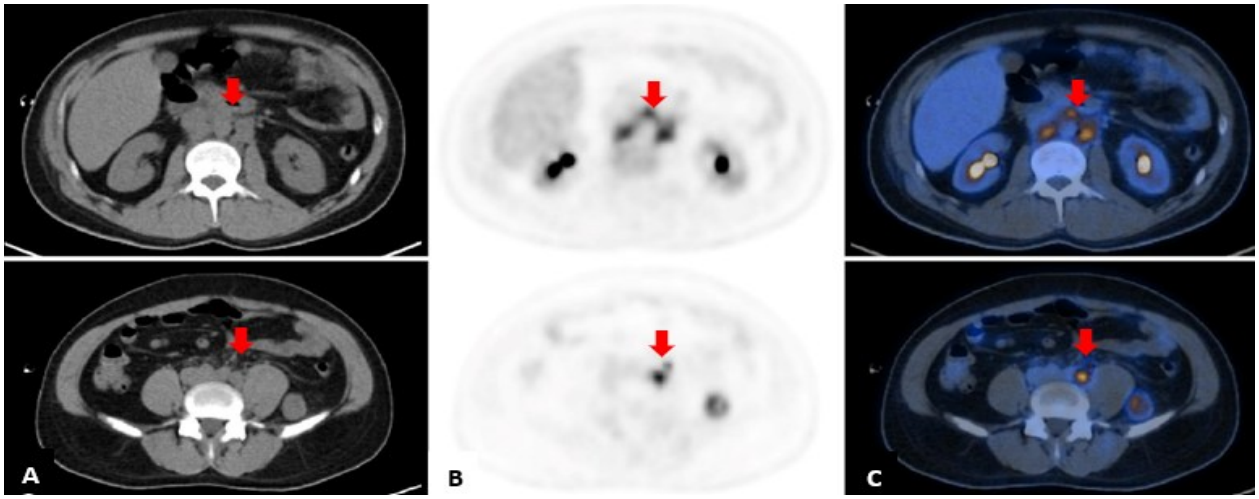

FIGURE 16 Axial view showing the (A) CT, (B) PET, and (C) fused PET/CT images of the patient's third whole-body PET/CT scan showing FDG-avid abdominal lymphadenopathies.

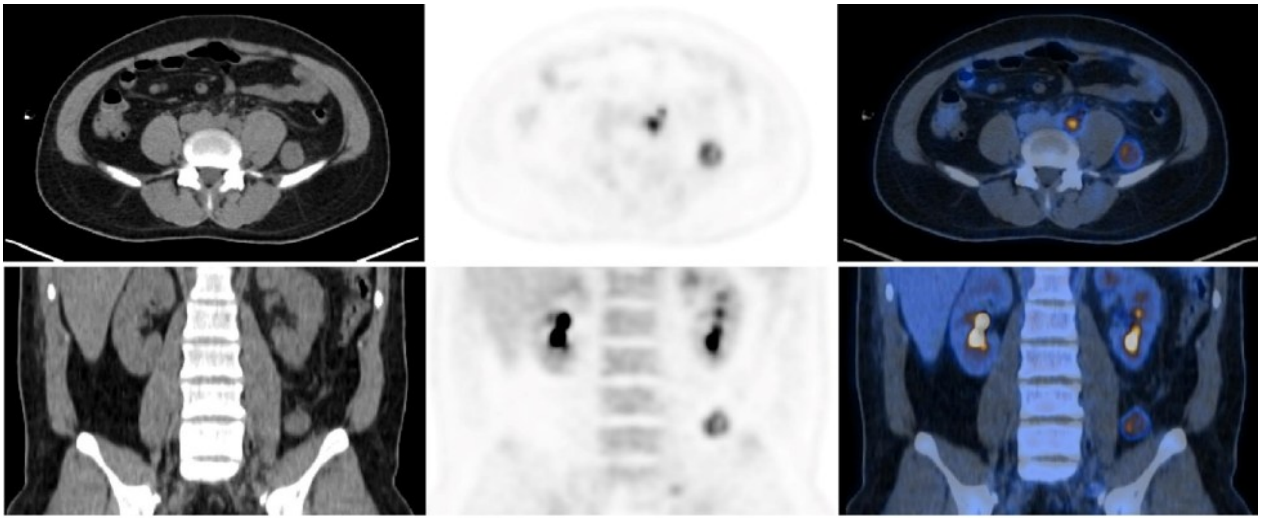

FIGURE 17 Axial and coronal view showing the (A) CT, (B) PET, and (C) fused PET/CT images of the patient's third whole-body PET/CT scan showing FDG-avid bilobed mass is identified in the left infrarenal retroperitoneal area.

Approximately 33% of patients have metastatic disease at diagnosis. Stage III patients with yolk sac elements display poorer prognosis with increased prevalence in late recurrences due to chemoresistance [4]. Based on the AJCC classification (Appendix A), the patient is classified as stage IIIC (pT1bN3M1a, S3) and is of poor prognosis with a 67% overall survival [8 - 9]. An online calculator provided by the International Germ Cell Cancer Collaborative Group (IGCCCG) Update Consortium predict a 3-year progression-free survival prediction of 63% (Figure 18) [10].

Positron emission tomography (PET) scan are becoming the mainstay nuclear medicine imaging technique for initial staging, evaluation of treatment response and disease monitoring in oncology. The modality allows measurement of both physiological and pathophysiological imaging. A radioactive tracer that decays by positron emission is used such as 2-[^{18}F]-fluoro-2-deoxyglucose (FDG). It is a glucose analogue that is transported intracellularly and phosphorylated to 2-[^{18}F]fluoro- 2-deoxyglucose-6-phosphate (FDG-6-phosphate) via the same pathways as glucose. Due to lesser amount of intracellular glucose phosphatase, 18F-FDG cannot be further metabolized and is trapped within the cancer cells [11 - 12]. This imaging modality is a hybrid of PET and CT technology that is able to provide both functional and anatomical information and is shown to improve diagnosing ang staging of most malignancies. The use of ^{18}F-FDG PET/CT scan in determining the disease stage, guiding treatment decisions, and monitoring treatment response played an important role in management of this case. Pure YST in adults are extremely rare and aggressive malignancy which metastasizes primarily through lymphatic spread. The advantage of hybrid PET/CT over purely anatomical imaging techniques, such as CT and MRI scans is that it enables clinicians to determine extent of the disease throughout the entire body as well as detect metabolic changes of the malignant lesions before structural changes occur. This aids in determining the need to use adjunct therapies (e.g. surgery, radiotherapy) for residual disease [13 - 14].

With increasing popularity of hybrid imaging, there are some documented cases of PYSTPPT with 18F-FDG PET/CT imaging done. García-G´omez et al (2021) have documented extensive highly metabolically active metastasis in the scrotal-inguinal, pelvic, mesenteric, retroperitoneal, hepatic, pulmonary, supradiaphragmatic regions and skeletal dissemination; and Wang et al (2015) documented lung and inguinal lymph node metastases [15 - 16].

The aggressive nature of PYSTPPT warranted close monitoring using tumor markers and diagnostic imaging. Compliance for laboratory and radiologic imaging has been fairly good for this patient, mostly attributed to private company health insurance, and financial, social and family support.

Management of testicular yolk sac tumor depends on the stage of the malignancy and primarily involves radical orchiectomy with or without chemotherapy, and dissection of retroperitoneal lymph nodes with monitoring with serum AFP (Table 2) [2, 8, 17 - 18]. Chemotherapy of choice is Bleomycin, Etoposide and Cisplatin which has shown to increase overall progression free survival rate and overall survival [9].

CONCLUSION

Pure yolk sac tumor post-pubertal type is an extremely rare and aggressive disease. A third of the known cases presents with metastases on diagnosis. Current management guidelines for advanced stages recommends orchiectomy with chemotherapy using Bleomycin, Etoposide and Cisplatin. FDG PET/CT scan is a very useful tool for clinicians in initial staging, treatment response, and long-term monitoring for malignancies. Given its inherent high sensitivity and ability to detect disease recurrence prior to anatomic change, the benefit of using FDG PET/CT for PYSTPPT is of value. An added benefit, the use of molecular imaging techniques presents a unique opportunity to further observe, study, and characterize the metabolism and aggressiveness this rare disease as well as by allowing a quick and comprehensive whole-body imaging.

INFORMED CONSENT

Informed consent for publishing this case report, accompanying images, histopathologic and laboratory results was obtained from the patient.

PATIENT PERSPECTIVE

The patient and relative are relieved following the excellent treatment response from chemotherapy. The hardships encountered has changed their outlook in life and has made more focus on their health.

DECLARATIONS

The authors declare no conflicts of interest, financial or otherwise.

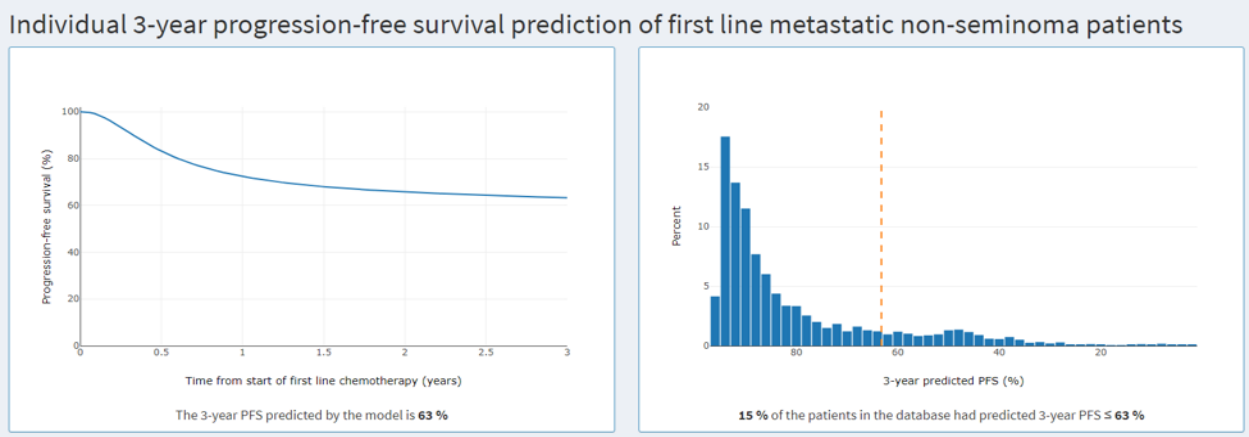

FIGURE 18 Progression-free survival of the patient based on the International Germ Cell Cancer Collaborative Group (IGCCCG) Update Consortium online calculator.

TABLE 2. Treatment of yolk sac tumor by stage

Stage 1

Disease is curative in almost all cases by radical inguinal orchiectomy

Choices for Stage 1A

Careful observation (surveillance): regular checkup every two months during the first year, with CT scans every four to six months. In the second year, regular checkup every three months, with CT scans every six to twelve months. For relapse, chemotherapy is indicated.

Nerve-sparing retroperitoneal lymph node dissection (RPLND)

Chemotherapy: giving the BEP regimen (bleomycin, etoposide, and cisplatin) for one cycle. Chemotherapy decreases the rate of relapse.

Stage 1S

Chemotherapy with three cycles of BEP or four cycles of EP (etoposide and cisplatin) is indicated if the alpha fetoprotein is still elevated post-orchiectomy with no evidence of mass on CT scan.

Stage 2

Surgery must be done first for all the cases.

Stage 2A

Tumor marker values after surgery as well as involvement of the retroperitoneal lymph nodes will decide the next step of management.

Normal tumor marker levels:

Retroperitoneal lymph node dissection (RPLND): If the lymph nodes contain cancer, then give two cycles of chemotherapy (BEP or EP). If no lymph nodes are involved, watch and monitor closely for signs of relapse.

Chemotherapy: 4 cycles of EP (etoposide and cisplatin) or three cycles of BEP (bleomycin, etoposide, and cisplatin).

High tumor markers post-orchiectomy should be treated using chemotherapy (EP or BEP). The number of cycles is determined after the risk stratification (good, intermediate, or poor).

Stage 2B

Normal tumor marker levels:

Chemotherapy: Four cycles of EP or three cycles of BEP should be given to treat the patients.

Retroperitoneal lymph node dissection (RPLND)

High tumor markers post-orchiectomy should be treated using chemotherapy (EP or BEP). The number of cycles is determined by the risk stratification (good, intermediate, or poor).

Stage 3

Patients with stage 3 disease should be treated with radical inguinal orchiectomy, followed by 3 to 4 cycles of the following chemotherapy regimens:

EP 4 cycles

BEP 3 or 4 cycles

VIP (etoposide, ifosfamide, and cisplatin) 4 cycles

High-dose chemotherapy and bone marrow transplant might be indicated in cancer resistance to usual dose chemotherapy.

Kattuoa Ml, Dunton CJ. Yolk Sac Tumors. [Updated 2023 Feb 4]. In: StatPearls [Internet]. Treasure Island (FL): StatPearls Publishing; 2024 Jan-. Available from: https://www.ncbi.nlm.nih.gov/books/NBK563163/

ACKNOWLEDGMENT

The author thanks Dr. Kathleen Ross Caligagan and Ms. Kristine Joy S. Calvario of the Cardinal Santos Medical Center for their precious suggestions and advice.

REFERENCES

1. Giona, S. (2022). The Epidemiology of Testicular Cancer. In N. Barber (Eds.) et. al., Urologic Cancers. Exon Publications. https://doi.org/10.36255/exon-publications-urologic-cancers-epidemiology-testicular-cancer.
2. Janugade, H., Monteiro, J., & Gouda, S. (2019). Pure yolk sac tumour, post-pubertal type, arising from cryptorchid testes. BMJ Case Reports, 12(7), e229541. https://doi.org/10.1136/bcr-2019-229541.
3. Williamson, S. R., Delahunt, B., Magi-Galluzzi, C., Algaba, F., Egevad, L., Ulbright, T. M., Tickoo, S. K., Srigley, J. R., Epstein, J. I., Berney, D. M., & Members of the ISUP Testicular Tumour Panel (2017). The World Health Organization 2016 classification of testicular germ cell tumours: a review and update from the International Society of Urological Pathology Testis Consultation Panel. Histopathology, 70(3), 335–346. https://doi.org/10.1111/his.13102.
4. Lobo J, Henrique R. Yolk sac tumor. PathologyOutlines.com website. April 27, 2023. [Internet]. [cited August 18th, 2024]. Available from: https://www.pathologyoutlines.com/topic/testisyst.html.
5. Patel, S., Satturwar, S., Khan, W., Ashman, D., & Quiroga-Garza, G. M. (2023). Pure post-pubertal yolk sac tumor of the testis: An extremely rare and aggressive entity. Annals of diagnostic pathology, 63, 152086. https://doi.org/10.1016/j.anndiagpath.2022.152086.
6. Shin, J., Kim, J. H., Jung, K. C., & Cho, K. J. (2022). A sinonasal yolk sac tumor in an adult. Journal of pathology and translational medicine, 56(3), 152–156. https://doi.org/10.4132/jptm.2021.12.09.
7. Fahim-Ul-Hassan, & Cook, G. J. (2012). PET/CT in oncology. Clinical medicine (London, England), 12(4), 368–372. https://doi.org/10.7861/clinmedicine.12-4-368.
8. GSRGT 2020: The International Germ Cell Cancer Collaborative Group (IGCCCG) update. [Internet]. 2020 [cited 2024 August]. Available from: https://www.urotoday.com/conference-highlights/gsrgt-2020/testicular-cancer/126571-gsrgt-2020-clinical-trials-corner-the-international-germ-cell-cancer-collaborative-group-igcccg-update.html.
9. Amin, M. B., Greene, F. L., Edge, S. B., Compton, C. C., Gershenwald, J. E., Brookland, R. K., Meyer, L., Gress, D. M., Byrd, D. R., & Winchester, D. P. (2017). The Eighth Edition AJCC Cancer Staging Manual: Continuing to build a bridge from a population-based to a more "personalized" approach to cancer staging. CA: a cancer journal for clinicians, 67(2), 93–99. https://doi.org/10.3322/caac.21388.
10. Gillessen, S., Sauvé, N., Collette, L., Daugaard, G., de Wit, R., Albany, C., Tryakin, A., Fizazi, K., Stahl, O., Gietema, J. A., De Giorgi, U., Cafferty, F. H., Hansen, A. R., Tandstad, T., Huddart, R. A., Necchi, A., Sweeney, C. J., Garcia-Del-Muro, X., Heng, D. Y. C., Lorch, A., … International Germ Cell Cancer Classification Update Consortium (2021). Predicting Outcomes in Men With Metastatic Nonseminomatous Germ Cell Tumors (NSGCT): Results From the IGCCCG Update Consortium. Journal of clinical oncology : official journal of the American Society of Clinical Oncology, 39(14), 1563–1574. https://doi.org/10.1200/JCO.20.03296.
11. Almuhaideb, A., Papathanasiou, N., & Bomanji, J. (2011). 18F-FDG PET/CT imaging in oncology. Annals of Saudi medicine, 31(1), 3–13. https://doi.org/10.4103/0256-4947.75771.
12. Ashraf MA, Goyal A. Fludeoxyglucose (18F) [Updated 2023 Aug 28]. [Internet]. [cited 2024 August]. Available from: https://www.ncbi.nlm.nih.gov/books/NBK557653/.
13. Parihar, A. S., Dehdashti, F., & Wahl, R. L. (2023). FDG PET/CT-based Response Assessment in Malignancies. Radiographics : a review publication of the Radiological Society of North America, Inc, 43(4), e220122. https://doi.org/10.1148/rg.220122.
14. Zhu, A., Lee, D., & Shim, H. (2011). Metabolic positron emission tomography imaging in cancer detection and therapy response. Seminars in oncology, 38(1), 55–69. https://doi.org/10.1053/j.seminoncol.2010.11.012.
15. García-Gómez, F. J., Villar-Rodríguez, J. L., Beato-Zambrano, C., de la Riva-Pérez, P. A., & Calvo-Morón, M. C. (2021). 18F-FDG PET/CT in pure testicular Yolk Sac Tumor in adult. International braz j urol : official journal of the Brazilian Society of Urology, 47(1), 202–204. https://doi.org/10.1590/S1677-5538.IBJU.2019.0780.
16. Wang, Z., Yan, B., Wei, Y. B., Yin, Z., Zhou, K. Q., & Yang, J. R. (2015). Adult metastatic yolk sac tumor descending from an intra-abdominal testis: A case report and review of the literature. Oncology letters, 10(6), 3647–3650. https://doi.org/10.3892/ol.2015.3817.
17. Kattuoa Ml, Dunton CJ. Yolk Sac Tumors. [Updated 2023 Feb 4]. [Internet]. 2023 [cited 2024 August]. Available from: https://www.ncbi.nlm.nih.gov/books/NBK563163/
18. Canete Portillo, S., Rais-Bahrami, S., & Magi-Galluzzi, C. (2022). Updates in 2022 on the staging of testicular germ cell tumors. Human pathology, 128, 152–160. https://doi.org/10.1016/j.humpath.2022.07.009.

Appendix

AJCC 8th edition TNM staging classification for testicular cancer

T	**Primary tumor**
TX	Primary tumor cannot be assessed
T0	No evidence of primary tumor
Tis	Germ cell neoplasia in situ
T1	Tumor limited to testis (including rete testis invasion) without LVI
T1a[a]	Tumor smaller than 3 cm
T1b[a]	Tumor 3 cm or larger
T2	Tumor limited to testis (including rete testis invasion) with LVI or Tumor invading hilar soft tissue or epididymis or penetrating visceral mesothelial layer covering the external surface of tunica albuginea with or without LVI
T3	Tumor directly invading spermatic cord soft tissue with or without LVI
T4	Tumor invading scrotum with or without LVI
N	**Regional lymph nodes**
NX	Regional lymph nodes cannot be assessed
N0	No regional lymph nodes metastasis
N1	Metastasis with a lymph node mass ≤2 cm in greatest dimension or multiple lymph nodes (≤5), none >2 cm in greatest dimension
N2	Metastasis with a lymph node mass >2 cm but not >5 cm in greatest dimension or multiple lymph nodes (>5), any one mass >2 cm but not >5 cm in greatest dimension or evidence of extranodal extension
N3	Metastasis with a lymph node mass >5 cm in greatest dimension
M	**Distant metastasis**
M0	No distant metastasis
M1	Distant metastases or discontinuous involvement of spermatic cord soft tissue
M1a	Nonretroperitoneal nodal or pulmonary metastases
M1b	Nonpulmonary visceral metastases
S	**Serum markers**
SX	Marker studies not available or nor performed
S0	Markers study levels within normal limits
S1	LDH < 1.5 × N• and hCG (mIU/mL) < 5000 *and* AFP (ng/mL) < 1000
S2	LDH 1.5–10 × N• and hCG (mIU/mL) 5000–50 000 *or* AFP (ng/mL) 1000–10 000
S3	LDH > 10 × N• and hCG (mIU/mL) > 50 000 *or* AFP (ng/mL) > 10 000

Association of Hemodynamic Changes with the Scan Parameters of a Dipyridamole-induced Stress Myocardial Perfusion Scintigraphy with Technetium-99m Sestamibi in Patients with Suspected Coronary Artery Disease

Noel Christi C. Macapagal, MD

Division of Nuclear Medicine, Philippine Heart Center
E-mail address: noel.macapagal@gmail.com

ABSTRACT

Background:

A dipyridamole induced stress myocardial perfusion scintigraphy with Tc-99m Sestamibi is utilized for diagnosing coronary artery diseases. The use of dipyridamole as form of pharmacologic stressor has expected hemodynamic changes.

Objective:

The objective of this study was to determine the association of these changes with the scan parameters in patients with suspected coronary artery disease (CAD).

Methodology:

A total of 101 patients, with suspected CAD, who underwent a dipyridamole-induced stress myocardial perfusion scintigraphy using Tc-99m Sestamibi from January 2019 to March 2020 were included in this study. The patient databases, monitoring sheets, and scan results were reviewed.

Results:

The blood pressure responses had no significant association with the scan parameters and results. The normal (> 1.2) and abnormal (< 1.2) heart rate ratios (HRR), which is the peak HR/baseline HR, likewise had no significant association with the scan results. However, in terms of the median HRR, the higher ratio of 1.29 (normal scan results) against the ratio of 1.25 (abnormal scan results) was determined to be significant (p-value of 0.032). The HRR also had a direct and indirect weak correlation with stress and rest Left Ventricular Ejection Fraction (LVEF) values (p-values of 0.09 and 0.011) and Summed Rest Score (p-value of 0.007), respectively. For the 12-L ECG, only the baseline normal (p-value of 0.018) and infarct findings (p-value of 0.017) were similarly associated with normal and abnormal scan results, respectively.

Conclusion:

For patients with suspected CAD, the higher HRRs and baseline 12-L ECG of normal and infarct findings relates to the expected scan result. For scan parameters, the higher HRRs were also correlated with higher stress and rest LVEF values, and normal SRS, albeit a weak correlation. Notably, the blood pressure and post-infusion 12-L ECG changes had no significant association. In summary, the higher HRRs indicates normal scan results, normal SRS, and better LVEF values which increases the diagnostic confidence in the interpretation and management, especially in some equivocal cases.

Keywords*: Dipyridamole, hemodynamic changes, myocardial perfusion scintigraphy*

INTRODUCTION

Coronary artery disease is chronic condition that affects the morbidity and quality of life and is the third leading cause of cardiovascular disease in the Philippines [1]. Therefore, a myocardial perfusion scintigraphy is used in determining the adequacy of blood flow to the myocardium. To increase its sensitivity, a form of stress is used which may be through exercise, or a pharmacologic stress agent. A vasodilator stress agent such as Dipyridamole produces indirect coronary dilation with a concomitant systemic vasodilatory effect wherein there is a decrease in blood pressure and reflex

tachycardia [2]. These hemodynamic changes may provide useful information in imaging abnormalities in coronary artery disease.

It has been well documented that the intravenous use of dipyridamole produces mild hemodynamic changes with a near peak effect at 3 minutes from its infusion with side effects of hypotension, headache, dizziness, and dyspnea [3]. These side effects have demonstrated a correlation with hemodynamic variables but did not affect the imaging or ECG findings [4]. A blunted heart rate response to Dipyridamole infusion was associated with an LVEF of less than 45% and was also an independent predictor of an elevated summed stress scores (SSS), higher resting heart rate, and lower HDL levels [2, 5].

However, several studies have noted that the clinical significance of these hemodynamic responses is currently debatable [6]. An abnormal HRR and systolic blood pressure response may suggest an inadequate patient response to dipyridamole infusion. The aim of this study was to determine the association of hemodynamic changes with the scan parameters of a dipyridamole-induced stress myocardial perfusion scintigraphy with Technetium-99m Sestamibi in patients with suspected CAD.

METHODOLOGY

This is a retrospective cross-sectional study that included 101 adult patients referred to the Division of Nuclear Medicine, Philippine Heart Center for a dipyridamole-induced stress myocardial perfusion scintigraphy with Tc-99m Sestamibi for the assessment of suspected coronary artery disease between January 2019 and March 2020. Patients with an incomplete information sheet, database, or images were excluded.

The patients included must have strictly followed the Standard Operating Procedure (SOP-M-AMS-NMD-023) for a dipyridamole-induced stress myocardial perfusion scintigraphy with Tc-99m Sestamibi of this institution. The data compiled was then checked for any inconsistencies/errors to the procedure.

The patients' data were obtained from their information sheet, databases, monitoring sheets, and official scan results. These included the following: demographic data, clinical history, blood pressure and heart rate readings, electrocardiographs, and scan results. The pertinent data were entered into the prepared collection forms/ spreadsheets for statistical analysis.

The patients were then categorized based on their recorded blood pressures and heart rates as normal or abnormal. A normal systolic blood pressure (SBP) response was defined as a reduction of more than or equal to 10 mmHg from the baseline and a normal heart rate response was based on the heart rate ratio (peak HR/baseline HR) of more than 1.2. An abnormal hemodynamic response was less than 10 mmHg from the baseline for SBP and less than or equal to 1.2 for the heart rate ratio (HRR) [7]. Other variables considered were the ECG findings before and after dipyridamole infusion, time when the hemodynamic change was noted, and side effects.

Dependent variables are the scan findings of perfusion defects interpreted as reversible (ischemia) or fixed (infarct/fibrosis) – which were noted in the official reports. The widely adopted American College of Cardiology/American Heart Association (ACC/AHA) 17 segment polar map of the left ventricle with a five-point score scale was used for the summed stress score (SSS), summed rest score (SRS), and the summed difference score (SDS). The left ventricle ejection fraction values (LVEF) at stress and rest were also included. The scan results were likewise determined as either having a normal or abnormal as indicated in the official reports. Normal scans were defined by the absence of any defect as seen in the final interpretation of the scan report and any finding that indicates otherwise were noted as abnormal.

Sample Size Calculation

With the G*Power 3.1.9.2, a minimum of 89 patients were needed for this study based on the average heart rate before (82) and after (92) the Dipyridamole test, common standard deviation of 10, 5% level of significance and 90% power.

Statistical Analysis

Descriptive statistics were used to summarize the demographic and clinical data of the patients. Frequency and proportion were then used for the categorical variables, median and inter quartile range for non-normally distributed continuous variables and mean and SD for normally distributed continuous variables. Independent Sample T-test, Mann-Whitney U, and Fisher's Exact/Chi-square test were used to determine the difference of mean, rank and frequency, respectively, between patients with normal versus abnormal result. Paired sample T-test was used to compare blood pressure and heart rate at baseline and after dipyridamole infusion. Spearman correlation analysis was used to determine the correlation of the difference

myocardial perfusion scores and LVEF values. Chi-square test for association was undertaken to establish the association of Myocardial Perfusion Score category and LVEF to Baseline ECG findings. Shapiro-Wilk was then used to test the normality of the other continuous variables. Missing variables were neither replaced nor approximated. Null hypotheses were rejected at 0.05 α- level of significance. STATA 13.1 was used for the entire data analysis.

RESULTS

In all, a total of 101 patients were included in this study with their demographic profile and test as seen in Table 1. There was a significant difference for the older age (p-value of 0.018) and female sex (p-value of 0.006) with the normal scan results.

A significant difference for patients with abnormal results was noted for those with chronic kidney disease (3.96%). Most of the patients were hypertensive (83.17%). Other demographic and procedural data such as the anthropometrics, administered activities (mCi), dipyridamole infused (0.56 mg/Kg), other comorbidities, and symptoms before infusion showed no significant difference.

The blood pressure and heart rate before and after dipyridamole infusion (Table 2) were statistically significant. This was also seen for both the normal and abnormal scan results (p value of < 0.001).

For the hemodynamic changes in a dipyridamole-induced stress (Table 3 & 4), twenty-two patients (21.78%) had an abnormal SBP decrease (< 10 mmHg) while 35 patients (34.65 %) had an abnormal HRR. Overall, 50 patients (49.5%) had abnormal SBP decrease and/or HRR.

The median SBP decrease was at 20 mmHg from the baseline. A normal SBP decrease (> 10 mmHg) was noted in majority of the patients (78.22%) with 52 patients (76.47%) corresponding with a normal scan result. An abnormal SBP decrease was also noted with the normal scan results of 16 patients (23.53%). However, these findings were not statistically significant.

For the HRR, the median ratio was 1.28 with a significantly lower ratio of 1.25 for the abnormal scan results compared to a ratio of 1.29 for a normal scan result (p-value of 0.032). Although, there was no statistically significant difference between the normal (> 1.2) or abnormal (<1.2) HRR and the scan results.

Other hemodynamic changes (Table 4), such as the DBP decrease and patients with abnormal SBP decrease and/or HRR were not statistically significant. In terms of the double product or rate pressure product, which is the product of the HR and SBP, only the post-infusion double product was determined to have a statistically significant difference with the scan results (p-value of 0.044). The post-infusion double product was noted to be higher for normal scans [10.68 (9.2 to 12.84)] than those with abnormal scan results [10.22 (8.46 to 11.18)]. There was also a statistically significant difference from the baseline to post-infusion change of the double product for entire study population and for the those with normal scans (p-value of < 0.001).

Most of the baseline ECG findings were normal (42.58%) and with no apparent change after dipyridamole infusion (87.13%). There was a statistically significant difference for the normal baseline (p-value of 0.018) and infarct ECG findings (p-value of 0.017); and normal/abnormal scan results, respectively. The changes in the ECG after dipyridamole infusion were only noted in 13 patients (12.87%), wherein 6 patients were noted with an ST segment depression and that only 2 patients had the presence of ischemia in their scan results. This, however, was not statistically significant.

For the frequency of myocardial perfusion scores (Table 6), majority of the patients had a normal SSS (81.19%), SRS (87.13%), and SDS (84.16%). Ischemia (51.61%) was the most common defect noted followed by fibrosis and infarct findings. As seen in Table 7, there was no statistically significant correlation between the SBP decrease and myocardial perfusion scores. The HRR showed a statistically significant direct/indirect weak correlation for the rest and stress LVEF values (p-values of 0.09 and 0.011) and SRS (p-value of 0.007). This implies that higher HRRs, the better LVEF values. This is also the case for SRS wherein a score of less than 4 is normal. However, the level of association was weak for these findings.

Table 8 shows the other findings monitored during the dipyridamole infusion period. For the time in which the peak HR (P-value of 0.003) was attained, patients with normal scan results had an average of 8.15 (± 2.94) minutes compared to 6.56 (± 2.21) minutes for those with abnormal results. The time attained for the lowest SBP decrease and symptom/s during infusion were not statistically significant. Chest heaviness (35.64%) was the most frequent symptom noted.

TABLE 1. Demographic profile and procedural data of the patients

	Scan result			p-value
	Total (n=101)	Abnormal (n=33)	Normal (n=68)	
	Frequency (%); Mean ± SD; Median (IQR)			
Age (years)	61.02 ± 14.4	56.18 ± 16.03	63.37 ± 13.02	**0.018**
Sex				**0.006**
Male	50 (49.5)	23 (69.7)	27 (39.71)	
Female	51 (50.5)	10 (30.3)	41 (60.29)	
Weight (kg)	67.15 ± 15.89	68.35 ± 16.79	66.57 ± 15.53	0.600
Height (cm)	159.40 ± 9.26	161.24 ± 8.68	158.5 ± 9.46	0.164
Administered Activity				
Rest (mCi)	327 (310 to 355)	326 (303 to 350)	328 (313 to 359)	0.304
Stress (mCi)	834 (815 to 870)	825 (808 to 857)	841 (818 to 873)	0.182
Dipyridamole (mg)	36.4 (31.8 to 44.3)	36.4 (32.4 to 43.7)	36.95 (31 to 44.5)	0.688
Comorbidities				
Hypertension	84 (83.17)	29 (87.88)	55 (80.88)	0.572
Dyslipidemia	44 (43.56)	13 (39.39)	31 (45.59)	0.670
Diabetes Mellitus	33 (32.67)	12 (36.36)	21 (30.88)	0.653
Smoker	7 (6.93)	3 (9.09)	4 (5.88)	0.680
ESRD	4 (3.96)	3 (9.09)	1 (1.47)	0.101
CKD	4 (3.96)	4 (12.12)	0	**0.010**
Symptoms before infusion				
Easy fatigability	24 (23.76)	8 (24.24)	16 (23.53)	1.000
Exertional dyspnea/DOB	23 (22.77)	11 (33.33)	12 (17.65)	0.127
Asymptomatic	17 (16.83)	4 (12.12)	13 (19.12)	0.572

TABLE 2. Blood pressure and heart rate before and after dipyridamole infusion

	Before	After	p-value
	Mean ± SD		
All patients			
SBP	137.62 ± 19.19	119.80 ± 21.4	**< 0.001**
DBP	83.26 ± 10.4	70.3 ± 12.37	**< 0.001**
Heart rate	69.89 ± 12.64	89.92 ± 13.47	**< 0.001**
Patients with Abnormal scan results			
SBP	136.91 ± 19.1	120.15 ± 19.2	**< 0.001**
DBP	81.31 ± 9.43	69.56 ± 11.12	**< 0.001**
Heart rate	71.06 ± 13.82	87.42 ± 13	**< 0.001**
Patients with Normal scan results			
SBP	139.09 ± 19.58	119.09 ± 25.66	**< 0.001**
DBP	87.27 ± 11.26	71.81 ± 14.67	**< 0.001**
Heart rate	69.32 ± 12.09	91.13 ± 13.62	**< 0.001**

TABLE 3. Hemodynamic changes in dipyridamole-induced stress

	Scan result			p-value
	Total (n=101)	Abnormal (n=33)	Normal (n=68)	
	Frequency (%); Median (IQR)			
SBP decrease	20 (30 to 10)	20 (30 to 10)	20 (30 to 10)	0.366
Normal SBP decrease (≥ 10 mm Hg)	79 (78.22)	27 (81.82)	52 (76.47)	0.615
Abnormal SBP decrease (< 10 mm Hg)	22 (21.78)	6 (18.18)	16 (23.53)	
HR Ratio (HRR)	1.28 (1.2 to 1.42)	1.25 (1.1 to 1.33)	1.29 (1.2 to 1.4)	**0.032**
Normal (> 1.2)	66 (65.35)	18 (54.55)	58 (70.59)	0.124
Abnormal (≤1.2)	35 (34.65)	15 (45.45)	20 (29.41)	

TABLE 4. Other hemodynamic changes in dipyridamole-induced stress

	Scan result			p-value
	Total (n=101)	Abnormal (n=33)	Normal (n=68)	
	Frequency (%); Median (IQR)			
DBP decrease	10 (20 to 10)	20 (20 to 10)	10 (20 to 0)	0.113
Abnormal SBP decrease and/or HRR	50 (49.5)	17 (51.52)	33 (48.53)	0.834
Double Product[i]				
Baseline	9.1 (7.93 to 10.64)	8.58 (7.93 to 10.4)	9.33 (7.92 to 11.05)	0.233
Post-Infusion	10.56 (9.02 to 12.18)	10.22 (8.46 to 11.18)	10.68 (9.2 to 12.84)	**0.044**
Difference	0.99 (-0.15 to 2.46)	0.78 (-0.49 to 1.84)	1.10 (0.03 to 2.75)	0.158
p-value (Baseline vs post-infusion)	**< 0.001**	0.061	**< 0.001**	

[i]Double Product = HR x SBP

TABLE 5. Blood pressure and heart rate before and after dipyridamole infusion

	Scan result			p-value
	Total (n=101)	Abnormal (n=33)	Normal (n=68)	
	Frequency (%); Mean ± SD			
Baseline ECG				
Normal	42 (42.58)	8 (24.24)	34 (50)	**0.018**
Conduction findings	39 (38.61)	14 (42.42)	25 (36.76)	0.665
Infarct findings	12 (11.88)	8 (24.24)	4 (5.88)	**0.017**
Ischemic findings	14 (13.86)	4 (12.12)	10 (14.71)	1.000
Hypertrophy findings	11 (10.89)	6 (18.18)	5 (7.35)	0.170
After Dipyridamole infusion				
ECG No change	88 (87.13)	26 (78.79)	62 (91.18)	0.113
With change	13 (12.87)	7 (21.21)	6 (8.82)	
ST segment depression	6 (46.15)	2 (33.33)	4 (57.14)	0.592
Other changes	7 (53.85)	4 (66.67)	3 (42.86)	

TABLE 6. Myocardial Perfusion Scores

	Frequency (%); Median (IQR)
Description of Defect (n=31)	
Ischemia	16 (51.61)
Infarct	4 (12.9)
Fibrosis	5 (16.13)
SSS	8 (4 to 19)
Normal (< 4)	82 (81.19)
Mild (4-8)	8 (7.92)
Moderate (9-12)	1 (0.99)
Severe (>12)	10 (9.90)
SRS	9 (4 to 16)
Normal (< 4)	88 (87.13)
Mild (4-8)	6 (5.94)
Moderate (9-12)	1 (0.99)
Severe (>12)	6 (5.94)
SDS	7 (3 to 15)
Normal (<2)	85 (84.16)
Mild (2-3)	5 (4.95)
Moderate (4-7)	3 (2.97)
Severe (>8)	8 (7.92)

TABLE 7. Correlation of SBP decrease and HRR to Myocardial Perfusion Scores and Left Ventricle Ejection Fractions

	Correlation coefficient	Level of association	p-value
SBP decrease			
SSS	-0.1426	Indirect weak correlation	0.155
SRS	-0.0988	Indirect weak correlation	0.325
SDS	-0.0605	Indirect weak correlation	0.548
Rest LVEF	0.0624	Direct weak correlation	0.536
Stress LVEF	0.0378	Direct weak correlation	0.707
HRR			
SSS	-0.0906	Indirect weak correlation	0.368
SRS	-0.2650	Indirect weak correlation	**0.007**
SDS	0.0013	Direct weak correlation	0.990
Rest LVEF	0.2591	Direct weak correlation	**0.009**
Stress LVEF	0.2516	Direct weak correlation	**0.011**

For the association of the baseline ECG findings with the myocardial perfusion scores (Tables 9, 10, and 11), the infarct findings showed statistically significant association with the SSS (p-value of < 0.001), SRS (p-value of < 0.001), and SDS (p-value of 0.005); and the normal baseline ECG with SRS (p-value of 0.028).

DISCUSSION

Dipyridamole is a phosphodiesterase enzyme inhibitor that indirectly increases myocardial perfusion by inhibiting the reuptake of endogenous adenosine [8]. Through this mechanism, it provides an alternative form of stress with expected hemodynamic changes which may have a clinical significance.

The hemodynamic changes in the SBP showed no significant difference between the myocardial perfusion scores (SSS, SRS & SDS), stress/rest LVEF, and the eventual scan result. The diastolic blood pressure changes likewise showed no significant difference. These findings were congruent with the study by Ghoobli, et. al. in 2017 wherein abnormal SBP changes are not associated abnormal scan findings and myocardial perfusion scores [2]. It was also noted that the absence of SBP response correlation may be affected by the presence of LV dysfunction in the study population.

The normal (> 1.2) /abnormal (< 1.2) heart rate ratios (HRR) also had no significant difference with the scan results while the median HRR was determined to have had a significant difference. The median HRR for this study was noted to be at 1.28 which is a normal response with a higher ratio of 1.29 for normal results compared to 1.25 for the abnormal results. This implies that a higher HRR or greater increase from the baseline HR is associated with normal scan results, but the cut-off value of 1.2, as previously defined, is uncertain for this study [9]. Though, it has likewise been suggested that further investigations are needed to determine the ideal limits for HR response to vasodilators as previous studies have reported a high number of abnormal HRRs [5, 9]. It has also been stated that reduced HRR to vasodilators is associated with increased risk and as well as an independent predictor of cardiac death [2, 5, 10]. For the myocardial perfusion scores, only the SRS had an indirect correlation with HRR albeit the level of association was weak. The stress and rest LVEF values also showed a direct weak correlation. Overall, the higher HRRs may indicate normal SRS (< 4) and higher stress/rest LVEF values which relates to normal scan results. This provides diagnostic confidence in understanding the effects of the Dipyridamole, particularly its effect on heart rate, wherein a substantial increase from baseline implies a normal myocardial perfusion.

For the double product or rate pressure product, the post-infusion value for the normal and abnormal scan results [10.68 (9.2 to 12.84) vs 10.22 (8.46 to 11.18)] was determined to have had a significant difference. The median post-infusion double product was 10.56 (9.02 to 12.18) for this study. The double product is used as a measure of myocardial oxygen demand and that dipyridamole causes a decrease in iBP and increase in HR which supports the values obtained for this study [11]. A preliminary study likewise had similar findings for post-infusion double product and observed a significant difference for Δ double product [11]. It was noted that the double product is related to sympathetic nervous system activity and decreased parasympathetic nervous system activity for which dipyridamole is not affected.

TABLE 8. Dipyridamole induced stress monitoring

	Scan result			**p-value**
	Total (n=101)	**Abnormal (n=33)**	**Normal (n=68)**	
	Frequency (%); Mean ± SD; Median (IQR)			
Time attained (minutes)				
Lowest SBP decrease	7.07 ± 3.13	7.45 ± 2.84	6.88 ± 3.27	0.392
Peak HR	7.08 ± 2.57	6.56 ± 2.21	8.15 ± 2.94	**0.003**
Symptom during infusion	5.86 ± 2.64	5.66 ± 2.53	6.37 ± 2.91	0.328
Symptom/s during infusion				
Chest heaviness/discomfort	36 (35.64)	10 (30.30)	26 (38.24)	0.510
Light headedness	24 (23.76)	9 (27.27)	15 (22.06)	0.621
Abdominal pain	23 (22.77)	7 (21.21)	16 (23.53)	1.000
Headache	21 (20.79)	6 (18.18)	15 (22.06)	0.796
Dizziness	9 (8.91)	1 (3.03)	8 (11.76)	0.265
SOB	6 (5.94)	1 (3.03)	5 (7.35)	0.661
Others	11 (10.89)	5 (15.15)	6 (8.82)	0.333

Baseline normal and infarct ECG findings showed a significant difference with normal and abnormal scan results, respectively. Myocardial perfusion scores (SSS, SRS, and SDS) correlated with the baseline infarct findings while only the SRS for the baseline normal ECG findings. Although, it should be noted that SDS is used as an index for ischemic burden and the most frequent defect noted for this study population was also ischemia. After dipyridamole infusion, most ECG findings remained unchanged with no significant difference for those 13 patients (12.87%) with only 6 developing the presence of ST segment depression. This is expected since dipyridamole does not induce absolute ischemia in most patients.

In terms of the demographic profile, patients that were younger (56.18 $\pm$ 16.03) had abnormal scan results. This suggests that these patients may have developed comorbidities earlier, hence the abnormal scan results. It should also be noted that these patients were preferably requested to undergo a dipyridamole induced stress rather than exercise; and are being considered for suspected CAD, which suggests a higher risk profile. Males were also noted to have an abnormal scan result, likely due to the greater influence of common factors (age, hypertension, etc.) than women thus the greater risk of cardiovascular disease [12, 13].

Another finding noted to be significant was the time (minutes) to reach the maximal HR upon dipyridamole infusion which was longer for those with normal scan results (8.15 $\pm$ 2.94 vs. 6.56 $\pm$ 2.21). This implies that a longer and possibly sustained increase in the HR may indicate a better HRR which would be congruent with a normal scan result as previously noted.

This retrospective study is limited as a single-center study referred to our institution for patients with suspected CAD. Cardiac autonomic dysfunction was also not confirmed which may help in understanding abnormal hemodynamic response.

CONCLUSION

In patients with suspected CAD who undergo a dipyridamole-induced stress myocardial perfusion scintigraphy –Tc-99m Sestamibi, the higher HRRs and baseline 12-L ECG (normal and infarct) findings, relates with the expected scan results. This implies that higher HRRs and normal baseline ECG finding are associated with normal scan results, and baseline infarct findings relate with abnormal scan results. The higher HRRs were also associated with the higher stress/rest LVEF and normal SRS, which supports a normal scan result .

However, there was no significant association for the blood pressure responses and post-infusion 12-L ECGs with any of the scan findings/results. Overall, the results may guide the clinician and reader in the study interpretation, thereby increasing diagnostic confidence and having a clearer understanding of the hemodynamic effects of Dipyridamole, especially in equivocal findings.

DECLARATIONS

The authors declare no conflicts of interest, financial or otherwise.

Acknowledgement

I would like to express gratitude to the consultants, co-residents, and staff of the Division of Nuclear Medicine, Philippine Heart Center for their unwavering support of this endeavor.

REFERENCES

1. Sison, J., Divinagracia, R., & Nailes, J. (2020). Asian management of hypertension: Current status, home blood pressure, and specific concerns in Philippines (a country report). Journal of clinical hypertension (Greenwich, Conn.), 22(3), 504–507. https://doi.org/10.1111/jch.13802.
2. Gholoobi, A., Ayati, N., Baghyari, A., Mouhebati, M., Atar, B., & Dabbagh Kakhki, V. R. (2017). Relationship between gated myocardial perfusion SPECT findings and hemodynamic, electrocardiographic, and heart rate changes after Dipyridamole infusion. The international journal of cardiovascular imaging, 33(6), 951–956. https://doi.org/10.1007/s10554-017-1074-6.
3. Ogilby, J. D., Kegel, J. G., Heo, J., & Iskandrian, A. E. (1998). Correlation between hemodynamic changes and tomographic sestamibi imaging during dipyridamole-induced coronary hyperemia. Journal of the American College of Cardiology, 31(1), 75–82. https://doi.org/10.1016/s0735-1097(97)00448-8.
4. Javadi, H., Shariati, M., Mogharrabi, M., Asli, I. N., Jallalat, S., Hooman, A., Seyedabadi, M., & Assadi, M. (2010). The association of dipyridamole side effects with hemodynamic parameters, ECG findings, and scintigraphy outcomes. Journal of nuclear medicine technology, 38(3), 149–152. https://doi.org/10.2967/jnmt.109.072629.
5. Gorur, G. D., Ciftci, E. A., Kozdag, G., Isgoren, S., Oc, M. A., Haksal, C., Gur, M., & Demir, H. (2012). Reduced heart rate response to dipyridamole in patients undergoing myocardial perfusion SPECT. Annals of nuclear medicine, 26(8), 609–615. https://doi.org/10.1007/s12149-012-0618-z.

TABLE 9. Association of Baseline ECG findings and SSS

Baseline ECG	Normal (n=82)	Mild (n=8)	Moderate (n=1)	Severe (n=10)	p-value
	Frequency (%)				
Normal	39 (47.56)	1 (12.5)	0	2 (20)	0.066
Infarct findings	5 (7.58)	1 (12.5)	1 (100)	5 (50)	**< 0.001**
Ischemic findings	12 (14.63)	1 (12.5)	0	1 (10)	1.000
Hypertrophy findings	8 (9.76)	0	1 (100)	2 (20)	0.073
Conduction findings	30 (36.59)	6 (75)	0	3 (30)	0.124

TABLE 10. Association of Baseline ECG findings and SRS

Baseline ECG	Normal (n=88)	Mild (n=6)	Moderate (n=1)	Severe (n=6)	p-value
	Frequency (%)				
Normal	41 (46.59)	0	0	1 (16.67)	**0.028**
Infarct findings	6 (6.82)	1 (16.67)	1 (100)	4 (66.67)	**< 0.001**
Ischemic findings	12 (13.64)	1 (16.67)	0	1 (16.67)	1.000
Hypertrophy findings	9 (10.23)	0	0	2 (33.33)	0.328
Conduction findings	33 (37.5)	5 (83.33)	0	1 (16.67)	0.054

TABLE 11. Association of Baseline ECG findings and SDS

Baseline ECG	Normal (n=85)	Mild (n=5)	Moderate (n=3)	Severe (n=8)	p-value
	Frequency (%)				
Normal	37 (43.53)	2 (40)	1 (33.33)	2 (25)	0.856
Infarct findings	6 (7.06)	1 (20)	1 (33.33)	4 (50)	**0.005**
Ischemic findings	14 (16.47)	0	0	0	0.782
Hypertrophy findings	8 (9.41)	1 (20)	1 (33.33)	1 (12.5)	0.231
Conduction findings	34 (40)	1 (20)	1 (33.33)	3 (37.5)	0.918

6. Mishra, R. K., Dorbala, S., Logsetty, G., Hassan, A., Heinonen, T., Schelbert, H. R., Di Carli, M. F., & RAMPART investigators (2005). Quantitative relation between hemodynamic changes during intravenous adenosine infusion and the magnitude of coronary hyperemia: implications for myocardial perfusion imaging. Journal of the American College of Cardiology, 45(4), 553–558. https://doi.org/10.1016/j.jacc.2004.10.064.
7. Hatutale, A., Vorster, M., Ankrah, A. O., Rheeder, P., & Sathekge, M. M. (2013). Association of hemodynamic response during dipyridamole stress testing with 99mTc-MIBI SPET myocardial perfusion image findings. Hellenic journal of nuclear medicine, 16(3), 181–185. https://doi.org/10.1967/s002449910096.
8. Gupta A, Samarany S. Dipyridamole Nuclear Stress Test. [Updated 2023 Jul 10]. In: StatPearls [Internet]. Treasure Island (FL): StatPearls Publishing; 2023 Jan-.[cited 2022 Oct] Available from: https://www.ncbi.nlm.nih.gov/books/NBK544321/.
9. Mathur, S., Shah, A. R., Ahlberg, A. W., Katten, D. M., & Heller, G. V. (2010). Blunted heart rate response as a predictor of cardiac death in patients undergoing vasodilator stress technetium-99m sestamibi gated SPECT myocardial perfusion imaging. Journal of nuclear cardiology : official publication of the American Society of Nuclear Cardiology, 17(4), 617–624. https://doi.org/10.1007/s12350-010-9242-2.
10. Bhatheja, R., Francis, G. S., Pothier, C. E., & Lauer, M. S. (2005). Heart rate response during dipyridamole stress as a predictor of mortality in patients with normal myocardial perfusion and normal electrocardiograms. The American journal of cardiology, 95(10), 1159–1164. https://doi.org/10.1016/j.amjcard.2005.01.042.
11. Ansari, M., Javadi, H., Pourbehi, M., Mogharrabi, M., Rayzan, M., Semnani, S., Jallalat, S., Amini, A., Abbaszadeh, M., Barekat, M., Nabipour, I., & Assadi, M. (2012). The association of rate pressure product (RPP) and myocardial perfusion imaging (MPI) findings: a preliminary study. Perfusion, 27(3), 207–213. https://doi.org/10.1177/0267659112436631.
12. Galiuto L, Locorotondo G. Gender differences in cardiovascular disease. J. Integr. Cardiol. 2015;1(1):20-2. doi: 10.15761/JIC.1000107.
13. Gao Z, Chen Z, Sun A, Deng X. Gender differences in cardiovascular disease. Medicine in Novel Technology and Devices. 2019 Dec 1;4:100025. doi.org/10.1016/j.medntd.2019.100025.

Prevalence and Clinical Profile of Osteoporosis Based on Central Bone Densitometry Among Filipinos Seen in a Tertiary Medical Institution: A Cross-Sectional Study

Charles Dale T. Solis, MD, Patrick Earl A. Fernando, MD

Department of Nuclear Medicine and Theranostics, St. Luke's Medical Center- Global City
E-mail address: charlesdalesolis@gmail.com

ABSTRACT

Background:

Osteoporosis, a severe metabolic bone disease, is a common cause of fragility fractures, disability, and reduced quality of life. Dual-energy X-ray absorptiometry (DXA) is widely recognized as the most reliable standard for diagnosing osteoporosis; however, few local data sets describe the prevalence and clinical characteristics of Filipino patients undergoing central bone densitometry. Most Philippine research uses historical populations or easily available data sets, underscoring the need for more current, institution-based information. The large DXA case load at St. Luke's Medical Center – Global City, which performs over 3,000 scans annually, highlights the value of generating local data from high-volume tertiary centers.

Objective:

To determine the prevalence of osteoporosis based on central DXA results in Filipino adults and to describe their clinico-demographic characteristics).

Methodology:

This analytic cross-sectional study included 244 Filipino patients who underwent DXA scanning at St. Luke's Medical Center – Global City from February to July 2025. Data on age, sex, comorbidities, dietary calcium intake, physical activity, caffeine intake, smoking, alcohol use, medication history, and family history of osteoporosis were obtained using an institutionally approved DXA questionnaire. DXA results were classified as normal, osteopenia, osteoporosis, or severe osteoporosis according to World Health Organization guidelines. Descriptive statistics summarized patient parameters. Chi-square and Fisher's exact tests were used to assess associations between risk factors and DXA classifications.

Results:

Most participants were women (92.6%) and were 51–65 years old (63.5%) The most common comorbidities were hypertension (27.9%) and diabetes (15.6%). According on DXA report, 49.6% had osteoporosis, 39.8% had osteopenia, 7.8% had normal bone mineral density, and 2.9% had severe osteoporosis. A statistically significant association was found between age group and DXA result ($p = 0.013$). Other factors—including sex, comorbidities, daily calcium intake, physical activity, caffeine intake, smoking, alcohol use, and family history of osteoporosis—were not significantly associated with bone density classification.

Conclusion:

Osteoporosis is highly prevalent in this cohort study, with almost 90% of patients had low bone mineral density, manifested as osteopenia (39.8%) or osteoporosis (49.6%). Among the examined variables, age was the only one significantly associated with the BMD classification, confirming the known impact of aging on bone deterioration. No significant associations with other clinical and lifestyle factors were found, reflecting a complex and multifactorial etiology of osteoporosis. These data confirm that routine performance of DXA screening, especially in the elderly and postmenopausal women, should be promoted in order to allow early detection, risk stratification, and intervention.

Keywords*: osteoporosis, dual-energy X-ray absorptiometry, bone mineral density, Filipino adults, prevalence, clinical profile*

INTRODUCTION

Osteoporosis is a metabolic bone disorder characterized by porous and brittle bones that are more vulnerable to low-impact trauma and falls. It can affect both men and women across all age groups and ethnicities, though it is more prevalent among older adults, particularly postmenopausal women. Osteoporosis is a major public health concern because it can lead to fractures of the hip, spine, and distal forearm, which in turn result in loss of independence, disability, decreased quality of life, and even death. One in three females and at least one in five males over the age of 50 may suffer from fractures related to osteoporosis. Multiple factors contribute to increased fracture risk in patients with osteoporosis. These include hormonal influences, use of medications such as glucocorticoids, smoking, inadequate calcium and vitamin D intake, physical inactivity, small body size, and family history of skeletal disorders [1]. Assessing the prevalence and clinical profile of patients with osteoporosis is therefore a crucial first step in addressing this condition. Through better understanding of these characteristics, clinicians can coordinate with primary care physicians to design effective interventions, management strategies, and treatment protocols.

In the Philippines, the number of studies describing the prevalence and clinical profile of osteoporosis is limited, particularly those using DXA—also known as central bone densitometry—as the diagnostic tool. Available studies have focused on specific subgroups or relied on older population-based data, highlighting the need for updated information using contemporary cohorts [2 – 9]. St. Luke's Medical Center – Global City performs more than 3,000 DXA scans annually, providing a valuable opportunity to generate institutional data that may approximate the local Filipino demographic seeking care in a tertiary medical center.

Dual-energy X-ray absorptiometry is a well-established method for assessing body composition and bone mineral density. It uses attenuation of X-ray beams at two different energies to distinguish between tissues with different mass attenuation coefficients and is considered the gold standard for diagnosing osteoporosis [2,3]. According to the World Health Organization (WHO) criteria, osteoporosis is diagnosed when the T-score is ≤ –2.5 in postmenopausal women and men aged 50 years or older, based on bone mineral density measures at the posteroanterior lumbar spine (L1–L4) and hip (femoral neck or total hip, whichever is lower) [4].

Globally, osteoporosis is highly prevalent. An estimated 200 million people are affected, and approximately 9 million fractures occur each year as a consequence of this condition [9]. Osteoporosis-related fractures—particularly of the wrist, spine, and hip—are associated with substantial morbidity, functional impairment, and increased mortality, as well as significant socioeconomic burden for patients, families, and health systems [10–13]. In the United States, for example, hip fractures can increase mortality by 10–20%, and up to 70% of survivors experience persistent disability [11,12].

OBJECTIVES

General Objective

To determine the prevalence and clinical profile of osteoporosis among Filipinos based on central dual energy Xray absorptiometry (DXA) scan done in St. Luke's Medical Center – Global City from February to July 2025.

Specific Objectives

1. To describe the clinico-demographic characteristics of Filipino adults who underwent central DXA scanning during the study period, specifically according to:
   i. Age group distribution (19–35, 36–50, 51–65, 66 – 75, 76–85, and >86 years)
   ii. Sex
   iii. Presence of comorbidities (e.g., hypertension, diabetes mellitus, hyperthyroidism, hypercortisolism, hyperparathyroidism, chronic kidney disease, hypogonadism, low testosterone, early menopause)
   iv. Medication history (e.g., glucocorticoids, thyroid medications, hormone-related therapies)
   v. Dietary calcium intake (low vs. adequate)
   vi. Physical activity level (low, moderate, high)
   vii. Lifestyle habits, including caffeine intake, smoking, and alcohol consumption
   viii. Family history of osteoporosis

2. To determine the proportion of patients with severe osteoporosis among those diagnosed with osteoporosis based on central DXA findings.

3. To determine the association between DXA classification (normal, osteopenia, osteoporosis, severe osteoporosis) and the following risk factors: age, sex, comorbidities, medication history, dietary calcium intake, physical activity level, caffeine intake smoking history, alcohol intake, family history of osteoporosis

METHODOLOGY

Study Design, Setting, and Population

This analytic cross-sectional study included Filipino adult patients who underwent central dual-energy X-ray absorptiometry scanning at the Department of Nuclear Medicine and Theranostics, St. Luke's Medical Center – Global City, from February to July 2025.

Inclusion Criteria

Patients were eligible if they:

1. provided informed consent;
2. were Filipino;
3. were Filipino males aged ≥50 years, or women who were postmenopausal or in the menopausal transition regardless of age; and
4. had a DXA scan performed at St. Luke's Medical Center – Global City between February and July 2025.

Exclusion Criteria

Patients were excluded if they:

1. were pregnant; or
2. were pediatric patients

OPERATIONAL DEFINITION OF TERMS

The following terms were provided with their operational definitions. The definitions listed were based on how these terms were used in the study, and the terms were arranged alphabetically.

Central Bone Densitometry: This refers to the diagnosis of osteoporosis based on the bone mineral densities of the regions of interest in the lumbar spine, total hip, or femoral neck.

Clinico-Demographic Profile: This referred to the baseline data of patients with osteoporosis. This included their age, sex, presence of comorbidities, history of medications, dietary intake, history of caffeine intake, smoking and drinking habits, and family history of osteoporosis.

Department of Nuclear Medicine and Theranostics - St. Luke's Medical Center – Global City: This was the declared research locale where actual cases of osteoporosis were obtained. This served as the main locale of data collection.

Dual Energy X-ray Absorptiometry (DXA): This was also known as central bone densitometry. This instrument used minute doses of ionizing radiation to produce images of the bone to diagnose osteoporosis. It was a simple, fast, and non-invasive tool for diagnosing osteoporosis.

Normal Bone Mineral Density: Defined as by bone mineral density (BMD) of T-scores equal to or greater than -1.0 standard deviations (SD) in postmenopausal women and men aged 50 and older.

Low Bone Mass (Osteopenia): This is defined by bone mineral density (BMD) T-scores between -1.0 and -2.5 standard deviations (SD) in BMD of postmenopausal women and men aged 50 and older.

Osteoporosis: This is the main condition of patients who will be included in the analysis. This refers to a bone disease that develops due to the decrease in the bone mineral and mass. Defined as a BMD T-score of -2.5 standard deviations (SD) or less below the lumbar spine, total hip, or femoral neck mean BMD in postmenopausal women and men aged 50 and older.

Severe or Established Osteoporosis: Clinically, severe osteoporosis may refer to cases where the T-score is significantly lower than -2.5 SD, with one or more past fractures due to osteoporosis.

Low or adequate calcium intake: Adults aged 19 to 50 are considered to have low calcium intake if they consume approximately less than 750 mg daily. For those aged above 50, intake is considered low if it falls below 800 mg per day.

Caffeine intake: Categorized into three levels based on daily consumption: low intake of less than or equal to three cups, moderate intake of four cups, and high intake of more than 4 cups

Smoking: Smoking is assessed in pack-years by multiplying the total years smoked by the number of packs per day. Smokers are classified into never smokers (0.0 pack-years), light smokers (0.1-20.0 pack-years), moderate smokers (20.1-40.0 pack-years), and heavy smokers (>40 pack-years). Current smokers are those who are currently smoking. Previous smokers are categorized based on smoking duration and time since quitting; short-term smokers are those with history of smoking of less than five years and cessation of more than one year, while long- term smokers have a smoking history of five or more years and cessation of six or more years.

Physical activity: Classified into three levels: Low, Moderate, and High. The Low category includes individuals who do not meet the criteria for moderate or high activity levels. Moderate activity is defined by meeting at least one of these criteria: engaging in vigorous activity for 20 minutes on 3 or more days, moderate activity or walking for 30 minutes on 5 or more days, or a combination of activities totaling sufficient exercise over the week. The High category is reached by either performing vigorous activity on 3 days or combining different activities across 7 days to achieve a substantial total of physical exertion.

Menopausal transition or Perimenopause: The period when women experience hormonal changes leading to menopause. It typically starts in the 40s but can vary due to genetics, lifestyle, or health factors.

DESCRIPTION OF STUDY PROCEDURES

As soon as permission was granted, the investigator began coordinating with the Nuclear Medicine Department to attach the research questionnaire and consent form in addition to the standard form used by the institution. Only those who affixed their signatures on the consent form were recruited into the study. Subjects were asked if proper preparations had been followed, such as the avoidance of calcium supplements for 24 hours. The subjects should have had no barium study or any CT scan with contrast a week before the DXA procedure. Subjects were asked to change into a hospital gown and to remove their shoes and accessories. Once enrolled, participants received an additional questionnaire to collect supplementary data not covered in the institutional DXA questionnaire, such as information on diabetes mellitus and chronic kidney disease, both of which could decrease BMD. The technician assisted the subjects in lying supine on the machine. Images of the hips and spine were acquired using a GE Lunar iDXA machine. The technologist processed the images using the vendor-provided software. All DXA scans were interpreted and qualified independently by two board-certified Nuclear Medicine physicians to ensure accuracy and consistency of the results. Once all medical charts were collected and reviewed, the researcher gathered the clinico-demographic profiles of the patients. This included their age, sex, presence of comorbidities, history of medications, dietary intake, caffeine intake history, smoking and drinking habits, and family history of osteoporosis. After these had been obtained, the main proponent determined the prevalence and risk factors for osteoporosis based on the dual-energy X-ray absorptiometry (DXA) findings. Patients were categorized according to normal bone density, osteopenia, osteoporosis, or severe osteoporosis, as well as their clinico-demographic profiles. The data were scored, tabulated, and subjected to statistical analysis (see Figure 1).

Type of Study, Time Period, and Target Population

This analytic cross-sectional study involved patients who underwent central dual-energy X-ray absorptiometry (DXA) scanning at St. Luke's Medical Center – Global City from February to July 2025.

Description of Outcome Measures

Assessment of bone mineral densities in the spine and bilateral hips.

Normal	≥ -1 SD
Osteopenia	Between -1 and -2.5 SD
Osteoporosis	≤ -2.5 SD
Severe osteoporosis	≤ -2.5 SD and ≥ 1 fragility fracture/s

Sampling Estimation

In the investigation that was conducted, the researcher covered patients diagnosed with osteoporosis using a DXA scan. In the institution where the data were collected, a monthly census of around 150 patients was encountered. Using this sampling technique, the presumed total number was recruited in this investigation, which was conducted within the study duration of February to July 2025. To compute the sample size, the researcher employed the proportion sampling technique. The formula is presented below:

$$n = \frac{DEFF \times N \times p(1-p)}{(d^2 / Z^2_{1-\alpha/2})(N-1) + p(1-p)}$$

Based on the formula presented above, the researcher set the design effect for the cluster survey at 1.0 with a 50% anticipated frequency. The confidence level was set at 95% with a 5% margin of error. Utilizing these values, only 244 participants were needed for the study. Once the total number of patients had been collected, the researcher stopped the data collection.

Statistical Treatment of Data

The researcher utilized Microsoft Excel version 2010 for the initial encoding of data. After this was completed, the investigator used the Statistical Package for the Social Sciences (SPSS) version 23 for Macintosh. The following statistical analyses were performed: (1) Frequency, percentage, and distribution were used to determine the significant association between the clinico-demographic profiles of patients and the prevalence of osteoporosis based on the dual-energy X-ray absorptiometry (DXA) scans performed at St. Luke's Medical Center – Global City from February to July 2025, (2) Chi-square and Fisher's Exact tests were used to determine the significant association between the prevalence of osteoporosis and the clinico-demographic profiles of patients.

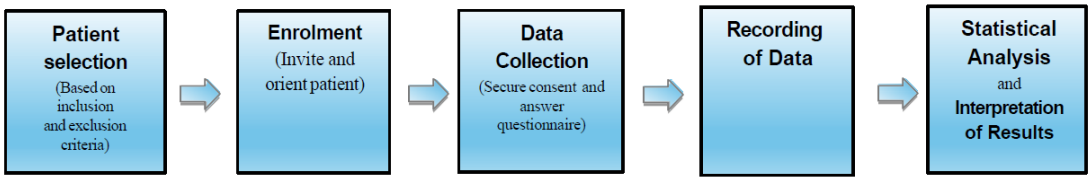

FIGURE 1 Study Schematic Diagram

RESULTS

Clinicodemographic Profile of Patients

Table 1 presents the clinicodemographic profile of 244 patients who underwent dual energy X-ray absorptiometry (DXA) at the Department of Nuclear Medicine and Theranostics, St. Luke's Medical Center – Global City. The majority of patients were aged 51 to 65 years (63.5%), followed by those aged 66 to 75 years (23.8%), while only a small proportion were older than 85 years (1.2%). Most of the participants were females (92.6%), with males comprising only 7.4% of the study population.

With regard to comorbidities, hypertension (27.9%) and diabetes mellitus (15.6%) were the most commonly reported, followed by hyperthyroidism (10.2%) and early menopause (14.3%). Other less frequent comorbidities included low testosterone (3.3%), chronic kidney disease (0.8%), hypercortisolism (0.8%), hyperparathyroidism (0.4%), and hypogonadism (0.4%).

More than half of the patients reported an adequate dietary calcium intake (53.7%), while 46.3% had low calcium intake. In terms of physical activity, moderate activity (52.5%) was the most common, followed by low activity (45.1%), and only 2.5% reported high activity levels. The majority did not consume caffeine (95.5%), did not smoke (96.7%), and did not drink alcohol (90.2%). Finally, 11.5% of participants had a family history of osteoporosis, while 88.5% reported none.

Prevalence of Osteoporosis Based on DXA Results

Table 2 presents the distribution of patients according to their dual energy X-ray absorptiometry (DXA) results. Out of the 244 patients assessed, 121 (49.6%) were classified as having osteoporosis, while 97 (39.8%) were found to have osteopenia. A smaller proportion, 19 patients (7.8%), exhibited normal bone mineral density, and only 7 patients (2.9%) were diagnosed with severe osteoporosis.

Association Between DXA Result and Demographic Factors

Table 3 shows the relationship between DXA results and the demographic characteristics of the patients. A statistically significant association was observed between age group and DXA result ($\chi^2 = 25.40$, $p = 0.013$), indicating that bone mineral density classification varied across different age categories. In contrast, sex was not significantly associated with DXA result ($\chi^2 = 5.61$, $p = 0.132$).

Association Between DXA Result and Clinical and Lifestyle Factors

Table 4 presents the relationship between DXA results and various clinical and lifestyle factors among the 244 patients included in the study. None of the evaluated variables showed a statistically significant association with DXA result, as all corresponding p-values were greater than 0.05.

Specifically, comorbid conditions such as hypertension ($p = 0.921$), diabetes mellitus ($p = 0.583$), hyperthyroidism ($p = 0.880$), and chronic kidney disease ($p = 0.562$) were not significantly related to bone density classifications. Similarly, hormonal and endocrine-related factors, including hypercortisolism ($p = 0.562$), hyperparathyroidism ($p = 0.796$), hypogonadism ($p = 0.796$), low testosterone ($p = 0.203$), early menopause ($p = 0.745$), and thyroid hormone medication ($p = 0.624$), did not demonstrate significant associations.

Lifestyle factors such as dietary calcium intake ($p = 0.375$), physical activity ($p = 0.552$), caffeine intake ($p = 0.488$), smoking ($p = 0.817$), drinking ($p = 0.140$), and family history of osteoporosis ($p = 0.434$) also showed no significant associations with DXA outcomes.

DISCUSSION

This study evaluated the clinicodemographic characteristics, prevalence, and associated factors of osteoporosis among adult patients who underwent dual energy X-ray absorptiometry (DXA) at St. Luke's Medical Center – Global City. The results showed that most patients were middle-aged to older adults, predominantly female, with common comorbidities such as hypertension, diabetes mellitus, and hyperthyroidism. Most participants reported adequate calcium intake and moderate physical activity, while only a small proportion had a family history of osteoporosis. These findings are consistent with established epidemiologic evidence showing that aging and female sex are the strongest nonmodifiable risk factors for osteoporosis, as both contribute significantly to bone mineral density (BMD) decline and fracture susceptibility [15].

The age distribution of patients revealed that most were between 51 and 65 years (63.5%), followed by those aged 66 to 75 years (23.8%). This reflects the well-documented acceleration of bone loss during the postmenopausal years as estrogen levels decline [14]. Estrogen helps regulate bone remodeling by suppressing bone resorption, and its deficiency leads to increased

TABLE 1. Clinicodemographic Profile of Patients with Osteoporosis Based on Dual Energy X-ray Absorptiometry (DXA) (n = 244)

Variable	Category	Frequency (Percentage %)
Age Group	36 - 50	15 (6.1)
	51 - 65	155 (63.5)
	66 - 75	58 (23.8)
	76 - 85	13 (5.3)
	> 86	3 (1.2)
Sex	Females	226 (92.6)
	Males	18 (7.4)
Co-morbidities	Hypertension	68 (27.9)
	Diabetes Mellitus	38 (15.6)
	Hyperthyroidism	25 (10.2)
	Hypercortisolism	2 (0.8)
	Hyperparathyroidism	1 (0.4)
	Hypogonadism	1 (0.4)
	Low Testosterone	8 (3.3)
	Early Menopause	35 (14.3)
	Chronic Kidney Disease	2 (0.8)
Dietary Calcium	Adequate	131 (53.7)
	Low	113 (46.3)
Physical Activity	Low	110 (45.1)
	Moderate	128 (52.5)
	High	6 (2.5)
Caffeine Intake	Yes	11 (4.5)
	No	233 (95.5)
Smoking	Yes	8 (3.3)
	No	236 (96.7)
Drinking Alcohol	Yes	24 (9.8)
	No	220 (90.2)
Family History of Osteoporosis	Yes	28 (11.5)
	No	216 (88.5)

TABLE 2. Prevalence of Patients with Osteoporosis Based on Dual Energy X-ray Absorptiometry (DXA) (n = 244)

DXA Result	Frequency (Percentage %)
Normal Bone Density	19 (7.8)
Osteopenia	97 (39.8)
Osteoporosis	121 (49.6)
Severe Osteoporosis	7 (2.9)
Total	**244**

TABLE 3. Association Between DXA Result and Demographic Factors (n = 244)

Variable	χ^2	df	p-value
Age Group	25.40	12	**0.013**
Sex	5.61	3	0.132

TABLE 4. Association Between DXA Result and Clinical and Lifestyle Factors (n = 244)

Variable	χ^2	df	p-value
Hypertension	0.49	3	0.921
Diabetes Mellitus	1.95	3	0.583
Hyperthyroidism	0.67	3	0.880
Hypercortisolism	2.05	3	0.562
Hyperparathyroidism	1.02	3	0.796
Hypogonadism	1.02	3	0.796
Low Testosterone	4.61	3	0.203
Early Menopause	1.23	3	0.745
Chronic Kidney Disease	2.05	3	0.562
Dietary Calcium Intake	3.11	3	0.375
Thyroid Hormone Medication	1.76	3	0.624
Physical Activity	4.93	6	0.552
Caffeine Intake	2.43	3	0.488
Smoking	0.94	3	0.817
Drinking Alcohol	5.48	3	0.140
Family History of Osteoporosis	2.74	3	0.434

osteoclastic activity and rapid bone loss [15]. The predominance of female patients (92.6%) also mirrors global trends, where osteoporosis affects women more frequently due to hormonal changes associated with menopause [1,14]. The smaller proportion of male patients in this study may also reflect underdiagnosis or under-screening, as osteoporosis in men often remains unrecognized until a fracture occurs [14].

Hypertension (27.9%), diabetes mellitus (15.6%), and hyperthyroidism (10.2%) were the most frequent comorbidities observed. These conditions have previously been linked to alterations in bone metabolism and mineral regulation [14]. Diabetes mellitus has been associated with both impaired bone formation and increased fracture risk due to oxidative stress and microvascular changes that impair bone quality [14]. Similarly, hyperthyroidism increases bone turnover, leading to cortical bone loss when thyroid hormone levels are inadequately controlled [14,16]. Despite these known mechanisms, the current study found no statistically significant association between these comorbidities and DXA classification. This may be attributed to the limited number of patients per category or adequate medical control of their conditions.

In terms of nutritional and lifestyle habits, 53.7% of patients reported adequate dietary calcium intake, while 46.3% had low intake. Calcium plays a vital role in maintaining bone mineralization, and insufficient intake has been associated with secondary hyperparathyroidism and increased bone resorption [9]. However, no significant association was found between calcium intake and DXA results. This suggests that while dietary calcium is important, it is not the sole determinant of bone mass. Other factors such as vitamin D status, genetics, and hormonal influences may have contributed more prominently to bone density outcomes [14]. The majority of patients (52.5%) reported moderate physical activity, which aligns with recommendations that regular weight-bearing exercise helps preserve bone strength and reduce fracture risk. Nevertheless, no significant relationship was found between activity level and DXA result, which could be related to differences in exercise type, intensity, or self-reporting accuracy.

The prevalence analysis revealed that 49.6% of patients had osteoporosis and 39.8% had osteopenia, with only 7.8% having normal bone density. This indicates that nearly nine in ten patients exhibited reduced bone mass. The prevalence observed in this study is higher than global estimates, which report osteoporosis prevalence of around 22% among postmenopausal women and 6% among men [4]. The higher proportion may reflect a referral bias, since patients undergoing DXA are often those already suspected of having low bone density or at risk for fractures. Nonetheless, this finding emphasizes the significant burden of osteoporosis in the Filipino population and the importance of early detection [5].

Among demographic factors, only age showed a statistically significant association with DXA result ($p = 0.013$). This finding reinforces the established relationship between aging and bone loss, as bone mass peaks in early adulthood and declines progressively due to reduced osteoblastic activity and increased resorption [15]. In contrast, sex did not exhibit a significant association with DXA classification, likely because nearly all participants were female, reducing variability. Similarly, comorbidities, medication use, calcium intake, lifestyle behaviors, and family history of osteoporosis did not demonstrate significant associations. Although smoking and alcohol use are recognized risk factors for bone loss, the very low prevalence of these habits in the sample (3.3% and 9.8%, respectively) likely limited statistical power [9,14].

The absence of significant associations for most clinical and lifestyle variables highlights the multifactorial nature of osteoporosis. Bone health is determined by complex interactions among genetic, hormonal, metabolic, nutritional, and environmental factors [14,15]. In this study, the lack of significant associations may also be influenced by unmeasured confounding variables such as medication use, vitamin D levels, or duration of exposure to risk factors. Pharmacologic management of chronic conditions may have also mitigated their impact on bone metabolism.

CONCLUSION

This study demonstrated that osteoporosis is highly prevalent among adult patients who underwent dual energy X-ray absorptiometry (DXA) at St. Luke's Medical Center – Global City, with nearly half diagnosed with osteoporosis and another substantial proportion exhibiting osteopenia. The findings revealed that the majority of affected individuals were middle-aged to older females, reflecting the established demographic trends in osteoporosis. Among all examined variables, only age showed a statistically significant association with DXA results, underscoring the strong influence of aging on bone mineral density. Other factors such as comorbidities, dietary calcium intake, physical activity, caffeine consumption, smoking, drinking, and family history did not demonstrate significant associations. These results highlight the need for continued attention to early detection and prevention of bone density loss, particularly in postmenopausal women and older adults.

Recommendations

Based on the findings, regular osteoporosis screening through DXA should be encouraged for women aged 50 years and older, and for men with identifiable risk factors. Health promotion programs should emphasize maintaining adequate calcium and vitamin D intake, engaging in regular weight-bearing exercise, and minimizing modifiable risk factors such as smoking and excessive alcohol consumption. Clinicians are encouraged to incorporate osteoporosis risk assessment into routine clinical evaluations, especially for patients with chronic diseases or those on long-term medications that may affect bone metabolism. Future research should include a larger and more diverse population, account for additional biochemical and hormonal parameters, and assess the long-term effects of lifestyle interventions and pharmacologic management on bone health outcomes.

DECLARATIONS

The authors declare no conflicts of interest, financial or otherwise.

REFERENCES

1. Lane N. E. (2006). Epidemiology, etiology, and diagnosis of osteoporosis. American journal of obstetrics and gynecology, 194(2 Suppl), S3–S11. https://doi.org/10.1016/j.ajog.2005.08.047.
2. Ellis K. J. (2000). Human body composition: in vivo methods. Physiological reviews, 80(2), 649–680. https://doi.org/10.1152/physrev.2000.80.2.649.
3. Laskey M. A. (1996). Dual-energy X-ray absorptiometry and body composition. Nutrition (Burbank, Los Angeles County, Calif.), 12(1), 45–51. https://doi.org/10.1016/0899-9007(95)00017-8.
4. Willers, C., Norton, N., Harvey, N. C., Jacobson, T., Johansson, H., Lorentzon, M., McCloskey, E. V., Borgström, F., Kanis, J. A., & SCOPE review panel of the IOF (2022). Osteoporosis in Europe: a compendium of country-specific reports. Archives of osteoporosis, 17(1), 23. https://doi.org/10.1007/s11657-021-00969-8.
5. International Osteoporosis Foundation. Facts and statistics. Available from: https://www.osteoporosis.foundation/factsstatistics#category-23
6. Burge, R., Dawson-Hughes, B., Solomon, D. H., Wong, J. B., King, A., & Tosteson, A. (2007). Incidence and economic burden of osteoporosis-related fractures in the United States, 2005-2025. Journal of bone and mineral research : the official journal of the American Society for Bone and Mineral Research, 22(3), 465–475. https://doi.org/10.1359/jbmr.061113.
7. Crabtree, N. J., Shaw, N. J., Bishop, N. J., Adams, J. E., Mughal, M. Z., Arundel, P., Fewtrell, M. S., Ahmed, S. F., Treadgold, L. A., Högler, W., Bebbington, N. A., Ward, K. A., & ALPHABET Study Team (2017). Amalgamated Reference Data for Size-Adjusted Bone Densitometry Measurements in 3598 Children and Young Adults-the ALPHABET Study. Journal of bone and mineral research : the official journal of the American Society for Bone and Mineral Research, 32(1), 172–180. https://doi.org/10.1002/jbmr.2935.
8. Lukaski H. C. (1993). Soft tissue composition and bone mineral status: evaluation by dual-energy X-ray absorptiometry. The Journal of nutrition, 123(2 Suppl), 438–443.
9. Pisani, P., Renna, M. D., Conversano, F., Casciaro, E., Di Paola, M., Quarta, E., Muratore, M., & Casciaro, S. (2016). Major osteoporotic fragility fractures: Risk factor updates and societal impact. World journal of orthopedics, 7(3), 171–181. https://doi.org/10.5312/wjo.v7.i3.171.
10. Bonjour, J. P., Ammann, P., & Rizzoli, R. (1999). Importance of preclinical studies in the development of drugs for treatment of osteoporosis: a review related to the 1998 WHO guidelines. Osteoporosis international : a journal established as result of cooperation between the European Foundation for Osteoporosis and the National Osteoporosis Foundation of the USA, 9(5), 379–393. https://doi.org/10.1007/s001980050161.
11. Warriner, A. H., Patkar, N. M., Curtis, J. R., Delzell, E., Gary, L., Kilgore, M., & Saag, K. (2011). Which fractures are most attributable to osteoporosis?. Journal of clinical epidemiology, 64(1), 46–53. https://doi.org/10.1016/j.jclinepi.2010.07.007.
12. Forte, M. L., Virnig, B. A., Swiontkowski, M. F., Bhandari, M., Feldman, R., Eberly, L. E., & Kane, R. L. (2010). Ninety-day mortality after intertrochanteric hip fracture: does provider volume matter?. The Journal of bone and joint surgery. American volume, 92(4), 799–806. https://doi.org/10.2106/JBJS.H.01204.
13. World Health Organization. WHO scientific group on the assessment of osteoporosis at primary health care level: summary meeting report. 2004. p. 5–7.
14. Black, D. M., & Rosen, C. J. (2016). Clinical Practice. Postmenopausal Osteoporosis. The New England journal of medicine, 374(3), 254–262. https://doi.org/10.1056/NEJMcp1513724.
15. Metcalfe D. (2008). The pathophysiology of osteoporotic hip fracture. McGill journal of medicine : MJM : an international forum for the advancement of medical sciences by students, 11(1), 51–57.
16. Shuhart, C., Cheung, A., Gill, R., Gani, L., Goel, H., & Szalat, A. (2024). Executive Summary of the 2023 Adult Position Development Conference of the International Society for Clinical Densitometry: DXA Reporting, Follow-up BMD Testing and Trabecular Bone Score Application and Reporting. Journal of clinical densitometry : the official journal of the International Society for Clinical Densitometry, 27(1), 101435. https://doi.org/10.1016/j.jocd.2023.101435.

UNITED IMAGING

Follow us on LinkedIn

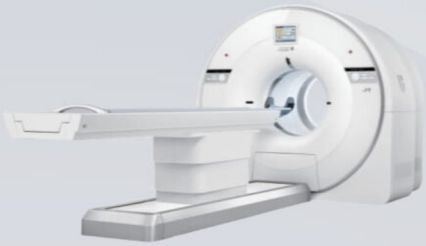

uMI 550
Digital. Attainable.

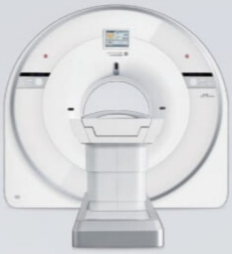

uMI Vista
Clarity. Profound.

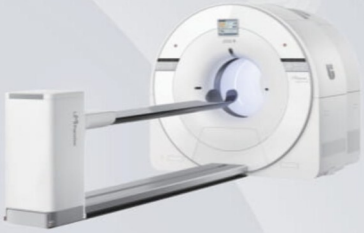

uMI Panvivo
Empowering Tomorrow for All

uMI Panorama
Digital High-Resolution PET/CT.

PASSION FOR *Change*

uEXPLORER
Total-body PET/CT.
Born to EXPLORE.

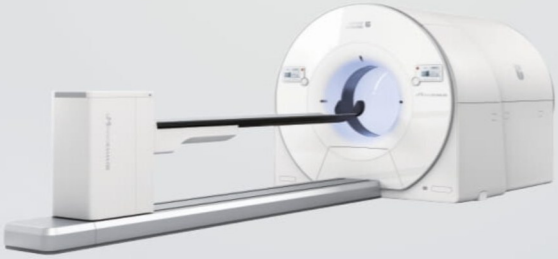

uMI Panorama GS
Next-Generation 148-cm
Whole-Body PET/CT.

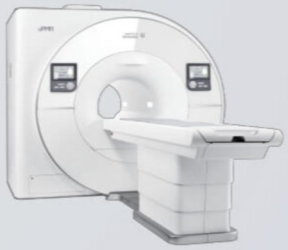

uPMR 790
Next Generation. Now Realized.

Leading innovations in molecular imaging, United Imaging has developed a complete portfolio of LYSO-based digital SiPM PET detector systems. Dedicated to revolutionizing user experiences from clinical applications to advanced research, our portfolio starts where others end. Together with our global customers, we're changing how we view Molecular Imaging today, and in the future.

UNITED IMAGING

uMI Panorama GS

Advancing Whole-Body Imaging

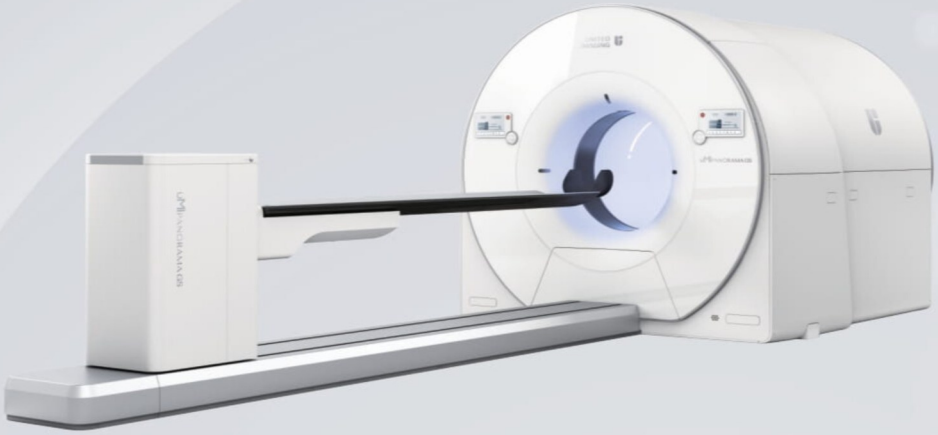

Expanding Whole-Body Imaging with 148 cm AFOV

- 148 cm axial FOV enables single-bed whole-body imaging, covering key nuclear medicine regions from the skull to the knees with high sensitivity.
- 25x sensitivity gain ensures precise line-of-response capture for unparalleled imaging clarity and superior sensitivity for diverse imaging needs, including low-dose, rapid scans for pediatrics and brain imaging.
- Fits within the footprint of standard FOV PET/CT systems.

Unlocking Precision without Compromise

- The 2.76 mm LYSO crystals provide a NEMA spatial resolution of 2.9 mm and 1.4 mm PSF+TOF spatial resolution with 100% SiPM coverage and ASIC technology, enabling sub-millimeter lesion detection and exceptional image clarity.
- Achieves 189 ps TOF and >3000 Peak-NECR, enhancing diagnostic accuracy with unparalleled details and contrast.
- AI-powered uExcel DPR and uExcel AIIR algorithms reduce noise and enhance contrast, while uExcel Focus corrects motion artifacts for improved quantification.

Enabling a Panoramic View for New Clinical and Research Dimensions

- Delivers precise PET imaging with ultra-low radiation through CT-Free attenuation correction (AC), ensuring safety without compromising quality.
- Supports advanced physiological and absolute quantitative analysis with innovative dynamic imaging technology (0.025/s Kernel Recon) and uKinetics.
- Achieves high-speed online reconstruction with average static scan times under 3 minutes, with options for parallel reconstruction and redundant acquisition.

Comparative Studies on the Utility of ^{68}Ga-FAPI PET/CT and ^{18}F-FDG PET/CT in Evaluating Head and Neck Carcinomas: A Systematic Review and Meta-Analysis

Christopher Timothy L. Azarraga, MD, Irene S. Bandong, MD, Christine Megan D. Nierras, MD

Department of Nuclear Medicine and Theranostics, St. Luke's Medical Center—Quezon City
E-mail address: timothyazarraga96@gmail.com

ABSTRACT

Background:

Head and neck squamous cell carcinomas (HNSCC) compose the majority of head and neck carcinomas with ^{18}F-Fluorodeoxyglucose (18F-FDG) PET/CT serving a vital role in the initial staging, treatment planning, and monitoring. Its limitations may include accumulation in inflammatory and benign processes, and variable physiologic tissue uptake. ^{68}Gallium-Fibroblast Activation Protein Inhibitor (^{68}Ga-FAPI) PET/CT, targeting the fibroblast activation protein (FAP), a major component of the tumor microenvironment, demonstrates potential as an alternative due to the lack of physiologic tissue uptake.

Objective:

This systematic review and meta-analysis evaluates the diagnostic performance of ^{68}Ga-FAPI compared to ^{18}F-FDG PET/CT in head and neck carcinomas.

Methodology:

A comprehensive literature search identified studies comparing ^{68}Ga-FAPI and ^{18}F-FDG PET/CT for primary tumors, tumor recurrence, nodal and distant metastases in head and neck carcinomas. A total of 12 studies involving 433 patients met the inclusion criteria. The reference standards were histopathology and radiologic characteristics. A random-effects model was used for the detection rate, pooled sensitivity, specificity, and diagnostic odds ratios (DOR).

Results:

^{68}Ga-FAPI demonstrated higher sensitivity for primary lesion detection (98%; 95% CI: 89–100%) compared to ^{18}F-FDG (94%; 95% CI: 75–100%). In detecting lymph node metastases, ^{18}F-FDG PET/CT had higher sensitivity (94%; 95% CI: 92–96%) than ^{68}Ga-FAPI (85%; 95% CI: 82–88%), while ^{68}Ga-FAPI showed superior specificity (94%; 95% CI: 91–96%). For distant metastases, ^{68}Ga-FAPI exhibited markedly higher sensitivity (98%; 95% CI: 93–99%) than ^{18}F-FDG (74%; 95% CI: 65–81%). Staging analysis comparison between ^{68}Ga-FAPI and ^{18}F-FDG showed ^{68}Ga-FAPI more effectively upstaged primary tumors and detected distant metastatic lesions but downstaged nodal involvement.

Conclusion:

^{68}Ga-FAPI PET/CT offers comparable or superior diagnostic performance when compared to ^{18}F-FDG PET/CT in head and neck carcinomas. It has the advantage in delineating primary tumor margins particularly in the challenging anatomical regions of the head and neck. However, it may underperform in detecting nodal disease compared to ^{18}F-FDG. Further research is warranted prior to the adoption of ^{68}Ga-FAPI into standard imaging protocols for HNSCC.

***Keywords**: Head and neck carcinoma, FAPI, FDG, PET, tumor staging*

INTRODUCTION

^{18}F-Fluorodeoxyglucose (FDG) is the most commonly utilized radiopharmaceutical in Positron Emission Tomography (PET). Its mechanism relies on the preferential glucose metabolism of cancer cells thru uptake via the GLUT transporters, enabling the functional assessment of tissues. By combining structural imaging techniques, such as computed tomography (CT) or magnetic resonance imaging (MRI), PET/CT or PET/MRI scans enable simultaneous assessment of both anatomy and metabolic activity [1].

Some limitations of ^{18}F-FDG PET scans include its non-specific accumulation in infectious and inflammatory processes. Furthermore, variable physiologic uptake in normal tissue, such as in the brain, lymphatics, and the urinary and gastrointestinal tract, can confound image interpretation and limit the utility of ^{18}F-FDG in such regions. Accumulation in a variety of inflammatory or hyperplastic benign processes, such as thyroid nodules or adrenal adenomas, are also potential confounders in malignancy evaluation. Tumors with low metabolic rate, such as well-differentiated neuroendocrine, prostate, and renal carcinomas, show minimal FDG uptake thus there has been an increasing interest in tracers with alternative mechanisms of uptake such as those that may bind to specific receptors or proteins on malignant cells, such as the somatostatin receptor (SSTR) or prostate-specific membrane antigen (PSMA) [2].

Fibroblast activation protein (FAP) is a transmembrane glycoprotein found in the tumor microenvironment that contributes to 90% of the tumor volume in epithelial carcinomas. Cancer-associated fibroblasts (CAF) promote tumor growth, invasion, and angiogenesis, and have been seen to be correlated with tumor aggressiveness and poor prognostication. With negligible expression of FAP in normal tissues and over-expression of FAP in certain malignancies, FAP-targeting ligands, such as ^{68}Gallium (^{68}Ga)-Fibroblast Activation Protein Inhibitor (FAPI), have been of interest for oncologic imaging and therapy [3].

Head and neck squamous cell carcinomas (HNSCC), comprise 90% of all head and neck carcinomas and are derived from the epithelial mucosa of the oral cavity, larynx, and nasopharyngeal regions, representing the 6th leading type of cancer worldwide. CT and MRI are the imaging modalities of choice for identifying and characterizing primary malignancies and for pre-operative staging and planning [4] ^{18}F-FDG PET is another important imaging modality, which enables the detection of occult primary tumor and distant metastatic disease, and assists in radiotherapy planning. However, ^{18}F-FDG has shown limitations, such as the assessment of tumor extension due to the complex anatomy and proximity of the structures in the head and neck, and the intense physiologic FDG uptake in the brain, salivary glands, vocal cords and brown fat, which may mask smaller-sized lesions [5].

This systematic review and meta-analysis aims to compare the performance of ^{18}F-FDG and ^{68}Ga-FAPI PET in head and neck carcinomas (HNC).

OBJECTIVE

Primary Objective

To compare the detection rate of ^{68}Ga-FAPI and ^{18}F-FDG PET/CT in the primary lesions and recurrent lesions of head and neck carcinomas.

Specific Objectives

- To determine the sensitivity, specificity, and diagnostic odds ratio (DOR) of ^{68}Ga-FAPI PET/CT for nodal disease of head and neck carcinomas
- To determine the sensitivity, specificity, and diagnostic odds ratio (DOR) of ^{18}F-FDG PET/CT for nodal disease of head and neck carcinomas
- To compare the detection rate of ^{68}Ga-FAPI and ^{18}F-FDG PET/CT in primary lesions of the following subclassifications: (1) Nasopharyngeal, (2) Oral Squamous, (3) Tonsillar
- To compare the detection rate of ^{68}Ga-FAPI and ^{18}F-FDG PET/CT in the distant metastatic lesions of head and neck carcinomas

METHODOLOGY

Eligibility Criteria/Criteria for considering studies for this review

All studies that met the following parameters were included:

(1) Population: Patients with HNSCC (Oral, Tonsillar, Nasopharyngeal, Unknown primary origin)
(2) Index Test: ^{68}Ga-FAPI PET/CT
(3) Comparator/Alternative tests: ^{18}F-FDG PET/CT
(4) Reference standard: Histopathologic sampling/ Radiologic imaging (Radiologic characteristics and follow-up)

(5) Outcomes
Primary outcome: Detection rate (DR) - Detected lesions on imaging / total number of lesions
(a) Primary lesion
(b) Recurrent lesions
Secondary outcomes:
Pooled sensitivity, pooled specificity, diagnostic odds ratio (DOR),
- Nodal metastasis (per lesion).
Detection Rate (DR)
- Distant metastatic disease (per lesion).

(6) Study Design: Systematic Review and Meta-Analysis
Included Articles: All cross-sectional analytical studies that directly compare ^{68}Ga-FAPI PET/CT with ^{18}F-FDG PET/CT in patients with HNSCC
Exclusion criteria include the following:
(1) studies with insufficient patient data
(2) studies that did not compare the index and comparator test
(3) studies with insufficient data to derive outcomes
(4) case studies, case series, review articles, editorials, and conference proceedings
(5) duplicated papers
(6) studies involving thyroid, lymphoma, or skin carcinomas. If repetitive studies involving the same patient pool were done, the more recent study/larger study would be included

Search methods for identification of studies

A comprehensive search of the following electronic databases was performed using PUBMED and Google Scholar. Journals and articles limited to the English language were extracted. The following keywords were used: ("PET" OR "POSITRON") AND ("FDG" OR "Fluorodeoxyglucose") AND ("FAPI" OR "FAP" OR "Fibroblast") AND ("Head" OR "Neck" OR "ORAL" OR "TONSIL" OR "NASOPHARYNX" OR "UNKNOWN" OR "SQUAMOUS" OR "TONGUE" OR "CHEEK" OR "NASAL" OR "PALATE"). All studies until August 2024 were included.

Data Extraction and Management

Three reviewers extracted pertinent data independently, resolving discrepancies through discussion and achieving consensus in cases of disagreement. The extracted data were then used to formulate 2-by-2 contingency tables to assess test performance.

The extracted data included (1) author's name and year, (2) study characteristics, country, total sample size, and analysis, (3) patient characteristics including sample size, age, gender, and histopathology, (4) technical characteristics including time in between scans, scanner type, tracer injected, scanning protocol, scanner modality, Standard Uptake Values Maximum (SUVMax), Metabolic Tumor Volume (MTV) or Functional Tumor Volume (FTV), Tumor-to-Background Ratio (TBR), (5) true positive, true negative, false positive, and false negative, and sensitivity and specificity per lesion, (6) information regarding primary malignancies, recurrence, nodal metastasis, and distant metastatic disease, (7) TNM and AJCC staging .

Assessment of risk of bias in individual studies

Two researchers used the Quality Assessment of Diagnostic Accuracy Studies (QUADAS - 2) to analyze the individual study's bias risk and applicability. The studies were assessed as having a low, unclear, or high risk of bias. The RevMan (version 5.3) software was used for the evaluation. An additional reviewer was engaged to resolve any potential disagreements .

Synthesis of results / Data synthesis

The data from the included studies were utilized, considering each study's relative importance. Analysis was done using a random-effect statistical model with the inverse variance method. The 95% confidence interval values were used. The I-square index was employed to assess the level of statistical heterogeneity within the papers included in the analysis. Statistical heterogeneity was considered significant if the I2 index exceeded 50%. In case of significant heterogeneity between studies, subgroup analysis was performed. The hierarchical summary receiver-operating characteristic (SROC) model was used to draw SROC curves and calculate the area under the curve (AUC).

The MetaDiSc 1.4 software was employed to perform pooled estimates of detection rates, sensitivity and specificity, positive predictive value, negative predictive value, positive and negative likelihood ratio, and diagnostic odds ratio (DOR) .

Risk of bias across studies

Funnel plots were used for assessment of publication bias .

Additional analyses

Subgroup analyses for primary tumors, lymph nodes, and distant metastatic disease, were done if with significant heterogeneity

RESULTS

Literature Search and Study Selection

The initial literature search identified 210 publications. After 104 duplicates were removed, 106 studies remained. Screening based on the abstracts further decreased the number of available studies to 15. After full-text review, three studies were excluded due to incomplete data. Thus, 12 studies were included in the review to compare the utility of ^{68}Ga-FAPI and ^{18}F-FDG PET/CT in head and neck carcinomas. Figure 1 shows the PRISMA flow chart summarizing the literature search.

Characteristics of the Included Studies

Table 1 summarizes the characteristics of the 12 studies included in the systematic review and meta-analysis. The included studies consisted of 433 participants with 5 main categories of head and neck carcinomas: 3 for general head and neck squamous; 4 for nasopharyngeal; 2 for oral squamous; 2 for tonsillar carcinomas, and 1 for unknown primary malignancy. The selected studies were published from 2020 to 2024 with 8 studies from China, 1 study from Thailand, and 3 studies from Germany. Eight (8) of the 12 studies were prospective studies, while the others were analyzed retrospectively. Eight (8) studies used histopathology or radiologic imaging as the reference standard, while 4 studies used only histopathology. Radiologic imaging (CT or MRI) as the reference standard was defined as typical malignant features confirmed by multiple-modality imaging or a significant reduction in size/number after anti-cancer treatment (chemotherapy, radiotherapy, immunotherapy, etc.) based on the RECIST criteria.

Three studies assessed both primary staging and tumor recurrence while 9 studies assessed only primary staging. Two studies administered [^{68}Ga]-Ga-DOTA-FAPi-46, while 9 studies used [^{68}Ga]-Ga-DOTA-FAPi-04 as the index tests. One study did not name the type of ^{68}Ga-FAPI tracer used. The PET images were semi-quantitatively analyzed using the SUV_{Max}, MTV or FTV, and the TBR. The background regions included the contralateral healthy tissue or contralateral muscle.

Risk of Bias and Applicability

The risk of bias and applicability for the included studies was assessed using the QUADAS-2 (see Figures 2 and 3). The index ^{68}Ga-FAPI and alternative test ^{18}F-FDG demonstrated more than 50% unclear risk of bias, as there was no mention of blinding of the individual test results. None of the studies were of low quality and the overall studies were satisfactory.

Quantitative Analysis (Meta-Analysis)

Based on the Primary Lesion Performance Analysis

The detection rates (Figure 4) of ^{68}Ga-FAPI and ^{18}F-FDG PET/CT in evaluating the primary lesions for HNC were 0.98 (95%CI: 0.89 -1.00; I^2 = 92%) and 0.94 (95%CI: 0.75 - 1.00; I^2 = 96%), respectively. Significant statistical heterogeneity (I^2 = 96%, p < 0.01) was noted between the two tracers (Appendix A).

Additional subgroup analysis (Appendix B and C) for detection rates of nasopharyngeal, oral squamous, and tonsillar carcinomas for ^{68}Ga-FAPI and ^{18}F-FDG PET/CT were obtained (Table 2).

Based on the Recurrent Disease Performance Analysis

The detection rates (Figure 5) of ^{68}Ga-FAPI and ^{18}F-FDG PET/CT in evaluating the recurrence for HNC were 0.73 (95%CI: 0.59 - 0.85; I^2 = 0%) and 0.73 (95%CI: 0.59 - 0.85; I^2 = 0%), respectively. There was no noted statistical heterogeneity (I^2 = 0%, p = 0.83).

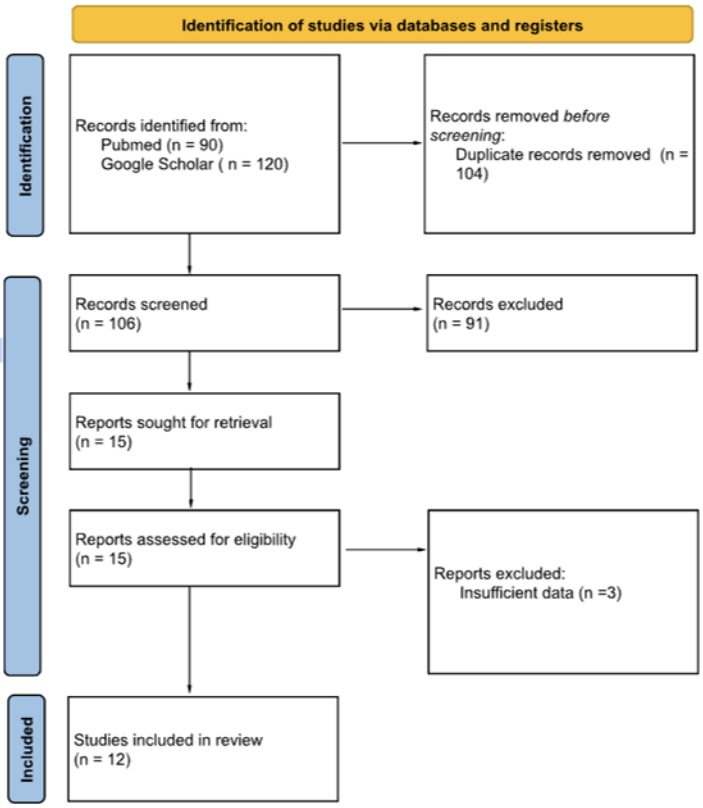

FIGURE 1 PRISMA flow diagram for selecting the included studies

TABLE 1. Characteristics of the Included Studies and Patient Population

	Author	Population	Age	Sex (M:F)	Reference Standard	Cancer Type
1	Promteangtrong et al. (2021) Thailand [6]	40	Mean: 57	27:13; (2:1)	Histopathology/ Follow-up imaging (CT or MRI)	Head and Neck Squamous
2	Jiang et al.(2022) China [7]	77	Mean: 58 (20 - 89)	61:16 (3:1)	Histopathology	Head and Neck Squamous
3	Wegen et al.(2022) Germany [8]	15	Median: 66 (37 - 82)	12:3 (4:1)	Histopathology/ Follow-up imaging (CT or MRI)	Head and Neck Squamous
4	Zheng et al. (2022)	47	52.3 ± 13.8	2:1	Histopathology/ Follow-	Nasopharyngeal
5	Qin et al. (2021) China	15	Mean 51.2 ±	1:1	Histopathology	Nasopharyngeal
6	Zhao et al. (2021) China [11]	45	median 50 (25 - 70)	3.5:1	Histopathology/ Follow-up imaging (MRI)	Nasopharyngeal
7	Ding et al. (2022) China	28	53 ± 11	4.6:1	Histopathology/ Follow-	Nasopharyngeal
8	Linz et al. (2021)	10	62 ± 9	4:1	Histopathology/ Follow-	Oral Squamous
9	Chen et al. (2022) China [14]	36	61.60 ± 10.49 (34 - 87)	4:1	Histopathology	Oral Squamous
10	Ji et al. (2024) China	21	55.05 ± 8.34	3.2 : 1	Histopathology/ Follow-	Tonsillar
11	Serfling et al. (2020) Germany [16]	8	62 (58 - 72)	3:1	Histopathology	Tonsillar
12	Gu et al. (2023) China [17]	91	median 60 (24 – 76)	4:1	Histopathology/ Follow-up imaging	Unknown primary

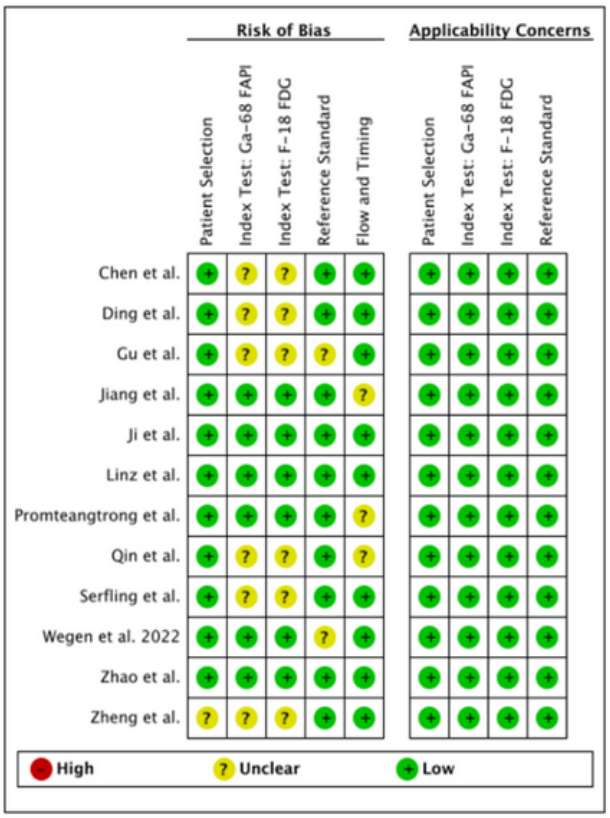

FIGURE 2 Study characteristics

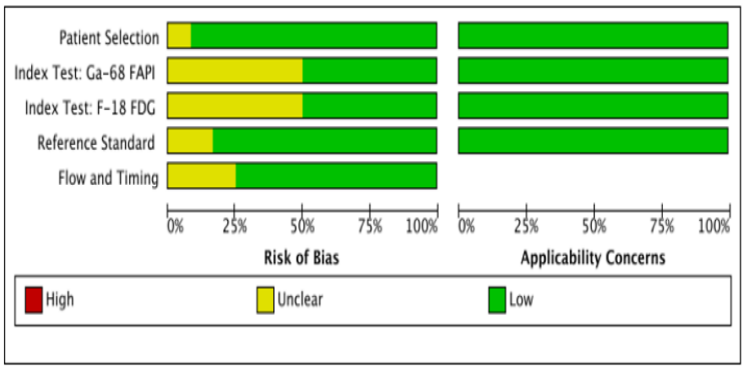

FIGURE 3 Quality of the Included Studies

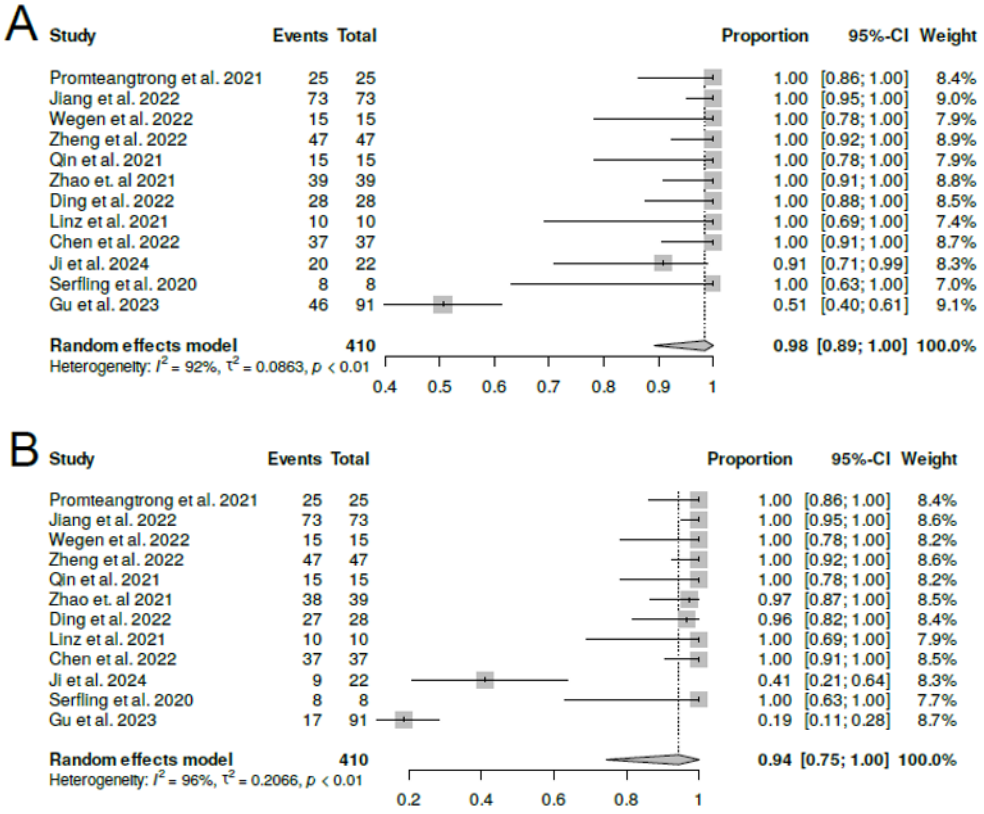

FIGURE 4 Forest plots of the sensitivity of (A) 68Ga-FAPI and (B) 18F-FDG PET/CT in the detection of primary HNC lesions.

TABLE 2. Subgroup Analysis Detection Rate of Primary Tumors

	FAPI PET/CT Detection Rates (95% CI)	**FDG PET/CT Detection Rates(95% CI)**
Nasopharyngeal	1.00 (95%CI: 0.99 -1.00;I^2=0%)	0.99 (95%CI: 0.96 -1.00;I^2=0%)
Oral Squamous	1.00 (95%CI: 0.97 - 1.00;I^2=0%)	1.00 (95%CI: 0.97 -1.00;I^2=0%)
Tonsillar	0.95 (95%CI: 0.82 -1.00;I^2=0%)	0.76 (95%CI: 0.09-1.00;I^2=92%)

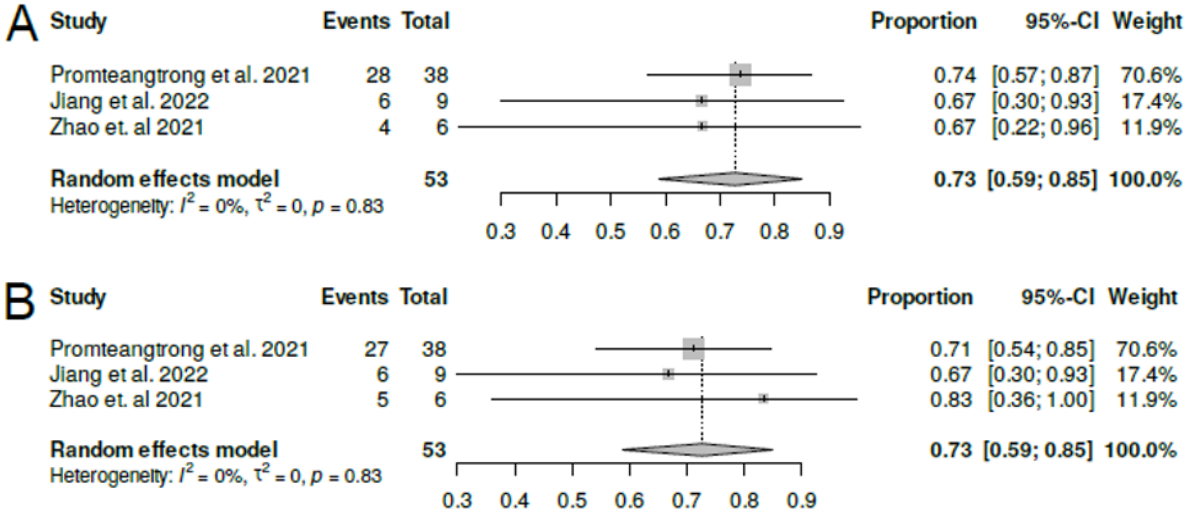

FIGURE 5 Forest plots of the sensitivity of (A) 68Ga-FAPI and (B) 18F-FDG PET/CT in the detection of recurrent HNC lesions

Based on the Lymph Node Performance Analysis

Seven (7) papers compared ^{68}Ga-FAPI and ^{18}F- FDG PET/CT in assessing the lymph node status to the reference standard. The per-lesion pooled sensitivity (Figure 6), specificity (Figure 7), and diagnostic odds ratios (Appendix D and E) ^{68}Ga-FAPI and ^{18}F-FDG PET/CT in the assessment of lymph node metastasis were 0.85 (95% mCI: 0.82 - 0.88; I^2 = 84.8%), 0.94 (95%CI: 0.91 - 0.96; I^2 = 92.3%), and 38.18 (95%CI: 11.61 - 125.54; I^2 = 67.9%), and 0.94 (95%CI: 0.92 - 0.96; I^2 = 75.9%); 0.78 (95% CI: 0.75 - 0.82; I^2 = 98.0%) and 27.46 (95%CI: 5.96 - 126.50; I^2 = 83.1%), respectively (see Table 3).

The relative summary receiver operating characteristics (SROCS) are shown in Figure 8. The Area under the Curve and Q* for ^{68}Ga-FAPI and ^{18}F-FDG PET/CT were 0.9263 and Q*=0.8607 and 0.9079 and Q*=0.8397, respectively.

Based on the Distant Metastatic Disease

The detection rates of ^{68}Ga-FAPI and ^{18}F-FDG PET/CT in evaluating distant metastatic disease for HNC were 0.98 (95%CI: 0.93 -0.99; I^2 = 45.5%) and 0.74 (95%CI: 0.65 - 0.81; I^2 = 85%), respectively (see Figure 9 and Table 4).

Nine (9) studies with a total of 285 patients, compared the ^{68}Ga-FAPI and ^{18}F-FDG TNM staging as shown in Table 5. The included studies showed ^{68}Ga-FAPI upstaged 47 and downstaged 1 T stage compared to the ^{18}F-FDG-based tumor staging. Thirty-nine (39) of the 47 patients were nasopharyngeal carcinoma primaries with skull-base involvement, intracranial extension, or invasion into the adjacent soft tissue structures that were not evident on ^{18}F-FDG PET/CT [7, 9, 10 - 12]. The remaining patients upstaged were tonsillar carcinoma primaries [15]. The T stage of 1 patient with nasopharyngeal carcinoma was underestimated in ^{68}Ga-FAPI when compared to ^{18}F-FDG PET/CT [12]. .

Ninety-six (96) out of 285 patients experienced changes in their N stage, with 76 patients under-staged in the ^{68}Ga-FAPI based TNM staging and 20 patients upstaged when compared to ^{18}F-FDG. 7 patients experienced changes in their M stages, with 6 patients demonstrating ^{68}Ga-FAPI upstaging for the detection of distant metastatic disease. In the study by Ding et al., ^{68}Ga-FAPI underestimated the M stage of one patient and missed a pulmonary nodule seen on ^{18}F-FDG PET/CT [7].

Seven (7) studies with a total number of 234 patients, compared the overall staging based on the American Joint Committee on Cancer (AJCC) Tumor Staging. 167 (71.1%) of all patients with head and neck carcinomas had no change in stage for both ^{68}Ga-FAPI and ^{18}F-FDG. ^{68}Ga-FAPI upstaged 37 (15.7%) patients with better tumoral extent/invasion delineation while 31 (13.2%) were downstaged due to better nodal evaluation of ^{18}F-FDG PET/CT.

DISCUSSION

This systematic review and meta-analysis is the first to quantitatively compare ^{68}Ga-FAPI and ^{18}F-FDG PET-CT for detecting primary, recurrent, nodal, and distant metastatic lesions for head and neck carcinomas.

Out of the 12 studies with a total of 410 lesions, based on a per-lesion evaluation of the primary tumor, ^{68}Ga-FAPI performed better than ^{18}F-FDG in HNC for detection of the primary lesion, with 0.98 (95%CI: 0.89 - 1.00) and 0.94 (95%CI: 0.75 - 1.00), respectively. 3 studies who compared ^{68}Ga-FAPI and ^{18}F-FDG in detection of recurrent disease, out of 53 total lesions, similar sensitivity was seen between ^{68}Ga-FAPI and ^{18}F-FDG PET-CT, 0.73 (95%CI: 0.59 - 0.85) and 0.73 (95% CI: 0.59 -0.85), respectively.

Per-lesion nodal analysis, ^{68}Ga-FAPI demonstrated inferior sensitivity compared to ^{18}F-FDG, with 0.85 (95% CI: 0.82 - 0.88) and 0.94 (95%CI: 0.92 - 0.96), however ^{68}Ga-FAPI showed superior specificity at 0.94 (95%CI: 0.92 - 0.96) and 0.78 (95% CI: 0.75 - 0.82), respectively.

Per-lesion distant metastatic disease, ^{68}Ga-FAPI appeared to be more sensitive than ^{18}F-FDG PET/CT, 0.98 (95%CI: 0.93 - 0.99) and 0.74 (95%CI: 0.65 - 0.81), respectively.

The study by Zheng et al., showed a significantly higher detection rate for soft tissue involvement of the primary nasopharyngeal tumors. ^{68}Ga-FAPI showed tumor extent with 100/111 (90.0%) compared to ^{18}F-FDG of 91/111 (82.0%). Additionally, ^{68}Ga-FAPI showed a superior detection for bone invasion in the regions of the corpus sphenoidal, petrous, and clivus with a total detection rate of of 207/207 (100%) compared to 177/207 (85.5%) for ^{18}F-FDG [9].

Our study demonstrated that ^{68}Ga-FAPI had a higher sensitivity in detecting tumor extension into the adjacent structure. This appears to be more evident in nasopharyngeal carcinomas as seen by the upstaging post ^{68}Ga-FAPI PET when compared to ^{18}F-FDG. The limited physiological uptake of ^{68}Ga-FAPI in brain, tonsillar regions, and neck tissues results in improved tumor-to-background ratios, facilitating accurate staging and evaluation of primary lesions.

All included studies assessed tumor characteristics, including SUV_{max} or tumor-to-background ratio (TBR). The studies by Zhao et al., and Gu et al., evaluating nasopharyngeal and carcinomas of unknown primary, reported significantly higher ^{68}Ga-FAPI SUV_{max} values compared to ^{18}F-FDG [11, 17]. Of the seven studies that compared TBR, the studies by Wegen et al., Ji et al., and Serfling et al., demonstrated significantly higher TBRs for ^{68}Ga-FAPI[8][15,16].

Furthermore, the studies by Promteangtrong et al., and Zhao et al., observed significantly larger functional tumor volumes with ^{68}Ga-FAPI compared to metabolic tumor volumes with ^{18}F-FDG [6, 11].

For nodal involvement, our study demonstrated that ^{68}Ga-FAPI had lower sensitivity and higher specificity when compared to ^{18}F-FDG. The studies by Jiang et al., and Zheng et al., attributed this observation to false-positive ^{18}F-FDG uptake in inflammatory lymph nodes and brown fat [7][9]. Despite the lower sensitivity for nodal detection, the high specificity of ^{68}Ga-FAPI enables a more precise preoperative staging, potentially minimizing the need for unnecessary nodal dissections [14].

Our study demonstrated a higher detection rate for ^{68}Ga-FAPI in the use of detecting distant metastatic disease. Small bone lesions detected by ^{68}Ga-FAPI were seen with the absence of ^{18}F-FDG uptake in the studies by Qin et al., and Zhao et al., and suggested that it may be due to the stroma-specific characteristics of FAPI towards activated fibroblasts/myofibroblasts in the bones [10][11].

Rizzo et al., conducted a prior meta-analysis showing a diagnostic sensitivity of 0.97 (95%CI: 0.95 - 0.99) for ^{68}Ga-FAPI in the initial evaluation and metastatic work-up of head and neck carcinomas [18]. Our study also yielded results consistent with other meta-analyses, in which they found ^{68}Ga-FAPI to be more sensitive than ^{18}F-FDG in the detection of the primary digestive, abdominal and pelvic, and liver tumors. The increased sensitivity of ^{68}Ga-FAPI is attributed to its ability to detect the strong fibrotic response that occurs early in the growth and invasion of adjacent tumors [19 - 22].

Despite its relatively high sensitivity and specificity, ^{68}Ga-FAPI can yield false-positive results in conditions such as degenerative osseous lesions, scarring and wound healing, chronic inflammatory processes in the head and mouth, and uterine and mammary findings. Thus, correlation with the patient's medical and clinical history remains essential [22]. However, ^{68}Ga-FAPI tracer uptake has been significantly higher in malignancy compared to benign lesions [11].

Several factors should be considered before the adoption of ^{68}Ga-FAPI over 18F-FDG PET/CT, such as availability, cost-effectiveness, and tumor classification. Close collaboration between the primary physician and the nuclear medicine specialist is essential to tailor the choice of radiotracer to the patient's specific needs, whether for improved delineation of the primary tumor before radiotherapy or evaluation of possible nodal metastasis. An additional potential benefit of ^{68}Ga-FAPI is the independence to blood glucose levels and lack of fasting or dietary preparation.

This meta-analysis has several limitations including significant heterogeneity across the studies which may be due to the diverse cancer types, and limited sample sizes. Seven studies were included to evaluate the per-lesion nodal specificity. Other studies did not include the number of true-negative or false-positive cases, hence the lack of specificity for primary, recurrent, and distant metastatic lesions. Future research with larger prospective studies may be included to help define the role of ^{68}Ga-FAPI over ^{18}F-FDG

CONCLUSION

The systematic review and meta-analysis has demonstrated that ^{68}Ga-FAPI PET/CT provides comparable or superior diagnostic performance when compared to ^{18}F-FDG PET/CT in the initial evaluation of head and neck carcinomas. ^{68}Ga-FAPI may be used for more accurate primary tumor extent, staging and the initial work-up, however, more robust studies are still recommended before its adoption as a first-line imaging test .

Disclosure

The authors have no conflict of interest to declare.

Clinical Relevance

This meta-analysis demonstrates comparable performance of ^{68}Ga-FAPI to the standard ^{18}F-FDG in the initial evaluation, staging and monitoring of head and neck squamous carcinomas. More robust studies are necessary to fully evaluate its clinical utility and establish its role as a possible first-line imaging modality. Practical considerations, such as tracer availability, may ultimately dictate the most suitable choice in clinical practice.

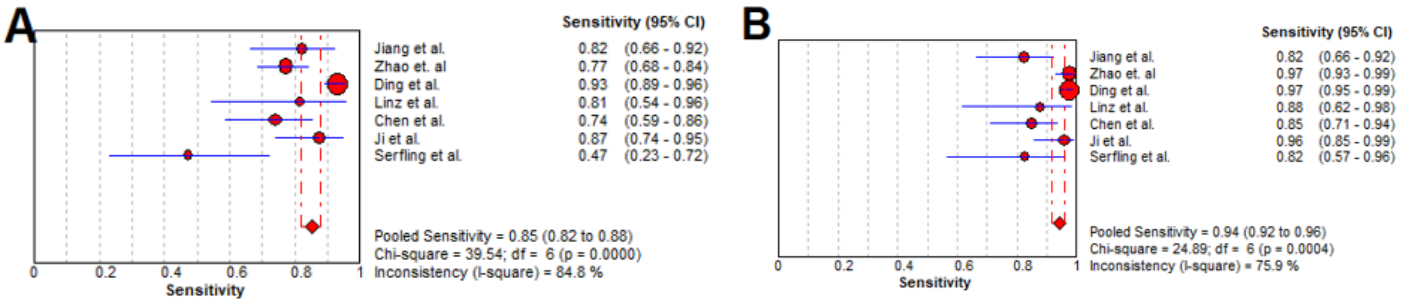

FIGURE 6 Forest plots of the sensitivity of (A) ^{68}Ga-FAPI and (B) ^{18}F-FDG PET/CT in detecting lymph nodes

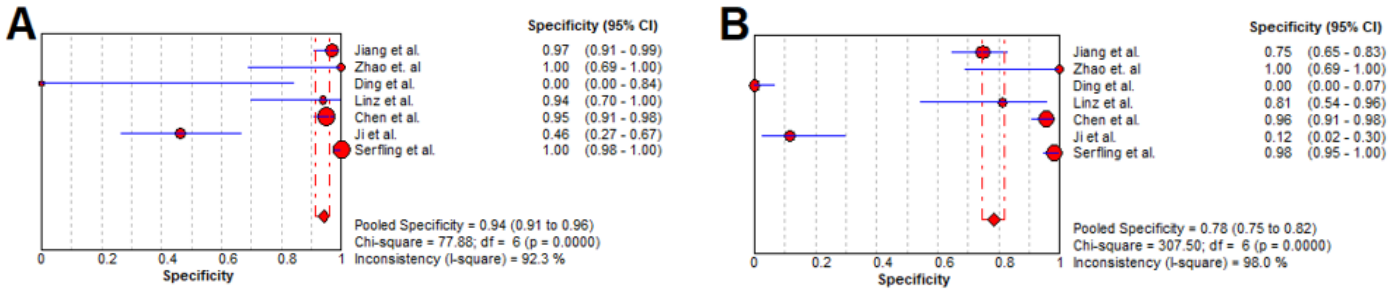

FIGURE 7 Forest plots of the specificity of (A) ^{68}Ga-FAPI and (B) ^{18}F-FDG PET/CT in detecting lymph nodes

TABLE 3. ^{68}Ga-FAPI vs ^{18}F-FDG in the evaluation of lymph nodes

	FAPI PET/CT Detection Rates (95% CI)	FDG PET/CT Detection Rates(95% CI)
Sensitivity	0.85 (95%CI: 0.82 - 0.88)	0.94 (95%CI: 0.92 - 0.96)
Specificity	0.94 (95%CI: 0.91 - 0.96)	0.78 (95% CI: 0.75 - 0.82)
Diagnostic Odds Ratio	38.18 (95%CI: 11.61 - 125.54)	27.46 (95%CI: 5.96 -126.50)
Area Under the Curve (AUC)	0.9263	0.9079
Q*	0.8607	0.8397

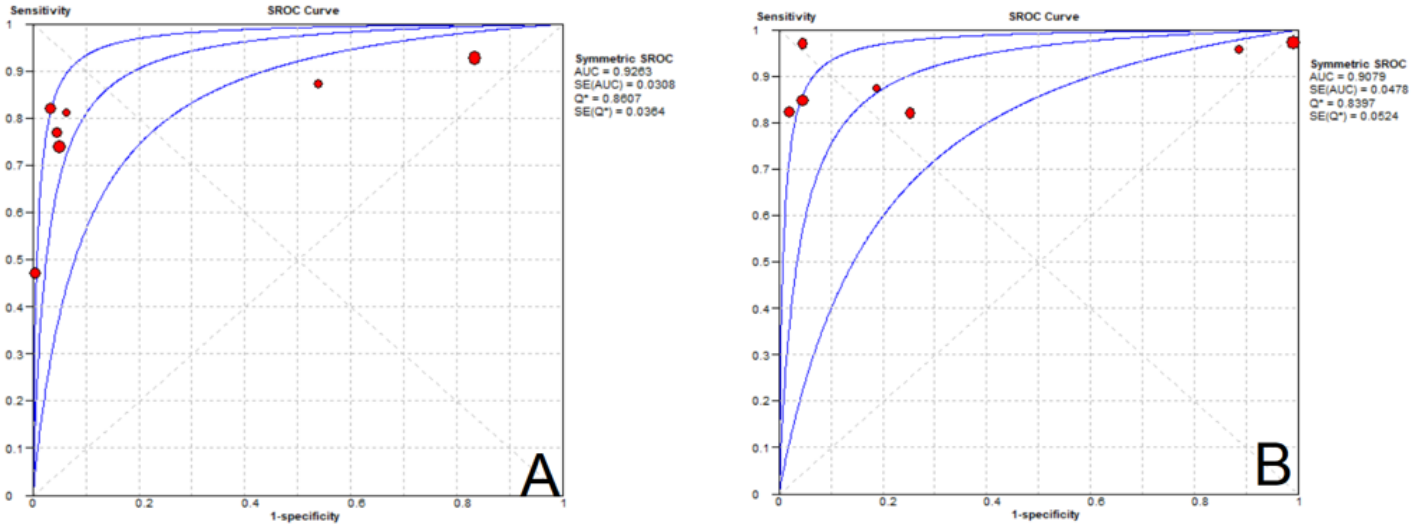

FIGURE 8 Summary Receiver Operating Characteristics (SROCs) (A) 68Ga-FAPI and (B) 18F-FDG in the detection of lymph nodes

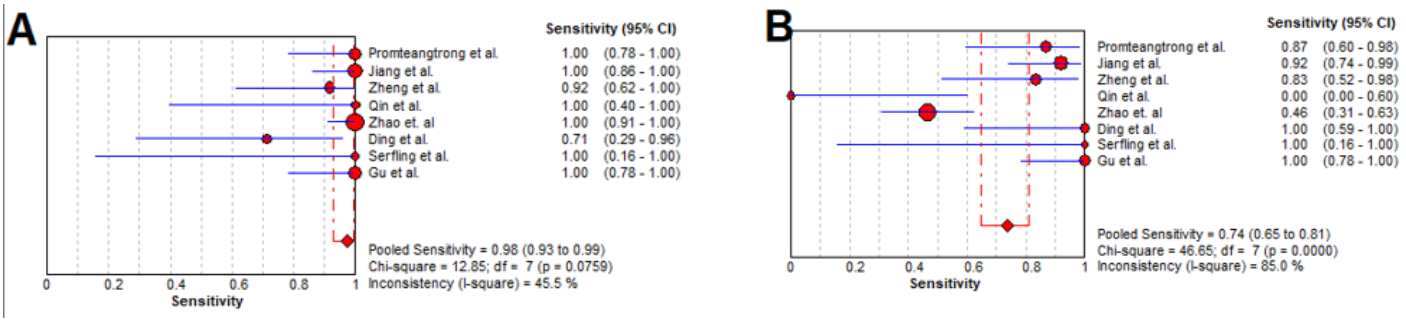

FIGURE 9 Forest plots of the sensitivity of (A) ^{68}Ga-FAPI and (B) ^{18}F-FDG PET/CT in the detection of distant metastatic lesions

TABLE 4. Subgroup Analysis Detection Rate of Primary Tumors

Lesion-Based Analysis	**FAPI PET/CT Sensitivity (95% CI)**	**FDG PET/CT Sensitivity (95% CI)**
Primary Lesions	0.98 (95%CI: 0.89 -1.00)	0.94 (95%CI: 0.75 -1.00)
Recurrent Lesions	0.73 (95%CI: 0.59 - 0.85)	0.73 (95%CI: 0.59 - 0.85)
Nodal Lesions	0.85 (95%CI: 0.82 - 0.88)	0.94 (95%CI: 0.92 - 0.96)
Distant Metastatic Lesions	0.98 (95%CI: 0.93 - 0.99)	0.74 (95%CI: 0.65 - 0.81)

TABLE 5. ^{68}Ga-FAPI vs ^{18}F-FDG TNM and AJCC staging

TNM Staging n = 285	**Patients Upstaged with ^{68}Ga-FAPI**	**Patients Downstaged with ^{68}Ga-FAPI**	**No Change in Staging**
Tumor	47 (16.4%)	1 (0.3%)	237 (83%)
Lymph Nodes	20 (7%)	76 (26%)	189 (66%)
Metastasis	6 (2%)	1(0.4%)	279(97.5%)
AJCC Staging n = 234	37(15.7%)	31(13.2%)	167(71.1%)

TABLE 6. Summary of other meta-analysis comparing ^{68}Ga-FAPI and ^{18}F-FDG

	Type of Malignancy	**FAPI Sensitivity (95% CI)**	**FAPI Specificity (95% CI)**	**FDG Sensitivity (95% CI)**	**FDG Specificity (95% CI)**
Rizzo et al. [18]	Head and Neck	0.97% (0.95 - 0.99)	None	None	None
Ouyang et al. [19]	Digestive System (Gastric, Liver, biliary)	0.98 (0.94 – .00)	0.81 (0.23 – 1.00)	0.73 (0.60 – 0.84)	0.77 (0.52 –0.95),
Liu et al. [20]	Abdominal and Pelvic (Gastric, Liver, Pancreatic, Colorectal)	0.98 (0.95 - 1.00)	None	0.76 (0.63 - 0.87)	None
Gege et al. [21]	Peritoneal metastasis	0.99 (0.99 - 1.00)	None	0.27 (0.11 - 0.43)	None
Singh et al. [22]	Liver tumors	0.94 (0.90 - 0.96)	0.89 (0.71 - 0.97)	0.56 (0.49 - 0.62)	0.96 (0.81 - 0.99)

REFERENCES

1. Anand, S. S., Singh, H., & Dash, A. K. (2009). Clinical Applications of PET and PET-CT. Medical journal, Armed Forces India, 65(4), 353–358. https://doi.org/10.1016/S0377-1237(09)80099-3.
2. Fletcher, J. W., Djulbegovic, B., Soares, H. P., Siegel, B. A., Lowe, V. J., Lyman, G. H., Coleman, R. E., Wahl, R., Paschold, J. C., Avril, N., Einhorn, L. H., Suh, W. W., Samson, D., Delbeke, D., Gorman, M., & Shields, A. F. (2008). Recommendations on the use of 18F-FDG PET in oncology. Journal of nuclear medicine : official publication, Society of Nuclear Medicine, 49(3), 480–508. https://doi.org/10.2967/jnumed.107.047787.
3. Chandekar, K. R., Prashanth, A., Vinjamuri, S., & Kumar, R. (2023). FAPI PET/CT Imaging-An Updated Review. Diagnostics (Basel, Switzerland), 13(12), 2018. https://doi.org/10.3390/diagnostics13122018.
4. López, F., Mäkitie, A., de Bree, R., Franchi, A., de Graaf, P., Hernández-Prera, J. C., Strojan, P., Zidar, N., Strojan Fležar, M., Rodrigo, J. P., Rinaldo, A., Centeno, B. A., & Ferlito, A. (2021). Qualitative and Quantitative Diagnosis in Head and Neck Cancer. Diagnostics (Basel, Switzerland), 11(9), 1526. https://doi.org/10.3390/diagnostics11091526.
5. Castaldi, P., Leccisotti, L., Bussu, F., Micciché, F., & Rufini, V. (2013). Role of (18)F-FDG PET-CT in head and neck squamous cell carcinoma. Acta otorhinolaryngologica Italica : organo ufficiale della Societa italiana di otorinolaringologia e chirurgia cervico-facciale, 33(1), 1–8.
6. Promteangtrong, C., Siripongsatian, D., Jantarato, A., Kunawudhi, A., Kiatkittikul, P., Yaset, S., Boonkawin, N., & Chotipanich, C. (2022). Head-to-Head Comparison of 68Ga -FAPI-46 and 18F-FDG PET/CT for Evaluation of Head and Neck Squamous Cell Carcinoma: A Single-Center Exploratory Study. Journal of nuclear medicine : official publication, Society of Nuclear Medicine, 63(8), 1155–1161. https://doi.org/10.2967/jnumed.121.262831.
7. Jiang, Y., Wen, B., Li, C., Tian, Y., Xiao, Z., Xu, K., Xing, D., Yu, Z., Huang, J., Jia, J., & He, Y. (2023). The performance of 68Ga-FAPI-04 PET/CT in head and neck squamous cell carcinoma: a prospective comparison with 18F-FDG PET/CT. European journal of nuclear medicine and molecular imaging, 50(7), 2114–2126. https://doi.org/10.1007/s00259-023-06138-y.
8. Wegen, S., van Heek, L., Linde, P., Claus, K., Akuamoa-Boateng, D., Baues, C., Sharma, S. J., Schomäcker, K., Fischer, T., Roth, K. S., Klußmann, J. P., Marnitz, S., Drzezga, A., & Kobe, C. (2022). Head-to-Head Comparison of [68 Ga]Ga-FAPI-46-PET/CT and [18F]F-FDG-PET/CT for Radiotherapy Planning in Head and Neck Cancer. Molecular imaging and biology, 24(6), 986–994. https://doi.org/10.1007/s11307-022-01749-7.
9. Zheng, J., Liu, F., Lin, K., Zhang, L., Huang, N., Zheng, W., Zhang, J., Yao, S., & Miao, W. (2022). [68Ga]Ga-FAPI PET/CT Improves the T Staging of Patients with Newly Diagnosed Nasopharyngeal Carcinoma: A Comparison with [18F]F-FDG. Molecular imaging and biology, 24(6), 973–985. https://doi.org/10.1007/s11307-022-01748-8.
10. Qin, C., Liu, F., Huang, J., Ruan, W., Liu, Q., Gai, Y., Hu, F., Jiang, D., Hu, Y., Yang, K., & Lan, X. (2021). A head-to-head comparison of 68Ga-DOTA-FAPI-04 and 18F-FDG PET/MR in patients with nasopharyngeal carcinoma: a prospective study. European journal of nuclear medicine and molecular imaging, 48(10), 3228–3237. https://doi.org/10.1007/s00259-021-05255-w.
11. Zhao, L., Pang, Y., Zheng, H., Han, C., Gu, J., Sun, L., Wu, H., Wu, S., Lin, Q., & Chen, H. (2021). Clinical utility of [68Ga]Ga-labeled fibroblast activation protein inhibitor (FAPI) positron emission tomography/computed tomography for primary staging and recurrence detection in nasopharyngeal carcinoma. European journal of nuclear medicine and molecular imaging, 48(11), 3606–3617. https://doi.org/10.1007/s00259-021-05336-w.
12. Ding, H., Liang, J., Qiu, L., Xu, T., Cai, L., Wan, Q., Wang, L., Liu, Y., & Chen, Y. (2022). Prospective comparison of 68Ga-FAPI-04 and 18F-FDG PET/CT for tumor staging in nasopharyngeal carcinoma. Frontiers in oncology, 12, 1047010. https://doi.org/10.3389/fonc.2022.1047010.
13. Linz, C., Brands, R. C., Kertels, O., Dierks, A., Brumberg, J., Gerhard-Hartmann, E., Hartmann, S., Schirbel, A., Serfling, S., Zhi, Y., Buck, A. K., Kübler, A., Hohm, J., Lapa, C., & Kircher, M. (2021). Targeting fibroblast activation protein in newly diagnosed squamous cell carcinoma of the oral cavity - initial experience and comparison to [18F]FDG PET/CT and MRI. European journal of nuclear medicine and molecular imaging, 48(12), 3951–3960. https://doi.org/10.1007/s00259-021-05422-z.
14. Chen, S., Chen, Z., Zou, G., Zheng, S., Zheng, K., Zhang, J., Huang, C., Yao, S., & Miao, W. (2022). Accurate preoperative staging with [68Ga]Ga-FAPI PET/CT for patients with oral squamous cell carcinoma: a comparison to 2-[18F]FDG PET/CT. European radiology, 32(9), 6070–6079. https://doi.org/10.1007/s00330-022-08686-7.
15. Ji, M., Ma, G., Liu, C., Gu, B., Du, X., Ou, X., Xu, X., Song, S., & Yang, Z. (2024). Head-to-head comparison of [68Ga]Ga-DOTA-FAPI-04 and [18F]FDG PET/CT for the evaluation of tonsil cancer and lymph node metastases: a single-centre retrospective study. Cancer imaging : the official publication of the International Cancer Imaging Society, 24 (1), 56. https://doi.org/10.1186/s40644-024-00699-3.
16. Serfling, S., Zhi, Y., Schirbel, A., Lindner, T., Meyer, T., Gerhard-Hartmann, E., Lapa, C., Hagen, R., Hackenberg, S., Buck, A. K., & Scherzad, A. (2021). Improved cancer detection in Waldeyer's tonsillar ring by 68Ga-FAPI PET/CT imaging. European journal of nuclear medicine and molecular imaging, 48(4), 1178–1187. https://doi.org/10.1007/s00259-020-05055-8.
17. Gu, B., Yang, Z., Du, X., Xu, X., Ou, X., Xia, Z., Guan, Q., Hu, S., Yang, Z., & Song, S. (2024). Imaging of Tumor Stroma Using 68Ga-FAPI PET/CT to Improve Diagnostic Accuracy of Primary Tumors in Head and Neck Cancer of Unknown Primary: A Comparative Imaging Trial. Journal of nuclear medicine : official publication, Society of Nuclear Medicine, 65(3), 365–371. https://doi.org/10.2967/jnumed.123.266556.

18. Rizzo, A., Miceli, A., Racca, M., Bauckneht, M., Morbelli, S., Albano, D., Dondi, F., Bertagna, F., Galizia, D., Muoio, B., Annunziata, S., & Treglia, G. (2023). Diagnostic Accuracy of [68Ga]Ga Labeled Fibroblast-Activation Protein Inhibitors in Detecting Head and Neck Cancer Lesions Using Positron Emission Tomography: A Systematic Review and a Meta-Analysis. Pharmaceuticals (Basel, Switzerland), 16 (12), 1664. https://doi.org/10.3390/ph16121664.
19. Ouyang, J., Ding, P., Zhang, R., & Lu, Y. (2023). Head-to-head comparison of 68Ga-FAPI-04 PET/CT and 18F-FDG PET/CT in the evaluation of primary digestive system cancer: a systematic review and meta-analysis. Frontiers in oncology, 13, 1202505. https://doi.org/10.3389/fonc.2023.1202505.
20. Liu, X., Liu, H., Gao, C., & Zeng, W. (2023). Comparison of 68Ga-FAPI and 18F-FDG PET/CT for the diagnosis of primary and metastatic lesions in abdominal and pelvic malignancies: A systematic review and meta-analysis. Frontiers in oncology, 13, 1093861. https://doi.org/10.3389/fonc.2023.1093861.
21. Gege, Z., Xueju, W., & Bin, J. (2023). Head-To-Head Comparison of 68Ga-FAPI PET/CT and FDG PET/CT for the Detection of Peritoneal Metastases: Systematic Review and Meta-Analysis. AJR. American journal of roentgenology, 220(4), 490–498. https://doi.org/10.2214/AJR.22.28402.
22. Singh, P., Singhal, T., Parida, G. K., Rahman, A., & Agrawal, K. (2024). Diagnostic Performance of FAPI PET/CT vs. 18F-FDG PET/CT in Evaluation of Liver Tumors: A Systematic Review and Meta-analysis. Molecular imaging and radionuclide therapy, 33(2), 77–89. https://doi.org/10.4274/mirt.galenos.2024.99705.
23. Kessler, L., Ferdinandus, J., Hirmas, N., Zarrad, F., Nader, M., Kersting, D., Weber, M., Kazek, S., Sraieb, M., Hamacher, R., Lueckerath, K., Umutlu, L., Fendler, W. P., & Rischpler, C. (2022). Pitfalls and Common Findings in 68Ga -FAPI PET: A Pictorial Analysis. Journal of nuclear medicine : official publication, Society of Nuclear Medicine, 63(6), 890–896. https://doi.org/10.2967/jnumed.121.262808.

APPENDIX :

A: Funnel Plots for Primary Tumor Detection Rate (A)^{68}Ga-FAPI (B) ^{18}F-FDG

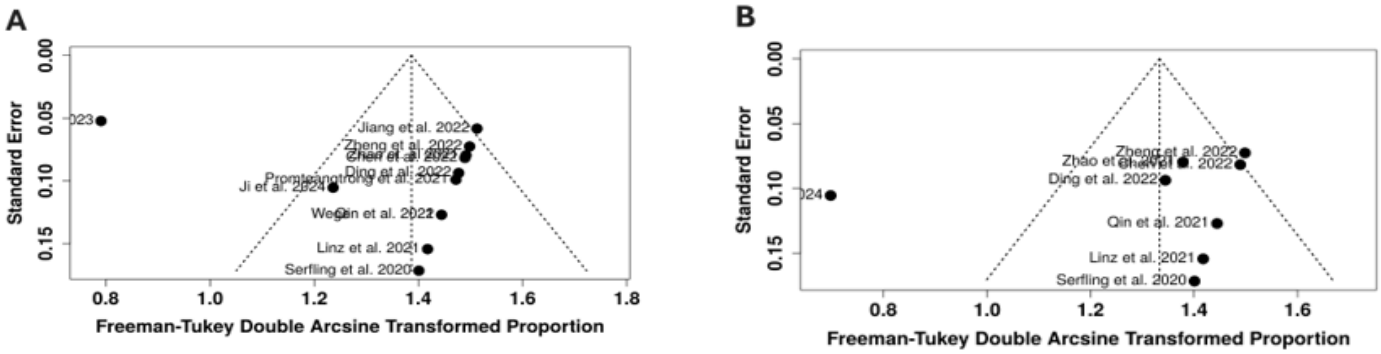

B: Subgroup Analysis Detection Rate of ^{68}Ga-FAPI in primary tumors

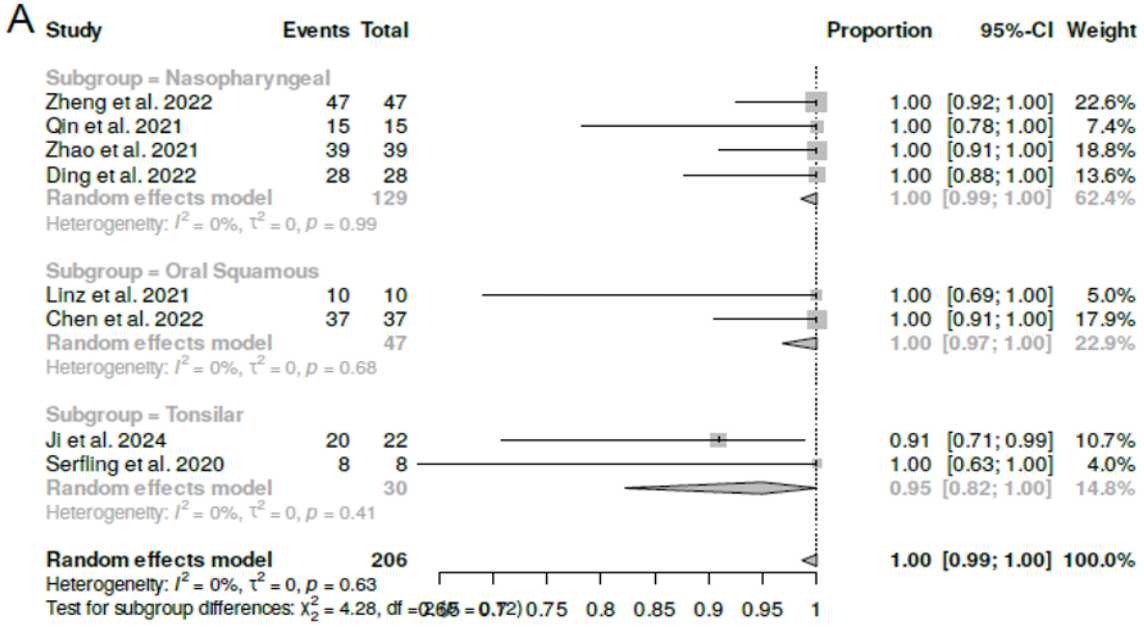

C: Subgroup Analysis Detection Rate of ^{18}F-FDG in primary tumors.

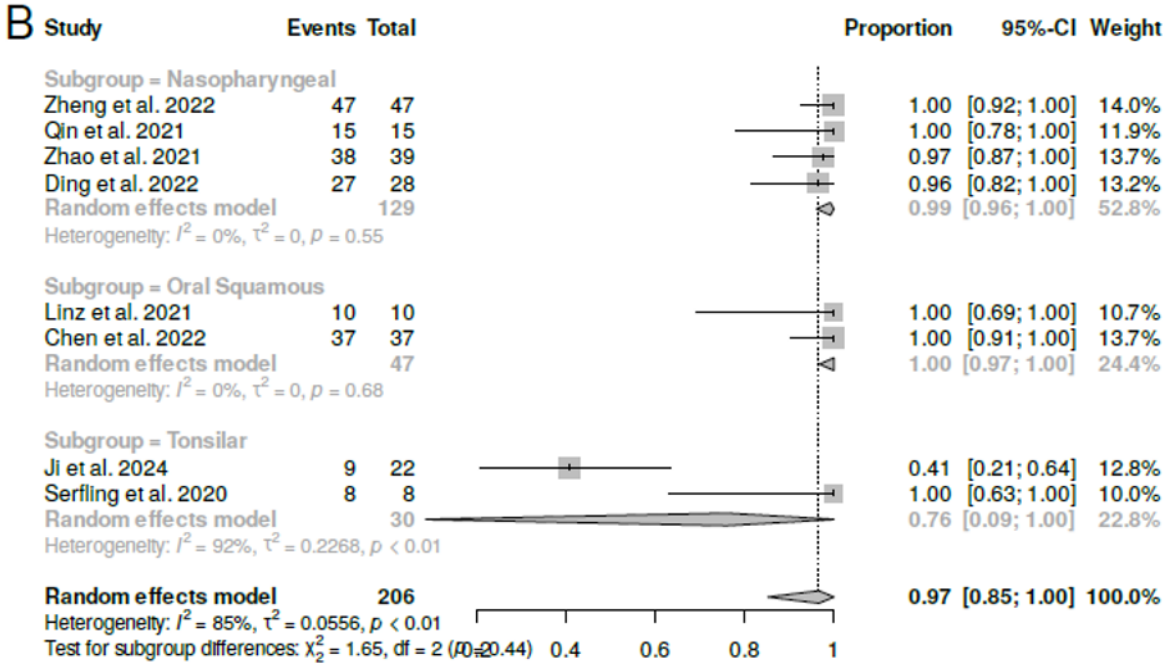

D: Diagnostic Odds Ratio of ^{68}Ga-FAPI in the assessment of lymph nodes

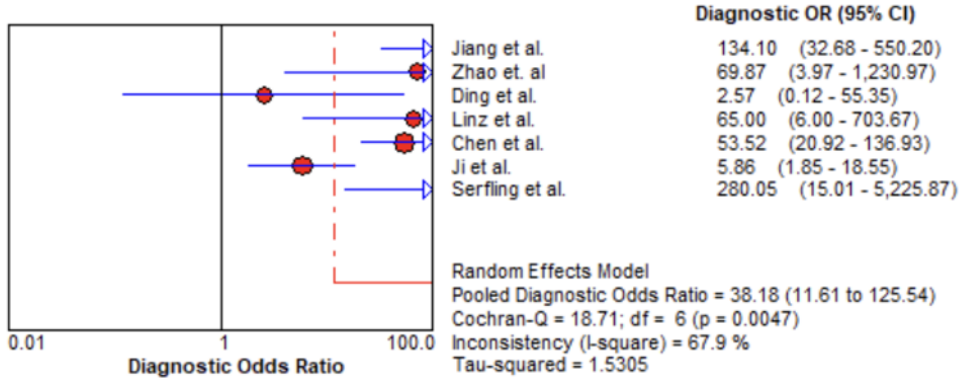

E: Diagnostic Odds Ratio of ^{18}F-FDG in the assessment of lymph nodes

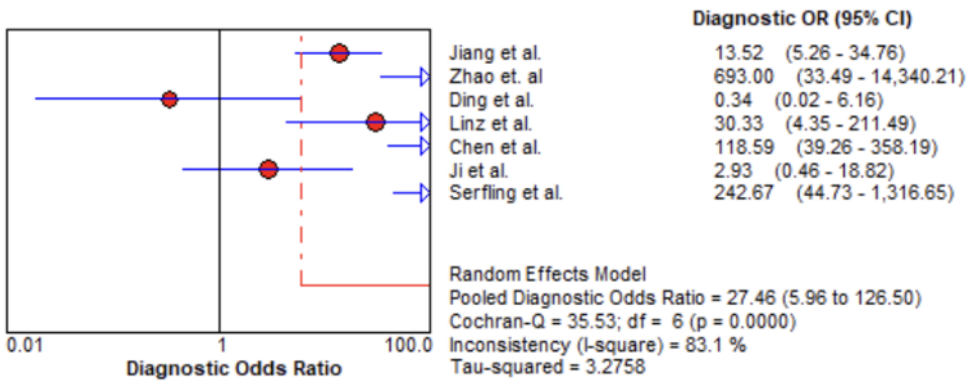

transmedic

Where the world's leading healthcare solutions meet the needs of our people

Offices in Singapore (HQ) | Malaysia | Thailand | Indonesia | Hong Kong | Philippines | Vietnam

The Role of Radioactive Iodine Therapy as Adjunctive Treatment in Papillary Thyroid Microcarcinoma: A Meta-Analysis

Jessica Elise A. Kuizon, MD, Mary Amie Gelina E. Dumatol, MD, Irene S. Bandong, MD

Nuclear Medicine Division, Philippine Heart Center
E-mail address: jeakuizonmd@gmail.com

ABSTRACT

Background:

With the increasing incidence of papillary thyroid microcarcinoma globally, controversy continues as to its optimal management. The appropriateness of RAI ablation, specifically in low and intermediate risk patients, remains to be a topic of debate among clinicians.

Objective:

This study aims to assess the effect of RAI ablation on the recurrence of PTMC in patients with low to intermediate risk.

Methodology:

A comprehensive literature search of PubMed, Cochrane library, Medline, Embase, and Google Scholar for studies comparing the recurrence rate of PTMC between patients treated with surgery followed by RAI vs. surgery alone was done according to the PRISMA guidelines. The meta-analysis was performed using review manager (Revman) version 5.4.

Results:

A total of 11 studies, which included 5167 eligible patients, were assessed. Any site recurrence rate for patients treated with surgery followed by RAI was lower than those treated with surgery alone (3.0% vs. 12.7%, RR = 0.19, p < 0.00001). Recurrence with structural evidence was also lower in patients treated with RAI compared to those treated with surgery alone (1.9% vs 4.7%, RR = 0.36, p = 0.0007).

Conclusion:

Radioiodine remnant ablation after surgery decreases cancer recurrence in low to intermediate risk PTMC patients .

MeSH Keywords*: papillary thyroid microcarcinoma, PTMC, thyroid papillary microcarcinoma, papillary microcarcinoma, radioactive iodine, RAI, radioactive iodine ablation, RRA, iodine-131 therapy, I-131*

INTRODUCTION

Thyroid carcinoma is the most common malignancy of the endocrine system with a global incidence of approximately 10/100,000 women and 3/100,000 men per year, with the incidence increasing worldwide in recent decades. Most of these tumors are papillary thyroid microcarcinomas (PTMC) [1, 3], a subset of papillary thyroid carcinomas, which are defined by the World Health Organization (WHO) as carcinomas ≤ 1 cm in the greatest dimension [2]. Prognosis for PTMC patients is usually excellent, with some studies reporting 5-year survival rates of as high as 95% [4, 5], locoregional recurrence rates of 2 - 4%, and distant metastases at 1 - 2% [6 - 8].

At present, several guidelines that suggest optimal management for PTMC exist, with most recommending surgery alone as sufficient management. Among these are the American Thyroid Association (ATA) guideline, the European Consensus Guideline, the German Society

of Nuclear Medicine, and the British Thyroid Association [10 - 13]. For most of these societies, limited surgical resection without RAI is sufficient in patients without high-risk features. The recently released Philippine Interim Clinical Practice Guidelines (CPG) for the diagnosis and management of well-differentiated thyroid cancer also does not recommend RAI for ATA low risk, unifocal or multifocal papillary microcarcinoma without adverse features. However, in a previous study, a significant part of low-risk DTC patients, for whom RAI is not recommended, presented with lymph-nodal involvement after I-131 whole body scan [31]. Studies also report disease recurrence in 4-16% of patients with many even developing distant metastasis [15 - 18, 20].

An appropriate balance between insufficient treatment and overtreatment must be found to avoid subjecting patients to unnecessary risks. Therefore, debates continue regarding the best treatment for PTMC, and it remains unclear whether RAI ablation could be beneficial in low to intermediate risk PTMC patients. While there have been previous meta-analysis studies done on the subject, results have been conflicting and to date, none have compared outcomes specifically in the low to intermediate risk group. With that in mind, this meta-analysis was done to determine if RAI remnant ablation truly has no role in the management of PTMC, or if it reduces disease recurrence in patients with low to intermediate risk features.

METHODOLOGY

This meta-analysis was performed in accordance with preferred reporting items for systematic reviews and meta-analyses [14]. Institutional review board approval was not required.

Literature-search strategy

The two reviewers performed an independent electronic literature search using the following resource databases: PubMed, Embase, Cochrane library, and Google Scholar. The latest search was performed on October 1, 2022, using one or more combinations of the following medical subject headings (mesh) keywords: “papillary thyroid microcarcinoma” or “PTMC” or “thyroid papillary microcarcinoma” or “papillary microcarcinoma” and “radioactive iodine” or “RAI” or “radioactive iodine ablation” or “RRA” or “iodine-131 therapy” or “I-131”. All the study titles from initial search results were then assessed for relevance before reviewing their respective abstracts. A review of the full texts was done only on the studies which were deemed relevant by the reviewers.

Inclusion and exclusion criteria

Studies which met the following criteria were included in the meta-analysis: (a): studies that included low risk and intermediate risk PTMC patients with no evidence of disease (NED) after initial therapy (total thyroidectomy or near-total thyroidectomy; (b) studies with RAI therapy vs. without RAI therapy groups; and (c) studies that provided data on disease recurrence. Studies were excluded if (a) full texts in English language were not available; (b) studies without a control group; (c) studies that included patients with gross extrathyroidal extension, distant metastasis, and/or incomplete tumor resection on initial diagnosis; and (d) lacking any necessary data .

Data extraction and Outcomes of interest

The two reviewers independently extracted data of interest from each study and summarized all the gathered data. The following details were extracted from each study: study title and reference details (author, year, and country), characteristics of the study population (total population size, median age, gender, extent of surgery, number of subjects treated with and without RAI), disease characteristics & ATA risk classification (presence or absence of risk factors), and outcome data. Efficacy outcomes collected included disease recurrence between with or without RAI ablation after. We defined recurrence as the development of tumor recurrence on imaging modalities (positive WBS, positive FDG-PET, positive histologic or cytologic pathology, including a detectable serum thyroglobulin level on follow up after an initial period of NED. In cases of disagreement, the consultant adviser arbitrated.

Quality assessment

Two reviewers independently assessed the included studies for risk of bias and quality using the modified Newcastle–Ottawa scale (NOS). The NOS criteria was comprised of (1) patient selection, (2) comparability of study groups, and (3) outcome assessment. A total of nine items were extracted, with each item assigned to a score of 1. Studies with scores of 5 or higher were considered to be of good quality.

Statistical analysis

The authors conducted this meta-analysis using review manager (Revman) version 5.4. Outcome data were

compared using a relative ratio (RR) with confidence intervals (CI) of 95%. A p value of < 0.05 was considered statistically significant. Statistical heterogeneity between studies was assessed by visual inspection of their Forest plots, with quantification using the $\chi 2$ -test and I2 statistic. Significance was set at p value < 0.1 and I2 > 50% .

RESULTS

Search Results

The initial search yielded a total of 684 studies; 673 of which were excluded following title or abstract review and full text review. Eleven (11) studies remained which met all the inclusion criteria (Table 1), with a corresponding total of 5,167 patients deemed eligible for inclusion in the study. The PRISMA flow diagram for this meta-analysis is shown in Figure 1.

Study characteristics

All included studies were retrospective cohorts (table 1). The study populations in the included studies ranged from 121 (RAI, n = 63 (52.1%), and no RAI, n = 58 (47.9%)) to 1932 (RAI, n = 1648 (85.3%), and no RAI, n = 284 (14.7%)) patients. All but one study scored NOS ratings of > 7 (considered a high rating), however all studies were considered to be of good quality. The quality assessment details can be seen in Table 2. All the other characteristics of the included studies, as well as available data on administered activities, are illustrated in Table 1.

Patient characteristics

A total of 5167 patients were included for analysis. The TT/NTT + RAI group included 3706 patients (71.7%) vs 1461 (28.3%) in the TT/NTT only group. All patients were considered either low or intermediate risk based on their tumor, node, and metastasis staging. The median follow-up ranged from 4.4 to 17.2 years.

Summary of the meta-analysis for the disease-recurrence rate in the overall population

A total of 11 studies performed the disease recurrence rate after TT/NTT with or without RAI remnant ablation treatment. Upon pooling the available data for any site recurrence of 5167 patients (Figure 2), the event rate in the surgery with RAI treated patients was 78 of 3706 (2.1%) and in surgery without RAI treated patients, it was 130 of 1461 (8.9%). Recurrence rate in those treated with surgery with RAI was lower than those treated with surgery alone with a risk ratio (RR) of 0.30. This was statistically significant (p = 0.03). However, this study group was heterogenous. An investigation into possible reasons for the heterogeneity was then done, one of which was the difference in the median length of follow up. We then performed a subgroup analysis using studies with median follow up of six years or shorter, and found that any site recurrence rate in patients treated with surgery with RAI was significantly lower than in those without RAI (3.0% vs. 12.7%, RR = 0.19, p < 0.00001). Fortunately, no heterogeneity was found within this subgroup (Figure 3).

Structural disease-recurrence rate in LR-IR PTMC patients

One other possible explanation for the heterogeneity could be a difference in what the studies recognized as cut-off values for serum thyroglobulin. This specific data was available in only a few of the studies that included the biochemical marker as evidence for recurrence. A meta-analysis between the structural recurrence (i.e., after exclusion of those with only biochemical evidence of disease) in those treated with surgery and RAI vs. those treated with surgery alone was also done (fig. 4) using 7 out of the 11 included studies. The result showed that RAI after surgery was able to significantly reduce structural disease recurrence rate compared to surgery alone (1.9% vs 4.7%, RR = 0.36, p = 0.0007). No significant heterogeneity was found for this subgroup as well.

Publication bias

Inverted funnel plots of the recurrence rates PTMC treated with and without RAI for each comparison group were produced to determine whether the articles had any publication bias. Figure 5 indicated publication bias in the research. This is possibly due to the heterogeneity between

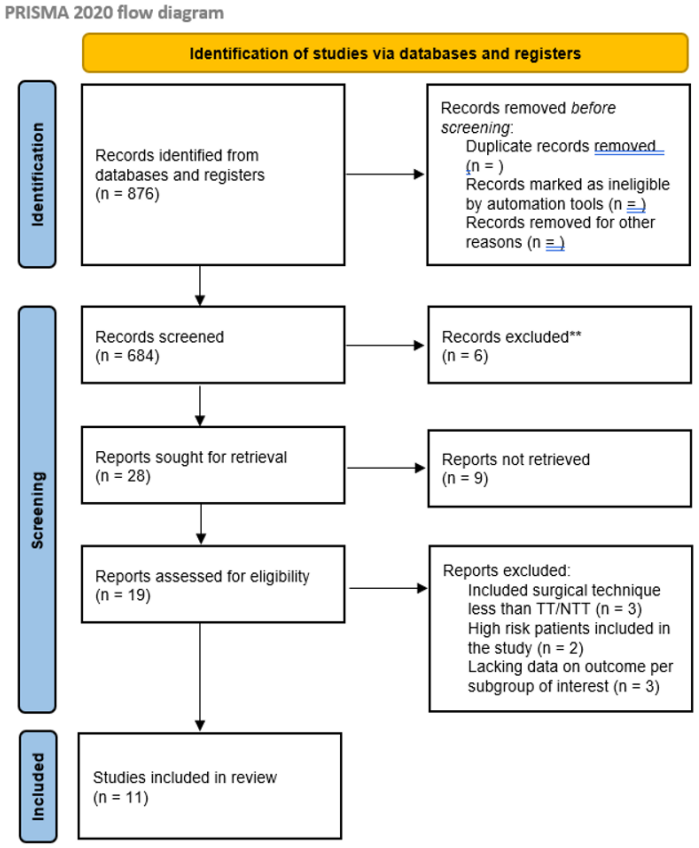

FIGURE 1 PRISMA 2020 flow diagram [32]

TABLE 1. Summary of characteristics of the included studies

Reference	Country	N	Mean age	Gender M/F	Histology	Mean tumor size (mm)	MF (%)	mETE (%)	LNM (%)	TT/ NTT	TT/NTT with RAI	Administered RAI activity (mCi)	Median follow up (yrs)
Chow *et al.* [17]	China	203	46.8	27/176	PTMC	7	31.0	20.7	24.6	187	136	80, 150	8.4
Creach *et al.* [19]	USA	407	45.0	86/321	PTMC	7	46.2	NA	NA	51	349	100	5.3
Dominguez *et al.* [21]	Chile	209	44.5	21/188	PTMC	6.2	38.8	17.7	16.7	209	183	90.4	4.4
Hay *et al.* [22]	USA	900	46	373/627	PTMC	7	NA	NA	NA	765	96	NA	17.2
Kim *et al.* [23]	Korea	704	47	73/631	PTMC	6	32.0	46.3	24.0	704	578	100	5.3
Kim *et al.* [24]	Korea	307	46	32/275	PTMC	8	32.0	38.0	37.0	173	163	100	5.4
Kwon *et al.* [25]	Korea	1932	50	243/1689	PTMC	7	33.1	71.5	29.2	1932	1648	80-150	8.3
Mihailovic *et al.* [26]	Serbia	130	44	22/108	PTMC	NA	27.3	NA	34.6	121	63	100	10
Moon *et al.* [27]	Korea	288	46.6	26/262	PTMC	6.2	20.5	30.9	33.7	181	114	30	6
Pelizzo *et*	Italy	403	Na	66/337	PTMC	NA	14.9	NA	11.7	359	260	NA	8.5
Xue *et al.* [29]	China	137	Na	36/101	PTMC	NA	75.2	92.0	92.0	137	94	30, 100, 150	NA

PTMC: papillary thyroid microcarcinoma; MF: multifocality; mETE: microscopic extrathyroidal extension; LNM: lymph-node metastasis; TT: total thyroidectomy; NTT: near total thyroidectomy.

the articles. Fortunately, however, subgroup analyses performed in the subgroup for any recurrence and the subgroup for structural recurrence (Figure 6) show no publication bias.

DISCUSSION

With the increasing incidence of papillary thyroid microcarcinoma, the debate surrounding its appropriate management continues with most guidelines recommending against radioiodine remnant ablation. While some scholars argue that RRA may only expose the patient to unnecessary risks without added benefit, there are still many that believe otherwise, especially in the Nuclear Medicine field [20, 23-24, 30]. In the Philippines, where I-131 whole body scan is not routinely done post-surgery and where active surveillance is not always an option due to low resource settings, risk factors such as distant metastasis in PTMC patients could go unnoticed and lead to a falsely low staging of disease. This meta-analysis was performed to determine whether RAI remnant ablation reduces disease-recurrence rate in low-to-intermediate risk PTMC patients.

TABLE 2. Methodological quality assessment (risk of bias) of included studies by modified Newcastle–Ottawa scale

References	Selection	Comparability	Outcome	Total score
Chow *et al.* [17]	★★★★	★☆	★★★	8
Creach *et al.* [19]	★★★★	★★	★★★	9
Dominguez *et al.* [21]	★★★★	★☆	★★★	8
Hay *et al.* [22]	★★★★	★☆	★★★	8
Kim *et al.* [23]	★★★★	★☆	★★★	8
Kim *et al.* [24]	★★★★	★☆	★★★	8
Kwon *et al.* [25]	★★★★	★☆	★★★	8
Mihailovic *et al.* [26]	★★★★	★☆	★★★	8
Moon *et al.* [27]	★★★★	★☆	★★★	8
Pelizzo *et al.* [28]	★★★☆	★☆	★★★	7
Xue *et al.* [29]	★★★☆	★★	★☆	6

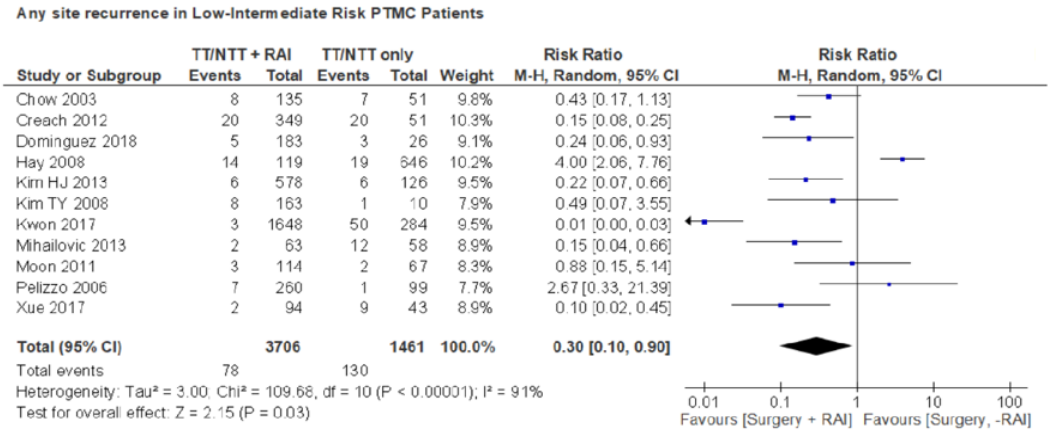

FIGURE 2 Any disease-recurrence in LR-IR PTMC patients

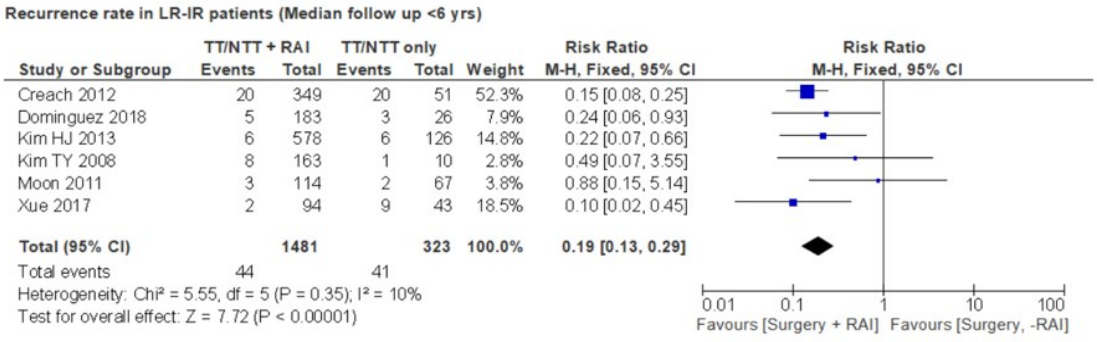

FIGURE 3 Any disease-recurrence rate in LR-IR PTMC patients (Median follow up < 6 years)

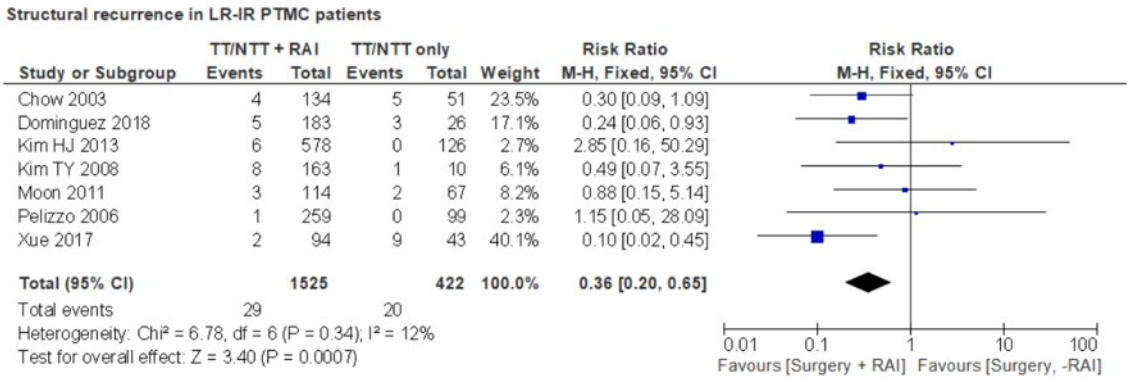

FIGURE 4 Structural recurrence in LR-IR PTMC patients

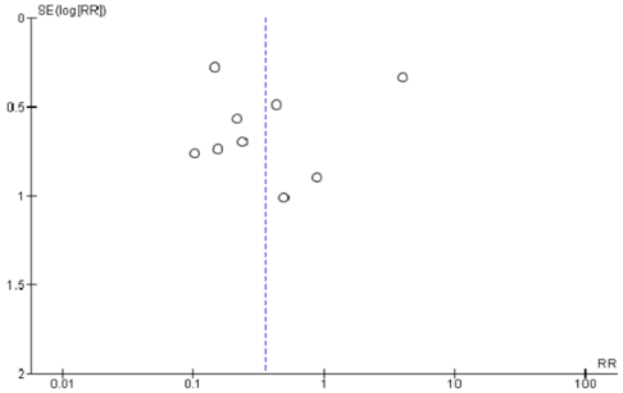

FIGURE 5 Funnel plot comparison of recurrence rates in LR-IR PTMC patients

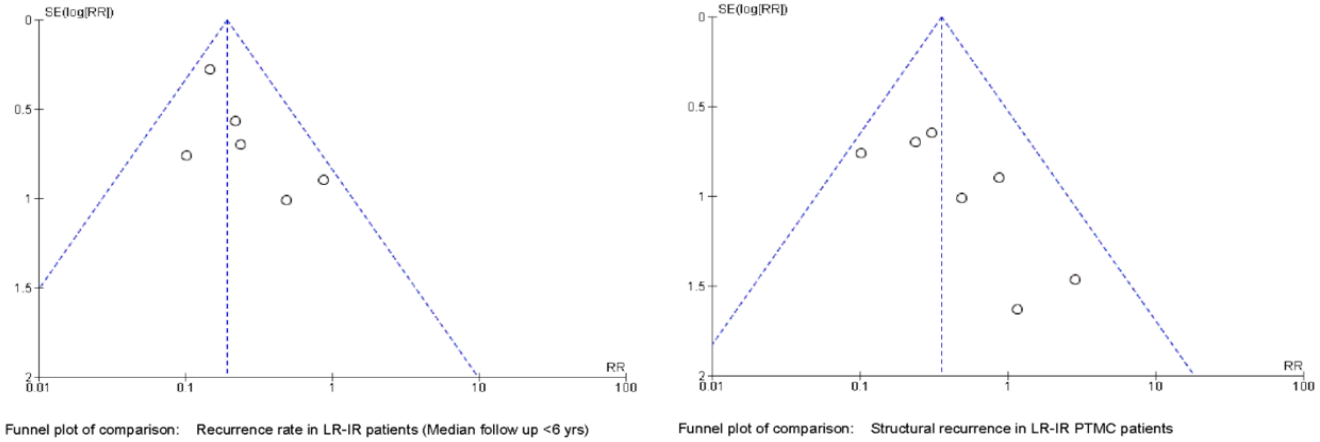

FIGURE 6 Funnel plot comparison any recurrence and structural recurrence subgroups, respectively.

The results showed that RAI ablation reduces the recurrence rate in low to intermediate risk patients, with both biochemical and structural evidence. These results are similar to two previous meta-analyses, which also showed reduced recurrence rates in intermediate risk patients, especially in those presenting with lymph node metastases, extrathyroidal extension, and multifocality which are well-known risk factors .

The limitations to this meta-analysis are as follows: first, all the included studies are retrospective cohorts since very few RCTs on PTMC exist. Some selection bias for treatment may inevitably arise because in practice, RAI ablation is more often given to patients with higher risk stratifications and more aggressive disease. Second, this meta-analysis did not account for the administered RAI activity because available data were not sufficient. Third, because of the small number of studies included, the reliability of the results may be affected. Lastly, the studies included were performed in different centers in different countries which may have resulted in the heterogeneity of the results.

CONCLUSION

Based on the results of this meta-analysis, we conclude that radioactive iodine ablation significantly reduces the recurrence of PTMC in low to intermediate risk patients post-surgery. However, large-volume, well-designed RCTs are still recommended before a definitive conclusion can be made.

Disclosure

The authors have no conflict of interest to declare.

Acknowledgements

The authors would like to sincerely thank the following: Dr. Michele D. Ogbac for her valuable inputs throughout the conduct of this study, Dr. Jerry M. Obaldo and Dr. Angelo O. Martinez for their support and expert guidance, and all of the staff at the Philippine Heart Center – Nuclear Medicine Division, without whom this study would not have been possible.

REFERENCES

1. Roti, E., degli Uberti, E. C., Bondanelli, M., & Braverman, L. E. (2008). Thyroid papillary microcarcinoma: a descriptive and meta-analysis study. European journal of endocrinology, 159(6), 659–673. https://doi.org/10.1530/EJE-07-0896.
2. Hedinger C, Williams E, Sobin L. (1988). Histologic types of thyroid tumors in World Health Organization histological classification of tumors; 2nd ed. Verlag: Springer; pp. 9–10.
3. Londero, S. C., Krogdahl, A., Bastholt, L., Overgaard, J., Trolle, W., Pedersen, H. B., Bentzen, J., Schytte, S., Christiansen, P., Godballe, C., & Danish Thyroid Cancer Group (2013). Papillary thyroid microcarcinoma in Denmark 1996-2008: a national study of epidemiology and clinical significance. Thyroid : official journal of the American Thyroid Association, 23(9), 1159–1164. https://doi.org/10.1089/thy.2012.0595 .
4. Hundahl, S. A., Fleming, I. D., Fremgen, A. M., & Menck, H. R. (1998). A National Cancer Data Base report on 53,856 cases of thyroid carcinoma treated in the U.S., 1985-1995 [see commetns]. Cancer, 83(12), 2638–2648. https://doi.org/10.1002/(sici)1097-0142(19981215)83:12<2638::aid-cncr31>3.0.co;2-1 .
5. Axelsson, T. A., Hrafnkelsson, J., Olafsdottir, E. J., & Jonasson, J. G. (2015). Tall cell variant of papillary thyroid carcinoma: a population-based study in Iceland. Thyroid : official journal of the American Thyroid Association, 25(2), 216–220. https://doi.org/10.1089/thy.2014.0075.
6. Siddiqui, S., White, M. G., Antic, T., Grogan, R. H., Angelos, P., Kaplan, E. L., & Cipriani, N. A. (2016). Clinical and Pathologic Predictors of Lymph Node Metastasis and Recurrence in Papillary Thyroid Microcarcinoma. Thyroid : official journal of the American Thyroid Association, 26(6), 807–815. https://doi.org/10.1089/thy.2015.0429.
7. Yu, X. M., Wan, Y., Sippel, R. S., & Chen, H. (2011). Should all papillary thyroid microcarcinomas be aggressively treated? An analysis of 18,445 cases. Annals of surgery, 254(4), 653–660. https://doi.org/10.1097/SLA.0b013e318230036d.
8. Jeon, M. J., Kim, W. G., Choi, Y. M., Kwon, H., Lee, Y. M., Sung, T. Y., Yoon, J. H., Chung, K. W., Hong, S. J., Kim, T. Y., Shong, Y. K., Song, D. E., & Kim, W. B. (2016). Features Predictive of Distant Metastasis in Papillary Thyroid Microcarcinomas. Thyroid : official journal of the American Thyroid Association, 26(1), 161–168. https://doi.org/10.1089/thy.2015.0375.
9. Davies, L., & Welch, H. G. (2014). Current thyroid cancer trends in the United States. JAMA otolaryngology-- head & neck surgery, 140(4), 317–322. https://doi.org/10.1001/jamaoto.2014.1.
10. American Thyroid Association (ATA) Guidelines Taskforce on Thyroid Nodules and Differentiated Thyroid Cancer, Cooper, D. S., Doherty, G. M., Haugen, B. R., Kloos, R. T., Lee, S. L., Mandel, S. J., Mazzaferri, E. L., McIver, B., Pacini, F., Schlumberger, M., Sherman, S. I., Steward, D. L., & Tuttle, R. M. (2009). Revised American Thyroid Association management guidelines for patients with thyroid nodules and differentiated thyroid cancer. Thyroid : official journal of the American Thyroid Association, 19(11), 1167–1214. https://doi.org/10.1089/thy.2009.0110.
11. Pacini, F., Schlumberger, M., Dralle, H., Elisei, R., Smit, J. W., Wiersinga, W., & European Thyroid Cancer Taskforce (2006). European consensus for the management of patients with differentiated thyroid carcinoma of the follicular epithelium. European journal of endocrinology, 154(6), 787–803. https://doi.org/10.1530/eje.1.02158.
12. Dietlein, M., Dressler, J., Eschner, W., Grünwald, F., Lassmann, M., Leisner, B., Luster, M., Moser, E., Reiners, C., Schicha, H., Schober, O., Deutsche Gesellschaft für Nuklearmedizin, & Deutsche Gesellschaft für Medizinische Physik (2007). Verfahrensanweisung zur Radioiodtherapie (RIT) beim differenzierten Schilddrüsenkarzinom (Version 3) [Procedure guidelines for radioiodine therapy of differentiated thyroid cancer (version 3)]. Nuklearmedizin. Nuclear medicine, 46(5), 213–219.
13. British Thyroid Association. Royal College of Physicians:guidelines for the management of thyroid cancer. Perros P, ed. 2nd ed. Report of the Thyroid Cancer Guidelines Update Group. London, England: Royal College of Physicians; 2007.
14. Moher, D., Shamseer, L., Clarke, M., Ghersi, D., Liberati, A., Petticrew, M., Shekelle, P., Stewart, L. A., & PRISMA-P Group (2015). Preferred reporting items for systematic review and meta-analysis protocols (PRISMA-P) 2015 statement. Systematic reviews, 4(1), 1. https://doi.org/10.1186/2046-4053-4-1.

15. Giordano, D., Gradoni, P., Oretti, G., Molina, E., & Ferri, T. (2010). Treatment and prognostic factors of papillary thyroid microcarcinoma. Clinical otolaryngology : official journal of ENT-UK ; official journal of Netherlands Society for Oto-Rhino-Laryngology & Cervico-Facial Surgery, 35(2), 118–124. https://doi.org/10.1111/j.1749-4486.2010.02085.x.
16. Arora, N., Turbendian, H. K., Kato, M. A., Moo, T. A., Zarnegar, R., & Fahey, T. J., 3rd (2009). Papillary thyroid carcinoma and microcarcinoma: is there a need to distinguish the two?. Thyroid : official journal of the American Thyroid Association, 19(5), 473–477. https://doi.org/10.1089/thy.2008.0185.
17. Chow, S. M., Law, S. C., Chan, J. K., Au, S. K., Yau, S., & Lau, W. H. (2003). Papillary microcarcinoma of the thyroid -Prognostic significance of lymph node metastasis and multifocality. Cancer, 98(1), 31–40. https://doi.org/10.1002/cncr.11442.
18. Ross, D. S., Litofsky, D., Ain, K. B., Bigos, T., Brierley, J. D., Cooper, D. S., Haugen, B. R., Jonklaas, J., Ladenson, P. W., Magner, J., Robbins, J., Skarulis, M. C., Steward, D. L., Maxon, H. R., & Sherman, S. I. (2009). Recurrence after treatment of micropapillary thyroid cancer. Thyroid : official journal of the American Thyroid Association, 19 (10), 1043–1048. https://doi.org/10.1089/thy.2008.0407.
19. Creach, K. M., Siegel, B. A., Nussenbaum, B., & Grigsby, P. W. (2012). Radioactive iodine therapy decreases recurrence in thyroid papillary microcarcinoma. ISRN endocrinology, 2012, 816386. https://doi.org/10.5402/2012/816386.
20. Al-Qurayshi, Z., Nilubol, N., Tufano, R. P., & Kandil, E. (2020). Wolf in Sheep's Clothing: Papillary Thyroid Microcarcinoma in the US. Journal of the American College of Surgeons, 230(4), 484–491. https://doi.org/10.1016/j.jamcollsurg.2019.12.036.
21. Domínguez, J. M., Nilo, F., Martínez, M. T., Massardo, J. M., Muñoz, S., Contreras, T., Carmona, R., Jerez, J., González, H., Droppelmann, N., & León, A. (2018). Papillary thyroid microcarcinoma: characteristics at presentation, and evaluation of clinical and histological features associated with a worse prognosis in a Latin American cohort. Archives of endocrinology and metabolism, 62(1), 6–13. https://doi.org/10.20945/2359-3997000000013.
22. Hay, I. D., Hutchinson, M. E., Gonzalez-Losada, T., McIver, B., Reinalda, M. E., Grant, C. S., Thompson, G. B., Sebo, T. J., & Goellner, J. R. (2008). Papillary thyroid microcarcinoma: a study of 900 cases observed in a 60-year period. Surgery, 144(6), 980–988. https://doi.org/10.1016/j.surg.2008.08.035.
23. Kim, H. J., & Kim, S. W. (2013). Radioactive iodine ablation does not prevent recurrences in patients with papillary thyroid microcarcinoma. Clinical endocrinology, 79(3), 445. https://doi.org/10.1111/cen.12131.
24. Kim, T. Y., Hong, S. J., Kim, J. M., Kim, W. G., Gong, G., Ryu, J. S., Kim, W. B., Yun, S. C., & Shong, Y. K. (2008). Prognostic parameters for recurrence of papillary thyroid microcarcinoma. BMC cancer, 8, 296. https://doi.org/10.1186/1471-2407-8-296.
25. Kwon, H., Jeon, M. J., Kim, W. G., Park, S., Kim, M., Kim, T. Y., Han, M., Song, D. E., Sung, T. Y., Yoon, J. H., Hong, S. J., Ryu, J. S., Shong, Y. K., & Kim, W. B. (2017). Lack of Efficacy of Radioiodine Remnant Ablation for Papillary Thyroid Microcarcinoma: Verification Using Inverse Probability of Treatment Weighting. Annals of surgical oncology, 24(9), 2596–2602. https://doi.org/10.1245/s10434-017-5910-7.
26. Mihailovic, J., Stefanovic, L., & Stankovic, R. (2013). Influence of initial treatment on the survival and recurrence in patients with differentiated thyroid microcarcinoma. Clinical nuclear medicine, 38(5), 332–338. https://doi.org/10.1097/RLU.0b013e3182872ed2.
27. Moon, H. J., Kim, E. K., Chung, W. Y., Yoon, J. H., & Kwak, J. Y. (2011). Minimal extrathyroidal extension in patients with papillary thyroid microcarcinoma: is it a real prognostic factor?. Annals of surgical oncology, 18(7), 1916–1923. https://doi.org/10.1245/s10434-011-1556-z.
28. Pelizzo, M. R., Boschin, I. M., Toniato, A., Piotto, A., Bernante, P., Pagetta, C., Rampin, L., & Rubello, D. (2006). Papillary thyroid microcarcinoma (PTMC): prognostic factors, management and outcome in 403 patients. European journal of surgical oncology : the journal of the European Society of Surgical Oncology and the British Association of Surgical Oncology, 32(10), 1144–1148. https://doi.org/10.1016/j.ejso.2006.07.001.
29. Xue, S., Wang, P., Liu, J., & Chen, G. (2017). Radioactive Iodine Ablation Decrease Recurrences in Papillary Thyroid Microcarcinoma with Lateral Lymph Node Metastasis in Chinese Patients. World journal of surgery, 41(12), 3139–3146. https://doi.org/10.1007/s00268-017-4134-0.
30. Neuhold, N., Schultheis, A., Hermann, M., Krotla, G., Koperek, O., & Birner, P. (2011). Incidental papillary microcarcinoma of the thyroid--further evidence of a very low malignant potential: a retrospective clinicopathological study with up to 30 years of follow-up. Annals of surgical oncology, 18(12), 3430–3436. https://doi.org/10.1245/s10434-011-1663-x.
31. Gallicchio, R., Giacomobono, S., Capacchione, D., Nardelli, A., Barbato, F., Nappi, A., Pellegrino, T., & Storto, G. (2013). Should patients with remnants from thyroid microcarcinoma really not be treated with iodine-131 ablation?. Endocrine, 44(2), 426–433. https://doi.org/10.1007/s12020-013-9935-9.
32. Page, M. J., McKenzie, J. E., Bossuyt, P. M., Boutron, I., Hoffmann, T. C., Mulrow, C. D., Shamseer, L., Tetzlaff, J. M., Akl, E. A., Brennan, S. E., Chou, R., Glanville, J., Grimshaw, J. M., Hróbjartsson, A., Lalu, M. M., Li, T., Loder, E. W., Mayo-Wilson, E., McDonald, S., McGuinness, L. A., … Moher, D. (2021). The PRISMA 2020 statement: an updated guideline for reporting systematic reviews. BMJ (Clinical research ed.), 372, n71. https://doi.org/10.1136/bmj.n71.

ASSURANCE CONTROLS TECHNOLOGIES CO., INC.

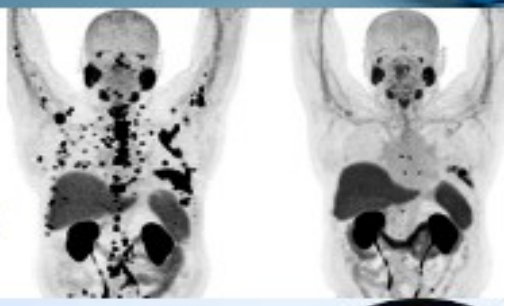

YOUR ONE STOP SHOP FOR ALL YOUR NUCLEAR MEDICINE NEEDS

Our innovation lies in our commitment to transforming the future of healthcare. Our flagship products in nuclear medicine are designed to deliver deeper insights, strengthen diagnostic confidence, and bring your patients closer to cutting-edge technology that matter.

YOUR PARTNER FOR:

- Radiopharmaceutical Products
- Theranostics Products
- Molecular Imaging Equipments
- Radiation Monitoring Devices
- Calibration Sources
- Hot Laboratory Equipment
- Radiation Protection Products

CONTACT

sales@assurancecontrols.com

1710 Annapolis Wilshire Plaza, Greenhills, San Juan

GMS
GLOBAL MEDICAL SOLUTIONS

THE SERVICE DIFFERENCE

PIONEER IN RADIOPHARMACY BUSINESS • WIDE PRODUCT PORTFOLIO
WORLDWIDE RADIOPHARMACEUTICAL MANUFACTURING NETWORK • WIDELY AND HIGHLY EXPERIENCED STAFF
VALUE ADDED SERVICE • CONSISTENT SUPPLY • PROMPT DELIVERY
STRINGENT QC/QA • VALUE FOR MONEY

GMS Pharmacy's mission is to be the premier provider of prepared time-critical radio-pharmaceuticals and comprehensive value-added pharmacy services that meet the needs of the professional health care community and their patients.

We are dedicated to providing quality services that exceed our customer's expectations and maintain their trust.

We work as a team which is the result of open communication and the free exchange of ideas and information in an environment that values and encourages respect and dignity for every individual. The health and safety of our employees, customers, and the community will never be compromised

PRODUCTS AND SERVICES

RADIOPHARMACY • RADIOMMUNOASSAY KITS • 1-125 BRACHY SEEDS • NUCLEAR MEDICINE EQUIPMENT
RADIOLOGIC EQUIPMENT • ULTRASOUND MACHINES • IVD REAGENTS • AFTER SALES SUPPORT

^{18}F-Fluorocholine (FCH) Positron Emission Tomography/Computed Tomography (PET/CT) in the Detection of Parathyroid Adenoma: A Case Series

Mea Glor L. Tumambing, MD, Irene S. Bandong, MD, Christopher Timothy L. Azarraga, MD

Department of Nuclear Medicine and Theranostics, St. Luke's Medical Center - Quezon City
E-mail address: mgl.tumambing@gmail.com

ABSTRACT

The emerging use of ^{18}F-fluorocholine (FCH) PET/CT has demonstrated superior diagnostic performance in the localization of parathyroid adenoma or hyperplasia attributed to its high spatial resolution, thus high sensitivity, shorter imaging time, and lower radiation dose.

This case series presented the FCH PET/CT findings in four adult female patients presenting with primary hyperparathyroidism and with a high clinical suspicion for parathyroid adenoma. The first patient, with discordant sonographic and scintigraphic results, had a focal increased FCH uptake inferoposterior to the right thyroid lobe, which aided in the localization of the parathyroid adenoma prior to surgery. Another patient, with a mediastinal lesion, initially suspected as an ectopic parathyroid adenoma, was later identified as a round to spindle cell neoplasm, showcasing FCH PET/CT's ability to detect other pathologies. Aside from the detection of parathyroid adenoma, one patient had a mildly FCH-avid focus in the right breast, highlighting the need for follow-up in incidental findings. The last patient, with multiglandular disease, had two FCH-positive foci posterior to the upper poles of both thyroid lobes not identified in parathyroid scintigraphy, confirmed by histopathology as parathyroid hyperplasia.

Despite its higher cost and limited availability in the Philippines, the study underscores the utility of FCH PET/CT in the detection and localization of hyperfunctioning parathyroid glands, especially in cases with negative or inconclusive conventional imaging, albeit its non-specific uptake in benign and malignant conditions requires careful interpretation of incidental findings.

***Keywords**: Primary hyperparathyroidism, parathyroid adenoma, parathyroid hyperplasia, parathyroid scintigraphy, 18F-fluorocholine PET/CT imaging*

INTRODUCTION

Primary hyperparathyroidism (PHPT) is a commonly encountered endocrine disorder, usually due to autonomous overproduction of parathyroid hormone (PTH) from one or more parathyroid glands. Solitary parathyroid adenoma accounts for 80-85% of cases, while approximately 15-20% of patients harbor multiple hyperfunctioning glands (i.e., hyperplasia, double or multiple adenomas), with parathyroid carcinoma being even rarer [1, 2]. Patients usually present with asymptomatic hypercalcemia; however, in developing countries where routine biochemical screening is lacking, patients may present with signs and symptoms such as bone pain, fractures, kidney stones, or even renal or neurologic impairment [3].

Once PHPT is diagnosed, surgical removal of the hyperfunctioning parathyroid gland remains the definitive treatment. Preoperative parathyroid imaging is recommended for localization of the abnormal parathyroid gland(s), since this can guide surgeons in performing selective parathyroidectomy, thus shortening surgery duration, minimizing damage to surrounding structures and complications, and even achieving a better cosmetic outcome [4, 5]. Cervical ultrasound, one of the initial imaging modalities widely used for localization of parathyroid adenoma, has a pooled sensitivity of 80% [6]. However, it has less sensitivity for parathyroid glands that are small, or have an ectopic, posterior, or intrathyroidal location. It also has limited use for patients with multiglandular disease and concomitant thyroid disease [5, 7].

Another initial imaging modality utilized is parathyroid scintigraphy, either using a dual-tracer or dual-phase imaging protocol. ^{99m}Tc-sestamibi is the most widely accepted radiopharmaceutical for parathyroid scintigraphy, which usually accumulates in the mitochondria. Parathyroid adenomas concentrate the radiotracer due to the increased number of mitochondria present in the oxyphil cells [8]. Compared to cervical ultrasound; it can detect ectopic or posteriorly located parathyroid adenomas. It has varying sensitivity of 41% to 96% using the dual-phase protocol, and 47% to 87% using the dual-tracer technique [7]. This is influenced by the protocol used, gland pathology (i.e., too small for the gamma camera resolution or too few oxyphil cells), and in multiglandular disease [5]. Addition of single photon emission computed tomography/ computed tomography (SPECT/CT) improves the localization of the parathyroid adenoma. Parathyroid scintigraphy is likewise usually done in combination with cervical ultrasound to increase the accuracy of localizing the abnormal gland if with concordant results [7].

Four-dimensional (4D) parathyroid computed tomography (CT) scan is also being used for preoperative imaging of patients with primary hyperparathyroidism. Even though it has shorter imaging time, the administration of iodinated contrast limits its use especially in patients with renal impairment, and has the risk of delivering higher radiation dose to patients. Likewise, the use of magnetic resonance imaging (MRI) for parathyroid localization is increasing, but studies evaluating its role for primary hyperparathyroidism are limited [5, 9].

The emergence of positron emission tomography/ computed tomography (PET/CT) using ^{18}F-fluorocholine (FCH) has improved the localization of hyperfunctioning parathyroid glands, especially in patients with inconclusive or discordant results in conventional imaging [5]. In a prospective study in the United States by Hope et al. (2021), the correct localization rate for the parathyroid adenoma using FCH PET/CT is 75%, while the localization rate of parathyroid imaging using ^{99m}Tc-sestamibi increased from 17% to 70% with FCH PET/CT [10]. This case series delves into the utility of novel imaging modality ^{18F}-FCH PET/CT scan in accurate localization of parathyroid adenoma in patients presenting with primary hyperparathyroidism in the Philippines.

OBJECTIVE

General Objective

To describe the PET/CT findings of adult patients with primary hyperparathyroidism who underwent ^{18}F-fluorocholine PET/CT at St. Luke's Medical Center - Quezon City

Specific Objectives

- To describe the outcomes of adult patients with primary hyperparathyroidism who underwent ^{18}F-fluorocholine PET/CT in St. Luke's Medical Center - Quezon City

- To describe the potential pitfalls of ^{18}F-fluorocholine PET/CT imaging

METHODOLOGY

This is a case series done at St. Luke's Medical Center - Quezon City from January 1, 2024 to September 30, 2024. The database of the PET/CT section was reviewed for possible inclusion of adult participants aged 18 years and above presenting with primary hyperparathyroidism who underwent ^{18}F-fluorocholine PET/CT for detection and localization of parathyroid adenoma.

Criteria for Participant Selection

Inclusion Criteria

Adult patients aged 18 years and older who present with primary hyperparathyroidism and have undergone ^{18}F-fluorocholine PET/CT imaging for the detection of parathyroid adenoma.

Exclusion Criteria

- Patients with prior thyroid surgeries or other surgeries of the head and neck

- Patients with incomplete or inaccessible medical records for review

Operational Definitions

- **Primary hyperparathyroidism** - Diagnosis made by a specialist (i.e., endocrinologist) in patients with hypercalcemia and elevated parathyroid hormone level, either patient is asymptomatic or symptomatic.
- **Positron Emission Tomography (PET) scan** - A non-invasive functional imaging modality in nuclear medicine which utilizes positron-emitting radionuclides to produce 3D images of tissues or organs.

- **^{18}Fluorine (^{18F})-fluorocholine (FCH)** - A positron emitter that is imaged using a PET scanner initially indicated for the evaluation of prostate carcinoma and also being used today for the preoperative localization of hyperfunctioning parathyroid glands.
- **Standard Uptake Value (SUV)** - A semiquantitative measure of the radiotracer uptake in the area of interest which takes into consideration the administered dose, time of injection, and the patient's body weight.
- **Dual-tracer parathyroid scintigraphy** - A nuclear medicine procedure that uses two radiopharmaceuticals: ^{99m}Technetium-pertechnetate (^{99m}Tc-O4-) and ^{99m}Technetium-sestamibi for the evaluation of parathyroid adenoma.
- **Dual-phase parathyroid scintigraphy** - A nuclear medicine procedure for evaluation of parathyroid adenoma performed at two time points: early phase (10-15 minutes post-injection of ^{99m}Tc-sestamibi) and delayed phase (up to 4 hours after tracer administration)
- **Single Photon Emission Computed Tomography and Computed Tomography (SPECT/CT)** - A hybrid imaging technique being utilized in nuclear medicine for anatomical localization.

Study Maneuver

The investigators reviewed the medical records of patients with primary hyperparathyroidism who underwent ^{18}F-fluorocholine PET/CT imaging in St. Luke's Medical Center - Quezon City, Philippines. The data gathered include the following: age, sex, symptoms at the time of examination, comorbidities, laboratory tests, and prior imaging modalities (i.e., ultrasound, parathyroid scintigraphy), PET/CT findings, and histopathologic reports if any.

Data Analysis

Descriptive statistics was used to summarize the patients' demographic characteristics and clinical data. All data analyses were performed using Microsoft Excel.

Ethical Approval

The study has been approved by the St. Luke's Institutional Scientific Review Committee (ISRC), and registered by the Institutional Ethics Review Committee (IERC). The study, EC Reference No. 25022, has been exempted from ethics review.

The study was conducted in accordance with the Good Clinical Practice (GCP) guidelines and National Ethical Guidelines for Health and Health-Related Research (NEG HHRR) [20], and adhered to the principles of the Declaration of Helsinki [21].

RESULTS

A total of four female patients were included in the study: two elderly, one middle-aged adult, and one young adult. All patients presented with hypercalcemia (mean ionized calcium of 1.74 mmol/L) and hyperparathyroidism (mean intact parathyroid hormone level of 353.68 pg/mL). One patient had an existing thyroid disease.

Case 1

A 24-year-old female initially presented with abdominal pain and early satiety, had several laboratory tests and imaging done to evaluate the possible cause (Table 1). Due to discordant results of neck ultrasound and parathyroid scintigraphy, the patient then underwent ^{18}F-fluorocholine (FCH) PET/CT scan to evaluate for parathyroid adenoma.

The patient underwent parathyroidectomy of the right inferior parathyroid gland, with the frozen section revealing enlarged hypercellular parathyroid. The histopathologic finding along with the decrease in the intact PTH level from 162.60 pg/mL (pre-incision) to 19.80 pg/mL (10 minutes post-excision) and eventually to 9.30 pg/mL (20 minutes post-excision) is consistent with parathyroid adenoma.

Case 2

The patient is an 81-year-old female who has elevated ionized calcium of 1.33 mmol/L and PTH of 188.90 pg/mL. Sonographic evaluation of the parathyroid gland showed no nodule or mass lesion, while dual-phase parathyroid scintigraphy with SPECT/CT scan showed a sestamibi-avid focus in the inferior aspect of the right thyroid lobe, as well as a sestamibi-avid lesion in the anterior mediastinum (Figure 2). A 4D CT scan of the parathyroid was also performed for further characterization of the lesions, and revealed an

TABLE 1. Summary of Laboratory and Imaging Results of Patient 1

Laboratory / Imaging Tests	Results
Urinalysis	Few calcium oxalate stones
Ionized calcium	1.48 mmol/L (Normal range: 1.0 - 1.3 mmol/L)
Intact parathyroid hormone (PTH)	233.50 pg/mL (Normal range: 18.5 - 88.0 pg/mL)
Total vitamin D	22.29 ng/mL (Normal range: 30 - 100 ng/mL)
Urine calcium	39.9 mg/dL (Normal range: 2.0 - 17.5 mg/dL)
Serum creatinine	0.52 mg/dL (Normal range: 0.55 - 1.02 mg/dL)
CT stonogram	Two lithiases in the lower pole calyces of the left kidney
Neck ultrasound	Heterogeneous hypoechoic solid nodule below the right thyroid lobe, which was hypervascular on color Doppler interrogation, to consider right parathyroid parenchymal disease.
Dual-tracer dual-phase parathyroid scintigraphy with SPECT/CT	No sestamibi-avid lesion in the neck and chest to suggest the presence of parathyroid adenoma.

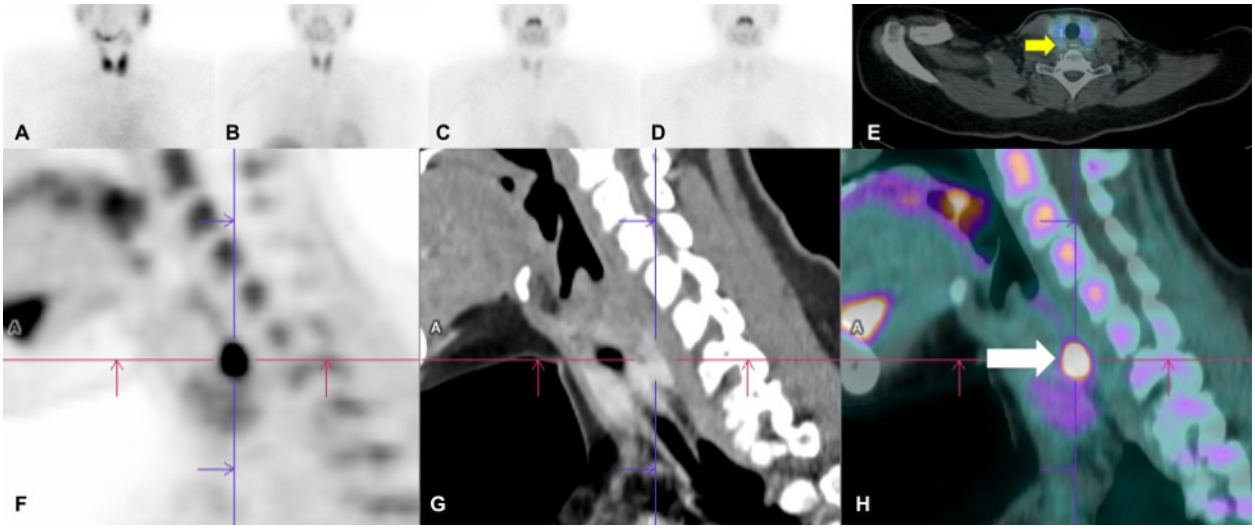

FIGURE 1 Dual-tracer dual-phase parathyroid scintigraphy showed no pertechnetate-avid (A) and no sestamibi-avid lesion in the initial image 10 minutes after 99mTc-sestamibi administration (B), as well as in the delayed 2-hour (C) and 4-hour images (D). Axial SPECT-CT image (E) showed a nodular density posterior to the right thyroid lobe with no corresponding sestamibi uptake (yellow arrow). Sagittal PET (F), CT (G) and fused PET/CT (H) images of the neck showed an FCH-avid enhancing nodular focus inferoposterior to the right thyroid lobe (white arrow) measuring 0.8 x 0.9 x 1.2 cm and with a standard uptake value (SUV) of 19.7, suggestive of a parathyroid adenoma.

elongated nodule near the inferior pole of the right thyroid lobe, isodense during the portal venous phase, exhibiting washout in the delayed phase and becoming hypodense. It also showed a lobulated soft tissue lesion with central necrotic area in the middle mediastinum exhibiting patchy arterial phase enhancement and progressive enhancement in the venous and delayed phases. An FCH PET/CT scan was then performed to evaluate for any FCH-positive lesions (Figures 3 and 4).

Two months after, the patient underwent percutaneous needle biopsy of the mediastinal mass with histopathologic finding of a round to spindle cell

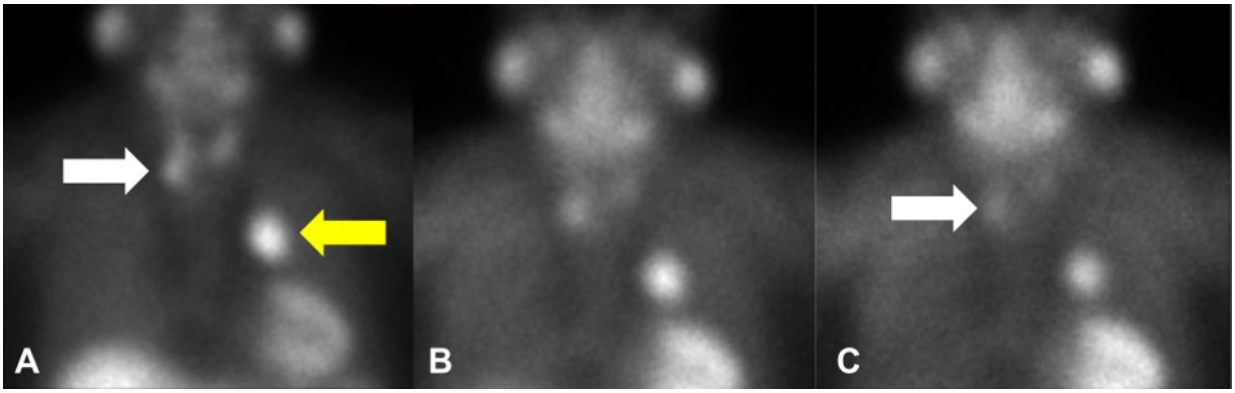

FIGURE 2 Dual-phase parathyroid scintigraphy showed a sestamibi-avid focus in the inferior third of the right thyroid lobe (white arrow) in the early phase of imaging 15 minutes post-sestamibi administration (A), which decreased in intensity on the delayed 4-hour image (C). A persistently sestamibi-avid focus is also seen in the mediastinum throughout the study (yellow arrow).

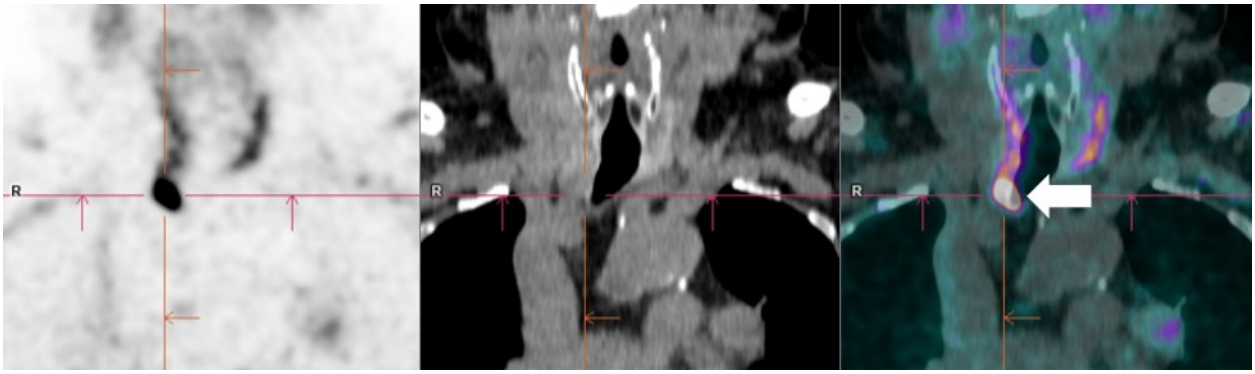

FIGURE 3 Coronal PET/CT images showed an FCH-avid (SUV of 16.6) focus in the inferior pole of the right thyroid lobe at the level of the sternoclavicular joint, between the proximal right common carotid artery and trachea at the level of the sternoclavicular joint (white arrow), measuring 1.5 x 0.9 x 0.6 cm. This is suggestive of a parathyroid adenoma.

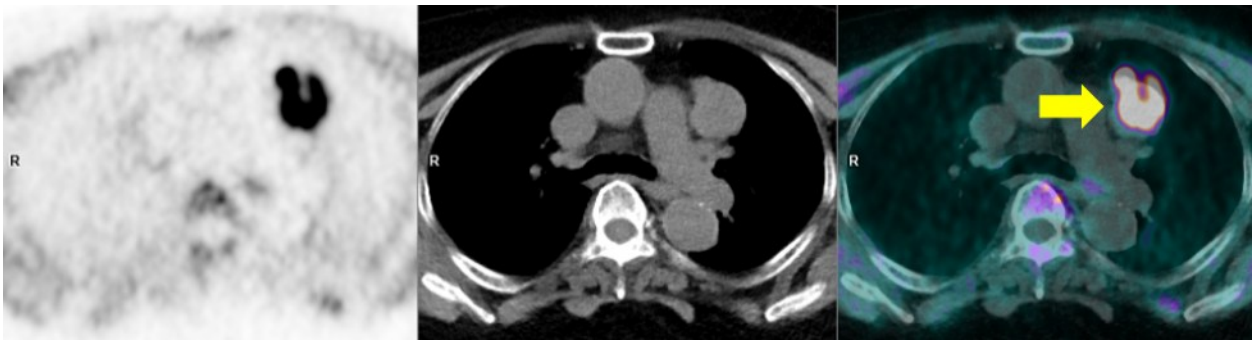

FIGURE 4 Axial PET/CT images of the chest showed an FCH-avid (SUV of 14.1) lobulated soft tissue mass in the middle mediastinum near the para-aortic region (yellow arrow), measuring 3.0 x 2.9 x 3.5 cm and showing a central region devoid of tracer uptake, which may be attributed to necrosis. Differentials include ectopic parathyroid tissue, enlarged lymph node with central necrosis, or another neoplastic process.

neoplasm. Immunohistochemical staining was recommended for a more definitive diagnosis, but was not done. A follow-up 4D CT scan of the parathyroid was done after 6 months, and the lobulated soft tissue mass in the middle mediastinum and nodule in the inferior pole of the right thyroid lobe are relatively stable. The patient is currently asymptomatic.

Case 3

The patient is a 50-year-old female, non-hypertensive, non-diabetic, with multinodular non-toxic goiter, and a known case of clear cell renal cell carcinoma who underwent left open radical nephrectomy and 12 cycles of Pembrolizumab. She came to the PET center presenting with elevated ionized calcium of 1.42 mmol/L

and a borderline high PTH of 64.40 pg/mL. Neck ultrasound only showed bilateral thyroid lobe nodules. An FCH PET/CT scan was performed to evaluate for parathyroid adenoma due to the negative ultrasound result (Figures 5 and 6).

The patient had undergone ultrasound-guided fine needle aspiration biopsy of the right thyroid lobe nodule showing atypia of undetermined significance, and the left thyroid lobe nodule which was suggestive of a benign follicular nodule. A month later, the patient proceeded with a parathyroidectomy of the right inferior parathyroid. The histopathologic features of the excised parathyroid, which is an enlarged hypercellular parathyroid, and the concomitant decrease in the PTH levels from 146.50 pg/mL pre-gland excision to 42.30 pg/mL 10 minutes post-gland excision, are compatible with a parathyroid adenoma. Total thyroidectomy was also performed and showed multifocal papillary thyroid carcinoma.

Case 4

The patient is an 85-year-old female, known to be hypertensive, diabetic, and dyslipidemic, presenting with drowsiness, easy fatigability, and disorientation. Workups revealed primary hyperparathyroidism, with high suspicion for a parathyroid adenoma (Table 2). An FCH PET/CT scan was performed due to negative sonographic and scintigraphic findings (Figure 7).

The patient underwent parathyroidectomy of the right and left superior pole nodules showing cellular parathyroid tissue, with the intraoperative PTH levels decreasing from 2,505.00 pg/mL to 639.80 pg/mL following excision of the right parathyroid gland and 441.20 pg/mL following removal of the left parathyroid gland, compatible with parathyroid hyperplasia. Postoperatively, normalization of ionized calcium at level of 1.12 mmol/L was also noted.

Summarized in Table 3 are the imaging and histopathologic findings of the four included patients in the study. FCH PET/CT scan localized the hyperfunctioning parathyroid glands in all patients, three of them underwent surgical removal.

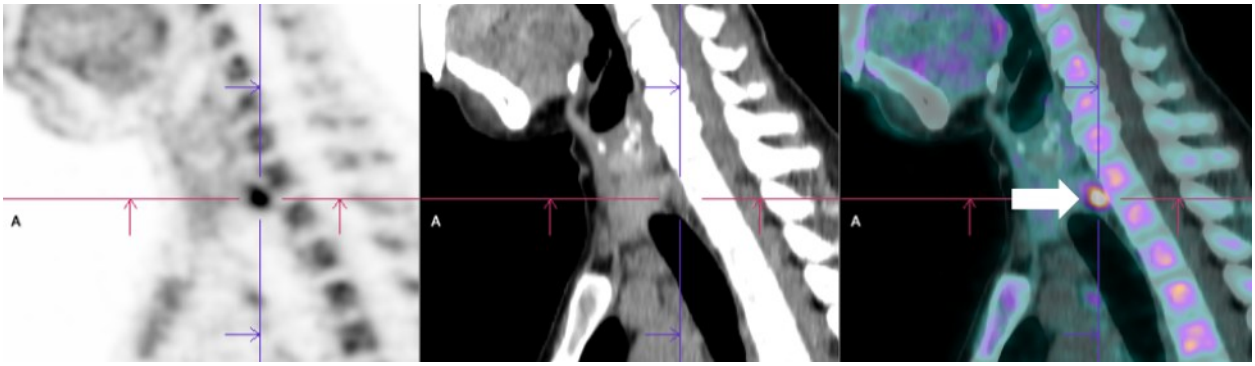

FIGURE 5 Sagittal PET/CT images of the neck and upper chest showed a focal increased FCH uptake inferoposterior to the right thyroid lobe at the tracheoesophageal groove with SUV of 7.9 (white arrow), suggestive of parathyroid adenoma.

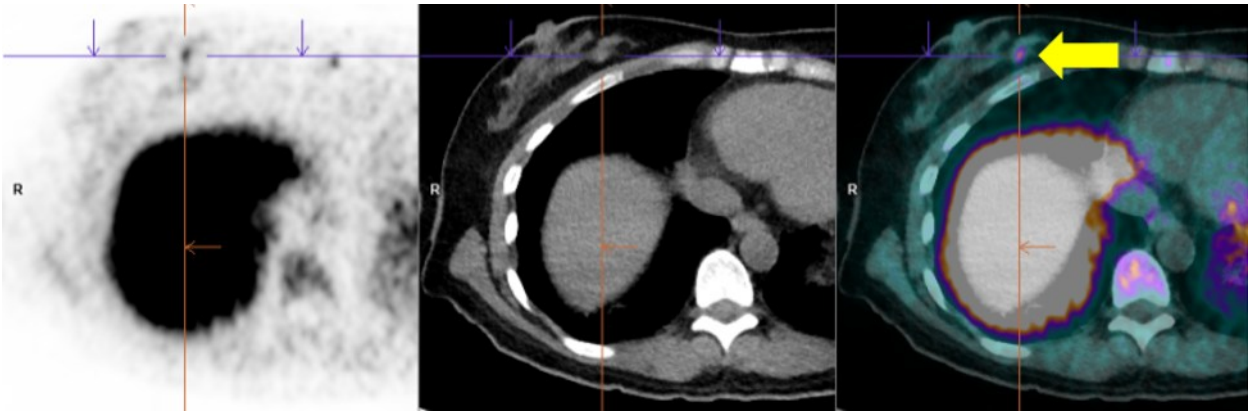

FIGURE 6 Axial PET/CT images of the chest show an incidental finding of a small mildly FCH-avid focus in the lower inner quadrant of the right breast, with SUV of 3.7 (yellow arrow).

TABLE 2. Summary of Laboratory and Imaging Findings of Patient 4

Laboratory / Imaging Tests	Results
Ionized calcium	2.74 mmol/L (Normal range: 1.09 - 1.30 mmol/L)
Intact parathyroid hormone (PTH)	927.90 pg/mL (Normal range: 18.5 - 88.0 pg/mL)
Serum creatinine	1.03 mg/dL (Normal range: 0.55 - 1.02 mg/dL); EGFR 48.9 mL/min/1.73m^2
Neck and thyroid ultrasound	Bilateral unenlarged cervical lymph nodes, and Bilateral lobe and isthmic nodules
Kidney and urinary bladder ultrasound	Non-obstructing left nephrolithiasis
Dual-tracer dual-phase parathyroid scintigraphy with SPECT/CT	Nodule in the inferior pole of the right thyroid lobe with decreased pertechnetate uptake and only mild sestamibi uptake (Figure 7A-D)

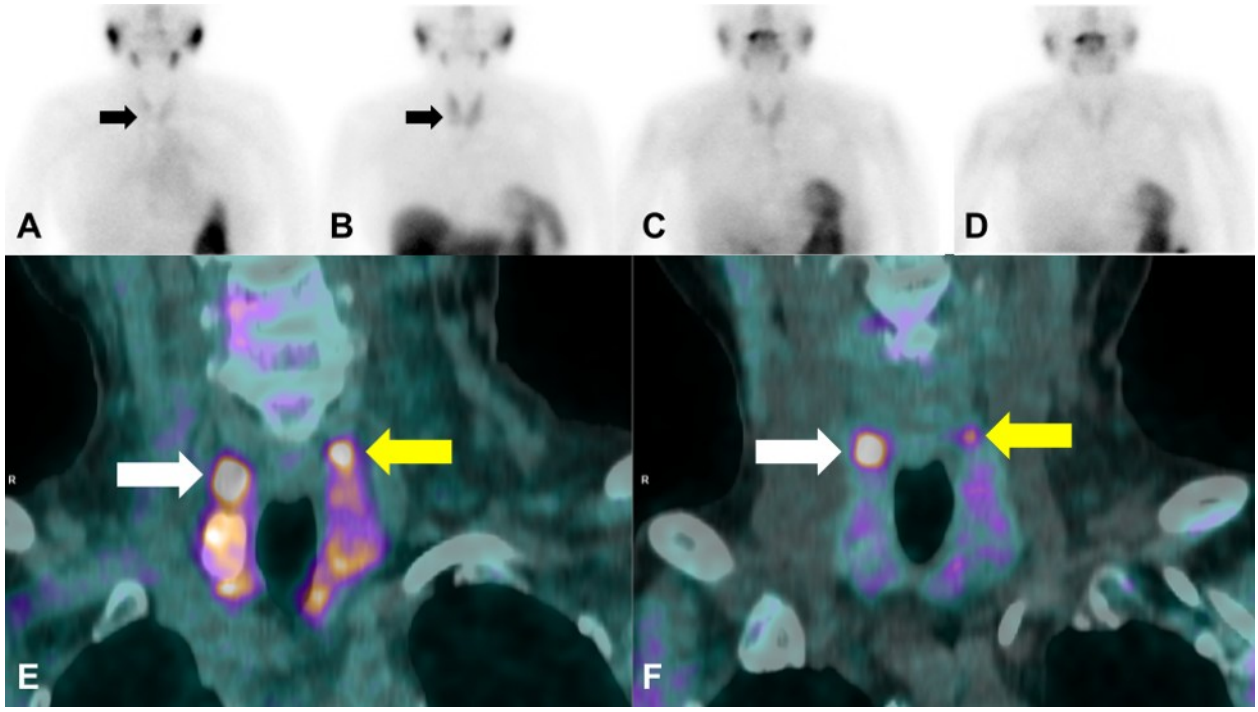

FIGURE 7 Dual-tracer, dual phase parathyroid scintigraphy showed a focus of decreased tracer uptake in the inferior third of the right thyroid lobe (black arrow) in the ^{99m}Tc-pertechnetate planar image (A). The similar focus has less sestamibi uptake compared to the rest of the thyroid gland evident in the early phase (B) and delayed phase (C, D) images. FCH PET/CT scan was done due to negative scintigraphic result and five minutes after tracer administration (E) showed FCH-avid foci posterior to the upper poles of both thyroid lobes, with an SUV of 31.6 on the right (white arrow) and 7.6 on the left (yellow arrow). Delayed fused PET/CT image one hour after tracer administration (F) showed the same FCH-avid foci with a decrease in intensity: SUVright 18.4 (white arrow) and SUVleft 4.0 (yellow arrow). These lesions measure 1.2 x 1 cm on the right and 0.8 x 0.6 cm on the left, and likely relate to hyperfunctioning parathyroid glands.

DISCUSSION

Recent advancements in the field of nuclear medicine have shifted focus to 18F-fluorocholine PET/CT imaging, which is now emerging as the preferred diagnostic tool for localization of parathyroid adenoma. Choline is an essential precursor of the phospholipids necessary for cell membrane synthesis. The phosphorylation of choline by choline kinase is responsible for its incorporation into the cell membrane. It has been studied that increased secretion of parathyroid hormone in hyperfunctioning

parathyroid glands upregulates choline kinase activity, hence its retention in the cells and subsequent increased choline uptake in PET/CT [5,10] Hyperfunctioning parathyroid glands are seen with focal increased tracer uptake in the neck relative to the background thyroid parenchyma [5].

In our study, Patient 1 has discordant sonographic and scintigraphic results. FCH PET/CT scan showed an FCH-avid focus inferoposterior to the right thyroid lobe, accurately localizing the parathyroid adenoma, supported by the surgical outcome and histopathologic findings. Similarly, in Patient 3 with negative ultrasound, FCH PET/CT imaging successfully localized the parathyroid adenoma preoperatively. A recent study by Nemir et al. (2024) evaluating the utility of the FCH PET/CT scan reported a detection rate of 92.81%, sensitivity of 100%, and positive predictive value of 94.74% in cases of primary hyperparathyroidism where conventional imaging methods are negative or inconclusive [11]. Moreover, a network meta-analysis by Lee et al. (2021) encompassing 119 studies and 8,495 patients reported that the FCH PET/CT scan has superior diagnostic performance in the localization of hyperfunctioning parathyroid glands compared to other modalities [12]. One of the factors associated with its superior diagnostic capability is the high spatial resolution and thus sensitivity, enabling the localization of small parathyroid adenomas which are usually missed by traditional imaging. Other strengths of FCH PET/CT include shorter acquisition time and lower radiation exposure, which has an effective dose of 2.0-4.0 millisievert (mSv) compared to 6.7-8.1 mSv in dual-phase parathyroid scintigraphy, not taking into account the dose received from CT [5, 9].

In the study of Medas et al., the sensitivity of ^{99m}Tc-sestamibi parathyroid scintigraphy for multigland disease is significantly lower compared to single gland disease (26.7% versus 92.6%), which may be attributed to the smaller size of the glands [13]. Although limited studies have been conducted, FCH PET/CT scan, being the most sensitive modality, may play a role in the detection of multigland disease. Sestamibi parathyroid scintigraphy was done in Patient 4, but failed to identify a focus of increased radiotracer uptake. The FCH PET/CT scan revealed two FCH-positive foci posterior to the upper poles of both thyroid lobes, which were surgically removed associated with an intraoperative decrease of PTH level, and the subsequent histopathology confirmed parathyroid gland hyperplasia. A similar case reported a patient being evaluated for primary hyperparathyroidism with negative cervical ultrasound, neck CT scan, and dual-tracer dual-phase parathyroid scintigraphy with SPECT/CT. The FCH PET/CT scan then revealed two foci of increased uptake, which were successfully excised evidenced by the normalization of calcium [14].

The biggest drawback of FCH PET/CT imaging is its higher cost and limited availability, particularly in the Philippines where, at present, only two institutions offer the radiotracer and imaging modality. However, a recent study by van Mossel et al. (2024) comparing the cost-effectiveness of FCH PET/CT imaging alone and the current practice of FCH PET/CT imaging after a negative or inconclusive cervical ultrasound and parathyroid scintigraphy with SPECT/CT showed similar costs and long-term health effects for both strategies, and such strategies can be utilized interchangeably [15].

Another disadvantage of ^{18}F-fluorocholine (FCH), being a non-specific radiotracer, is the tendency to accumulate in benign conditions like inflammation or even in malignant processes since tumor cells have rapid proliferation supported by the upregulation of choline kinase activity [16]. In Patient 2, a sestamibi-avid and FCH-avid mediastinal lesion was seen, initially suspected to be an ectopic parathyroid adenoma. Histopathology then revealed a round to spindle cell neoplasm. This is supported by the retrospective analysis of Cegla et al., which revealed that it is not uncommon to detect another malignancy using FCH PET/CT scan in patients diagnosed or being evaluated for prostate cancer [17]. In the study, 6.6% of the patients were suspected to have a second primary malignancy, of which 29.2% were confirmed to be malignant.

In addition, a study by Broos et al. (2022) evaluating incidental findings on FCH PET/CT scan for parathyroid imaging revealed that 7 out of 10 patients with focal increased tracer uptake in the breast were found to be malignant [18]. In Patient 3, a mildly FCH-avid focus was seen in the right breast; however, no follow-up was done to determine whether the patient had a dedicated breast imaging to further characterize the lesion. Attention to incidental breast lesions on FCH PET/CT scan is important since it was found that choline accumulation is strongly correlated with choline kinase overexpression, which may suggest high tumor activity [19]. These incidental findings underscore the dual utility and challenge of FCH PET/CT imaging, as it not only aids in localizing abnormal parathyroid glands but also

necessitates attention to potentially significant, unrelated pathologies.

CONCLUSION

All four cases demonstrated positive findings on ^{18}F-fluorocholine (FCH) PET/CT scan, with two confirmed as parathyroid adenomas and one as parathyroid hyperplasia on histopathology, while the remaining case was clinically diagnosed as a parathyroid adenoma. Notably, two of the four cases also exhibited non-parathyroid FCH-avid lesions.

This highlights the utility of ^{18}F-fluorocholine (FCH) PET/CT imaging in patients presenting with primary hyperparathyroidism necessitating precise localization of parathyroid adenoma and even parathyroid hyperplasia, particularly those with negative, discordant, or inconclusive initial imaging tests.

In addition, careful interpretation by nuclear medicine physicians is necessary due to the non-specific nature of the radiotracer ^{18}F-fluorocholine, accumulating in other benign or malignant processes. Incidental detection of malignancy remains a notable concern, underscoring the importance of thorough follow-up assessments.

Advancements in nuclear medicine, particularly with FCH PET/CT imaging, have become a valuable tool for enabling the detection and accurate localization of hyperfunctioning parathyroid glands due to its superior spatial resolution and sensitivity, improving surgical planning and thus better patient outcomes.

DISCLOSURE

The authors have no conflict of interest to declare.

TAKE HOME MESSAGE

F-18 Fluorocholine PET/CT imaging should be recommended in patients with suspected parathyroid adenoma, particularly those with inconclusive conventional imaging results.

REFERENCES

1. Potts J, Jüppner H. Chapter 410: Disorders of the Parathyroid Gland and Calcium Homeostasis. In: Loscalzo J, Fauci A, Kasper D, Hauser S, Longo D, Jameson JL, editors. Harrison's Principles of Internal Medicine. 21st ed. McGraw-Hill; 2022. p. 3169–3190.
2. Quak, E., Cavarec, M., Ciappuccini, R., Girault, G., Rouzier, R., & Lequesne, J. (2023). Detection, resection and cure: a systematic review and meta-analysis of 18F-choline PET in primary hyperparathyroidism. The quarterly journal of nuclear medicine and molecular imaging : official publication of the Italian Association of Nuclear Medicine (AIMN) [and] the International Association of Radiopharmacology (IAR), [and] Section of the Society of..., 67(2), 122–129. https://doi.org/10.23736/S1824-4785.23.03512-4.
3. Minisola, S., Arnold, A., Belaya, Z., Brandi, M. L., Clarke, B. L., Hannan, F. M., Hofbauer, L. C., Insogna, K. L., Lacroix, A., Liberman, U., Palermo, A., Pepe, J., Rizzoli, R., Wermers, R., & Thakker, R. V. (2022). Epidemiology, Pathophysiology, and Genetics of Primary Hyperparathyroidism. Journal of bone and mineral research : the official journal of the American Society for Bone and Mineral Research, 37(11), 2315–2329. https://doi.org/10.1002/jbmr.4665.
4. Bilezikian, J. P., Khan, A. A., Silverberg, S. J., Fuleihan, G. E., Marcocci, C., Minisola, S., Perrier, N., Sitges-Serra, A., Thakker, R. V., Guyatt, G., Mannstadt, M., Potts, J. T., Clarke, B. L., Brandi, M. L., & International Workshop on Primary Hyperparathyroidism (2022). Evaluation and Management of Primary Hyperparathyroidism: Summary Statement and Guidelines from the Fifth International Workshop. Journal of bone and mineral research : the official journal of the American Society for Bone and Mineral Research, 37(11), 2293–2314. https://doi.org/10.1002/jbmr.4677.
5. Petranović Ovčariček, P., Giovanella, L., Carrió Gasset, I., Hindié, E., Huellner, M. W., Luster, M., Piccardo, A., Weber, T., Talbot, J. N., & Verburg, F. A. (2021). The EANM practice guidelines for parathyroid imaging. European journal of nuclear medicine and molecular imaging, 48(9), 2801–2822. https://doi.org/10.1007/s00259-021-05334-y.
6. Nafisi Moghadam, R., Amlelshahbaz, A. P., Namiranian, N., Sobhan-Ardekani, M., Emami-Meybodi, M., Dehghan, A., Rahmanian, M., & Razavi-Ratki, S. K. (2017). Comparative Diagnostic Performance of Ultrasonography and 99mTc-Sestamibi Scintigraphy for Parathyroid Adenoma in Primary Hyperparathyroidism; Systematic Review and Meta- Analysis. Asian Pacific journal of cancer prevention : APJCP, 18(12), 3195–3200. https://doi.org/10.22034/APJCP.2017.18.12.3195.
7. Expert Panel on Neurological Imaging, Zander, D., Bunch, P. M., Policeni, B., Juliano, A. F., Carneiro-Pla, D., Dubey, P., Gule-Monroe, M. K., Hagiwara, M., Hoang, J. K., Jain, V., Kim, L. T., Moonis, G., Parsons, M. S., Rath, T. J., Solórzano, C. C., Subramaniam, R. M., Taheri, M. R., DuChene Thoma, K., Trout, A. T., … Corey, A. S. (2021). ACR Appropriateness Criteria® Parathyroid Adenoma. Journal of the American College of Radiology : JACR, 18(11S), S406–S422. https://doi.org/10.1016/j.jacr.2021.08.013.
8. O'Malley JP, Zeissman H, Thrall J. Nuclear medicine and molecular imaging: The requisites. Philadelphia: Elsevier; 2021.

9. Hindié, E., Schwartz, P., Avram, A. M., Imperiale, A., Sebag, F., & Taïeb, D. (2021). Primary Hyperparathyroidism: Defining the Appropriate Preoperative Imaging Algorithm. Journal of nuclear medicine : official publication, Society of Nuclear Medicine, 62(Suppl 2), 3S–12S. https://doi.org/10.2967/jnumed.120.245993.
10. Noskovicova, L., Balogova, S., Aveline, C., Tassart, M., Zhang-Yin, J., Kerrou, K., Jaksic, I., Montravers, F., & Talbot, J. N. (2024). 18F-Fluorocholine-Positron Emission Tomography/Computerized Tomography (FCH PET/CT) Imaging for Detecting Abnormal Parathyroid Glands: Indication, Practice, Interpretation and Diagnostic Performance. Seminars in nuclear medicine, 54(6), 875–895. https://doi.org/10.1053/j.semnuclmed.2024.08.002.
11. Pasini Nemir, E., Fares, S., Rogić, I., Golubić, A. T., & Huić, D. (2025). 18F-fluorocholine PET/CT imaging in primary hyperparathyroidism after negative or inconclusive cervical ultrasonography and 99mTc-MIBI scintigraphy. Japanese journal of radiology, 43(4), 687–695. https://doi.org/10.1007/s11604-024-01698-x.
12. Lee, S. W., Shim, S. R., Jeong, S. Y., & Kim, S. J. (2021). Direct Comparison of Preoperative Imaging Modalities for Localization of Primary Hyperparathyroidism: A Systematic Review and Network Meta-analysis. JAMA otolaryngology--head & neck surgery, 147(8), 692–706. https://doi.org/10.1001/jamaoto.2021.0915.
13. Medas, F., Erdas, E., Longheu, A., Gordini, L., Pisano, G., Nicolosi, A., & Calò, P. G. (2016). Retrospective evaluation of the pre- and postoperative factors influencing the sensitivity of localization studies in primary hyperparathyroidism. International journal of surgery (London, England), 25, 82–87. https://doi.org/10.1016/j.ijsu.2015.11.045.
14. Nocuń, A., Kędra, M., Stefaniak, B., & Chrapko, B. (2017). Parathyroid hyperplasia detected by F-18-Choline PET/CT, negative on Tc-99m-MIBI SPECT/CT and F-18-Deoxyglucose PET/CT scans. Nuclear medicine review. Central & Eastern Europe, 20(1), 60–61. https://doi.org/10.5603/NMR.2017.0005.
15. van Mossel, S., Saing, S., Appelman-Dijkstra, N. et al. Cost-effectiveness of one-stop-shop [18F]Fluorocholine PET/CT to localise parathyroid adenomas in patients suffering from primary hyperparathyroidism. Eur J Nucl Med Mol Imaging 51, 3585–3595 (2024). https://doi.org/10.1007/s00259-024-06771-1.
16. Calabria, F., Chiaravalloti, A., Cicciò, C., Gangemi, V., Gullà, D., Rocca, F., Gallo, G., Cascini, G. L., & Schillaci, O. (2017). PET/CT with 18F-choline: Physiological whole bio-distribution in male and female subjects and diagnostic pitfalls on 1000 prostate cancer patients: 18F-choline PET/CT bio-distribution and pitfalls. A southern Italian experience. Nuclear medicine and biology, 51, 40–54. https://doi.org/10.1016/j.nucmedbio.2017.04.004.
17. Cegla, P., Scibisz-Dziedzic, K., Witkowska, K., Kubiak, A., Wierzchoslawska, E., Kycler, W., Chrapko, B., & Czepczyński, R. (2022). Detection of a second primary cancer in a 18F-fluorocholine PET/CT - multicentre retrospective analysis on a group of 1345 prostate cancer patients. Nuclear medicine review. Central & Eastern Europe, 25(1), 25–30. https://doi.org/10.5603/NMR.a2022.0006.
18. Broos, W. A. M., Knol, R. J. J., Zant, F. M. V., Schaper, N. C., & Wondergem, M. (2022). Incidental Findings on 18 F-Fluorocholine PET/CT for Parathyroid Imaging. World journal of nuclear medicine, 21(3), 192–199. https://doi.org/10.1055/s-0042-1751031.
19. Ozawa, A., Iwasaki, M., Yokoyama, K., Tsuchiya, J., Kawano, R., Nishihara, H., & Tateishi, U. (2023). Correlation between choline kinase alpha expression and 11C-choline accumulation in breast cancer using positron emission tomography/computed tomography: a retrospective study. Scientific reports, 13(1), 17620. https://doi.org/10.1038/s41598-023-44542-4.
20. Philippine Health Ethics Research Board. National Ethical Guidelines for Health and Health-related Research. DOST - PCHRD. 2017. Available from: https://ethics.healthresearch.ph/index.php/2012-04-19-05-10-10/297-2017-nationalethical-guidelines-revision.
21. World Medical Association (2013). World Medical Association Declaration of Helsinki: ethical principles for medical research involving human subjects. JAMA, 310 (20), 2191–2194. https://doi.org/10.1001/jama.2013.281053.

Switch lighting: A Case Report of Prostate Cancer with Neuroendocrine Dedifferentiation

Dan Joseph Olpindo, MD

Section of Nuclear Medicine and PET/CT Center, Department of Radiologic Sciences
Cardinal Santos Medical Center, Metro Manila, Philippines
E-mail address: djvolpindo.sbcm@gmail.com

ABSTRACT

We report on a 72-year-old patient with an initial diagnosis of metastatic prostate acinar adenocarcinoma, who was monitored by means 18F-prostate-specific membrane antigen, positron emission tomography/computed tomography (18FPSMA PET/CT). Baseline PET/CT revealed nodal and osseous metastases with good response to android deprivation therapy. Approximately 2 years later, there was a significant progression of primary and metastatic lesions on 18F-PSMA PET/CT, where further imaging of 18F-Fluorodeoxyglucose (FDG) PET/CT revealed multiple FDG-avid lesions. The switch of metabolic activity of prostate cancer lesions from predominantly PSMA-avid to FDG-avid on PET/CT warranted histopathologic evaluation for confirmation of prostate carcinoma with neuroendocrine dedifferentiation (NED). Biopsy of the prostate and hepatic metastasis further strengthen the diagnosis of NED that is small cell carcinoma. Interestingly, on further workup using Ga-68Dotatate PET/CT scan some of the metastatic lesions are nonavid, and hypermetabolic lesions are significantly more FDG-avid than that of Dotatate. These findings indeed reflect that a more aggressive type of neuroendocrine dedifferentiation with a poorer outcome and limited treatment options or hyperplasia attributed to its high spatial resolution, thus high sensitivity, shorter imaging time, and lower radiation dose.

***Keywords**: Prostate acinar adenocarcinoma, prostate carcinoma with neuroendocrine dedifferentiation, 18F-PSMA PET/CT, 18F-FDG PET/CT, Ga-68Dotatate PET/CT*

INTRODUCTION

Prostate cancer is the most commonly diagnosed malignancy in men globally and the fifth leading cause of cancer-related deaths [1]. According to the World Health Organization (WHO), it is the third most common type of cancer among Filipino men. In 2022, almost 10,000 Filipino men were diagnosed with the disease, with some developing into an aggressive type called castration-resistant prostate cancer (CRPC). Some further progress into the most aggressive form which is neuroendocrine dedifferentiation (NED), where standard treatments no longer work and patients succumb to the disease [2].

The human prostate consists of epithelial cells luminal, basal, and 1% neuroendocrine cells. Prostate cancer develops through cell growth and proliferation which strongly rely on the androgen-androgen receptor (AR) axis. Therefore, prostate cancer is initially treated with surgical resection, radiotherapy, and androgen deprivation therapy (ADT). Reports suggest that NED originates from trans-differentiation of adenocarcinoma, and drives focal neuroendocrine dedifferentiation to castration-resistant prostate carcinoma (CRPC). These patients are further treated with next-generation ADTs (enzalutamide or abiraterone). During the course of CRPC treatment, 30% develop NED, in which tumor cells often acquire neuroendocrine features, showing low to absent AR expression and negative or low PSA levels, that has very limited therapeutic response [3].

In the most recent classification of the World Health Organization (WHO), Neuroendocrine prostate carcinomas are classified as, adenocarcinoma with Paneth-like cell neurodifferentiation, carcinoid tumor, large cell neuroendocrine carcinoma, small cell neuroendocrine carcinoma and usual adenocarcinoma with neuroendocrine differentiation [4]. Neuroendocrine differentiation (NED) includes cases of typical acinar or ductal adenocarcinoma with focal or diffuse neoplastic neuroendocrine cells detected by immunohistochemical stains. It may differentiate into an aggressive, high-grade tumor of Small Cell Neuroendocrine Carcinoma [4].

The incidence of neuroendocrine prostate carcinoma increases after hormonal therapy and represents a challenge both in the radiological and pathological diagnosis, as well as in the clinical management. Advancements in imaging techniques with various radiopharmaceuticals have improved the ability to detect and characterize prostate cancer. Positron emission tomography/computed tomography (PET/CT) may assess treatment efficacy, detecting potential recurrence and dedifferentiation of prostate carcinoma.

In this report, we present a diagnosed case of prostate adenocarcinoma, who received androgen deprivation, targeted therapy, and chemotherapy. His response was monitored by serial serum PSA level and 18F-PSMA PET/CT scans, and later on evaluated using Ga-68 Dotatate PET/CT and 18F-FDG PET/CT for neuroendocrine dedifferentiation.

OBJECTIVE

This case study aims to discuss the patterns of prostate carcinoma neuroendocrine dedifferentiation that may be encountered in PET/CT scans using different radiopharmaceuticals for early recognition of aggressive disease.

CASE DESCRIPTION

A 72-year-old, married, Filipino patient with no known comorbidity or prior history of hospitalization presented with sudden onset of dysuria and hematuria prompting hospital admission. Upon work-up, he was found to have bladder mass, enlarged prostate, and elevated PSA level of 127 ng/mL. Otherwise, all other laboratory tests were unremarkable. Cystoscopy with transurethral resection of the bladder tumor and prostate biopsy was facilitated, revealed histopathologic findings of low-grade papillary urothelial carcinoma and prostatic acinar adenocarcinoma, Gleason score 8 (4+4) present in 90% of the tissue. A baseline 18F-PSMA PET/CT scan identified high PSMA expression of the enlarged prostate gland with extension to seminal vesicles and urinary bladder floor. PSMA-avid pelvic and extra pelvic lymph nodes are present with multiple PSMA-avid osseous metastases. (Figure 1). Androgen deprivation therapy (Bicalutamide), GnRHagonist (Triptorelin), and Denosumab were initiated.

Follow-up after 6 months and 1-year interval, show a significant decrease in the PSA level with values of 0.28 ng/mL then 2.72 ng/mL. The primary prostate disease showed metabolic stability with gradual anatomic improvement in 18F-PSMA PET/CT throughout the course of therapy. Pelvic and extra pelvic lymph nodes achieved metabolic resolution, while osseous metastases demonstrated metabolic regression (Figure 2).

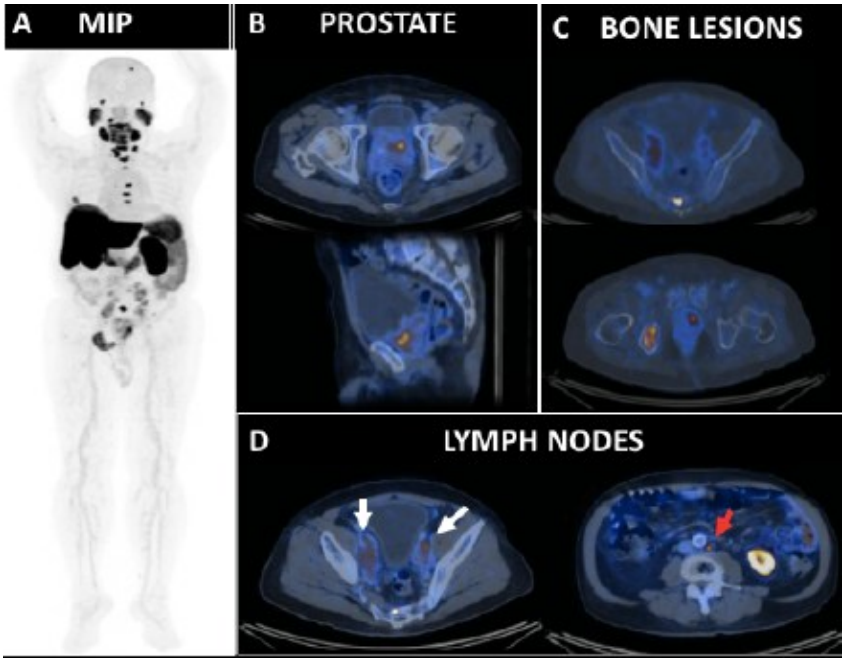

FIGURE 1 Baseline 18F-PSMA PET/CT performed for staging of known primary prostate carcinoma.
A: Maximum intensity projection. **B:** Prostate gland axial and sagittal PET/CT. **C:** Bone lesions axial PET/CT.
D:external iliac nodes (white arrow) and abdominal aortic node (red arrow) axial PET/CT

A rise in serum PSA level of 15.45 ng/mL is observed on the 20th month following the ADT, GnRh, and targeted therapy. 18F-PSMA PET/CT revealed stable PSMA-avid and enlarged prostate gland, with increased metabolic activity and the number of osseous metastases (Figure 3). Bicalutamide was shifted to next-generation ADT (Enzalutamide), while Triptorelin and Denosumab were continued.

On subsequent follow-up after 6-month treatment of Enzalutamide together with Triptorelin and Denosumab, a drop in serum PSA level was observed (PSA: 0.411 ng/mL). However, on the 18F-PSMA PET scan, there is a discordant change in the prostate gland, showing a significant increase in size but decreased PSMA activity. The osteoblastic metastases are grossly stable with almost complete resolution of PSMA activity. There is an interval appearance of non-PSMA avid perivesical and hepatic lesions (Figure 4).

The characteristics of low PSMA expression with gross development of new nodal and hepatic lesions in 18F PSMA PET scan, in the background of sudden nadir in PSMA level are suspicious for dedifferentiation or metasynchronous disease. After a week, an 18FFDG PET/CT scan was performed and revealed an intensely hypermetabolic/FDG-avid prostate gland, along with hypermetabolic perivesical lymph node and hepatic lesions (Figure 5).

The patient underwent cystoscopy with biopsy of the prostate and bladder as well as the liver lesions. Histopathology and immunohistochemistry (diffusely positive synaptophysin and chromogranin) examination confirmed neuroendocrine differentiation (i.e. small cell carcinoma), given a history of androgen deprivation therapy, a prostatic origin is favored. Bladder wall histopathology reveals benign urothelial cells leading to a diagnosis of neuroendocrine prostate dedifferentiation (Small cell Neuroendocrine Ca).

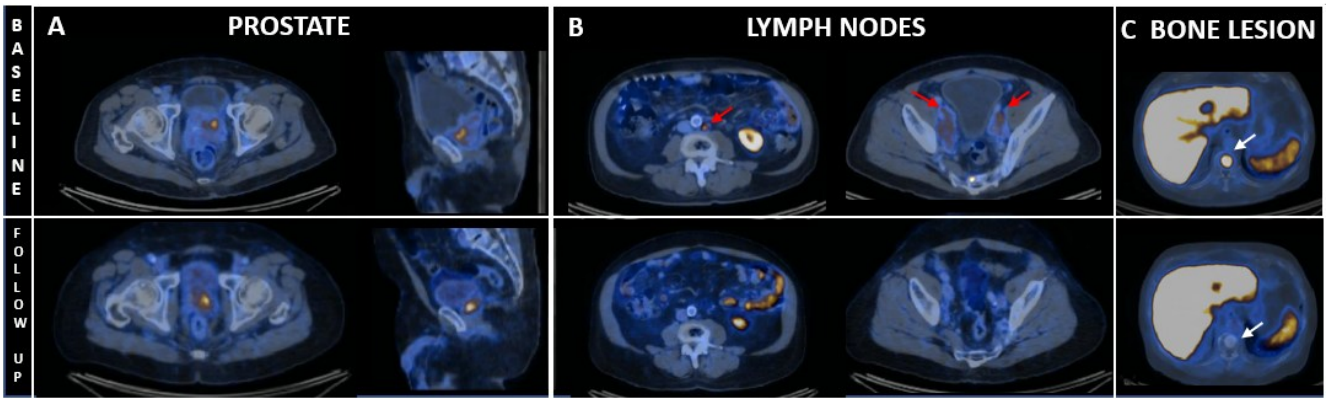

FIGURE 2 Serial fused F-18 PSMA PET/CT images captured from baseline to follow up.
A: Prostate gland axial and sagittal PET/CT, gradual size regression in primary prostate malignancy with stable PSMA uptake **B:** Complete metabolic response (red arrow) was achieved for a few extra pelvic and pelvic lymph nodes axial PET/CT **C:** Bone lesions axial PET/CT. Metabolic resolution was achieved for some osseous metastasis

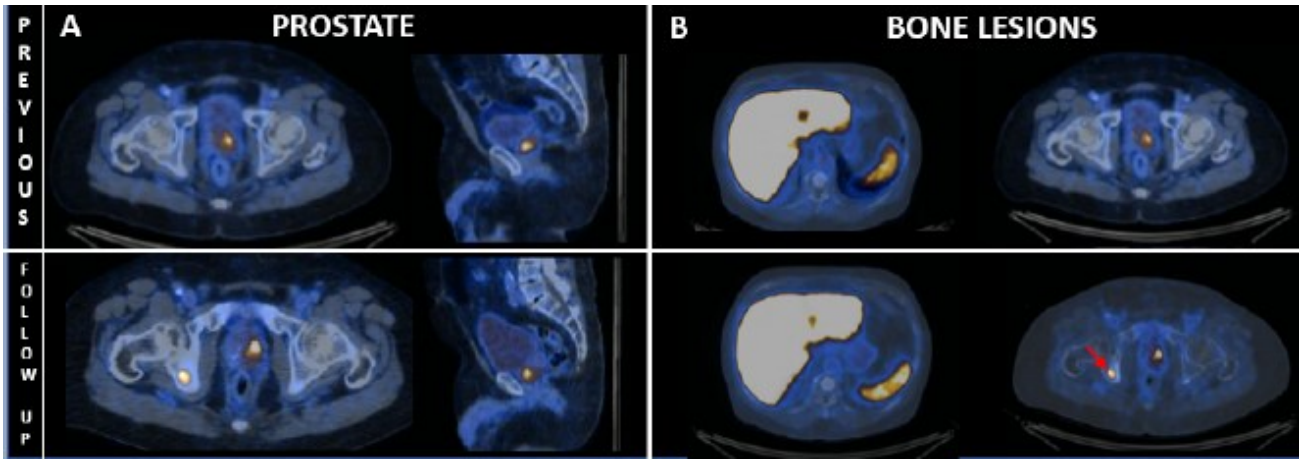

FIGURE 3 Comparison of serial fused F-18 PSMA PET/CT images captured during follow-up.
A: Prostate gland axial and sagittal PET/CT, Gross size progression in primary prostate malignancy still with stable PSMA uptake, **B:** Bone lesions axial PET/CT with stable and some new of osteoblastic lesion (red arrow)

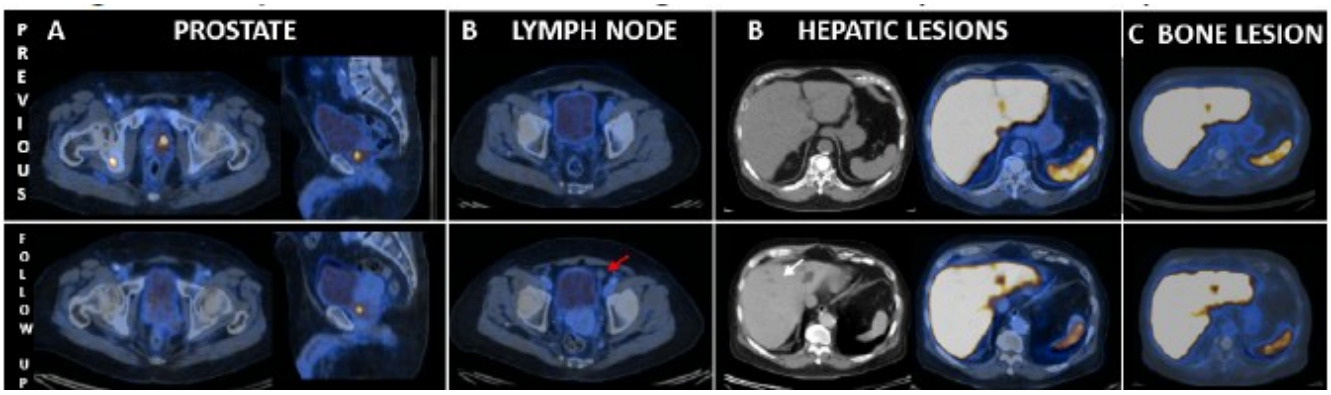

FIGURE 4 Comparison of serial fused F-18 PSMA PET/CT images captured during follow-up after 6 months of next-generation ADT (Enzalutamide).

A: Prostate gland axial and sagittal PET/CT, Gross size progression in primary prostate malignancy still with stable PSMA uptake, **B:** new non-PSMA avid perivesical lymph node (red arrow) axial PET/CT **C:** New non-PSMA-avid hepatic (white arrow) lesions axial CT an PET/CT **D:** Bone lesions axial PET/CT with stable lesion

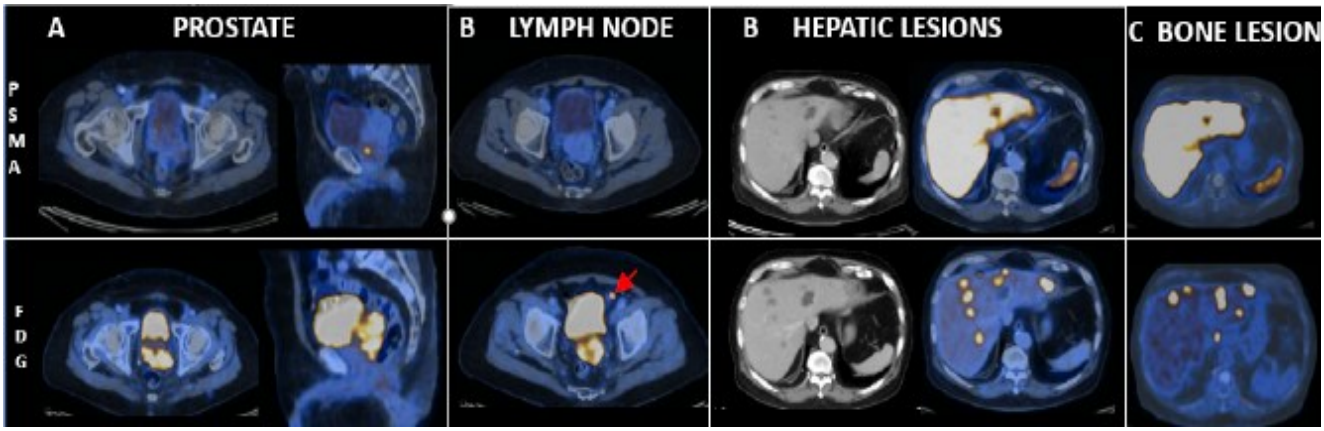

FIGURE 5 Comparison of fused F-18 PSMA PET/CT and F-18 FDG PET/CT images with a 1-week interval .

A: Intensely FDG avid prostate gland axial and sagittal PET/CT **B:** FDG-avid perivesical lymph node (red arrow) **C:** liver nodules with similar intense FDG uptake as the prostate. **D:** None to low-FDG-avid bone metastases

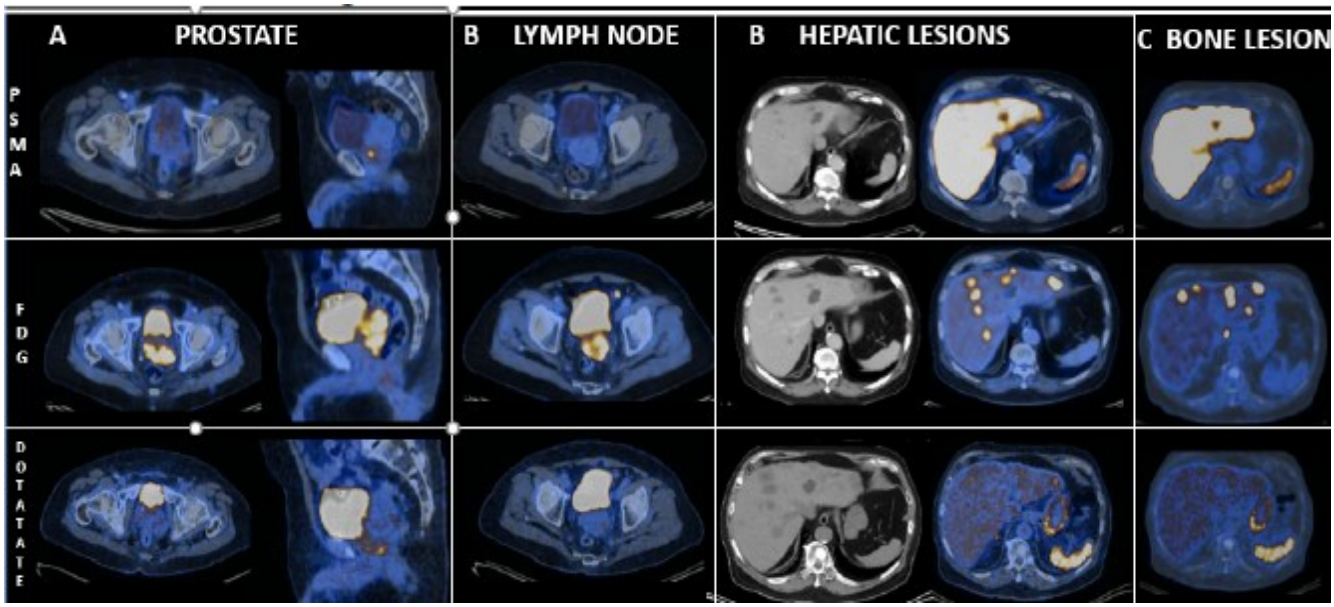

FIGURE 6 Comparison of fused F-18 PSMA PET/ CT, F-18 FDG PET/CT and Ga-68 Dotatate PET/CT images.

A: Prostate gland axial and sagittal PET/CT, with significant FDG activity than PSMA and Dotatate **B:** Prominent FDG avid perivesical lymph node a non-PSMA and non-Dotatate avid **C:** Increase in sized of FDG-avid and Dotatate-avid hepatic lesions axial PET/CT **D:** Stable non-metabolic bone lesions axial PET/CT

In order to explore the possibility of undertaking Lutetium Dotatate peptide receptor radionuclide therapy (PRRT), a Ga-68 Dotatate-PET/CT was performed, which revealed tracer uptake in the prostate gland and hepatic masses (Krenning 2-3) in which FDG uptake is significantly more intense than that of the Dotatate uptake. The perivesical lymph node and pulmonary nodules are non-Dotatate-avid (Figure 6). Given the evidence of exclusionary Dotatate-negative lesions and heterogeneous expression of Dotatate across metastatic sites, the patient was not submitted to Lutetium Dotatate PRRT, and chemotherapy with Paclitaxel and Etoposide was initiated instead.

After six cycles of therapy, the PSA level remains low (2.67 ng/mL) with PET scan features of disease progression. 18F-FDG PET/CT revealed new FDG-avid hilar, perivesical, and pulmonary lesions, there is persistent high tracer uptake in the preexisting metastases (Figure 7). Consequently, the therapeutic regimen was shifted to targeted therapy, Olaparib, a poly (adenosine diphosphate–ribose) polymerase (PARP) inhibitor used for treatment-related neuroendocrine prostate cancer with a BRCA2 mutation.

The patient remains able to do activities of daily living (ECOG 1), with good compliance in therapeutic management and follow-ups.

DISCUSSION

Looking back at the serial 18F-PSMA PET/CT images, the baseline image depicted a hypermetabolic prostate gland, pelvic/extra-pelvic lymph nodes, and multiple osseous lesions, indicative of active metastatic lesions from prostate adenocarcinoma. It has been recognized that androgen binds to the androgen receptor (AR), and activates AR signaling which promotes the development and proliferation of prostate adenocarcinoma. Androgen deprivation therapy (ADT) with gonadotropin-releasing hormone (GnRH) agonists is the mainstay treatment for advanced-stage prostate cancer treatment. Both drug classes decrease levels of testosterone. During the course of these treatments, disease regression was observed in the patient as evidenced by a drastic decrease in PSA level and regression/resolution of PSMA uptake in the identified lesions in PSMA PET/CT. After approximately 1 ½ half years of treatment, a rise in serum PSA is observed, with noted new lesions in PSMA PET/CT. Bicalutamide was shifted to a newer ADT which is Enzalutamide, an androgen receptor inhibitor that is indicated for the treatment of metastatic, castration-resistant, prostate cancer (mCRPC) that has progressed despite treatment of first-line therapies. The efficacy of this medication is demonstrated in many clinical trials, however, approximately 25 – 35% of exhibit primary resistance to these agents.

Recognizing recurrence or progression is a complex challenge in clinical practice and conventional imaging. After 6 months of treatment with Enzalutamide, the PSA level decreased, however on PSMA PET/CT scan noted a significant increase in the size of the prostate gland with decreased PSMA activity, the appearance of new bone and hepatic lesions with low to non-PSMA activity are also evident. With these developments in PET CT findings and in the background of low PSA level, neuroendocrine prostate dedifferentiation is considered.

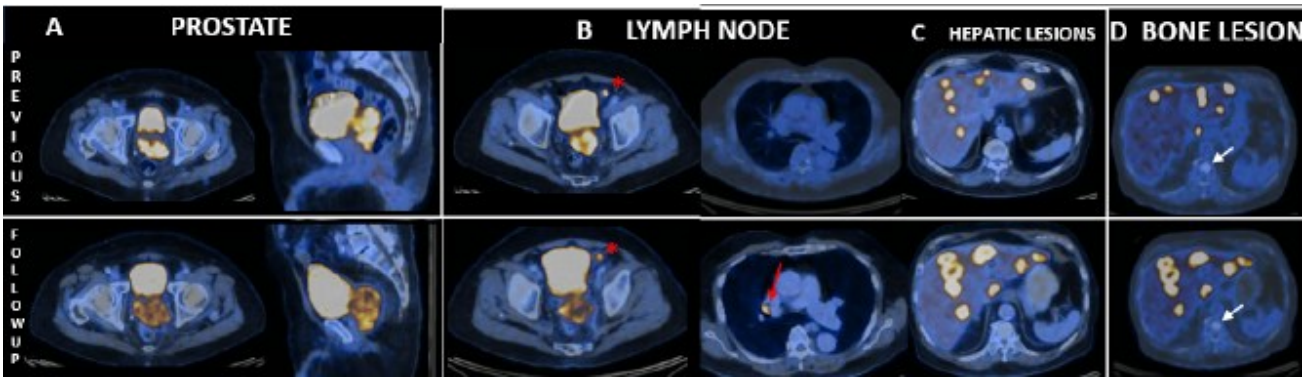

FIGURE 7 Comparison of fused serial F-18 FDG PET/CT with 7-month intervals after 6 cycles of chemotherapy.
A: Prostate gland axial and sagittal PET/CT, size progression with decrease FDG-uptake in primary prostate malignancy **B:** Prominent perivesical lymph node with higher FDG activity (asterisk) axial PET/CT, New FDG-avid right hilar lymph node (red arrow) **C:** Increase in sized of hepatic FDG-avid hepatic lesions axial PET/CT **D:** Stable non-FDG-avid bone lesions axial PET/CT

The utilization of 18F-FDG PET/CT has been employed to identify dedifferentiation in patients with indolent prostate cancer subsequent to ADT therapy. The patient's 18F FDG PET/CT scan revealed an increased FDG activity in the prostate gland, lymph nodes, and hepatic lesions. One mechanism behind this process is the histologic transformation from adenocarcinoma to a poorly differentiated neuroendocrine (NE) carcinoma with absent or low AR expression levels. The induction of trans-differentiation and lineage plasticity by AR inhibition leads to the suppression of PSMA, implying that PSMA-targeted imaging could not effectively visualize neuroendocrine prostate cancers (NEPCs). PSMA suppression correlates with GLUT12 suppression and glucokinase upregulation, which is positively associated with higher glucose uptake in conventional 18F-FDG PET imaging. These suggest a limited utility of PSMA-based theragnostic and imaging in the management of NEPC.

With this progression, prostate and liver biopsy with immunohistochemical profiling was done and revealed neuroendocrine differentiation with higher expression of neuroendocrine markers, such as synaptophysin and chromogranin, strengthening the diagnosis for prostate carcinoma with neuroendocrine dedifferentiation of small cell carcinoma. Treating Prostate carcinoma with NED remains challenging because of broad therapy resistance, platinoids combined with etoposide/taxanes are the most used and internationally [10]. 177Lu-DOTATATE Peptide Receptor Radionuclide Therapy (PRRT) is an approved therapy that has shown reasonable benefit in treatment outcome and improvement in quality of life of well-differentiated neuroendocrine tumors. Ga-68 Dotatate PET/CT scan was done to evaluate efficacy and eligibility for PRRT therapy. The scan shows Dotatate-avid prostate gland and hepatic lesions (Krenning score 2-3), which is significantly more FDG-avid than Dotatate. Some of the lesions such as perivesicular and periprostatic which are FDG-avid are non-Dotatate-avid. These represent tumor heterogeneity that implies the presence of variable cellular populations having different genomic characteristics in different tumor sites of the same patient. Imaging is important in for determination of tumor behavior. 18F-fluorodeoxyglucose (FDG) is a marker of tumor metabolism and uptake increases with more aggressive tumors, correlates with worse outcomes, and has been shown to outperform pathologic grading and less suitable candidates and poor response for PRRT [11].

Chemotherapeutic agents such as Etoposide and Paclitaxel were initiated. Platinoids combined with etoposide/taxanes are the most used and internationally endorsed regimens. However, the prognosis remains poor9. Despite the novel potential of these drugs, repeat F-18 FDG PET/CT scans revealed overall disease progression. Therefore, the identification of tissue germlines and biomarkers are potentially useful in the treatment of such disease. The patient was started on Olaparib, a selective inhibitor, that exploits synthetic lethality against CRPC after androgen deprivation therapy (ADT) and expression of neuroendocrine markers in patients with BRCA mutations. The patient was to be evaluated using an 18F FDG PET/CT scan after 3 months of treatment, with anticipation of a good treatment response.

Treatment-induced neuroendocrine differentiation of mCRPC is associated with a deeply divergent transcriptional profile with limited treatment options and poorer survival as compared to classic adenocarcinoma. Further studies should evaluate the association with other treatments targeting the neuroendocrine component potentially assisting clinicians in predicting patient outcomes and optimizing treatment strategies.

CONCLUSION

PET/CT scans holds fundamental importance in evaluating prostate carcinoma, for treatment planning and monitoring of treatment response. 18-F PSMA PET/CT is a transmembrane cell surface protein that is overexpressed in 95% of PCa cells. However, application of this imaging modality requires a comprehensive knowledge of the various influencing factors that can affect the diagnostic outcome, such as prostate cancer dedifferentiation wherein prostatic lesions loses PSMA activity. 18F-FDG PET/CT emerges as a valuable marker of tumor metabolism, and uptake increases with more aggressive tumors such poorly differentiated tumors and neuroendocrine dedifferentiation. Prostate carcinoma with neuroendocrine dedifferentiation having divergent transcriptional profile with limited treatment options, optimization of treatment strategy must be explored. A 68Ga-DOTATATE PET/CT imaging is used to assess patient suitability for PRRT, highlighting the presence of somatostatin receptors (SSTR) to which PRRT selectively binds. Currently, the best treatment option for Prostate Ca NED is unclear, and treatment remains challenging because of broad therapy resistance. Various PET/CT approaches may help improve clinical management for recognizing the tumor behavior, monitoring and potential therapeutic interventions.

DISCLOSURE

The authors have no conflict of interest to declare.

REFERENCES

1. Leslie SW, Soon-Sutton TL, Skelton WP. Prostate Cancer. [Updated 2024 Oct 4]. In: StatPearls [Internet]. Treasure Island (FL): StatPearls Publishing; 2024 Jan-. Available from: https://www.ncbi.nlm.nih.gov/books/NBK470550/.
2. Sampang, L., & Sampang, L. (2024, July 19). UP study pinpoints key player in aggressive type of prostate cancer. SCIENCE - University of the Philippines Diliman -. https://science.upd.edu.ph/up-study-pinpoints-key-player-inaggressive- type-of-prostate-cancer/.
3. Patel, G. K., Chugh, N., & Tripathi, M. (2019). Neuroendocrine Differentiation of Prostate Cancer-An Intriguing Example of Tumor Evolution at Play. Cancers, 11 (10), 1405. https://doi.org/10.3390/cancers11101405.
4. Taher, A., Jensen, C. T., Yedururi, S., Surasi, D. S., Faria, S. C., Bathala, T. K., Mujtaba, B., Bhosale, P., Wagner-Bartak, N., & Morani, A. C. (2021). Imaging of Neuroendocrine Prostatic Carcinoma. Cancers, 13(22), 5765. https://doi.org/10.3390/cancers13225765.
5. Yamada, Y., & Beltran, H. (2021). Clinical and Biological Features of Neuroendocrine Prostate Cancer. Current oncology reports, 23(2), 15. https://doi.org/10.1007/s11912-020-01003-9.
6. Ghosh, A., & Heston, W. D. (2004). Tumor target prostate specific membrane antigen (PSMA) and its regulation in prostate cancer. Journal of cellular biochemistry, 91(3), 528–539. https://doi.org/10.1002/jcb.10661.
7. Bergamini, M., Dalla Volta, A., Caramella, I., Bercich, L., Fisogni, S., Bertoli, M., Valcamonico, F., Grisanti, S., Poliani, P. L., Bertagna, F., & Berruti, A. (2022). Case Report: 18F-PSMA PET/CT Scan in Castration Resistant Prostate Cancer With Aggressive Neuroendocrine Differentiation. Frontiers in oncology, 12, 937713. https://doi.org/10.3389/fonc.2022.937713.
8. Sheikhbahaei, S., Afshar-Oromieh, A., Eiber, M., Solnes, L. B., Javadi, M. S., Ross, A. E., Pienta, K. J., Allaf, M. E., Haberkorn, U., Pomper, M. G., Gorin, M. A., & Rowe, S. P. (2017). Pearls and pitfalls in clinical interpretation of prostate-specific membrane antigen (PSMA)-targeted PET imaging. European journal of nuclear medicine and molecular imaging, 44(12), 2117–2136. https://doi.org/10.1007/s00259-017-3780-7.
9. Bakht, M. K., Lovnicki, J. M., Tubman, J., Stringer, K. F., Chiaramonte, J., Reynolds, M. R., Derecichei, I., Ferraiuolo, R. M., Fifield, B. A., Lubanska, D., Oh, S. W., Cheon, G. J., Kwak, C., Jeong, C. W., Kang, K. W., Trant, J. F., Morrissey, C., Coleman, I. M., Wang, Y., Ahmadzadehfar, H., … Porter, L. A. (2020). Differential Expression of Glucose Transporters and Hexokinases in Prostate Cancer with a Neuroendocrine Gene Signature: A Mechanistic Perspective for 18F-FDG Imaging of PSMA-Suppressed Tumors. Journal of nuclear medicine : official publication, Society of Nuclear Medicine, 61(6), 904–910. https://doi.org/10.2967/jnumed.119.231068.
10. Farinea, G., Calabrese, M., Carfi, F., Saporita, I., Poletto, S., Delcuratolo, M. D., Turco, F., Audisio, M., Di Stefano, F. R., Tucci, M., & Buttigliero, C. (2024). Impact of Neuroendocrine Differentiation (NED) on Enzalutamide and Abiraterone Efficacy in Metastatic Castration-Resistant Prostate Cancer (mCRPC): A Retrospective Analysis. Cells, 13(16), 1396. https://doi.org/10.3390/cells13161396.
11. Sargos, P., Ferretti, L., Gross-Goupil, M., Orre, M., Cornelis, F., Henriques de Figueiredo, B., Houédé, N., Merino, C., Roubaud, G., Dallaudiére, B., Richaud, P., & Fléchon, A. (2014). Characterization of prostate neuroendocrine cancers and therapeutic management: a literature review. Prostate cancer and prostatic diseases, 17(3), 220–226. https://doi.org/10.1038/pcan.2014.17.
12. Binderup, T., Knigge, U., Johnbeck, C. B., Loft, A., Berthelsen, A. K., Oturai, P., Mortensen, J., Federspiel, B., Langer, S. W., & Kjaer, A. (2021). 18F-FDG PET is Superior to WHO Grading as a Prognostic Tool in Neuroendocrine Neoplasms and Useful in Guiding PRRT: A Prospective 10-Year Follow-up Study. Journal of nuclear medicine : official publication, Society of Nuclear Medicine, 62(6), 808–815. https://doi.org/10.2967/jnumed.120.244798.
13. Zhang, Y., Zheng, D., Zhou, T., Song, H., Hulsurkar, M., Su, N., Liu, Y., Wang, Z., Shao, L., Ittmann, M., Gleave, M., Han, H., Xu, F., Liao, W., Wang, H., & Li, W. (2018). Androgen deprivation promotes neuroendocrine differentiation and angiogenesis through CREB-EZH2-TSP1 pathway in prostate cancers. Nature communications, 9 (1), 4080. https://doi.org/10.1038/s41467-018-06177-2.

MedChoice

Thyroid & Diabetes HEALTHCARE

Todo Aruga

MEDICAL EQUIPMENT PRODUCT LINE

General Radiography System

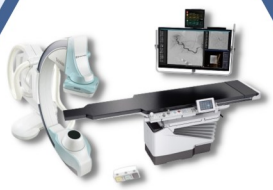

Cardiac & Angiography

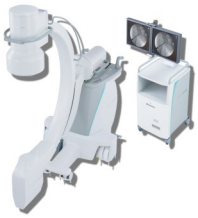

Mobile C-Arm Imaging System

Mobile X-Ray System

Digital Radiography System

R/F System

SHIMADZU
Philippines Corporation

For inquiries, contact: SHINE MIRANDA | shine@shimadzu.com.ph | 7955-1110 Loc. 309

shimadzu.com.ph facebook.com/ShimadzuPH/ linkedin.com/company/shimadzu-philippines-corp youtube.com/c/ShimadzuPhilippinesCorporation

Diagnostic Accuracy of Bone Scintigraphy versus F-18 FDG PET-CT in Detecting Bone Metastasis among Breast Cancer Patients: A Systematic Review and Meta-Analysis

Wendelyn Shanel G. Lim, MD[1], Chris Patrick G. Ignacio, MD[2], Patrick Earl A. Fernando, MD[1]

[1] *Department of Nuclear Medicine and Theranostics, St. Luke's Medical Center—Global City, Taguig, Philippines*

[2] *Institute of Radiology, St. Luke's Medical Center—Global City, Taguig, Philippines*

E-mail address: wendelynshanel.lim@gmail.com

ABSTRACT

Objective:

This systematic review and meta-analysis aimed to compare the diagnostic accuracy of F18-FDG PET-CT and bone scintigraphy (BS) in the detection of bone metastases among patients with breast cancer.

Methodology:

Electronic databases (PubMed, EMBASE, Medline, and Cochrane Library) were searched for studies published between 2010 and 2023 comparing both modalities. A random-effects model was used to pool sensitivity, specificity, diagnostic odds ratios (DOR), and likelihood ratios. Hierarchical Summary Receiver Operating Characteristic (HSROC) curves were constructed to assess overall test performance.

Results:

F-18 FDG PET-CT demonstrated superior diagnostic performance across all parameters. The pooled sensitivity and specificity for PET-CT were 93% and 84%, respectively, compared to 89% and 77% for bone scintigraphy. PET-CT yielded a significantly higher DOR of 66.89 and an AUC of 0.94, while bone scintigraphy yielded a DOR of 26.99 and an AUC of 0.89. The negative likelihood ratio (NLR) for PET-CT was 0.08, indicating a 92% reduction in the odds of disease following a negative result, whereas bone scintigraphy showed a higher NLR of 0.14.

Conclusion:

F18-FDG PET-CT significantly outperforms bone scintigraphy in detecting skeletal metastases, particularly in identifying early marrow involvement and lytic lesions. With a superior DOR and a more reliable NLR, F18-FDG PET-CT should be considered the preferred modality for definitive staging and ruling out bone metastases. However, given the high cost and limited availability of PET/CT in regions like the Philippines, bone scintigraphy remains a more accessible, albeit less specific, clinical alternative.

Keywords*: Breast Cancer, Bone Metastasis, F18-FDG PET-CT Bone Scintigraphy, Meta-analysis*

INTRODUCTION

Breast cancer is the most common cancer affecting women worldwide, and second most common global cancer. It is the fifth cause of cancer deaths and third most fatal type of cancer among Filipino women with an incidence rate of 27,163 cases annually [1]. Majority of the Filipino women are diagnosed at an advanced stage with a mortality rate of 27 deaths per 100,000 people [2].

The most common sites of distant metastases include the bone, liver, lung, and brain. Bone lesions are frequently seen as a site of metastasis or disease recurrence in breast cancer, and it significantly affects the prognosis and quality of life of the patient [3]. Bone metastases are classified as osteolytic, osteoblastic or mixed, but are predominantly osteolytic, and 15% to 20% of cases have an osteoblastic component [4].

With advances in technology in molecular and hybrid imaging non-invasive detection and diagnosis of bone

metastasis becomes more precise and accurate, thereby improving identification of patients who are in an advanced stage of the disease. Based on the NCCN Clinical Practice Guidelines in Oncology (NCCN Guidelines®), systemic imaging is not recommended or indicated in stage I, II or operable III breast carcinoma in the absence of signs and symptoms of advanced disease. Molecular imaging is recommended in patients with high suspicion of metastatic disease. Bone scan and F-18 FDG PET-CT scan is indicated in patients with localized bone pain or elevated Alkaline phosphatase [5]. Bone scintigraphy (BS) is commonly used and referred as the conventional imaging, it detects osseous remodeling and osteoblastic activities, while advanced imaging like F-18 FDG PET-CT evaluates glycolytic metabolism of both bone and visceral metastases in patients with malignancy (6).

Some Nuclear Medicine departments in the Philippines offer both bone scintigraphy and F-18 FDG PET-CT, while most of them only offer the former. Physicians would then question which is more sensitive and specific, as well as more economically efficient for financially challenged patients. Thus, a systematic review and meta-analysis comparing both methods are important to further guide physicians in individualizing diagnostic requests.

OBJECTIVE

This systematic review and meta-analysis aimed to compare the diagnostic accuracy of F18-FDG PET-CT and bone scintigraphy (BS) in the detection of bone metastases among patients with breast cancer.

METHODOLOGY

Search Strategy

Journals evaluating F18-FDG PET-CT and bone scintigraphy in detecting bone metastases in breast cancer patients published from 2010 to 2023 are collated from electronic databases such as PubMed, EMBASE, Medline and Cochrane Library. Algorithm was based on the combination of terms: (1) Bone scan OR bone scintigraphy, (2) PET-CT OR positron emission tomography, (3) Breast cancer, (4) Bone metastases. References were screened to determine all the key information for this study.

Study Selection

Journals considered for this review were screened with the following eligible criteria: (1) Journals that compare bone scan and F-18 FDG PET-CT scan in diagnosing bone metastases in patient with breast cancer; (2) Journals should be diagnostic test studies; (3) Journal that provides the sensitivity, specificity and analytic statistics of their study; (4) Journal that detects bone metastasis in breast cancer patients, regardless of treatment regimen.

Data Extraction

Two (2) reviewers extracted the journals independently and based on their availability in the electronic resources. Controversies were resolved with discussion with the third reviewer. For each journal, authors, country of origin, number of participants, inclusion and exclusions, study design, and imaging methods (bone scan and F-18 FDG PET-CT) were recorded.

Quality Assessment

The quality of the included studies was assessed according to the quality assessment of diagnostic accuracy studies (QUADAS-2), which includes patient selection, reference standard, index text and flow of patients through the study/timing of index tests, and relevant reference standard.

Statistical Analysis

The study used a random effect model and pooled the sensitivity and specificity of both diagnostic imaging and construct hierarchy summary receiver operating characteristic (HSROC) curves of both F-18 FDG PET-CT and bone scan to account for the heterogeneity of the studies. With the following data, likelihood radio, diagnostic odd ratio (DOR), positive likelihood ratio (PLR), negative likelihood ratio (NLR) was obtained.

RESULTS

Eligible studies

The electronic search showed 266 journals; 253 were excluded by reading the abstract, while 13 were read and 8 were rejected due to lacking some data. Four (4) journals are recognized to have all the inclusion criteria with 403 patients are read and enrolled and are listed in Table 1.

Quality Assessment

The study used QUADAS-2 (Quality Assessment of Diagnostic Accuracy Studies 2) to evaluate the quality of six studies based on the four key domains of risk of bias and applicability. All patients were diagnosed with breast cancer and were undergoing staging. Nearly all received both index tests. While biopsy is the gold standard for diagnosing bone metastases, it is highly invasive, so all studies confirmed the findings by correlating them with

TABLE 1 Baseline characteristics for included studies

Author	Year	Country	Age	Sample Size
Caglar et al. [10]	2015	Turkey	27 to 85 years old	150
Balci et al. [11]	2012	Turkey	Mean age of 50.6 years old	162
Teke et al. (12)	2015	Turkey	28 to 81 years old	62
Hahn et al. (14)	2011	Germany	35 to 78 years old	29

TABLE 2 Risk of bias and applicability judgements in QUADAS - 2

Studies	Patient Selection	Index Test	Reference Standard	Flow and Timing	Applicability
Caglar et al. [10]	Low	Low	Low	Low	High
Balci et al. [11]	Low	Low	Low	Low	High
Teke et al. (12)	Low	Low	Low	Low	High
Hahn et al. (14)	Low	Low	Low	Low	HIgh

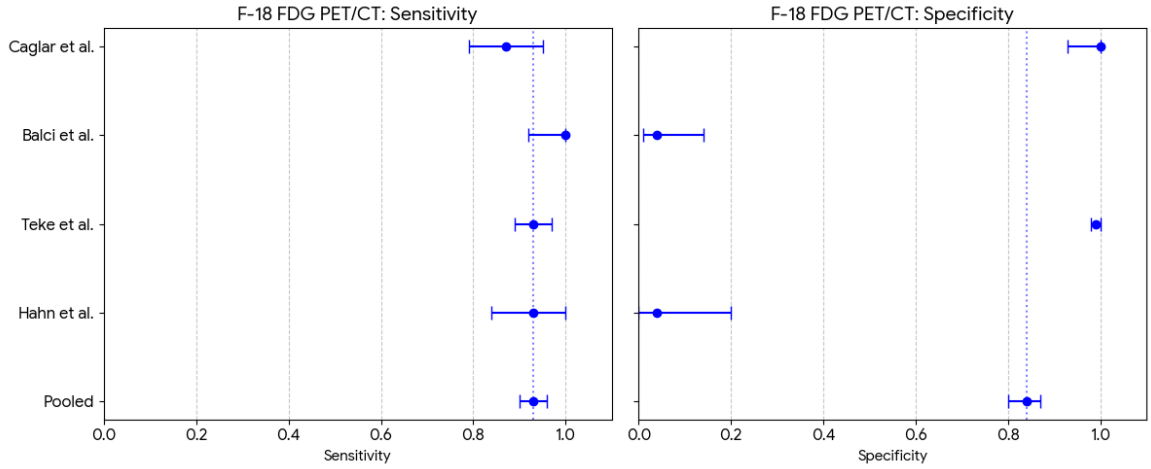

FIGURE 1 Forest plot of study-specific sensitivity and specificity estimates with pooled diagnostic accuracy for F18-FDG PET-CT

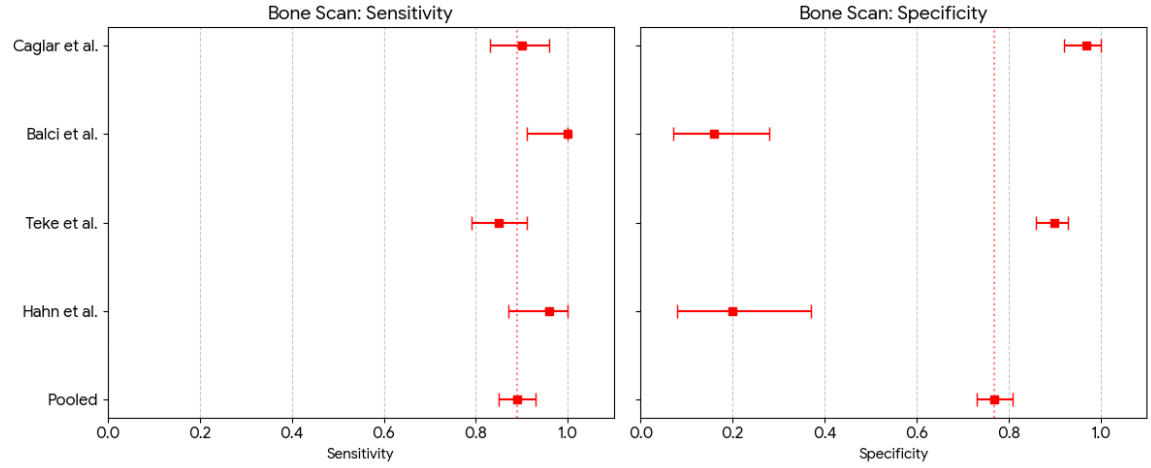

FIGURE 2 Forest plot of study-specific sensitivity and specificity estimates with pooled diagnostic accuracy for Bone Scintigraphy

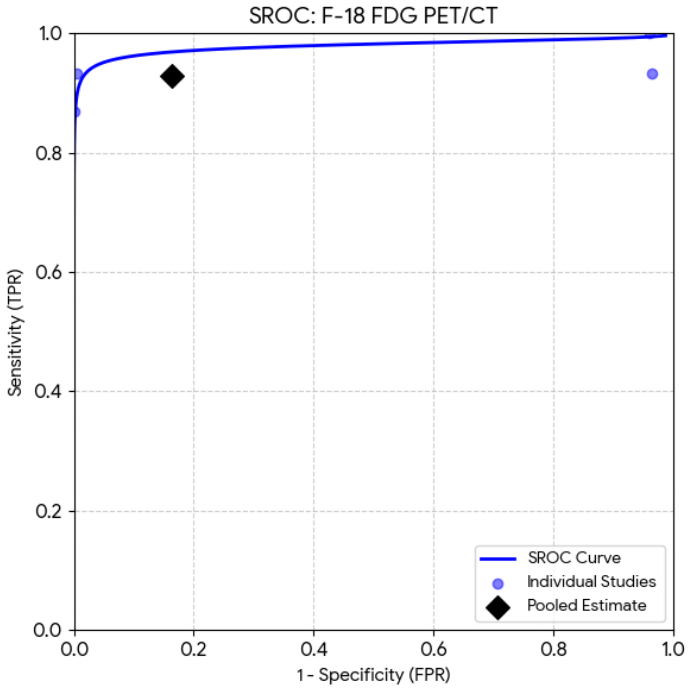

FIGURE 3 Hierarchical SROC curve for summary diagnostic performance of F-18 FDG PET-CT

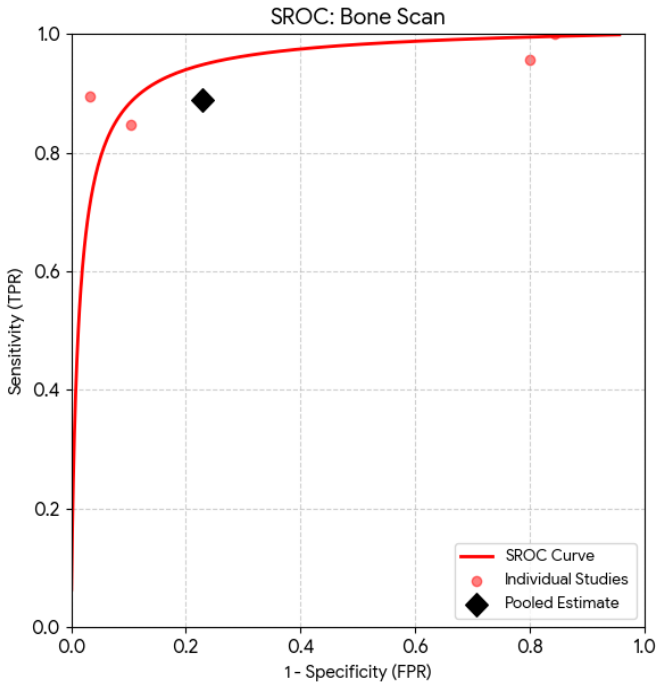

FIGURE 4 Hierarchical SROC curve for summary diagnostic performance of Bone Scintigraphy

other conventional imaging methods, including X-rays, CT scans, and MRIs, with minimal to no dropouts (see Table 2).

Summary estimates of sensitivity, specificity, DOR, PLR, NLR

Forest plot

Using the random effects model and as shown in the forest plot (Figures 1 and 2), the pooled sensitivity and specificity are noted. The p-values indicate that the sensitivity and specificity of the pooled studies support the diagnostic test's high accuracy which might be an indication of its reliable performance. The pooled sensitivity and specificity of F18-FDG PET-CT were 0.93 [95% CI: 0.90, 0.96; $p < 0.01$] and 0.84 [95% CI: 0.80, 0.87; $p < 0.01$], respectively, and on average the diagnostic test correctly identifies 93% of true positive cases and 84% true negative cases, with estimated positive likelihood ratio (PLR = 5.66), negative test result of 92% (NLR = 0.08) and diagnostic odds ratio (DOR) of 66.89. The pooled sensitivity, specificity, PLR, NLR and DOR for bone scan were 0.89 [95% CI: 0.85, 093; $p < 0.01$] and 0.77 [95% CI: 0.73, 0.81; $p < 0.01$], 89%, 77%, 3.87, 0.14, and 26.99, respectively (see Appendix).

HSROC curve

The HSROC curves provide a comprehensive overview of the test performance, with an overall area under the curve (AUC) of 0.94 for F-18 FDG PET-CT scan, representing excellent discriminative ability, and 0.89 for the bone scintigraphy, categorized as good.

DISCUSSION

Staging breast cancer patients is crucial for determining the most appropriate therapeutic approach and assessing prognosis. In the Philippines, most women are diagnosed at an advanced stage of breast cancer [2]. Bone metastases are the most common site of spread, occurring in approximately 70% of advanced cases [7]. Non-invasive detection of bone metastases is typically achieved through imaging studies. Bone scintigraphy, the conventional imaging method, is widely used to detect osseous remodeling and osteoblastic activity. However, it has limitations, particularly in identifying osteolytic lesions unless bone marrow involvement is already present. In contrast, hybrid imaging techniques such as F-18 FDG PET-CT, which combines anatomical and metabolic imaging, may offer significant advantages in detecting bone metastases [8].

In this meta-analysis, we investigated the diagnostic performance of F-18 FDG PET-CT and bone scintigraphy in detecting bone metastasis in breast cancer patients. Pooled data indicated that F-18 FDG PET-CT demonstrates superior sensitivity, specificity, and overall accuracy compared to bone scintigraphy. While both modalities reflect high overall test accuracy, the F-18

(DOR) of 66.89 and an AUC of 0.94, compared to the bone scintigraphy's DOR of 26.99 and AUC of 0.89. This nearly 2.5-fold difference in the DOR underscores that PET-CT is a more robust discriminatory tool, capable of maintaining higher precision between true positive and false positive results.

The clinical utility of these findings is further highlighted by the likelihood ratios. The pooled data for F-18 FDG PET-CT yielded an estimated positive likelihood ratio (PLR) of 5.66, suggesting that a positive result significantly increases the post-test probability of metastatic disease. Furthermore, its negative likelihood ratio (NLR) of 0.08 indicates that a negative test result reduces the odds of the disease by approximately 92%, demonstrating excellent utility in ruling out bone involvement. In contrast, bone scintigraphy yielded an estimated PLR of 3.87 and an NLR of 0.14. This higher NLR suggests that bone scintigraphy is less effective at excluding disease; consequently, while both are useful, a negative PET-CT result carries more diagnostic weight as a standalone guide for ruling out bone metastases in breast cancer patients.

The superior sensitivity of F-18 FDG PET-CT is fundamentally rooted in its ability to detect early marrow involvement and lytic lesions [9]. Because bone metastases originate in the bone marrow, F-18 FDG PET-CT can identify malignant cells via their high glycolytic activity while they are still confined to the medullary space [7]. In contrast, bone scintigraphy relies on the bone remodeling process, which can lead to an "osteoblastic lag" where the scan remains negative if bone destruction outpaces formation or if the remodeling response is delayed or absent [10].

The findings suggest that bone scintigraphy is less consistent across different patient populations, as evidenced by its higher NLR and the variability in pooled specificity across the included studies. Factors such as degenerative changes or healing fractures may contribute to this inconsistency, potentially confounding the results [6]. While both modalities remain clinically valuable in the management of breast cancer [5], F-18 FDG PET-CT offers a more definitive diagnostic profile. Its superior ability to detect early-stage metastasis and its higher reliability in ruling out the disease make it the more effective modality for the staging and management of bone metastasis compared to traditional bone scintigraphy [11].

Due to the limited availability of molecular imaging in the Philippines as of 2024, bone scintigraphy is more accessible and significantly more affordable compared to F-18 FDG PET-CT scans. In Manila, the cost of a bone scintigraphy ranges from PHP 3,599 to PHP 10,913, whereas a whole-body F-18 FDG PET-CT scan (plain) costs between PHP 43,000 and PHP 72,896. Although the PET-CT scan offers higher sensitivity and specificity, it is not commonly offered to Filipino patients due to its availability and cost.

CONCLUSION

F-18 FDG PET-CT outperforms bone scintigraphy in detecting bone metastases in breast cancer patients and should be considered the preferred imaging method for detection of bone metastases. By providing accurate staging, PET-CT enables timely treatment, which enhances prognosis and ultimately reduces overall treatment costs.

As a recommendation, a randomized controlled trial (RCT) could be conducted to evaluate the effectiveness of F-18 FDG PET-CT imaging compared to bone scintigraphy in detecting bone metastasis. Additionally, the trial could also assess the clinical value of F-18 FDG PET-CT as both a diagnostic tool and a treatment method for specific diseases. We should also highlight the availability of F-18 FDG PET-CT in the Philippines, considering that several PET-CT centers are being established with varying price ranges, although most are still situated in the national capital region.

DISCLOSURE

The authors have no conflict of interest to declare.

REFERENCES

1. Villanueva, R., Porcalla, D. 2023. Breast cancer 3rd " most fatal type" among Filipino women. Retrieved from: Breast cancer 3rd 'most fatal type' among Filipino women | Philstar.com
2. Brook, N., Brook, E., Dharmarajan, A., Dass, C. R., & Chan, A. (2018). Breast cancer bone metastases: pathogenesis and therapeutic targets. The international journal of biochemistry & cell biology, 96, 63–78. https://doi.org/10.1016/j.biocel.2018.01.003.
3. McDonald, M., Hertz, R., Lowenthal, S., 2008. The burden of cancer in Asia. https://cdn.pfizer.com/pfizercom/products/cancer_in_asia.pdf. Accessed April 3, 2022. [Ref list].

4. Venetis, K., Piciotti, R., Sajjadi, E., Invernizzi, M., Morganti, S., Criscitiello, C., & Fusco, N. (2021). Breast Cancer with Bone Metastasis: Molecular Insights and Clinical Management. Cells, 10(6), 1377. https://doi.org/10.3390/cells10061377.
5. National Comprehensive Cancer Network.2024. Breast cancer (version 3.2024). Retrieved from breast.pdf (nccn.org).
6. Pesapane, F., Downey, K., Rotili, A., Cassano, E., & Koh, D. M. (2020). Imaging diagnosis of metastatic breast cancer. Insights into imaging, 11(1), 79. https://doi.org/10.1186/s13244-020-00885-4.
7. Pang, L., Gan, C., Xu, J., Jia, Y., Chai, J., Huang, R., Li, A., Ge, H., Yu, S., & Cheng, H. (2022). Bone Metastasis of Breast Cancer: Molecular Mechanisms and Therapeutic Strategies. Cancers, 14(23), 5727. https://doi.org/10.3390/cancers14235727.
8. Ouvrard, E., Kaseb, A., Poterszman, N., Porot, C., Somme, F., & Imperiale, A. (2024). Nuclear medicine imaging for bone metastases assessment: what else besides bone scintigraphy in the era of personalized medicine?. Frontiers in medicine, 10, 1320574. https://doi.org/10.3389/fmed.2023.1320574.
9. Tahara, R. K., Brewer, T. M., Theriault, R. L., & Ueno, N. T. (2019). Bone Metastasis of Breast Cancer. Advances in experimental medicine and biology, 1152, 105–129. https://doi.org/10.1007/978-3-030-20301-6_7.
10. Ben-Haim, S., & Israel, O. (2009). Breast cancer: role of SPECT and PET in imaging bone metastases. Seminars in nuclear medicine, 39(6), 408–415. https://doi.org/10.1053/j.semnuclmed.2009.05.002.
11. Caglar, M., Kupik, O., Karabulut, E., & Høilund-Carlsen, P. F. (2016). Detection of bone metastases in breast cancer patients in the PET/CT era: Do we still need the bone scan?. Revista espanola de medicina nuclear e imagen molecular, 35(1), 3–11. https://doi.org/10.1016/j.remn.2015.08.006.
12. Balci, T. A., Koc, Z. P., & Komek, H. (2012). Bone scan or (18)f-fluorodeoxyglucose positron emission tomography/computed tomography; which modality better shows bone metastases of breast cancer?. Breast care (Basel, Switzerland), 7(5), 389–393. https://doi.org/10.1159/000341559.
13. Teke, F., Teke, M., Inal, A., Kaplan, M. A., Kucukoner, M., Aksu, R., Urakci, Z., Tasdemir, B., & Isikdogan, A. (2015). Significance of hormone receptor status in comparison of 18F -FDG-PET/CT and 99mTc-MDP bone scintigraphy for evaluating bone metastases in patients with breast cancer: single center experience. Asian Pacific journal of cancer prevention : APJCP, 16(1), 387–391. https://doi.org/10.7314/apjcp.2015.16.1.387.
14. Hahn, S., Heusner, T., Kümmel, S., Köninger, A., Nagarajah, J., Müller, S., Boy, C., Forsting, M., Bockisch, A., Antoch, G., & Stahl, A. (2011). Comparison of FDG-PET/CT and bone scintigraphy for detection of bone metastases in breast cancer. Acta radiologica (Stockholm, Sweden : 1987), 52(9), 1009–1014. https://doi.org/10.1258/ar.2011.100507.

APPENDIX : Study-specific estimates and the overall pooled performance for F-18 FDG PET-CT versus Bone Scan.

Summary of values for F-18 FDG PET-CT

	TP	FN	TN	FP	Sensitivity (95% CI)	Specificity (95% CI)
Caglar et al.	60	9	51	0	0.87 (0.79–0.95)	1.00 (0.93–1.00)
Balci et al.	47	0	2	49	1.00 (0.92–1.00)	0.04 (0.01–0.14)
Teke et al.	141	10	343	2	0.93 (0.89–0.97)	0.99 (0.98–1.00)
Hahn et al.	28	2	1	27	0.93 (0.84–1.00)	0.04 (0.00–0.20)
Pooled					**0.93 (0.90–0.96)**	**0.84 (0.80–0.87)**

Summary of values for Bone Scan

	TP	FN	TN	FP	**Sensitivity (95% CI)**	**Specificity (95% CI)**
Caglar et al.	77	9	59	2	0.90 (0.83–0.96)	0.97 (0.92–1.00)
Balci et al.	40	0	9	49	1.00 (0.91–1.00)	0.16 (0.07–0.28)
Teke et al.	127	23	310	36	0.85 (0.79–0.91)	0.90 (0.86–0.93)
Hahn et al.	22	1	7	28	0.96 (0.87–1.00)	0.20 (0.08–0.37)
Pooled					**0.89 (0.85–0.93)**	**0.77 (0.73–0.81)**

The Vanishing Jaw: Gorham-Stout Disease of the Mandible

Aaron Kim T. Cheng, MD, Jose Carlos T. Chanyungco, MD

Division of Nuclear Medicine, Department of Medicine, University of the Philippines - Philippine General Hosspital
E-mail address: aktchengmd@gmail.com

ABSTRACT

Background:

Gorham-Stout disease is a rare idiopathic disorder characterized by progressive osteolysis and replacement of normal bone with vascular or lymphatic tissue. Mandibular involvement is uncommon and may pose a diagnostic challenge because of its nonspecific clinical presentation. Bone scintigraphy has been described as a useful adjunct in the evaluation of disease extent and activity.

Case Presentation:

A 19-year-old female presented with a five-year history of a gradually enlarging, painless submental mass. Neck ultrasound demonstrated a large complex cystic lesion in the sublingual and submandibular regions, while computed tomography revealed a lobulated hypodense mass associated with lytic destruction of the mandible. Whole-body Tc-99m MDP bone scintigraphy demonstrated absent radiotracer uptake in the body and angle of the mandible, with increased uptake corresponding to the anterior neck mass. SPECT/CT confirmed extensive mandibular osteolysis. The patient subsequently underwent radiotherapy followed by surgical excision of the submandibular mass. Histopathologic examination demonstrated vascular channels with lymphoid follicles, consistent with angiolymphangioma, supporting the diagnosis of Gorham-Stout disease.

Conclusion:

Gorham-Stout disease should be considered in the differential diagnosis of progressive mandibular osteolysis. Bone scintigraphy, despite its limitations, remains valuable in the diagnosis and management of the disease. It can aid in assessing the extent of the disease, monitoring its progression, evaluating treatment response, and distinguishing the disease from other pathologies. Correlation of clinical findings, multimodality imaging, and histopathologic examination remains essential for accurate diagnosis and management.

Keywords*: Gorham-Stout disease, bone scintigraphy, mandibular osteolysis*

INTRODUCTION

Gorham-Stout disease is a rare condition characterized by spontaneous and progressive bone resorption. It involves idiopathic osteolysis that may extend beyond joint borders and is often linked to benign vascular or lymphatic proliferation, leading to the destruction of the bone matrix [1 - 4].

The first documented case of Gorham-Stout disease dates back to 1838, when Jackson described an adult male experiencing complete humeral bone resorption over an 11-year period [5]. More than a century later, in 1955, Gorham and Stout formally characterized the condition as a syndrome after reviewing 24 previously reported cases [4, 6].

Gorham-Stout disease presents with a wide range of clinical manifestations depending on the site of involvement, and diagnosis may take months to years. In some instances, the condition manifests acutely, often with debilitating pain, and initial symptoms may include spontaneous fractures. In other cases, it follows a more insidious course, marked by progressive muscle weakness [2].

This disease can involve various bones, though it is most commonly localized to the maxillofacial region, upper limbs, cranium, shoulder, and pelvis [2,3]. Romer first reported a case of jaw involvement in 1924, while Thoma documented complete mandibular lysis in 1933 [4].

We present a case of a 19-year-old female who developed massive osteolysis of the mandible with an associated submandibular mass. Bone scintigraphy was performed to aid in diagnosis. The patient subsequently received radiotherapy and surgical treatment.

CASE PRESENTATION

A 19-year-old female presented with a five-year history of a gradually enlarging soft, movable, non-tender submental mass. The patient reported no other symptoms suggestive of thyroid or malignant diseases, such as sudden weight loss, fever, weakness, palpitations, tremors, insomnia, menstrual irregularities, heat/cold intolerance, or changes in bowel movement. Concern over its progressive growth prompted the patient to seek medical evaluation.

A neck ultrasound showed a large, well-defined complex cystic mass located in the sublingual and submandibular regions. A CT scan revealed a lobulated, non-enhancing hypodense mass extending from the submandibular to the submental regions, with associated mandibular lytic changes. The mass measured 6.1 x 8.2 x 5.1 cm and contained multiple punctate calcifications. Vascular structures within the mass appeared to originate from both inferior thyroid arteries.

Whole body bone scintigraphy was performed, revealing absent Tc-99m MDP uptake in the body and angle of the mandible. Increased tracer uptake was observed in the anterior neck region, corresponding with the known mass (Figures 1 and 2). The scintigraphic images were interpreted by a board-certified nuclear medicine physician.

The patient underwent radiotherapy to manage the progression of the osteolytic process, followed by excision of the submandibular mass. Histopathologic examination showed vascular channels with lymphoid follicles, consistent with angiolymphangioma.

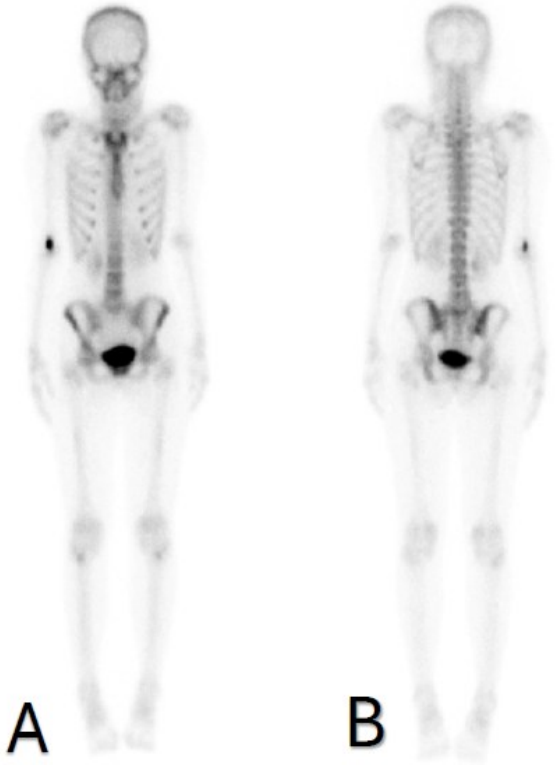

FIGURE 1 (A) Anterior and (B) posterior images of Tc-99m MDP whole body bone scintigraphy. Absent tracer uptake was noted in the body and angle of the mandible for Bone Scintigraphy.

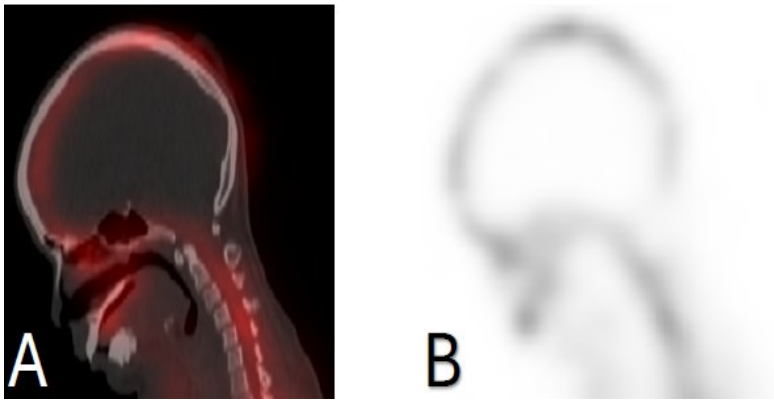

FIGURE 2 Fused SPECT-CT (A) and SPECT (B) images of the head and neck (sagittal view). Absent tracer uptake was noted in the mandibular area. Bone resorption with lytic changes

DISCUSSION

Gorham-Stout disease, also known as disappearing bone disease, massive osteolysis, or vanishing bone disease, is a rare idiopathic condition marked by extensive bone loss. To date, approximately 200 cases have been documented in literature, highlighting the rarity of this condition [2,7].

It was first described by Jackson in 1838 when he documented a case of complete humeral bone resorption over an 11-year period. Later, in 1955, Gorham and Stout reviewed previously reported cases and formally defined the condition as a syndrome [2,5,7,8].

The disease is characterized by the replacement of normal bone with aggressively expanding non-neoplastic vascular tissue, resembling hemangiomas or lymphangiomas. Its primary lesions include osteolysis and lymphatic tissue proliferation without malignancy. It is nonexpansile but locally aggressive, often leading to bone resorption. In some cases, the vascular lesion may spread into surrounding soft tissue and adjacent bones [4,7,9].

The exact etiology and pathophysiology of Gorham-Stout disease remain unknown. Gorham and Stout associated the condition with angiomatosis of blood and lymph vessels, proposing hyperemia, local pH alterations, and mechanical forces as potential factors for bone absorption while excluding osteoclast involvement. In contrast, some studies have suggested a role for osteoclasts [2,7]. Increased osteoclast activity has been linked to elevated interleukin-6 levels, as suggested by Devlin et al., while Moller et al. and Hirayama et al. proposed an enhanced sensitivity of osteoclast precursors to humoral factors that drive bone resorption [10–12]. It has also been suggested that it may originate from a silent hamartoma that becomes active and initiates bone resorption following minor trauma [13]. Despite these theories, the mechanisms behind Gorham-Stout disease remain unclear.

Gorham-Stout disease is diagnosed primarily through exclusion, requiring the elimination of other common causes of osteolysis, such as infections, cancers (primary or metastatic), and endocrine or inflammatory diseases. The diagnosis is confirmed through biopsy, which serves as the gold standard. Histopathology reveals no evidence of malignant, neuropathic, or infectious components but identifies the presence of lymphovascular malformations within the affected bone, a hallmark feature that distinguishes it from other conditions [2,7].

In this case report, the histopathologic examination of the excised mass revealed vascular channels with lymphoid follicles, which is consistent with the histologic findings described in literature for Gorham-Stout disease [2,7].

Imaging studies such as x-ray, CT, MRI, and bone scintigraphy have been used in the evaluation of Gorham -Stout disease [14]. Bone scintigraphy, in particular, is a highly sensitive nuclear medicine imaging technique commonly used to evaluate active bone formation associated with malignant or benign diseases [15]. However, in Gorham-Stout disease, bone scintigraphy is utilized differently. Unlike its typical use in conditions such as bone metastases, where active bone remodeling or formation is assessed, bone scintigraphy in Gorham-Stout disease primarily evaluates the osteolytic nature of the condition [16,17].

In the early stages of the disease, bone scintigraphy typically shows increased radiotracer uptake in areas of active osteolysis. This uptake is thought to result from increased vascular proliferation and bone surface activity. As the disease progresses and bone resorption becomes complete, the affected areas show an absence of radiotracer uptake due to the lack of bone matrix [14,17]. This biphasic pattern aligns with the two stages of the disease: an initial phase characterized by vascular proliferation and active osteolysis, and a later phase in which fibrous tissue replaces the resorbed bone without regeneration [9,16,18].

In the present case report, bone scintigraphy was performed in the latter stage of the disease, demonstrating absent radiotracer uptake in the affected region, consistent with advanced bone resorption.

In some cases, multifocal, noncontiguous osteolysis has also been observed in patients with Gorham-Stout disease [19,20], and whole body bone scintigraphy may be a valuable tool in evaluating these multifocal lesions. In one reported case, bone scintigraphy was utilized to monitor disease progression and evaluate the response to treatment after one year of pamidronate therapy [16]. Furthermore, the absence of radiotracer uptake in the resorbed sites distinguishes the disease from other pathologies, such as primary bone tumors, metastases,or osteomyelitis [9,16,18].

Due to the rarity of this pathological condition, there is no established standard treatment. Proposed approaches include medical treatment such as bisphosphonates or interferon α-2b, surgical intervention, radiotherapy, and/or combinations of these methods [2,7,21–23]. However, the management generally focuses on radiation therapy to control large, painful lesions and surgical intervention to address pathological progression that could result in significant functional limitations. Surgical options include resection of the affected segment, reconstruction with bone grafts, or the use of prostheses [14,24]. Three phase bone scintigraphy may be done to assess the viability of the grafts [25]. However, the osteolytic nature of the disease compromises the structural integrity and long-term effectiveness of reconstruction, as bone grafts undergo resorption within weeks after grafting [14,24].

CONCLUSION

Gorham-Stout disease is a rare condition characterized by progressive osteolysis and replacement of bone with vascular fibrous connective tissue. Its etiology and pathogenesis remain unclear.

Bone scintigraphy, despite its limitations, remains valuable in the diagnosis and management of the disease. It can aid in assessing the extent of the disease, monitoring its progression, evaluating treatment response, and distinguishing the disease from other pathologies.

While no definitive therapy has been established, most patients are treated with radiotherapy and surgical procedures. Given its unpredictable clinical course and lack of established therapies, early detection through clinical suspicion, diagnostic imaging, and confirmation with histopathological examination are essential.

DISCLOSURE

The authors have no conflict of interest to declare.

REFERENCES

1. Choma, N. D., Biscotti, C. V., Bauer, T. W., Mehta, A. C., & Licata, A. A. (1987). Gorham's syndrome: a case report and review of the literature. The American journal of medicine, 83(6), 1151–1156. https://doi.org/10.1016/0002-9343(87)90959-4.
2. Sá, P., Marques, P., Oliveira, C., Rodrigues, A. S., Amorim, N., & Pinto, R. (2015). Gorham's disease: clinical case. Revista brasileira de ortopedia, 50(2), 239–242. https://doi.org/10.1016/j.rboe.2015.03.004.
3. Bosco, F., Giustra, F., Faccenda, C., Boffano, M., Ratto, N., & Piana, R. (2022). Gorham-Stout disease: A rare bone disorder. Journal of Orthopaedic Reports, 1(2), 100028. https://doi.org/10.1016/j.jorep.2022.04.005.
4. Saify, F. Y., & Gosavi, S. R. (2014). Gorham's disease: A diagnostic challenge. Journal of oral and maxillofacial pathology : JOMFP, 18(3), 411–414. https://doi.org/10.4103/0973-029X.151333.
5. Jackson, J.B.S. (1838) A boneless arm. Boston Med Surg J 18:368–369. https://doi.org/10.1056/NEJM183807110182305.
6. Gorham, L. W., & Stout, A. P. (1955). Massive osteolysis (acute spontaneous absorption of bone, phantom bone, disappearing bone); its relation to hemangiomatosis. The Journal of bone and joint surgery. American volume, 37-A (5), 985–1004.
7. Wang, P., Liao, W., Cao, G., & Jiang, Y. (2019). A rare case of Gorham-stout syndrome involving the thoracic spine with progressive bilateral chylothorax: a case report. BMC musculoskeletal disorders, 20(1), 154. https://doi.org/10.1186/s12891-019-2542-z.
8. Evrenos, M. K., Özkaya, M., Yaman, M., & Proff, L. Y. (2016). Case Report: Gorham-Stoute Syndrome with Involvement of Majority of Mandible, and Partial Maxillary, Temporal and Zygomatic Bones. Journal of maxillofacial and oral surgery, 15(Suppl 2), 335–338. https://doi.org/10.1007/s12663-015-0869-z.
9. Parihar, V., Yadav, Y. R., & Sharma, D. (2008). Gorham's disease involving the left parietal bone: a case report. Cases journal, 1(1), 258. https://doi.org/10.1186/1757-1626-1-258.
10. Devlin, R. D., Bone, H. G., 3rd, & Roodman, G. D. (1996). Interleukin-6: a potential mediator of the massive osteolysis in patients with Gorham-Stout disease. The Journal of clinical endocrinology and metabolism, 81(5), 1893–1897. https://doi.org/10.1210/jcem.81.5.8626854.
11. Möller, G., Priemel, M., Amling, M., Werner, M., Kuhlmey, A. S., & Delling, G. (1999). The Gorham-Stout syndrome (Gorham's massive osteolysis). A report of six cases with histopathological findings. The Journal of bone and joint surgery. British volume, 81(3), 501–506. https://doi.org/10.1302/0301-620x.81b3.9468.
12. Hirayama, T., Sabokbar, A., Itonaga, I., Watt-Smith, S., & Athanasou, N. A. (2001). Cellular and humoral mechanisms of osteoclast formation and bone resorption in Gorham-Stout disease. The Journal of pathology, 195 (5), 624–630. https://doi.org/10.1002/path.989.
13. El-Kouba, G., de Araújo Santos, R., Pilluski, P. C., Severo, A., & Lech, O. (2015). GORHAM-STOUT SYNDROME: PHANTOM BONE DISEASE. Revista brasileira de ortopedia, 45(6), 618–622. https://doi.org/10.1016/S2255-4971(15)30313-X.
14. Agyeman, K., Pretell-Mazzini, J., Subhawong, T., Kerr, D. A., & Jose, J. (2017). Gorham Disease. American journal of orthopedics (Belle Mead, N.J.), 46(6), E458–E462.

15. Van den Wyngaert, T., Strobel, K., Kampen, W. U., Kuwert, T., van der Bruggen, W., Mohan, H. K., Gnanasegaran, G., Delgado-Bolton, R., Weber, W. A., Beheshti, M., Langsteger, W., Giammarile, F., Mottaghy, F. M., Paycha, F., & EANM Bone & Joint Committee and the Oncology Committee (2016). The EANM practice guidelines for bone scintigraphy. European journal of nuclear medicine and molecular imaging, 43(9), 1723–1738. https://doi.org/10.1007/s00259-016-3415-4.
16. Park, S. B., Choi, J. Y., & Kim, S. J. (2017). Gorham-Stout Disease Affecting the Mandible: Bone Scintigraphy and Computed Tomography Findings. Clinical nuclear medicine, 42(10), 779–781. https://doi.org/10.1097/RLU.0000000000001800.
17. Spieth, M. E., Greenspan, A., Forrester, D. M., Ansari, A. N., Kimura, R. L., & Gleason-Jordan, I. (1997). Gorham's disease of the radius: radiographic, scintigraphic, and MRI findings with pathologic correlation. A case report and review of the literature. Skeletal radiology, 26(11), 659–663. https://doi.org/10.1007/s002560050306.
18. Johnson, P. M., & McClure, J. G. (1958). Observations on massive osteolysis; a review of the literature and report of a case. Radiology, 71(1), 28–42. https://doi.org/10.1148/71.1.28
19. Wang, L., Mo, X., Shen, H., & Zhang, S. (2024). Multifocal Gorham-Stout disease in a thirteen-year-old boy with horseshoe kidney: A case report. Radiology case reports, 19(11), 5066–5070. https://doi.org/10.1016/j.radcr.2024.07.170.
20. Ozbayrak, M., Yilmaz, M. H., Kantarci, F., Ozer, H., Harmanci, K., Babacan, M., & Dervisoglu, S. (2013). A case of an idiopathic massive osteolysis with skip lesions. Korean journal of radiology, 14(6), 946–950. https://doi.org/10.3348/kjr.2013.14.6.946.
21. Dunbar, S. F., Rosenberg, A., Mankin, H., Rosenthal, D., & Suit, H. D. (1993). Gorham's massive osteolysis: the role of radiation therapy and a review of the literature. International journal of radiation oncology, biology, physics, 26(3), 491–497. https://doi.org/10.1016/0360-3016(93)90968-2.
22. Hammer, F., Kenn, W., Wesselmann, U., Hofbauer, L. C., Delling, G., Allolio, B., & Arlt, W. (2005). Gorham-Stout disease--stabilization during bisphosphonate treatment. Journal of bone and mineral research : the official journal of the American Society for Bone and Mineral Research, 20(2), 350–353. https://doi.org/10.1359/JBMR.041113.
23. Hagberg, H., Lamberg, K., & Aström, G. (1997). Alpha-2b interferon and oral clodronate for Gorham's disease. Lancet (London, England), 350(9094), 1822–1823. https://doi.org/10.1016/S0140-6736(05)63639-2.
24. Al-Jamali, J., Glaum, R., Kassem, A., Voss, P. J., Schmelzeisen, R., & Schön, R. (2012). Gorham-Stout syndrome of the facial bones: a review of pathogenesis and treatment modalities and report of a case with a rare cutaneous manifestations. Oral surgery, oral medicine, oral pathology and oral radiology, 114(6), e23–e29. https://doi.org/10.1016/j.oooo.2011.08.016.
25. Buyukdereli, G., Guney, I. B., Ozerdem, G., & Kesiktas, E. (2006). Evaluation of vascularized graft reconstruction of the mandible with Tc-99m MDP bone scintigraphy. Annals of nuclear medicine, 20(2), 89–93. https://doi.org/10.1007/BF02985619.

ESCO
LIFESCIENCES GROUP

Improving Lives Through Science

DIRECT MANUFACTURER

- Animal Research Workstation
- Biosafety Safety Cabinet
- CO_2 Incubator
- Ducted Fume Hood
- Ductless Fume Hood
- Filtered Storage Cabinet
- Laboratory Centrifuge
- Laboratory Oven and Incubator
- Laboratory Refrigerator and Freezer
- Laboratory Shaker
- Laminar Flow Cabinet
- PCR Cabinet
- PCR Thermal Cycler
- Powder Weighing Balance Enclosure
- Ultra-low Temperature Freezer

ESCO
LIFESCIENCES

- Airflow Containment
- Cross-Contamination Facility Integrated Barrier
- Isolation Containment
- Ventilation Containment
- Radiopharmacy
- Adherent Cell Bioreactors
- Adherent Automated Cell Harvesting System
- Cell Culture Monitoring Tools
- Single-use Consumables for Bioprocessing

ESCO
MEDICAL

- Time-Lapse Incubator
- Benchtop Incubator
- ART Workstation
- CO_2 Incubator
- Anti-Vibration Table
- Gas Analyser

ESCO
ASTER

CRDMO Services

www.escolifesciences.com


PHILMED DYNASTY
SUPPLIES CORP.


PHILMED DYNASTY
SUPPLIES CORP.

Inter Medical

MultiCam

with 1 or 2 detectors

Crystal Probe-*automatic*™

Gamma probe system with CZT technology
for radioguided surgery

SLN Sentinel lymph node

ROLL Radioguided occult lesion localization

Crystal Photonics

Biograph Trinion PET/CT

Future-forward by design

siemens-healthineers.com/en-ph/biograph-trinion

Launch your future forward with a PET/CT that puts you confidently ahead of the curve and easily adapts to evolving clinical possibilities: Biograph Trinion™ with myExam Companion™.

Biograph Trinion PET/CT fully integrates best-in-class hardware and software to create one high-performance platform. A brand-new imaging experience puts patients more at ease, while users gain efficiency from a modern design and AI-supported workflow. Always the right fit, Biograph Trinion provides a sustainable investment from today onward—delivering reduced costs through its compact footprint, automated energy-saving features, and on-site scalability.

SIEMENS Healthineers

Symbia Pro.specta SPECT/CT
with myExam Companion

Modernize to MAXIMIZE

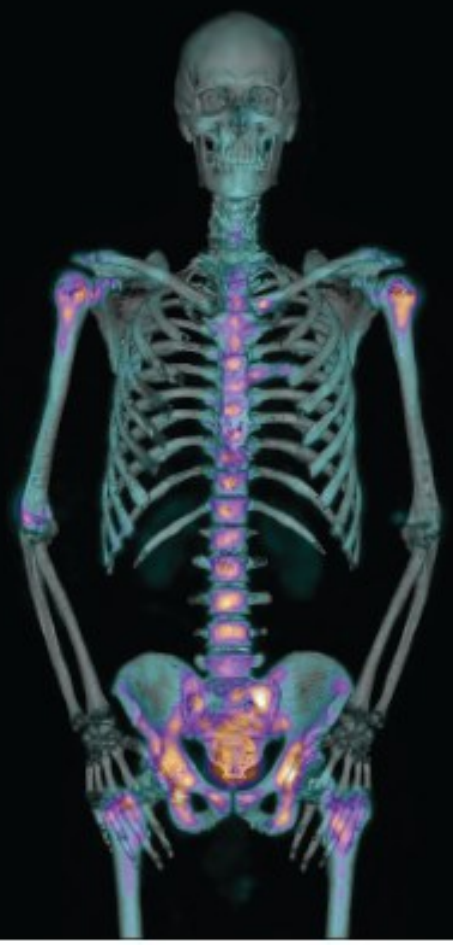

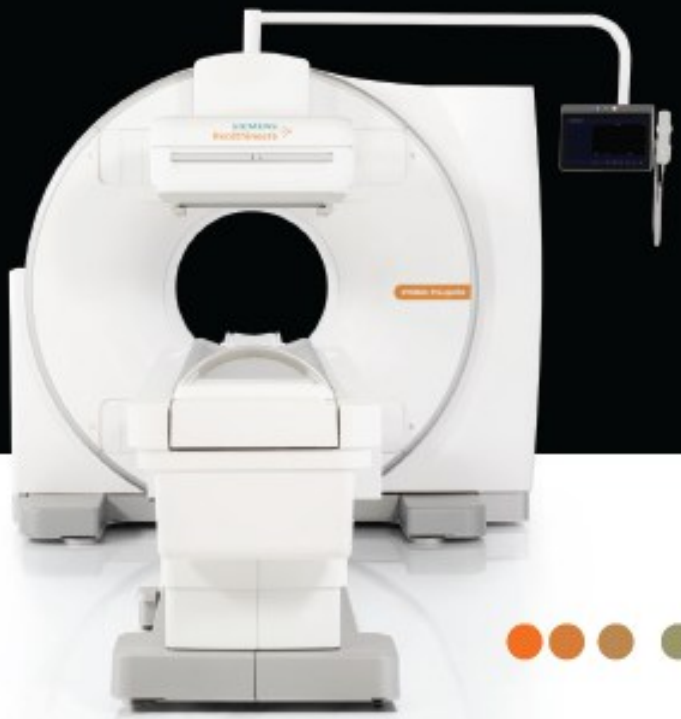

Take your nuclear medicine department into the future with intelligent SPECT/CT imaging. Symbia Pro.specta™ with myExam Companion™ gives you the power of more.

Redefine performance with new standards for SPECT/CT

Automatic SPECT motion correction and up to 64-slice CT enable faster scanning at the highest image quality.[1]

Reach your full potential with a smart workflow

A single, intuitive interface automates steps across the entire workflow—helping you achieve high-quality, reproducible results.

Achieve optimized imaging from dedicated clinical tools

A multi-purpose SPECT/CT that transforms into a specialized camera for cardiology, neurology, oncology, theranostics, and more.

[1] *Based on competitive literature at time of publication. Data on file.*

Symbia Pro.specta SPECT/CT is not commercially available in all countries. Future availability cannot be guaranteed. Please contact your local Siemens Healthineers organization for further details.

Learn more at siemens-healthineers.com/symbia-prospecta

SIEMENS Healthineers